

# **Cystatin C and Alzheimer's Disease**

**Abigail J. Williams**

**A thesis submitted for the degree of Doctor of Philosophy**

**September 2014**

**Department of Molecular Biology and Biotechnology**

**University of Sheffield**

## Abstract

Aggregation of amyloid- $\beta$  in Alzheimer's disease (AD) is modulated in the presence of other amyloidogenic proteins including human cystatin C (hCC), which directly protects neuronal cells from A $\beta$ -induced toxicity and inhibits fibril formation. Determination of the relevant conformations of the interacting A $\beta$  and hCC is a key step to uncovering the molecular mechanism of hCC's activity in AD.

A system for the production of recombinant A $\beta_{1-40}$  has been established and is described here. It is also shown that hCC readily produces stable oligomeric species upon incubation in aggregating conditions, a phenomenon that has not been observed for other members of the cystatin family. Novel structural differences between amyloid fibrils produced by hCC and cystatin B have also been identified using limited proteolysis, indicating that hCC does not retain a monomer-like fold within the fibril and that the N-terminal is disordered and not part of the fibril core.

The work presented here shows that hCC inhibits fibril production by A $\beta$  in a dose-dependent manner, instead promoting the production of amorphous aggregates and small assemblies, with 2:1 molar ratios of hCC to A $\beta$  being required for complete inhibition. It is unclear if the assemblies observed are toxic protofibrils or an alternative non-toxic species. A comparison of the inhibitory activity of the monomeric and dimeric forms of hCC was carried out, and indicated that the active region could be the hydrophobic loop involved in protease inhibition. Characterisation of binding by NMR HSQC experiments revealed that no observable complex was being formed between monomeric A $\beta$  and folded monomeric hCC. Taken together these results suggest that hCC is selectively binding to an oligomeric species of A $\beta$  and trapping the peptide in a non-toxic state.

## Acknowledgements

First and foremost I must thank my supervisor Rosie Staniforth who has been wonderful, both for offering me this PhD in the first place and for all her guidance, support and encouragement throughout the last four years. I would also like to thank Jon Waltho, Mike Williamson and Jeremy Craven for all their help and guidance, as well as my advisors Neil Hunter and Stuart Wilson. Andrea Hounslow has been amazing, assisting me with the NMR experiments and analysis, and also thank you to Simon Thorpe for help with the MS. Thanks to Svet Tzokov for all of his help with EM and his constant reassurance that I hadn't broken the microscope.

Thank you also to the cystatin group, particularly Pete, Amy and Sirwan. I'm sorry for filling the office with ducks and owls and lobsters. Pete has been simply awesome, full of knowledge and ideas and always around for a chat. Amy and Sirwan have made D07 such an enjoyable place to work for the last two years, with lots of fun and laughter (and celebrity gossip!). Much of my research has been based on the findings of Adham and Emma, for which I am very grateful. The NMR group have been great; it would be impossible to name everybody (and I would undoubtedly forget someone), but thank you all so much for the friendships, discussions and advice. Cake Friday definitely brightens up the week, and there have been some pretty impressive concoctions (forever immortalised in the brilliant NMR cookbook).

I have met many amazing people since moving to Sheffield, but special thanks must go to Wednesday Club, to Sophie, Simon, Katie, Sarah, Suze and Lucy (and Larry of course!). Thank you for keeping me sane, for our many hours spent in the Uni Arms, and the greatest farm trip ever. I'm so glad I met you all, and I definitely wouldn't have made it through without you. Also thank you to George for his words of encouragement and sense of perspective over the last few weeks of writing up. Massive thanks to the fabulous Hannah and Simon for many awesome weekends of cocktails and culture, and for reminding me that there is a life outside of science.

Thank you to my wonderful family, to Mum, Dad and Elle for all your love and support, it means so much to me and I am truly grateful.

Last but not least, thank you to Simon for moving to Sheffield, for putting up with me and for always believing in me. I couldn't have done it without you.

## Table of Contents

<b>Chapter One: Introduction</b> .....	<b>1</b>
1.1. Amyloid.....	1
1.1.1. The Importance of Protein Folding .....	3
1.1.2. Conversion to an Amyloid-forming Competent State .....	6
1.1.3. Mechanism of Fibril Formation.....	7
1.1.4. High Molecular Weight Oligomers .....	11
1.1.5. Fibril Structure.....	13
1.1.6. Therapeutics .....	23
1.1.7. Natural regulation of amyloid formation <i>in vivo</i> .....	24
1.2. Amyloidogenic Disease .....	26
1.2.1. Cytotoxicity.....	27
1.2.2. Alzheimer’s Disease .....	29
1.2.3. Cerebral Amyloid Angiopathies.....	31
1.2.4. Amyloid- $\beta$ .....	32
1.3. Cystatins .....	34
1.3.1. Cystatin C.....	35
1.3.2. Biological role of hCC .....	36
1.3.3. Inhibition Mechanism.....	37
1.3.4. Structure of hCC .....	37
1.3.5. L68Q Variant of hCC .....	40
1.3.6. Cystatins and Disease .....	40
1.4. Interactions with A $\beta$ .....	41
1.4.1. Albumin .....	42
1.4.2. Amyloidogenic Proteins .....	43
1.5. Overview of Thesis .....	50
<b>Chapter Two: Materials and Methods</b> .....	<b>51</b>
2.1. Buffers and Reagents.....	51
2.2. DNA Manipulation.....	51
2.2.1. Expression Vectors.....	51
2.2.2. Plasmid Extraction .....	51
2.2.3. Primer Sequences.....	51

2.2.4. Quantification of DNA.....	52
2.2.5. Competent Cells.....	52
2.2.5. Site-Directed Mutagenesis .....	53
2.2.6. Transformations .....	53
2.2.7. DNA Sequencing .....	53
2.3. Growth Media and Solutions.....	53
2.3.1. Luria-Bertani Media.....	53
2.3.2. M9 Minimal Media .....	53
2.3.3. Antibiotic Solutions.....	55
2.3.4. Isopropyl- $\beta$ -D-galactosidase (IPTG).....	55
2.4. Protein Expression and Purification .....	56
2.4.1. Protein Characteristics.....	56
2.4.2. Cystatin C.....	56
2.5. Protein Procedures.....	59
2.5.1. SDS Polyacrylamide Gel Electrophoresis .....	59
2.5.2. Tricine SDS Polyacrylamide Gel Electrophoresis .....	60
2.5.3. Determination of Protein Concentration .....	62
2.5.4. Protein Concentration and Buffer Exchange .....	62
2.5.5. Analytical Size Exclusion Chromatography.....	62
2.6. Spectroscopic Techniques.....	62
2.6.1. Fluorescence Spectroscopy.....	62
2.6.2. Nuclear Magnetic Resonance (NMR).....	63
2.6.3. Transmission Electron Microscopy (TEM).....	63
<b>Chapter Three: Purification of A<math>\beta</math><sub>1-40</sub> Using a Ubiquitin Tag .....</b>	<b>64</b>
3.1. Introduction .....	64
3.2. Materials and Methods.....	66
3.2.1. His <sub>6</sub> Ub-A $\beta$ <sub>1-40</sub> Construct.....	66
3.2.2. Expression and Purification of GST-YUH1 .....	66
3.2.3. Expression and Purification of His <sub>6</sub> Ub-A $\beta$ <sub>1-40</sub> .....	67
3.2.4. Hydrolysis of His <sub>6</sub> Ub-A $\beta$ <sub>1-40</sub> .....	68
3.2.5. Separation of A $\beta$ <sub>1-40</sub> from the Ubiquitin tag.....	69
3.2.6. Preparation of Monomeric A $\beta$ <sub>1-40</sub> .....	70

3.3. Results.....	71
3.3.1. Cleavage of His <sub>6</sub> Ub-A $\beta$ <sub>1-40</sub> .....	71
3.3.2. Separation of A $\beta$ <sub>1-40</sub> Peptide from Ubiquitin .....	71
3.3.3. Characterisation of the Purified Peptide after SEC.....	80
3.3.4. Fibrillisation .....	85
3.3.5. Overview of Final Purification .....	86
3.4. Conclusions .....	86
<b>Chapter Four: Structural Studies of Cystatin C .....</b>	<b>88</b>
4.1. Introduction .....	88
4.2. Materials and Methods .....	89
4.2.1. hCC Fibril Formation .....	89
4.2.2. ThT Fluorescence .....	90
4.2.3. SEC-HPLC .....	90
4.2.4. Purification of Oligomeric Species.....	90
4.2.5. Purification of Fibrils.....	90
4.2.6. Limited Proteolysis .....	91
4.3. Results and Discussion.....	97
4.3.1. Fibrillisation of hCC .....	97
4.3.2. Oligomeric Intermediates.....	108
4.3.3. Limited Proteolysis of hCC Fibrils with Elastase .....	123
<b>Chapter Five: Interaction of Cystatin C and A<math>\beta</math><sub>1-42</sub>.....</b>	<b>136</b>
5.1. Introduction .....	136
5.1.1. hCC and A $\beta$ .....	137
5.2. Materials and Methods .....	141
5.2.1. Preparation of Monomeric A $\beta$ <sub>1-42</sub> .....	141
5.2.2. A $\beta$ <sub>1-42</sub> Fibril Formation .....	141
5.2.3. Preparation of hCC Species .....	144
5.2.4. Analytical Size Exclusion Chromatography (SEC).....	144
5.2.5. Nuclear Magnetic Resonance Spectroscopy .....	145
3. Results .....	148
5.3.1. A $\beta$ <sub>1-42</sub> Fibrillisation .....	148
5.3.2. Addition of hCC to A $\beta$ <sub>1-42</sub> Fibrillisation .....	151

5.3.3. Time-course of A $\beta$ <sub>1-42</sub> and hCC.....	156
5.3.4. Comparison of Different Species .....	165
5.3.5. Addition at Different Time-Points.....	167
5.3.6. Addition of Different Species .....	169
5.3.7. NMR Spectroscopy .....	174
5.4. Discussion.....	190
<b>Chapter Six: Final Conclusions and Future Work .....</b>	<b>196</b>
<b>References .....</b>	<b>201</b>

## List of Figures

### **Chapter One: Introduction**

Figure 1.1. Amyloid Fibril Structure.....	2
Figure 1.2. Free Energy Surface for Protein Folding and Amyloid Formation.....	3
Figure 1.3. Thermodynamics of Folding.....	5
Figure 1.4. Fibrillisation Reaction and Pathway.....	8
Figure 1.5. Models of Fibril Formation.....	10
Figure 1.6. Large Molecular Weight Oligomers.....	12
Figure 1.7. Amyloid Fibre X-ray Diffraction Pattern and Corresponding Structure.....	15
Figure 1.8. Electron Microscopy of Amyloid.....	16
Figure 1.9. A $\beta$ Fibril Structure Model.....	20
Figure 1.10. Oligomeric Forms of A $\beta$ Peptides.....	23
Figure 1.11. Possible Drug Targets for Amyloid Disease.....	24
Figure 1.12. Postulated Cell-Surface Receptors for A $\beta$ with Different Roles in Cytotoxicity.....	29
Figure 1.13. Initial Events in the Amyloid Cascade Hypothesis.....	31
Figure 1.14. Processing of APP.....	33
Figure 1.15. Schematic of Cystatin Primary Structure.....	35
Figure 1.16. Structure of hCC.....	39

### **Chapter Two: Materials and Methods**

Figure 2.1. Purification of Cystatin C.....	58
Figure 2.2. Precision Plus Protein Dual Xtra Standards (Bio-Rad) .....	60

### **Chapter Three: Purification of A $\beta$ <sub>1-40</sub> Using a Ubiquitin Tag**

Figure 3.1. Hydrolysis Reaction.....	71
Figure 3.2. Separation of Hydrolysis Products by Reverse-Phase HPLC.....	72
Figure 3.3. Separation of Hydrolysis Products by Size-Exclusion HPLC.....	73
Figure 3.4. SEC-HPLC of His <sub>6</sub> Ub-A $\beta$ <sub>1-40</sub> in Varying Concentrations of	

Acetonitrile.....	74
Figure 3.5. Separation of Hydrolysis Products by SEC-HPLC in 40% Acetonitrile.....	75
Figure 3.6. Size-Exclusion Chromatography and SDS-PAGE Analysis.....	76
Figure 3.7. Isolation of A $\beta$ <sub>1-40</sub> by Fibrillisation at pH 2.0.....	77
Figure 3.8. Isolation of A $\beta$ <sub>1-40</sub> by Fibrillisation at pH 7.4 with 100 $\mu$ M ZnCl <sub>2</sub> .....	78
Figure 3.9. Ni <sup>2+</sup> -NTA Chromatography of Hydrolysis Reaction.....	79
Figure 3.10. Analytical SEC of Purified A $\beta$ <sub>1-40</sub> .....	80
Figure 3.11. SEC-HPLC Analysis of Purified A $\beta$ <sub>1-40</sub> .....	82
Figure 3.12. Mass Spectrometry Analysis of Purified A $\beta$ <sub>1-40</sub> .....	84
Figure 3.13. Fibrillisation of A $\beta$ <sub>1-40</sub> .....	85
Figure 3.14. Outline of the optimised protocol for A $\beta$ <sub>1-40</sub> purification.....	87

#### **Chapter Four: Structural Studies of Cystatin C**

Figure 4.1. Current models of Cystatin Fibril Structures.....	89
Figure 4.2. Limited Proteolysis Sample Preparation.....	93
Figure 4.3. Topology Map of Cystatin C with Predicted Elastase Cut Sites.....	94
Figure 4.4. Limited Proteolysis Fragment Analysis.....	96
Figure 4.5. Fibrillisation of Cystatin C at pH 4.0.....	98
Figure 4.6. Fibrillisation of Cystatin C at pH 2.0.....	99
Figure 4.7. pH Dependence of hCC Fibril Formation.....	102
Figure 4.8. Electron Microscopy of hCC Fibrils at pH 4.0.....	104
Figure 4.9. Electron Microscopy of hCC Fibrils at pH 2.0.....	105
Figure 4.10. Fibril Width Measurements.....	106
Figure 4.11. TEM of L68Q Fibrils.....	107
Figure 4.12. TEM Time-Course of hCC Fibrillisation at pH 4.0.....	110
Figure 4.13. TEM Time-course of hCC Fibrillisation at pH 2.0.....	113
Figure 4.14. Incubation of Cystatin C Fibrils at Different Ionic Strengths.....	116

Figure 4.15. Incubation of Cystatin C Fibrils with Denaturant.....	117
Figure 4.16. Incubation of Cystatin C Fibrils – Mechanical Perturbations.....	118
Figure 4.17. Incubation of Cystatin C Fibrils at Different pH.....	119
Figure 4.18. Oligomer Measurements.....	121
Figure 4.19. TEM of Limited Proteolysis.....	124
Figure 4.20. Digestion Map of Cystatin C Fibrils at Predicted Cut Sites.....	128
Figure 4.21. Cystatin C Topology Identifying Positions of Hydrolysis.....	129
Figure 4.22. Models of Cystatin Fibril Structure.....	132
Figure 4.23. Loop Protrusion.....	133
Figure 4.24. Digestion Map of Cystatin C Fibrils with no constraints on possible cut sites.....	135

## **Chapter Five: Interaction of Cystatin C and A $\beta$ <sub>1-42</sub>**

Figure 5.1. The Aggregation of A $\beta$ <sub>1-42</sub> and Different Methods of Modulation.....	137
Figure 5.2. The Interaction between Cystatin C and A $\beta$ in the Literature.....	139
Figure 5.3. Curve Fitting.....	143
Figure 5.4. Fibrillisation of A $\beta$ <sub>1-42</sub> using Different Systems.....	149
Figure 5.5. TEM of A $\beta$ <sub>1-42</sub> Fibrillisation using Different Systems.....	150
Figure 5.6. A $\beta$ + Cystatin C Dose Dependence .....	152
Figure 5.7. Calculated Kinetic Parameters.....	153
Figure 5.8. TEM of Incubation of A $\beta$ <sub>1-42</sub> in the Presence of hCC .....	155
Figure 5.9. Electron Microscopy Time-Course.....	157
Figure 5.10. SEC Time-course of Fibrillisation of A $\beta$ <sub>1-42</sub> .....	160
Figure 5.11. SEC Time-course of A $\beta$ <sub>1-42</sub> Fibrillisation in the Presence of hCC...	162
Figure 5.12. Peak Heights from SEC-HPLC Time-course.....	164
Figure 5.13. Comparison of Different Species by TEM.....	165
Figure 5.14. Addition of Cystatin C at Different Points.....	168
Figure 5.15. Addition of Cystatin C Dimer.....	170

Figure 5.16. TEM of Cystatin C Oligomer with A $\beta$ <sub>1-42</sub> .....	172
Figure 5.17. Addition of Cystatin C Oligomer.....	173
Figure 5.18. HSQC Spectrum of Cystatin C at 278 K.....	175
Figure 5.19. Titration of Cystatin C with A $\beta$ <sub>1-42</sub> .....	176
Figure 5.20. Amide Chemical Shifts.....	177
Figure 5.21. Amide Peak Intensity.....	180
Figure 5.22. Changes in Amide Peak Intensity.....	181
Figure 5.23. HSQC Spectrum of Cystatin C at 303 K.....	183
Figure 5.24. Time-course of Cystatin C in the Presence of A $\beta$ <sub>1-42</sub> .....	184
Figure 5.25. Amide Chemical Shift Changes for hCC and A $\beta$ <sub>1-42</sub> Time-course...	185
Figure 5.26. Amide Peak Intensity.....	186
Figure 5.27. Changes in Amide Peak Intensity.....	187
Figure 5.28. Intensity Change Mapped onto Cystatin C Structure.....	188
Figure 5.29. TEM of NMR Time-course.....	189
Figure 5.30. Proposed Modulation of A $\beta$ <sub>1-42</sub> by Cystatin C.....	195

## List of Tables

### **Chapter One: Introduction**

Table 1.1. Summary of Human Proteins Linked with an Amyloid Disease.....27

Table 1.2. Physiological Concentrations of hCC.....36

### **Chapter Two: Materials and Methods**

Table 2.1. Primer Sequences.....52

Table 2.2. Predicted Protein Characteristics.....56

### **Chapter Three: Purification of A $\beta$ <sub>1-40</sub> Using a Ubiquitin Tag**

Table 3.1. Production Strategies for A $\beta$ <sub>1-40</sub>.....65

### **Chapter Four: Structural Studies of Cystatin C**

Table 4.1. Buffer Conditions for Fibril Stability Tests.....91

Table 4.2. Incubation of Cystatin C Fibrils in Different Conditions.....114

Table 4.3. Fragments Observed from Elastase Digest of Cystatin C Fibril.....127

## List of Abbreviations

A $\beta$	Amyloid $\beta$
AD	Alzheimer's Disease
ALS	Amyloid Lateral Sclerosis
AFM	Atomic Force Microscopy
AUC	Analytical Ultracentrifugation
$\beta$ 2m	$\beta$ 2-Microglobulin
C-terminal	Protein Region – Carboxylate End
CAA	Cerebral Amyloid Angiopathy
cC	Chicken Cystatin
CD	Circular Dichroism Spectroscopy
EDTA	Ethylenediaminetetraacetic Acid
EGCG	Epigallocatechin-Gallate
EM	Electron Microscopy
EPR	Electron Paramagnetic Resonance Spectroscopy
ESI-MS	Electrospray-Ionisation Mass Spectroscopy
FAP	Familial Amyloidotic Polyneuropathy
FTIR	Fourier Transform Infrared Spectroscopy
hCC	Human Cystatin C
H/D	Hydrogen/Deuterium Exchange
HSQC	Hetero-Nuclear Single Quantum Coherence NMR Spectroscopy
LP	Limited Proteolysis
MPL	Mass Per Unit Length
MS	Mass Spectroscopy
MWCO	Molecular Weight Cut-Off
N-terminal	Protein Region – Amide End
NMR	Nuclear Magnetic Resonance Spectroscopy
OD	Optical Density
PES	Polyethersulfone
PMSF	Phenylmethanesulfonyl Fluoride

PrP <sup>C</sup>	Prion Protein (Cellular)
RP-HPLC	Reverse-Phase High Pressure Liquid Chromatography
SDM	Site-Directed Mutagenesis
SDS-PAGE	Sodium Dodecyl Sulphate Polyacrylamide Gel Electrophoresis
SEC HPLC	Size Exclusion Chromatography High Pressure Liquid Chromatography
ssNMR	Solid State Nuclear Magnetic Resonance Spectroscopy
STEM	Scanning Transmission Electron Microscopy
TEM	Transmission Electron Microscopy
TFE	2,2,2, Trifluoroethanol
ThT	Thioflavin T
TTR	Transthyretin
UV	Ultra-Violet

## Chapter One: Introduction

The deposition of amyloid is linked to several major incurable diseases, such as Alzheimer's disease (AD) (Selkoe and Schenk, 2003), Huntington's disease (Perutz, 1999), Parkinson's disease (Lang and Lozano, 1998) and the prion diseases (Collinge, 2001, Prusiner, 1998). Alzheimer's disease is the most common cause of dementia, affecting 6% of people over the age of 65 in Western Europe (Burns and Iliffe, 2009), and costing the UK government alone £26 billion per annum (Alzheimer's Society, UK, 2014). As the world's population ages and these late-onset diseases become more prevalent, an understanding of the underlying mechanisms of amyloidogenesis, the process by which amyloid fibrils form, becomes increasingly important. The last 15 years have produced huge advances in the understanding of protein aggregation, have defined many of the structural properties of amyloid fibrils and explored how misfolded species can become deleterious to life.

In order to establish novel ways of targeting the process of amyloid formation for therapeutic purposes, either through small molecules or other factors, it is essential to understand the methods for modulating this process that are already found in nature. An increasing number of studies are emerging in which different amyloidogenic proteins perturb the assembly of others under physiological conditions (Li and Buxbaum, 2011, Li et al., 2013, Kinghorn et al., 2006, Chiou et al., 2009, Sastre et al., 2004, Lauren et al., 2009). Genetic links, co-localisation and physiological responses in the form of changes in expression levels are further evidence for the multiple layers of *in vivo* regulation of these processes. As we search for a cure, the purpose of this thesis is to study the natural regulation of amyloid  $\beta$  aggregation by another amyloidogenic protein, cystatin C (hCC).

### 1.1. Amyloid

Amyloids are long unbranched fibrils with a diameter of 4-20 nm and a length stretching to several microns (Fandrich, 2012, Kodali and Wetzel, 2007). They are composed of a single protein type and, remarkably, have been shown to exhibit a common cross- $\beta$  fold consisting of an organised core of  $\beta$ -strands that run perpendicular to the fibril axis (Figure 1.1) (Blake and Serpell, 1996, Sunde et al., 1997). Given the variety of different folds that amyloidogenic proteins exhibit in their native states (all  $\alpha$ , all  $\beta$ ,  $\alpha/\beta$  and unstructured), the mechanism of the formation of amyloids is an

aggregation reaction according to the definition of Cleland *et al.* (1993), where unfolding of the protein chain is a pre-requisite to assembly:

Self-association – a reversible process involving the interactions of two or more native protein molecules (with reversible precipitation of the protein as a possible consequence)

Aggregation – interaction of two or more denatured protein molecules (which often leads to practically irreversible precipitation)

Ohnishi and Takano (2004) highlight an additional level of complexity suggesting that the precise ordering of amyloids compared to amorphous aggregates calls for a separate definition that still recognises the possible cross-overs between pathways to amyloids and less ordered aggregates.

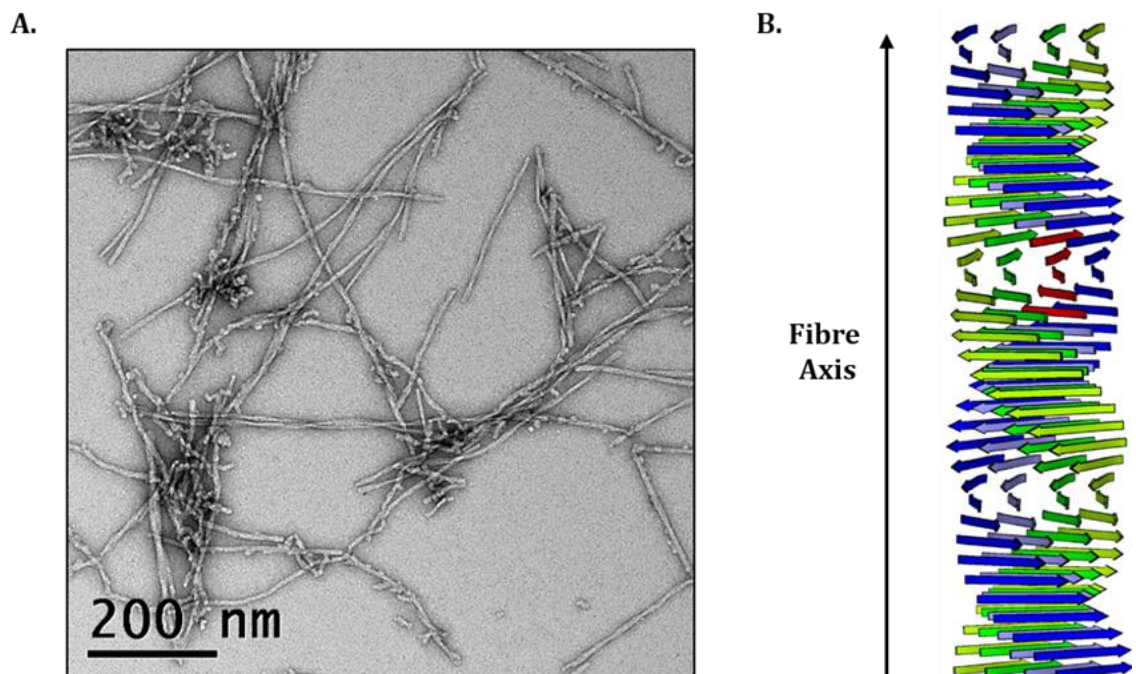


**Figure 1.1. Amyloid Fibril Structure**

*Electron micrograph (A) of negatively stained  $A\beta_{1-42}$  amyloid fibrils. Model of the cross- $\beta$  fibril structure (B) consisting of  $\beta$ -strands running perpendicular to the fibril axis, with inter-strand hydrogen bonds in the direction of the axis. Adapted by Prof. Peter Artymiuk from (Sunde *et al.*, 1997) with permission from Elsevier.*

### 1.1.1. The Importance of Protein Folding

A greater understanding of the mechanism of fibril formation can be gained from an understanding of protein folding, since amyloid formation necessarily involves the unfolding then refolding of much of the protein chain en bloc. The most popular concept to describe protein folding is the free energy landscape (Figure 1.2) (Dill and Chan, 1997), where funnel-shaped energy profiles defined by kinetics and thermodynamics depict the folding properties of proteins (Ohnishi and Takano, 2004). The native state is normally situated at the lowest minimum of the funnel (Figure 1.2), thus suggesting this is the most stable configuration.

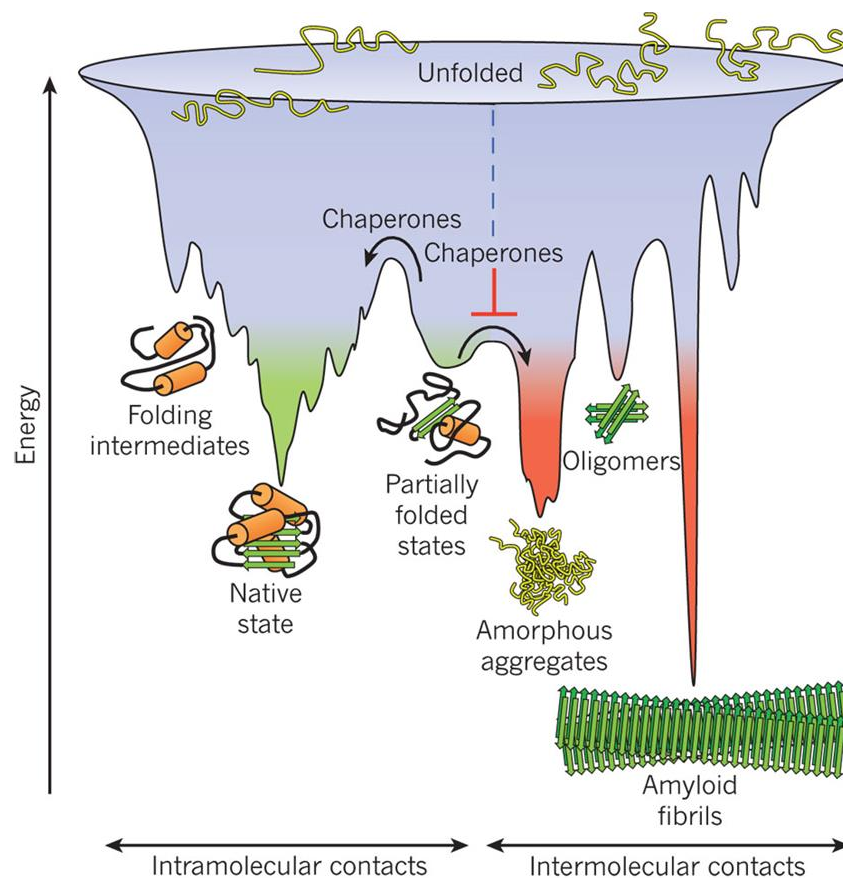


**Figure 1.2. Free Energy Surface for Protein Folding and Amyloid Formation**

*Scheme depicting the funnel-shaped landscape that proteins explore as they move towards the native state (green) through the formation of intramolecular contacts. The uneven nature of this landscape leads to the accumulation of kinetically trapped conformations that need to overcome free energy barriers in order to reach a favourable downhill path. These steps are often assisted by chaperones in vivo. Several molecules folding simultaneously in the same compartment can lead to the free-energy surface of folding overlapping with that of intermolecular aggregation, resulting in the formation of amyloid fibrils, oligomers or amorphous aggregates (red). Image taken from (Hartl et al., 2011) with permission from Macmillan Publishers Ltd.*

Proteins explore an uneven landscape as they move towards the native state, leading to the accumulation of kinetically trapped conformations that are required to overcome free energy barriers in order to reach a favourable downhill path (Hartl et al., 2011). *In vivo* this process is often assisted by chaperones. The folding of several molecules simultaneously in the same compartment can lead to the free-energy surface of folding overlapping with that of intermolecular aggregation, resulting in the formation of amyloid fibrils, oligomers or amorphous aggregates. Current work reveals that, whereas under physiological conditions proteins readily find their native state as the energy barrier separating the folded state from the unfolded state is easily overcome, the formation of amyloid is separated by a significant free energy barrier.

The propensity of polypeptide chains to form fibrils appears to be a general property (Chiti and Dobson, 2009) and appears to be almost independent of amino acid sequence or composition (Tycko 2011). For proteins that fold, the aggregation reaction leading to fibrillar amyloids competes with functional folding and constitutes an alternative pathway of assembly. The observation that amyloid may be a universal feature of a protein's energy landscape led to the suggestion that amyloid formation may be a fundamentally different process to protein folding, the first dictated by non-specific backbone interactions, the latter specific to the protein's sequence (Fandrich and Dobson, 2002).

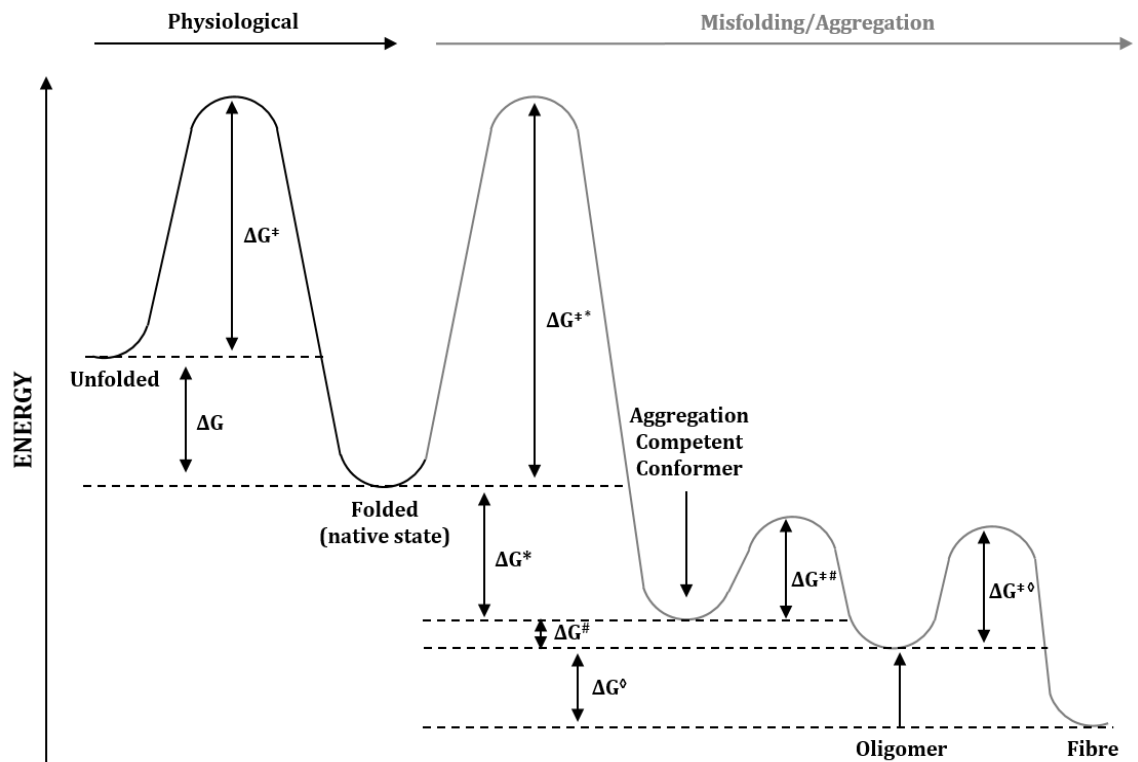


**Figure 1.3. Thermodynamics of Folding**

*Under physiological conditions proteins readily find their native state as  $\Delta G^\ddagger$ , which governs the rate of conversion, is easily overcome and the folded state is more stable than the unfolded ( $\Delta G$  dictates relative populations of folded and unfolded). In misfolding conditions, aggregated states may be energetically favoured over natively folded states.  $\Delta G^{\ddagger*}$  defines the rate of conversion to aggregation-competent forms, while  $\Delta G^*$  determines relative populations;  $\Delta G^{\ddagger\#}$  dictates the rate of formation of oligomeric species and  $\Delta G^\#$  indicates the relative populations;  $\Delta G^{\ddagger\circ}$  is the rate of conversion to amyloid fibril, with  $\Delta G^\circ$  defining the amount of fibril formed. Figure adapted from (Cohen and Kelly, 2003) with permission from Macmillan Publishers Ltd.*

Structural work reveals that the general framework of the mature fibril is defined by main chain interactions; however, at the same time, interactions between the amino acid side chains are clearly responsible for stabilisation of the fibril and fibril variations (Ma and Nussinov, 2006, Makin *et al.*, 2005, Zanuy *et al.*, 2004, Tjernberg *et al.*, 2002). It is likely therefore that the key mechanisms of amyloid formation bear some resemblance to those of protein folding, within a more restricted secondary structural space but expanded to include the possibility of extensive inter-chain bonding prior to the adoption of a stable tertiary fold. The increased free energy barrier required to form amyloid relative to the folded state of the protein can be explained using concepts based on the nucleation polymerisation model proposed by Jarrett & Lansbury (1993). They state that initial assembly steps are energetically unfavourable and a critical nucleus size

needs to be established before elongation becomes a favourable process. Energetically the entropic cost of association is initially too great compared with any energy gains made from the formation of intermolecular bonds and so the nucleus is rarely populated (Chothia and Janin, 1975). Once the nucleus is large enough, there are more sites for monomer addition and the numerous contacts possible render the process energetically favourable.

### 1.1.2. Conversion to an Amyloid-forming Competent State

In order to understand the mechanism of amyloid formation, it is important to understand the mechanism of conformational conversion. It has been demonstrated that under destabilising conditions proteins not involved with amyloid diseases can form fibrils (Fandrich et al., 2001), leading to the hypothesis that proteins may share the potential for amyloid deposition and that this is not limited to a few disease-associated proteins (Guijarro et al., 1998). As mentioned earlier, the formation of amyloid fibrils is similar to amorphous aggregation and requires at least partial unfolding. Amorphous aggregation is thought to be driven by hydrophobic interactions between exposed protein interiors (Ohnishi and Takano, 2004) but, in addition, must be stabilised by more specific interactions which occur as a result of self-complementary sections of the polypeptide chains. The fully folded state of the protein is therefore not converted directly into amyloid fibrils. The absence or destabilisation of side chain interactions, for example through mutation or changes in the environment can lead to an increase in partially folded or unfolded proteins, and as a result increases exposure of hydrophobic residues and the normally buried main chain to the solvent (Dobson, 2003). A key driving force in amyloid formation is the favourable burial of exposed hydrophobic groups and the need for partially unfolded proteins to find an alternative low energy conformation that is kinetically accessible under a given set of conditions (Chiti and Dobson, 2006).

### 1.1.3. Mechanism of Fibril Formation

Amyloidogenic proteins differ in both native fold and primary sequence, however this diverse group of proteins are thought to form amyloid through a similar mechanism (Glabe, 2006). Amyloid formation has been shown to have three stages with typical sigmoidal kinetics (Figure 1.4A). An initial lag phase is followed by an exponential elongation phase before the reaction reaches an equilibrium plateau. The protein species that are present during both the lag and elongation phases are not clearly defined, and these may vary in different systems (Figure 1.4B). Before the formation of amyloid fibrils, small soluble oligomeric structures are formed, which can differ in size, morphology and toxicity (Kayed et al., 2009). Coalescence of the oligomers is thought to form protofibrils, which are short beaded fibrils. Finally, either through a conformational change or through association of the protofibrils, mature fibrils are formed.

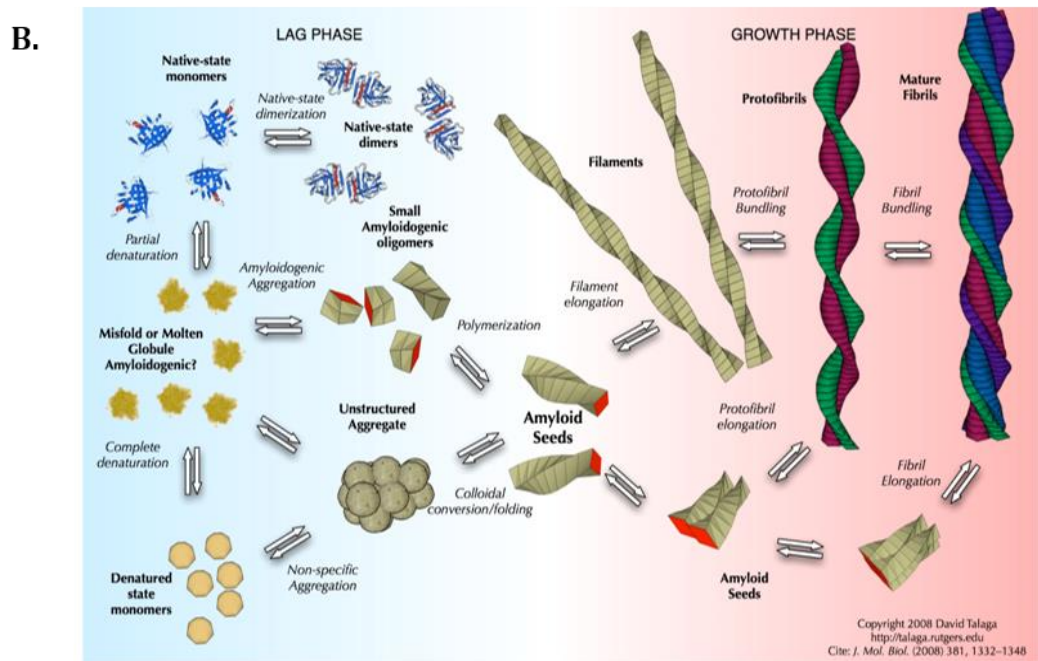
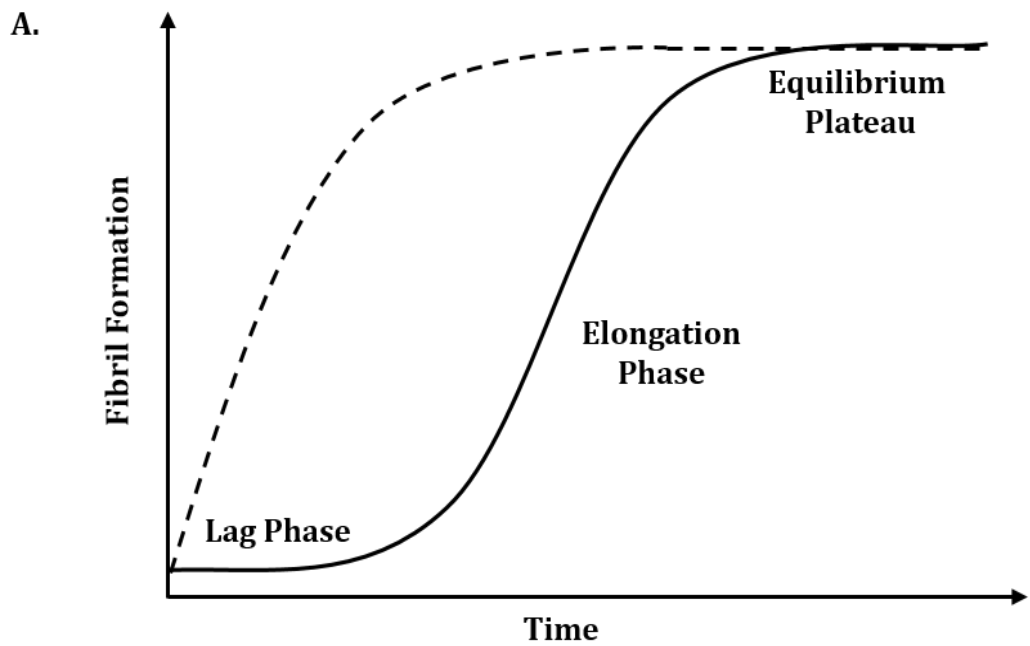


**Figure 1.4. Fibrillisation Reaction and Pathway**

Characteristic kinetic profile of amyloid fibril formation (A), illustrating the lag phase, growth phase and thermodynamic equilibrium. At high protein concentrations, or in favourable conditions, nucleation is very rapid resulting in no observable lag phase (dashed line); this phenomenon is also seen when the reaction is seeded (Jarrett and Lansbury, 1993). Nucleation may occur but is no longer sigmoidal due to the presence of pre-formed nucleation sites. Fibril formation (B) is defined by the aggregation of monomeric species to form small amyloid seeds (lag phase), which then extend to form stable protofibrils (growth phase). Protofibrils then bundle together to form the mature fibril. Image taken from Giurleo et al. (2008) with permission.

### 1.1.3.1. Kinetic Models

There are four prominent models of amyloid formation, the latest of which, nucleated conformational conversion, combines elements of the other three (Figure 1.5) (Kelly, 2000, Serio et al., 2000). The first is described as templated assembly in which a pre-assembled amyloidogenic (A-state) nucleus binds with a soluble amyloid-incompetent (S-state) peptide, causing a rate-determining conformational change in the latter and allowing addition of the peptide to the growing amyloid fibril (Griffith, 1967). This model predicts that the lag phase will be directly affected by the soluble protein concentration, but there will be no change in the rate of fibril elongation, and that addition of a seed should cause a reduction in lag phase. The second mechanism is monomer-directed conversion, where a monomeric peptide will undergo conversion into an amyloid-competent species (Prusiner, 1982). This species will propagate the conversion of further monomeric peptides which initiates polymerisation. This model will not be affected by the addition of a seed, as the rate-limiting step occurs with the conversion of the soluble protein. The third mechanism is nucleated polymerisation (Jarrett and Lansbury, 1993). In this case soluble amyloid-competent species associate to form a nucleus which will propagate fibril formation through addition of assembly competent monomers to the nucleus. These amyloid-competent species are in equilibrium with amyloid-incompetent protein, with the equilibrium heavily favouring the incompetent species. Therefore the rate-limiting step is the association of amyloid-competent species to form a nucleus. This model predicts that the lag time should decrease, and the rate of fibril elongation increase, with an increase in soluble protein concentration. The addition of a seed will remove the lag time of the reaction. The nucleation model covers a number of well-defined processes, in addition to amyloid fibril formation, such as protein crystallisation, actin polymerisation and microtubule association (Jarrett and Lansbury, 1993). The final mechanism is nucleated conformational conversion (Serio et al., 2000) where it is proposed that structurally dynamic oligomers undergo conformational rearrangements to induce the formation of nuclei. These oligomers lack a defined quaternary structure, but it is suggested that they could have a micelle-like structure. Nuclei will then interact with a structurally flexible oligomer with a distribution of subunits, causing the addition of this subunit group onto the end of the fibril.

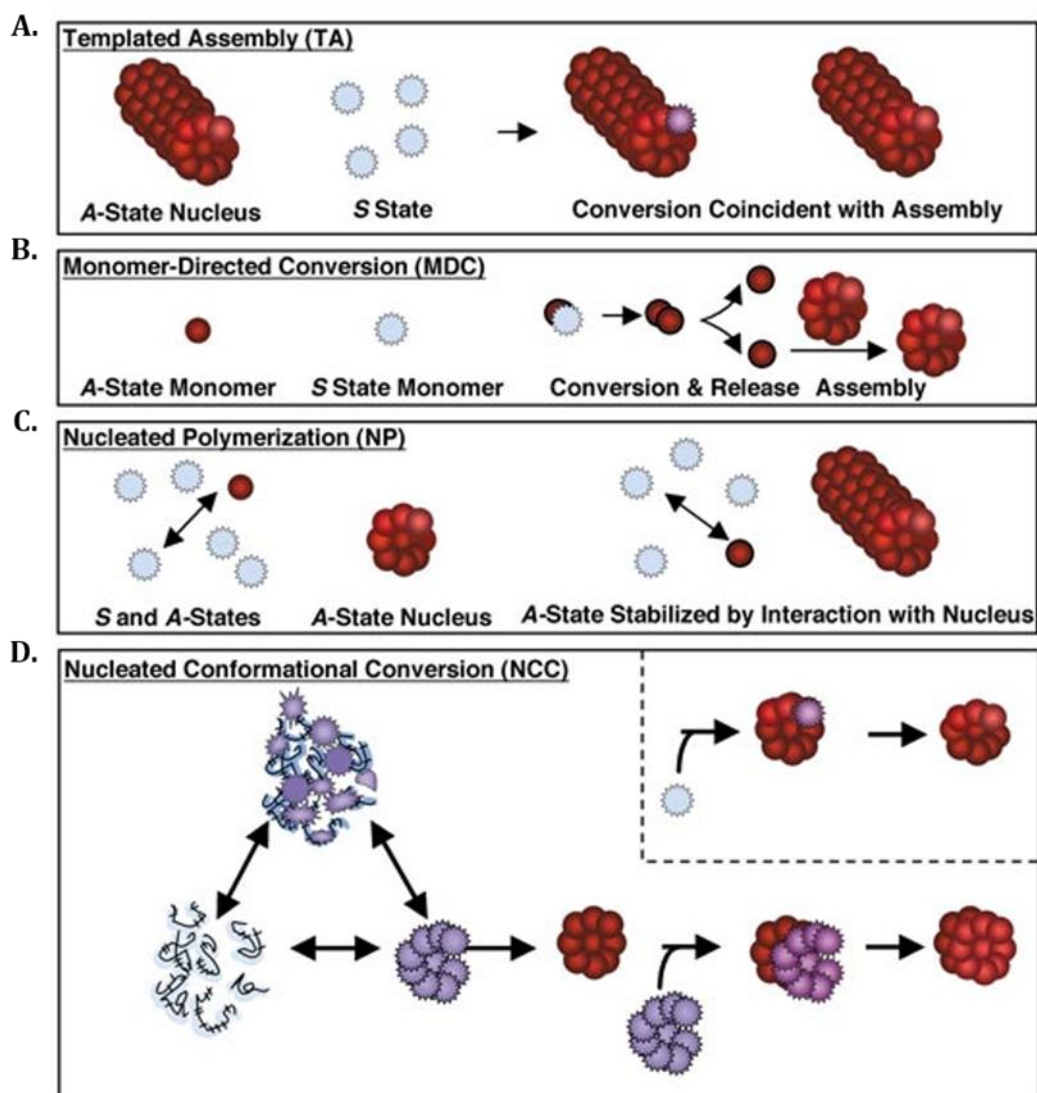


**Figure 1.5. Models of Fibril Formation**

*Proposed models for amyloidogenic peptide conversion into amyloid fibrils. Jagged circles represent soluble (S-state) protein, smooth circles represent amyloid-competent (A-state) protein which takes a similar structure to that adopted in amyloid fibrils and open circles represent potential conformational heterogeneity in A) templated assembly, B) monomer-directed conversion, C) nucleated polymerisation and D) nucleated conformational conversion. Figure taken from (Kelly, 2000) with permission from Macmillan Publishers Ltd.*

A new layer of complexity to the concentration dependence of fibril formation has been added with the discovery of secondary processes that can be involved in nuclei formation, making the nucleation process highly dependent on the aggregates formed during the assembly reaction (Buell et al., 2014). These secondary processes include fragmentation and secondary nucleation. Upon reaching a critical concentration, existing fibrillar aggregates act as a surface to catalyse nuclei formation, leading to

rapid proliferation of toxic oligomeric species and amyloid fibrils in a secondary nucleation event (Cohen et al., 2013). Fragmentation of amyloid fibrils increases the number of extension sites available for the attachment of soluble protein molecules, again leading to rapid proliferation of fibrils (Xue et al., 2009a, Xue and Radford, 2013). In some cases this can lead to a negative concentration dependence on fibril assembly, as low concentrations will favour fragmentation and therefore increase the concentration of seed (Xue et al., 2009a, Bernacki and Murphy, 2009).

It is difficult to find a consensus or a general model for the intrinsically complex and heterogeneous mechanism of assembly. Nucleation remains a key feature of most models and seeding is a defined property of most amyloids. However, only with the most complete data sets which include data, not only on monomer disappearance, but also fibril concentration and intermediate species quantification, will it be possible to clearly differentiate various mechanisms as discussed by Bernacki and Murphy (2009).

#### 1.1.4. High Molecular Weight Oligomers

Soluble oligomeric intermediates form both on and off-pathway to amyloid fibril production and, using the A $\beta$  peptide as an example, can range from dimers through small 3-10mers up to large macromolecular structures several mega-Daltons in size (Haas and Selkoe, 2007). These intermediates are often transient heterogeneous structures, making them incredibly difficult to study. It is proposed that soluble oligomeric species could be the pathogenic agents, making the study of these species highly relevant (Lansbury, 1999). Amyloid intermediates can be grouped into different classes including protofibrils, annular aggregates and oligomers (Fandrich, 2012). Within these classes there is thought to be a plethora of different states and subspecies, making classification of diverse intermediates complicated (Figure 1.6).

Most structurally similar to the mature amyloid fibril, protofibrillar intermediates are thought to represent a late stage in the amyloid pathway. Whilst lacking the periodic symmetry and very high order of mature fibrils, protofibrils are shorter, thinner and often curved (Walsh et al., 1999, Goldsbury et al., 2000). Their interaction with the amyloid staining dyes Congo red and thioflavin T is weaker than for mature fibrils, however a signal can still be monitored. A $\beta$  protofibrils stabilised using a protofibril specific antibody (B10AP) have been shown to have high levels of regular  $\beta$ -sheet structure, which were revealed by ssNMR to encompass two  $\beta$ -strands stretching from residues 16-22 and 30-36 (Scheidt et al., 2011). These regions are shorter than those

present in the mature fibrils but consistent with protofibrils representing a precursor to the fibrils.

Annular aggregates have a donut-like shape enclosing a central channel, which is thought to be filled with water (Lashuel et al., 2002). Several amyloidogenic proteins, such as variants of  $\alpha$ -synuclein and A $\beta$ , have been reported to form ring-like aggregates (Caughey and Lansbury, 2003, Lashuel et al., 2002). These samples are often highly heterogeneous, making it difficult to examine their detailed molecular structure; however their similarity to pore forming toxins has led to the proposal that these species can pierce the cell, disrupting the membrane integrity and causing cell death (Fandrich, 2012, Caughey and Lansbury, 2003, Butterfield and Lashuel, 2010).

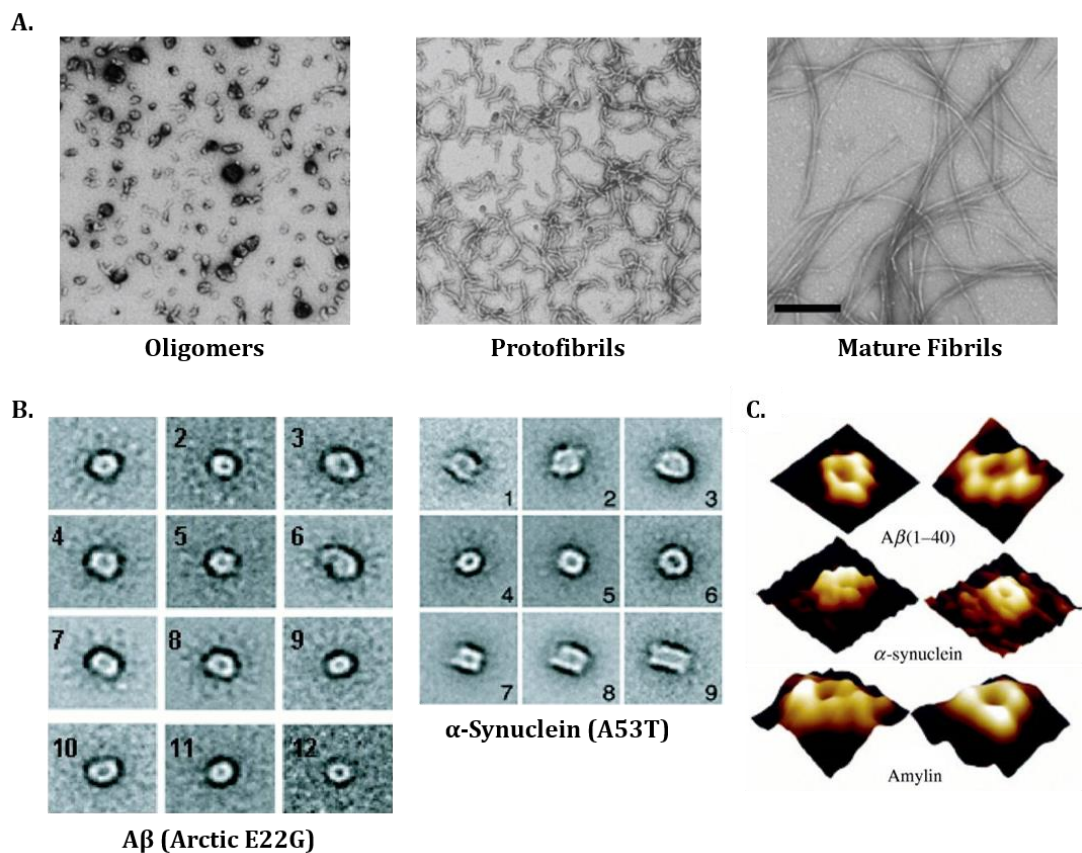


**Figure 1.6. Large Molecular Weight Oligomers**

Images representing **A)** the different forms of amyloid- $\beta$  typically described as spherical oligomers, protofibrils and, for comparison, mature fibrils taken from (Fandrich, 2012) with permission from Elsevier. The scale-bar represents 200 nm. **B)** EM images of annular, water-filled aggregates of A $\beta$  and  $\alpha$ -synuclein, and **C)** the same structures and amylin (IAPP) seen by AFM. Images taken from (Lashuel and Lansbury, 2006).

Representing early kinetic intermediates in the amyloid formation pathway, oligomeric species occur as metastable states which undergo a conversion into conformations that are more thermodynamically favourable (Fandrich, 2012). The transient nature of these structures causes difficulty in obtaining detailed structural information, and makes it necessary to devise methods of trapping the intermediates, such as ligand binding or lyophilisation (Scheidt et al., 2011, Chimon et al., 2007). Although these trapped stable states may not play an actual role in the kinetic process of fibril assembly, they can still be considered intermediates in this process as they may represent transitional properties not seen in other conformers and could provide key information about other kinetic intermediates (Fandrich, 2012).

It is well established that amyloid fibrils have a characteristic cross- $\beta$  structure; however a similar generic conformation (a structural element common to *all*) has not yet been discovered for oligomers (Fandrich, 2012). As both  $\beta$ -sheet and random coil conformations have been identified in different oligomeric species, it is thought characteristic secondary structure can vary considerably (Sandberg et al., 2010, Habicht et al., 2007, Campioni et al., 2010). Nonetheless oligomer-specific antibodies such as A11 interact with oligomer preparations from different polypeptides (Kayed et al., 2003) and these preparations produce similar effects in cell metabolic assays (Bucciantini et al., 2002), suggesting that key structural commonalities do exist. Oligomers are highly polymorphic, with differences in structure occurring within the same sample, or from different preparation protocols (Glabe, 2008). Due to their dynamic, transient nature, oligomeric assemblies often aggregate further and progress to more mature species (Fandrich, 2012).

#### 1.1.5. Fibril Structure

Despite there being very little structural and sequence similarity between amyloidogenic proteins involved in disease, the mature fibrils formed have a similar structure as well as similar toxicity mechanisms (Makin and Serpell, 2005). In order to understand better the implications of structural and mechanistic studies of amyloids, it is useful to review common biophysical methods for their characterisation.

Amyloid fibrils are large, heterogeneous and insoluble, making it difficult to obtain structural information from conventional high-resolution experimental techniques such as solution NMR and X-ray crystallography (Serpell, 2000). However, biophysical techniques such as solid-state NMR (ssNMR) and X-ray fibre diffraction can be used to

great effect, in conjunction with microscopy techniques (electron microscopy and atomic force microscopy), limited proteolysis, hydrogen-deuterium (H/D) exchange and electron paramagnetic resonance spectroscopy (EPR) to develop structural constraints leading to refinement of structural models. Although atomic resolution models for fibrils formed from natively unfolded peptides such as A $\beta$  and the folded protein Het-s have been determined, there is still a way to go before it is possible to boast a similar understanding of other systems.

#### *1.1.5.1. Dye-binding Assays*

Identification of amyloid is aided through characteristic properties displayed upon binding to certain dyes, notably Congo red and thioflavin T (ThT). A key diagnostic tool, fibrils turn a characteristic pink-orange colour under a light microscope and will display green birefringence (double refraction) when viewed under cross-polarised light upon specific binding to Congo red (Sipe and Cohen, 2000). When Congo red binds amyloid fibrils, the associated birefringence is an indication of an ordered sub-microscopic structure (Glennner et al., 1972). Amyloid fibrils also bind specifically to the benzothiazole dye ThT, leading to an enhanced fluorescence and a shift in emission from 445 nm to 482 nm. Monitoring this change in fluorescence allows aggregation to be followed in solution over long periods of time. It is suggested that these changes arise from molecular alignment of the dye molecules as they bind to a specific epitope displayed by the fibrils. It is thought that binding is specific and associative, either through extended  $\beta$ -sheet or intercalation (Wolfe et al., 2010).

#### *1.1.5.2. X-Ray Fibre Diffraction*

X-ray fibre diffraction is a technique that has provided many key findings about the structure of amyloid fibrils. A characteristic feature of fibrils is their X-ray fibre diffraction pattern (Figure 1.7) which indicates an ordered, repeating  $\beta$ -sheet conformation running perpendicular to the fibril axis, known as a cross- $\beta$  structure (Blake and Serpell, 1996). The hydrogen bonding distance between  $\beta$ -strands perpendicular to the fibril axis is derived from the strong reflection at 4.7 Å which dominates the diffraction patterns in the meridian direction. 10 Å equatorial reflections are indicative of the distance between the  $\beta$ -sheets, allowing a crucial structural model to be established. Moreover, the helical twist of the  $\beta$ -sheets along the fibril axis is illustrated by higher order reflections in the meridian direction (Sunde et al., 1997). Similar high-resolution diffraction patterns confirmed that, regardless of the precursor

protein, amyloid fibrils share a common protofilament sub-structure. The simplicity of this pattern not only allows the proposal of simple structural models but can also be used powerfully to discount other more complex models which would imply the presence of further reflections (Jahn et al., 2010).

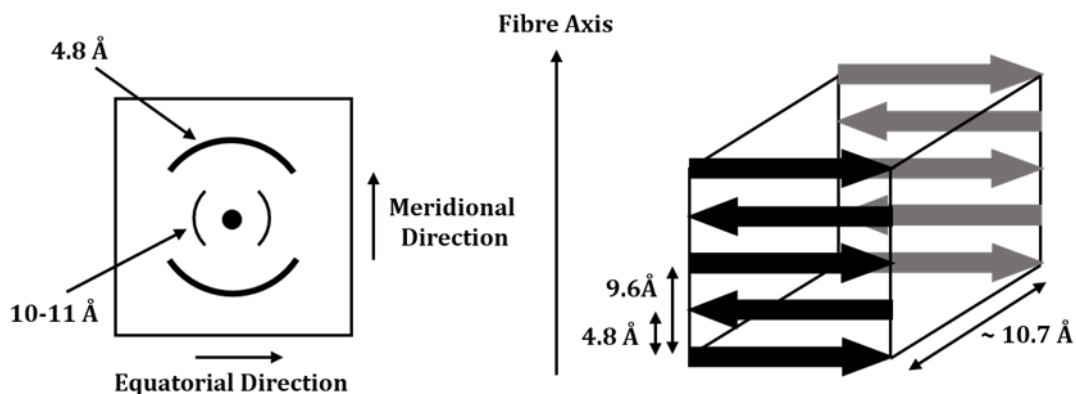


**Figure 1.7. Amyloid Fibril X-ray Diffraction Pattern and Corresponding Structure**

*X-ray fibre diffraction pattern from amyloid fibrils (left), consistent with the characteristic cross- $\beta$  structure. The strong 4.8 Å reflection in the meridional direction corresponds to the distance between  $\beta$ -strands (right) and the weaker 10-11 Å reflection in the equatorial direction indicates the inter-sheet distance of  $\sim 10.7$  Å. Figure taken from (Serpell, 2000) with permission from Elsevier.*

### 1.1.5.3. Microscopy Techniques

Electron microscopy showed early on that fibrils are straight and unbranching, with a diameter of 70-120 Å (Shiraham and Cohen, 1967), and consist of several protofibrils arranged parallel to each other. Transmission electron microscopy (TEM) and atomic force microscopy (AFM) are crucial techniques for not only identifying amyloid fibrils, but also providing information on the morphology and dimensions of both the fibrils and their intermediates. The formation of both oligomeric and fibrous structures can be followed by these microscopic techniques, and the development of real-time AFM methods could provide some exciting insights into the mechanism of fibrillisation.

Cryo-electron microscopy can be used to produce three-dimensional reconstructions of amyloid fibrils, by averaging multiple EM images of fibril cross-sections. Whilst this technique does not allow high-resolution structural detail to be determined, it is a useful tool to aid structural modelling as shown in Figure 1.8.

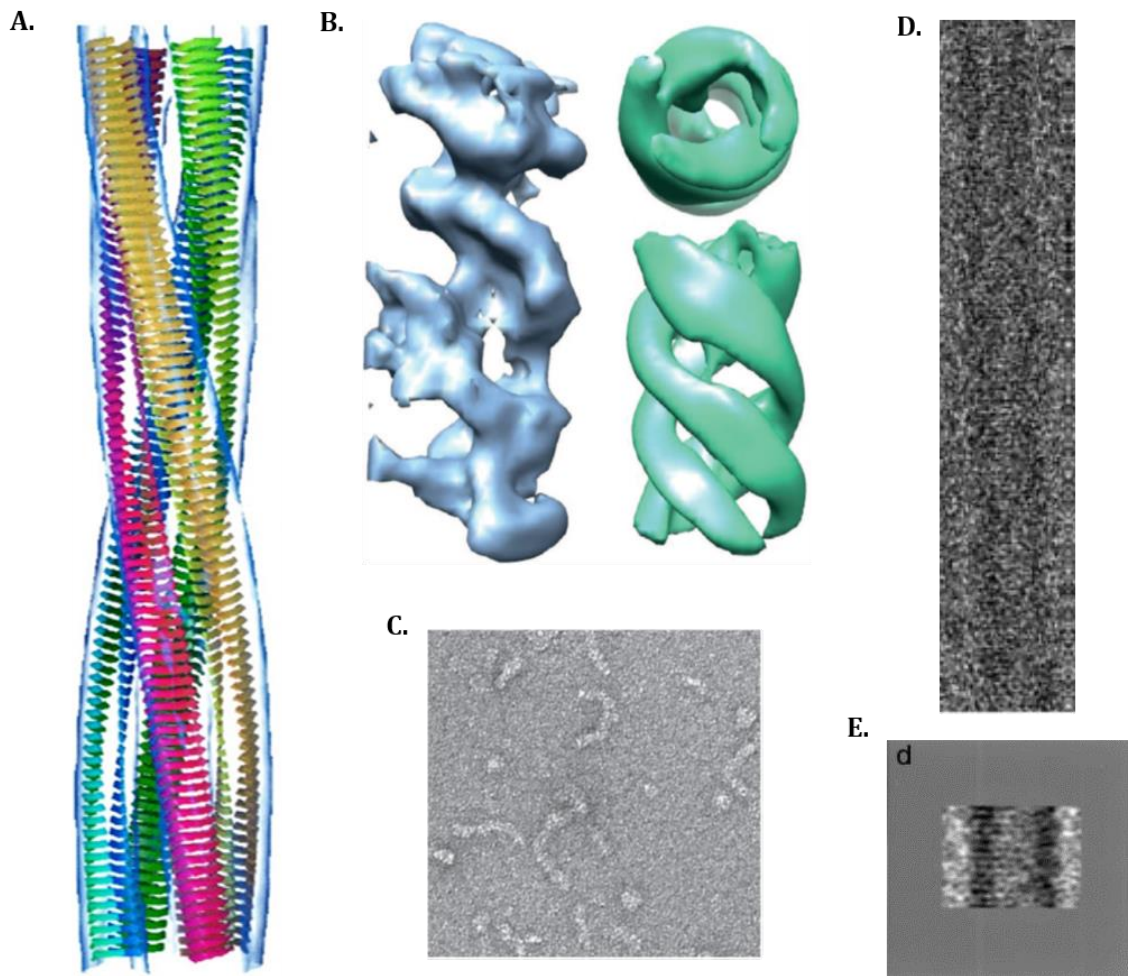


**Figure 1.8. Electron Microscopy of Amyloid**

*Model of insulin fibrils (A) based on cryo-electron microscopy images, taken from (Jimenez et al., 2002). Also shown are reconstructions (B) of prion-bound A $\beta$  oligomers and an original micrograph (C) of the sample. Taken from (Nicoll et al., 2013). Peptides from the central region of the A $\beta$  peptide (11-25) form fibrils where the secondary structure can be directly visualised by negative-stain TEM (D). A number of regions of these fibrils which were aligned then added together (E). Taken from Serpell & Smith (2000) with permission from Elsevier.*

Models determined this way include the SH3 domain (Jimenez et al., 1999), insulin (Jimenez et al., 2002) and  $\beta_2$ -microglobulin (White et al., 2009). Cryo-EM analysis provides evidence for the cross- $\beta$  model, as striations can be seen running across the fibril with a 4.7 Å repeat in fibrils formed from a central peptide fragment of A $\beta$  (A $\beta_{11-25}$ ) (Serpell and Smith, 2000). This visualisation also indicates that the  $\beta$ -strands are in direct register and running perpendicular to the fibril axis. More recently, a model of prion-bound oligomeric A $\beta$  structures termed “nanotubes” has been examined using negative stain electron microscopy and tomography techniques. This novel structure is triple helical in shape with a 7.8 nm repeat and a 10 nm diameter (Nicoll et al., 2013).

Microscopy is particularly useful when identifying common species within a mixture as the different structural families can be studied separately.

In all structural reconstructions, mass per unit length (MPL) measurements are used as a complementary measurement to model different densities of protein molecules into the observed framework. These measurements are made using a specialised scanning transmission electron microscope (STEM), giving a relatively precise indication of the mass per unit length of the fibril.

#### *1.1.5.4. Solid-State Nuclear Magnetic Resonance*

Solid-state NMR (ssNMR) has become one of the leading techniques for amyloid structure determination (Tycko, 2011) providing high-resolution information which is not available using other techniques. Complex and sophisticated, a variety of ssNMR experiments have been used to determine experimental constraints and consequently, in conjunction with techniques such as EM, X-ray diffraction and computational methods, full molecular structural models. A range of techniques have been devised which mean that essentially very similar experiments to those run in solution can be run on solid samples. The limiting factor is that the resolution of the spectra obtained is generally very poor. In order to tackle this problem, labelling techniques have been developed to reduce the number of peaks seen in each spectrum. The addition of different forms of labelled glycerol to growth media results in different patterns of isotopic labelling ( $^{15}\text{N}$  and  $^{13}\text{C}$ ) according to residue type. This allows assignment followed by measurements of inter-residue distances, which provide information on secondary, tertiary and quaternary structures as well as dynamic data.

#### *1.1.5.5. Limited Proteolysis*

In a similar fashion to hydrogen/deuterium exchange, limited proteolysis provides information on accessible regions of the amyloid fibril (Hubbard 1998). Regions with regular secondary structure will be protected from proteolytic activity whereas areas with high chain mobility will be highly susceptible, allowing the protected fibril core to be determined. Structural information has been obtained for amyloid fibrils from several systems including lysozyme (Frare et al., 2006), A $\beta$  (Kheterpal et al., 2001), HET-s (Balguerie et al., 2003),  $\beta_2$ -microglobulin (Myers et al., 2006) and cystatin B (Davis, 2013).

#### 1.1.5.6. Hydrogen/Deuterium Exchange

Quenched hydrogen/deuterium (H/D) exchange experiments can be used to determine protected regions of both single protein molecules and larger molecular weight structures such as amyloid fibrils. By observing the rate at which amide protons within the peptide backbone exchange with solvent deuterons (or vice versa) solvent accessible regions can be mapped, as the rate of exchange is dependent on the accessibility of the amide protons. Amides involved in stable hydrogen-bonding networks or incorporated in structured regions will be protected from the solvent, and therefore will have a slower rate of exchange than amides that are highly exposed which will exchange rapidly. Quenching the reaction after different exchange times by freezing, removal of the solvent by lyophilisation, then solubilisation in the non-exchanging solvent DMSO allows for the determination of protection patterns using NMR spectroscopy and/or mass spectrometry (Alexandrescu, 2001). Observation by NMR provides residue-specific information making this the more desirable method of analysis (Hoshino et al., 2002). However using mass spectrometry as a complementary approach can give useful information on the populations of partially and fully exchanged species and the homogeneity of the sample. H/D exchange has been used to provide dynamic information on the amyloid fibril, demonstrating that molecules can dissociate and re-associate with the main fibril (Sanchez et al., 2011, Carulla et al., 2005). The SH3 study suggested recycling of half of the molecules from an average fibril of 100 nm would occur within days (between 2 and 20 days).

#### 1.1.5.7. A $\beta$ Fibril Structure

Despite the problems of hydrophobicity and insolubility, the structure of the A $\beta$  peptide in solution has been extensively studied by NMR, CD and FTIR (Serpell, 2000). Differences in pH, concentration and incubation time all have significant effects on the structure. In organic solvents the peptide is often seen to form an  $\alpha$ -helical conformation, whereas in aqueous buffer the  $\beta$ -sheet is more prevalent (Shao et al., 1999, Coles et al., 1998, Sticht et al., 1995). This propensity to be helical is thought to reflect physiological preferences as A $\beta$  is produced at the membrane surface. Later, as the peptide diffuses away, a conformational switch is thought to be initiated by the N-terminal, as deprotonation of certain key residues causes destabilisation of the  $\alpha$ -helix (Zagorski and Barrow, 1992). Alternatively, the  $\alpha$ -helical form is postulated to associate

with others and form membrane penetrating pores leading to toxicity (Butterfield and Lashuel, 2010).

Excitingly, a molecular structural model has recently been published of A $\beta$ <sub>1-40</sub> fibrils seeded from Alzheimer's disease brain tissue (Figure 1.9), determined using data from ssNMR and EM (Lu et al., 2013). Unique structures were produced from two AD patients with different clinical histories, suggesting that structural variations could be responsible for variations within the disease. Samples taken from different areas of the brain produced similar structures in both cases; this observation is intriguing as polymorphism is an inherent property of formation of A $\beta$  fibrils. This could signify that fibrils may spread from a single nucleation site throughout the brain, or that different clearance mechanisms within patients promote different nucleation events. Unique assignments were obtained of all <sup>15</sup>N and <sup>13</sup>C chemical shifts with strong sharp signals, indicating that the entire peptide sequence is part of the ordered, relatively rigid, molecular structure. In conjunction with MPL data, a structure with a 3-fold symmetry was determined, similar to fibrils formed *in vitro* which have a twisted morphology (Paravastu et al., 2008, Goldsbury et al., 2005). Other *in vitro* fibrils have exhibited 2-fold symmetry, illustrating how different conditions can lead to different structures (Meinhardt et al., 2009, Bertini et al., 2011, Petkova et al., 2006, Zhang et al., 2009). Nearly all A $\beta$  fibril structures have shown a parallel in-register intermolecular alignment, however in one instance, a mutated form of A $\beta$ <sub>1-40</sub> (D23N), which leads to a familial form of cerebral amyloid angiopathy (CAA), has been shown to adopt an anti-parallel alignment with a radically different conformation (Tycko et al., 2009). It remains to be seen whether this is a hallmark of CAA.

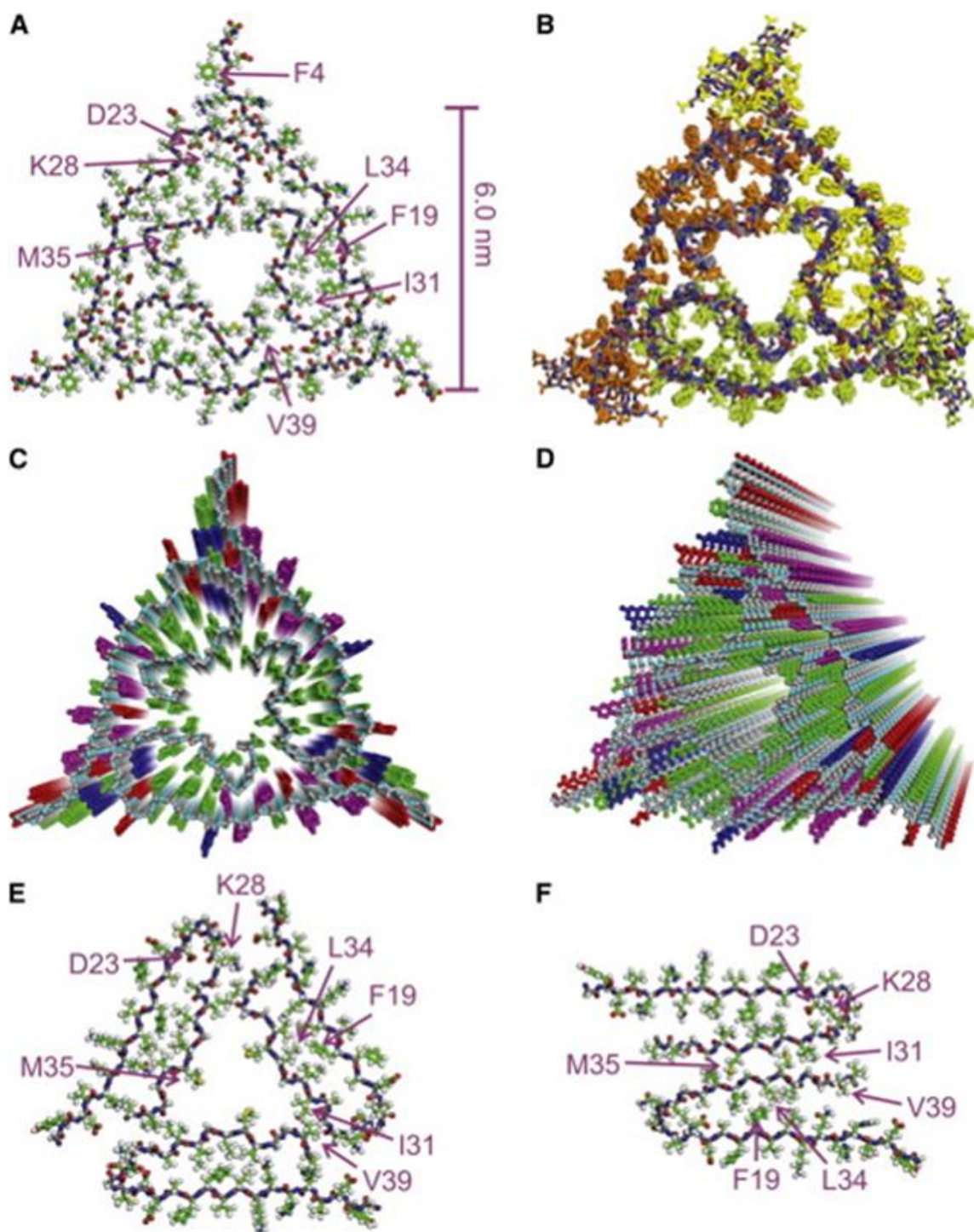


**Figure 1.9. A $\beta$  Fibril Structure Model**

*In A-D are different visualisations of the structure of an A $\beta$  amyloid seeded from material taken from different regions of the brain of a patient with Alzheimer's disease. Although the structure obtained is the same across the brain, these structures differ from structures obtained from fibrils grown in vitro. These latter structures are shown in E and F. Image taken from (Lu et al, 2013) with permission.*

#### 1.1.5.8. A $\beta$ Fibril Formation

There are numerous theories for what induces the structural transformation of the A $\beta$  peptide into amyloid. Early literature suggested that the C-terminal region of the A $\beta$  peptide could be crucial for *in vivo* fibril formation (Jarrett et al., 1993). This region of the peptide is part of the putative transmembrane region of APP, since the C-terminal sequence contains 14 consecutive hydrophobic residues, with a striking predominance of branched residues valine and isoleucine (Jarrett and Lansbury 1993). In a manner similar to that of silk protein sequences (which contain the consensus sequence (GAGS)<sub>n</sub>) there is a regular occurrence of glycine at every fourth position. The conformational flexibility of this residue, which enables it to explore new regions of the Ramachandran plot, may promote more rapid, low energy switching. The identification of a precise sequence involved in a nucleation event is assumed to be a requirement in a process which is demonstrably sequence-specific (Jarrett and Lansbury 1993).

A $\beta$  forms amyloid fibrils in a concentration-dependent manner consistent with the nucleation polymerisation mechanism (Kelly, 2000, Jarrett and Lansbury, 1993). Factors such as temperature, solvent and pH have a significant effect on the structure of A $\beta$  fibrils and the rate of A $\beta$  fibril formation is highly pH dependent (Barrow and Zagorski, 1991). Normal blood pH is 7.3, however as this becomes more acidic the propensity of A $\beta$  to form amyloid increases, with the maximum rate of fibril formation occurring at pH 5.5. This is close to that found in some intracellular organelles such as late endosomes or lysosomes, and there is evidence that A $\beta$  species can accumulate in these organelles (Zhi et al., 2011, Koo & Squazzo, 1994, Haass et al., 1992).

A further theory, which can be combined with the endosomal location of the peptide, is as follows. As expression levels of A $\beta$  remain constant in sporadic AD, it is proposed that membrane interactions are responsible for increased A $\beta$  aggregation (Yamamoto et al., 2004). In the presence of either detergent or ganglioside micelles soluble A $\beta$  will spontaneously form fibrils. It is thought that initiation of fibril formation occurs at the interface between the micelle surface and the aqueous environment. The *in vivo* binding of the protein at the surface causes partial unfolding and allows fibril formation to commence. Gangliosides, such as GM1, are found in lipid rafts in neuron membranes within the brain (Matsuzaki, 2007), and it is suggested that GM1-A $\beta$  may act as a seed for A $\beta$  aggregation. Cholesterol strengthens the interaction between these two species, as well as increasing the formation of amyloidogenic A $\beta$  peptides.

#### 1.1.5.9. A $\beta$ Oligomers

As well as readily forming amyloid fibrils, A $\beta$  peptides aggregate to form a diverse range of oligomeric species. It is thought that these intermediates are responsible for cytotoxicity in AD. Soluble A $\beta$  oligomers, formed within specific intracellular vesicles and secreted from the cell, block hippocampal long-term potentiation at nanomolar concentrations (Walsh et al., 2002), as well as impairing rodent spatial memory (Lesne et al., 2006) and causing dendritic spine retraction from pyramidal cells (Shankar et al., 2007). The number of different properties attributed to A $\beta$  oligomers, and the lack of standard protocols for the preparation of these species, means that establishing common ground across different studies is hindered. A scheme is shown in Figure 1.10 which describes the range of species reported as presented in a review by Benilova et al. (2012).

As discussed previously, A $\beta$  oligomers as well as the fibrils, benefit from some of the more advanced structural studies carried out on amyloidogenic proteins. The secondary structure of A $\beta$  protofibrils stabilised by a fibril-specific antibody (B10AP) was recently resolved by ssNMR by Scheidt et al. (2011). Assignment was complete and chemical shifts obtained were consistent with the presence of two  $\beta$ -strands, encompassing residues 16-22 and 30-36. The remaining N-terminal and central region remain structured but not in a regular  $\beta$ -sheet conformer. The predicted  $\phi/\psi$  angles for the peptide bonds indicated a low twist sheet structure. The relevance of this work to the many different forms of A $\beta$  oligomers documented will reveal itself in time.



the amyloid proteins and have beneficial effects on a range of amyloidogenic proteins. A popular benchmark is epigallocatechin gallate (EGCG).

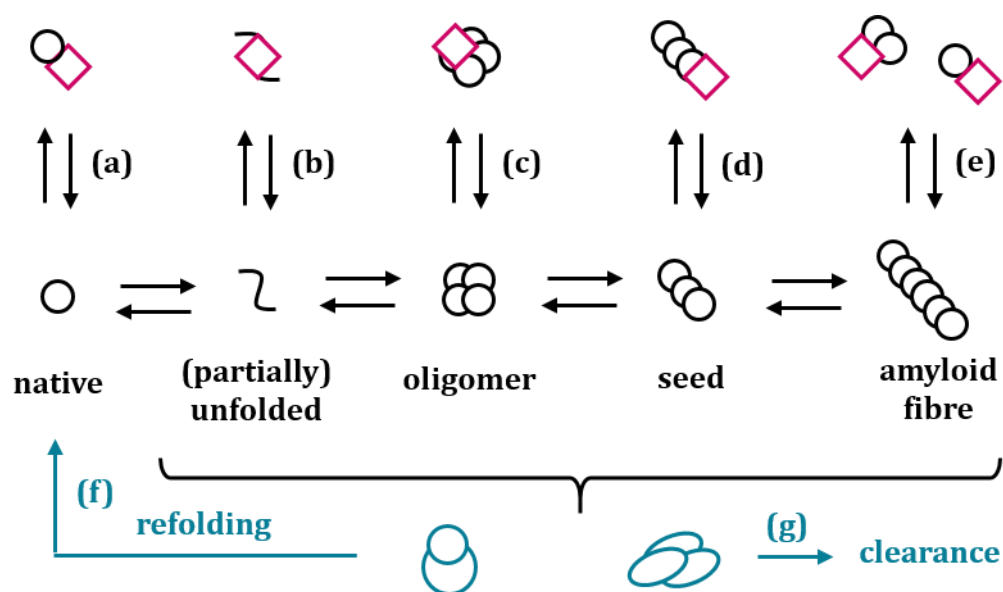


**Figure 1.11. Possible Drug Targets for Amyloid Disease**

The amyloid assembly reaction is shown in black. A pink (diamond-shaped) drug molecule is shown to be interacting with a number of possible targets labelled (a) through (e). Alternative mechanisms would be to enhance clearance (g) or correct refolding (f) of the amyloidogenic protein. Image adapted from (Hard and Lendl, 2012) with permission from Elsevier.

### 1.1.7. Natural regulation of amyloid formation *in vivo*

Amyloid is predominantly associated with pathological conditions, however there are several inherent mechanisms present to prevent its formation. Proteins have the fundamental ability to form amyloid due to the simple backbone interactions present in  $\beta$ -sheets; however in most cases nature prevents this by shielding the amyloid-prone regions. Self-complementary sections are rarely found on the protein surface, suggesting that such segments are prevented from interacting with each other through evolved chaperoning effects (Goldschmidt et al., 2010). Proteins are designed to prevent  $\beta$ -sheets from propagating by protecting their free edge strands through formation of  $\beta$ -barrels or by covering the strand with structural loops (Richardson and Richardson, 2002). In other cases the edge strand will be short or irregular, again making it unsuitable for further propagation. This is an example of negative design, where the overall structure is not improved by these additions but rather they are present to prevent an undesirable alternative.

Yet amyloid is not always damaging. Amyloid fibrils have several unique physical and mechanical properties which have been harnessed by lower organisms for structural purposes (Fowler et al., 2007). Extracellular amyloid (curli) and chaplins modulate development of aerial structures and biofilm formation in bacteria, and curli are also involved in host invasion and pathogenesis (Barnhart and Chapman, 2006, Chapman et al., 2002). Prions such as HET-s, URE2p and Sup35p have regulatory roles in fungi (Uptain and Lindquist, 2002), and the hydrophobins are involved in fungal coat and aerial structure formation (Butko et al., 2001), whereas chorion proteins are a major component in insect and fish eggshells (Iconomidou et al., 2000). Perhaps most interesting is the discovery that amyloid has a functional role in mammals, including humans. Amyloid formed from the glycoprotein Pmel17 is involved in facilitating and regulating the biosynthesis of melanin in melanosomes by acting as a multivalent receptor that templates small molecule precursor polymerisation (Fowler et al., 2006). It is also hypothesised that amyloid could play a regulatory role in coagulation and blood clot clearance mechanisms (Kranenburg et al., 2002).

Due to the potential pathogenicity of amyloid formation, and the many diseases associated with amyloid deposition, the regulation of these functional processes are crucial. The properties that make amyloid appealing as a system, such as protease resistance, could also be the features that are most dangerous should these processes go wrong. Yeast use a system of chaperones to control prion propagation, function and degradation and prevent toxicity (Uptain and Lindquist, 2002). In humans, Pmel17 aggregation is highly regulated through two mechanisms. The full-length protein will not form amyloid, and this can only occur after proteolytic cleavage in the melanosome, protecting upstream organelles. The fibrillisation process is thought to proceed via an energetically favourable downhill polymerisation mechanism. This rapid progression prevents the generation of toxic oligomeric assemblies, therefore bypassing one of the fundamental problems of amyloidogenesis (Fowler et al., 2006). A greater understanding of these regulatory mechanisms could lead to development of a novel therapeutic for amyloid disease.

The subject of this thesis, which is to understand better how different amyloidogenic proteins may regulate each other's ability to fibrillise *in vivo*, will be explored in further sections. It is worth noting here the hypothesis that a mammalian disaggregation activity exists. It was first shown in *Caenorhabditis elegans* that post-nuclear supernatant

(PNS) will disaggregate A $\beta$ <sub>1-40</sub> amyloid fibrils (Cohen et al., 2006, Bieschke et al., 2009). It is possible to uncouple proteolysis and disaggregation activities either by heating the nematode homogenate to 80°C or by protease inhibition. Both of these methods eradicate proteolysis but retain disaggregation, thereby indicating that *C. elegans* disaggregation activity is not reliant on proteolysis. A similar mechanism was discovered in homogenates from both mouse and human cells, as both A $\beta$ <sub>1-40</sub> and gelsolin fragment fibrils were disaggregated *in vitro* (Murray et al., 2010). Again, the proteolytic and disaggregation activities could be uncoupled by the addition of protease inhibitors; although unlike the *C. elegans* system disaggregation activity could be inactivated through proteinase K digestion, highlighting that this activity is protein based. It is of great interest to identify the molecular mechanism of this disaggregation system, and the molecular machinery involved.

## 1.2. Amyloidogenic Disease

Amyloidogenic diseases are defined by the abnormal extracellular deposition of insoluble amyloid fibrils into plaques (Caughey and Lansbury, 2003). In these diseases, a specific protein or peptide either does not fold into, or does not remain in, its native conformational state and consequently loses its normal function (Chiti and Dobson, 2006). In some cases the formation of amyloid causes a toxic gain of function. Table 1.1. gives a summary of some of these diseases and the associated amyloidogenic protein (Sipe et al., 2010, Hard and Lendel, 2012). Currently 27 proteins have been identified as forming extracellular amyloid plaques, and several more give rise to disease-associated intracellular amyloid-like deposits (Sipe et al., 2010). Three broad groups can be used to describe amyloidogenic diseases: non-neuropathic systemic amyloidosis where aggregation occurs in multiple tissues, non-neuropathic localised amyloidosis where the deposition is confined to a single type of tissue, and neurodegenerative conditions where the amyloid plaques form solely in the brain (Chiti and Dobson, 2006). Familial amyloidogenic diseases can arise from specific hereditary mutations (10%), however most are sporadic (85%). The spongiform encephalopathies can be transmissible in other mammals as well as humans (5%). Additional species such as heparin, collagen, ApoE, glycosaminoglycans and metal ions (Hirschfield and Hawkins, 2003, Alexandrescu, 2005) are found associated with the amyloid deposits. However, *in vitro* self-assembly will occur in the absence of these components, indicating that other factors are not essential for amyloid formation (Dobson, 2004).

<b>Protein</b>	<b>Native Structure</b>	<b>Disease</b>	<b>Location of Amyloid</b>
<b>A<math>\beta</math></b>	Unfolded	Alzheimer's Cerebrovascular amyloidosis Down's syndrome	Brain
<b><math>\alpha</math>-Synuclein</b>	Unfolded	Parkinson's Dementia with Lewy bodies	Brain
<b><math>\beta_2</math>-Microglobulin</b>	$\beta$ -sheet	Haemodialysis-related amyloidosis	Musculoskeletal system Gastrointestinal & urogenital tracts
<b>Cystatin C</b>	$\alpha/\beta$	Hereditary cystatin C amyloid angiopathy	Brain
<b>Huntingtin (polyQ)</b>	$\alpha$ -helical/unfolded	Huntington's	Brain
<b>Insulin</b>	$\alpha$ -helical	Injection-localised amyloidosis	Site of injection
<b>IAPP (amylin)</b>	Unfolded	Type II diabetes	Pancreas
<b>Lysozyme</b>	$\alpha/\beta$	Hereditary systemic amyloidosis	A number of visceral organs & tissues
<b>PrP (prion)</b>	Unfolded/ $\alpha$ -helical	Spongiform encephalopathies	Brain
<b>Tau</b>	Unfolded	Alzheimer's Frontotemporal dementia	Brain
<b>Transthyretin</b>	$\beta$ -sheet	Familial amyloid polyneuropathy type I Senile systemic amyloidosis	Virtually all tissues & organs

**Table 1.1. Summary of Human Proteins Linked with Amyloid Disease.**

### 1.2.1. Cytotoxicity

The relationship between amyloid fibrils and cytotoxicity is unclear and often controversial. The formation of fibrils is pathogenic, as demonstrated by the correlation between disease and amyloid deposition (Rochet and Lansbury, 2000), and injection of amyloid fibrils into mouse brains causes AD (Meyer-Luehmann et al., 2006, Stoehr et al., 2014, Watts et al., 2014). The difficulties come when trying to determine the specific pathogenic agent: is it the fibrils themselves or some other intermediate species that causes toxicity? Substantial amounts of aggregated protein, up to kilograms, are often found in systemic amyloid diseases, and are thought to be the major cause of clinical symptoms (Pepys, 1996). However there is no clear correlation between the amount of amyloid deposited and the severity of the pathology; a severe case may show little or no amyloid plaques during post-mortem (Näslund et al., 2000, Lue et al., 2000, McLean et al., 1999, Wang et al., 1999). In neurodegenerative diseases there is

significant evidence to show that it is the soluble oligomeric species and short fibrils that are toxic rather than the insoluble mature fibrils (Caughey and Lansbury, 2003, Kaye et al., 2003), and that cytotoxicity may be directly linked to the interaction of aggregates with the components of the cell surface (Lorenzo and Yankner, 1994, Thomas et al., 1996). Neurotoxicity has been seen from a protofibril-only fraction and it has been suggested that amyloid formation could be a protective measure, as early prefibrillar aggregates can be highly damaging to the cell in comparison to the mature fibril (Caughey and Lansbury, 2003). Experiments using non-disease-associated proteins under amyloid forming conditions demonstrated that early species in the aggregation pathway were inherently cytotoxic (Bucciantini et al., 2002). This could suggest a common mechanism of pathogenicity in protein misfolding diseases, relating to the structure of early aggregates. Both fibrils and oligomers display a wide variety of morphologies, and these polymorphs could explain the lack of correlation between fibril load and the severity of symptoms observed due to differences in physicochemical properties on the fibril surface in different polymorphs (Colletier et al., 2011, Paravastu et al., 2008, Petkova et al., 2005, Paravastu et al., 2009, Yoshiike et al., 2007).

Samples containing fibrils of human  $\beta_2$ -microglobulin have been shown to disrupt model liposome membranes and reduce cell viability, whereas prefibrillar oligomeric species of the same protein show no membrane disruption (Xue et al., 2009b). By reducing the length of the fibril an increase in cytotoxicity was observed, suggesting that the cytotoxic potential of the fibrils is modulated by their physical dimensions. It could be that cellular toxic responses are enhanced by fibril breakage; consequently fragmentation of fibrils not only enhances amyloid cytotoxicity but also provides a mechanism to rapidly increase fibril load.

Although it is undeniable that oligomeric fractions of amyloidogenic proteins are capable of disrupting biological membranes, it is also clear that the process of cytotoxicity is likely to involve a number of further complexities and a number of different protein receptors have been proposed to mediate the different pathophysiological effects of these species (Figure 1.12). In AD, this includes the prion protein but also receptor tyrosine kinases such as EphB2 that are believed to affect  $Ca^{2+}$  influx via the NMDA receptor. Neuroimmune receptors Fc $\gamma$ RIIb and LILRB2 are other candidates who mediate an inflammatory response. Genetic manipulation of these

receptors by either up- or down-regulating their expression produces results consistent with an active role in A $\beta$ -mediated cytotoxicity (Benilova and De Strooper, 2013).

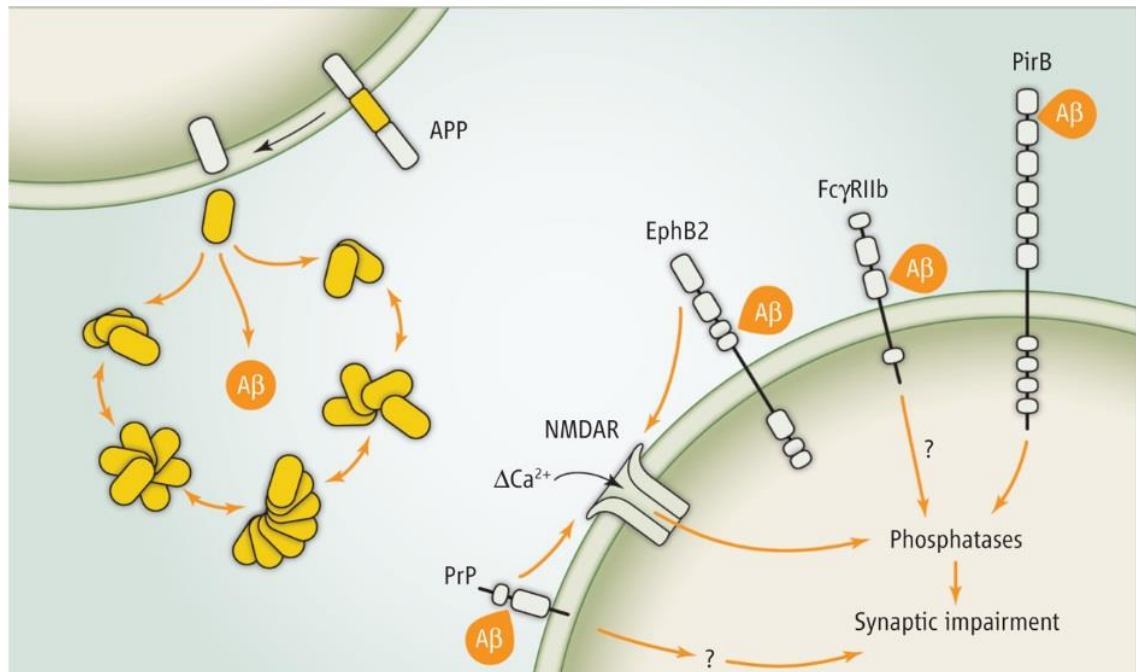


**Figure 1.12. Postulated Cell-Surface Receptors for A $\beta$  with Different Roles in Cytotoxicity**

There are currently a number of different receptors postulated for A $\beta$  at the cell surface which could either alone or synergistically lead to the observed pathology. They include the prion protein and the EphB2 receptor which mediate their toxicity via Ca<sup>2+</sup> influx from the NMDA receptor and more recently identified neuro-immune receptors Fc $\gamma$ RIIb and PirB/LilrB2 who mediate their activity directly via inflammatory cascades. Orange arrows indicate possible binding sites for A $\beta$ . Figure taken from (Benilova and De Strooper, 2013) with permission from AAAS.

### 1.2.2. Alzheimer's Disease

Alzheimer's disease (AD) is the most common cause of dementia, with 37 million people affected worldwide (Rushworth and Hooper, 2010) and 6% of people over the age of 65 affected (Burns and Iliffe, 2009). The incidence of the disease increases with age, affecting almost 50% of the population over 85 (Irvine et al., 2008). Although there are specific criteria used to diagnose AD, at the moment the only accurate method of diagnosis is post-mortem autopsy. Advances in the use of magnetic resonance imaging (MRI) and/or single photon emission computed tomography (SPECT) imaging will improve diagnosis and allow the identification of pre-symptomatic patients.

AD is characterised by the presence of extracellular amyloid plaques and intracellular neurofibrillary tangles (NFT) in the brain (Annaert and De Strooper, 2002). The former consist of fibrils mainly formed from the A $\beta$  peptide, whereas the latter are composed of

hyper-phosphorylated tau protein. In addition to the plaques and tangles, there is a progressive loss of cognitive function due to an overall loss of grey matter, particularly in cortical layers III and V (Caughey and Lansbury, 2003, Deng et al., 2001). A hallmark of the AD brain is A $\beta$  amyloid plaques in neurophil and cerebral vessel walls (Caughey and Lansbury, 2003, Serpell, 2000). The molecular link between A $\beta$  peptide and neurotoxicity is poorly understood (Annaert and De Strooper, 2002). A $\beta$  is thought to be involved in several toxic processes such as apoptosis, activation of complement, generation of radicals, disrupted calcium homeostasis and the generation of pores in the cell membrane (Small et al., 2001), Benilova et al., 2012) and the prominent hypothesis is that the oligomeric forms of A $\beta$  are the toxic species responsible for degeneration.

Late-onset AD, or sporadic AD, is the most common form of the disease, accounting for over 90% of cases, however insight into the root causes of this disease can be gained from studying familial cases. Familial AD is early-onset, and usually involves a mutation that either increases the amount of A $\beta$ <sub>1-42</sub> or its propensity to form fibrils (Caughey and Lansbury, 2003). The most common of these genetic polymorphisms are missense mutations in the presenilin-1 gene (*PS1*) which encodes one of the enzymes responsible for the cleavage of the A $\beta$  peptide from its precursor protein ( $\gamma$ -secretase), causing an increase in both extracellular and brain concentrations of A $\beta$ <sub>1-42</sub> (Scheuner et al., 1996). Mutations are also found in the presenilin-2 (*PS2*) encoding a further processing enzyme for A $\beta$  and the amyloid precursor protein (*APP*) gene itself which causes increased concentrations of both A $\beta$ <sub>1-40</sub> and A $\beta$ <sub>1-42</sub> or alter the spectrum of A $\beta$  peptides produced (Ancolio et al., 1999, Kumar-Singh et al., 2000). These polymorphisms can also be associated with late-onset AD and cerebral amyloid angiopathy (CAA) (Yamada, 2000, Yamada et al., 1997).

The amyloid cascade hypothesis (Hardy, 1997, Hardy and Selkoe, 1999, Sisodia et al., 2001, Annaert and De Strooper, 2002) was proposed as a result of these discoveries and stated that the amyloid  $\beta$  peptide, and more specifically, its aggregation into amyloid-like fibrils was responsible for all the pathophysiology of Alzheimer's disease, including the characteristic hyper-phosphorylation of tau proteins and the ensuing formation of intracellular tangles (Figure 1.13).

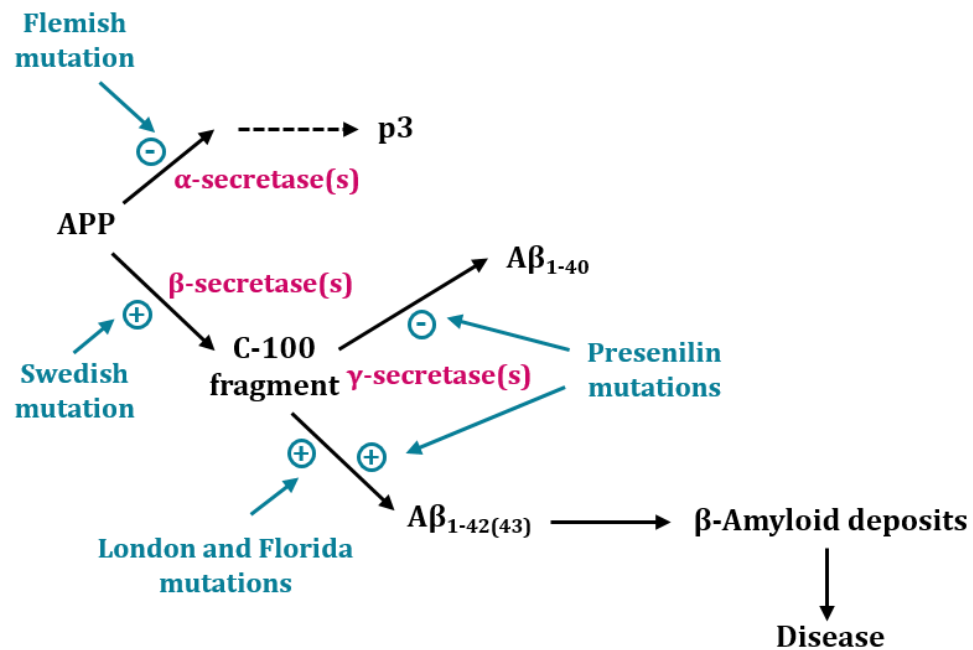


**Figure 1.13. Initial Events in the Amyloid Cascade Hypothesis**

Evidence that the levels of Aβ peptide measured in the CSF are directly causative to Alzheimer's disease come from a combination of direct measurements, studies of genetic penetrance and injection of β-amyloid directly into the brains of mice. The C-100 fragment is the C-terminal fragment of APP generated from cleavage by BACE, starting at Met261. p3 is generated from α-secretase cleavage of APP and is non-pathogenic. Adapted from (Hardy, 1997) with permission from Elsevier.

### 1.2.3. Cerebral Amyloid Angiopathies

More than 80% of patients with Alzheimer's disease also suffer from vascular deposition of amyloid, a condition known as cerebral amyloid angiopathy (CAA). CAAs are caused by the deposition of amyloid in the central nervous system (CNS) (Revesz et al., 2003). These plaques cause thickening of the blood vessels, leading to dementia and cerebral haemorrhage. The majority of CAA cases are sporadic with 46% of individuals over seventy years old having some degree of CAA. CAA is found associated with Alzheimer's disease (Yamada, 2000), but also with Downs syndrome, cerebral infarction and intracranial haemorrhage (Maruyama et al., 1990). The overlap with AD is such that it is believed that the CAA not only contributes to, but in some cases actually causes cognitive decline and therefore dementia, possibly by preventing drainage of Aβ from the brain (Weller and Nicoll, 2003). It is of note that whereas most amyloidoses are linked to the misfolding of a single protein, CAA shows that these pathological conditions are not obligatory single protein diseases. Around half a dozen proteins are known to form cerebrovascular amyloid as well as Aβ and include the prion

protein, hCC, transthyretin and gelsolin (Yamada, 2000). Severe CAA is often associated with mutations in these proteins, and polymorphisms in several risk factors are also linked to an increased risk of CAA or CAA-related haemorrhage (Yamada, 2000, Revesz et al., 2003).

#### 1.2.4. Amyloid- $\beta$

Amyloid- $\beta$  ( $A\beta$ ) is a short peptide formed through cleavage of the amyloid precursor protein (APP). The  $A\beta$  fragments vary in length from 38-43 amino acids (Benilova et al., 2012), however the most common are  $A\beta_{1-40}$  and  $A\beta_{1-42}$  (Jarrett et al., 1993). Studies have suggested that while  $A\beta_{1-40}$  is the predominant form,  $A\beta_{1-42}$  is the more toxic form of the protein (Storey and Cappai, 1999). Although it has been proposed that these different alloforms of  $A\beta$  peptide oligomerise through different assembly pathways, there is much evidence to support that similar intermediates are populated by both peptides, albeit at different concentrations of the peptide (Bitan et al., 2003).

##### 1.2.4.1. Processing of APP

Proteolytic cleavage of the amyloid precursor protein (APP) by transmembrane aspartyl proteases (Irvine et al., 2008) leads to the production of  $A\beta$  peptides. APP is a type I integral membrane protein (Kang et al., 1987) found in lipid rafts, and is composed of a cytoplasmic domain and an extracellular domain in addition to the membrane-spanning domain. APP is expressed in most tissues, including the brain; however its function is unknown. It is suggested that APP could be involved in cell survival, cell adhesion, synaptogenesis and regulation of neurite outgrowth (Vetrivel and Thinakaran, 2010). It is proposed that there are two different pathways for APP cleavage; it is either internalised and degraded via the lysosome or cleaved within the  $A\beta$  region (either at the plasma membrane or in endosomal vesicles) causing the ectodomain to be secreted (Figure 1.14) (Lamb et al., 1993).

Amyloidogenic cleavage of APP requires the activity of two enzymes;  $\beta$ -secretase and  $\gamma$ -secretase (De Strooper and Annaert, 2000). The initial cleavage by  $\beta$ -site APP-cleaving enzyme 1 (BACE1) produces a soluble ectodomain, leaving the C-terminal portion of the protein (containing  $A\beta$ ) in the membrane. Cleavage of the C-terminal transmembrane section by the  $\gamma$ -secretase complex produces the  $A\beta$  peptide. The multi-enzyme  $\gamma$ -secretase complex consists of PEN2, nicastrin, APH1 and either presenilin 1 or 2, and has heterogeneous site preference, thereby producing fragments of different

lengths. Cleavage in this manner exposes hydrophobic residues from the C terminal of the peptide; these residues are normally buried in the cell membrane and when exposed have a propensity to aggregate.

Initial cleavage of APP can also occur by  $\alpha$ -secretase activity. This is non-amyloidogenic, as the  $\alpha$ -secretase enzyme cleaves downstream of BACE1. Consequently the C-terminal fragment is truncated, and the p3  $\beta$ -peptide produced by  $\gamma$ -secretase cleavage is shortened. The fragment produced by  $\alpha$ -secretase cleavage, sAPP $\alpha$ , could protect neurons from A $\beta$ -induced damage (Goodman and Mattson, 1994, Thornton et al., 2006). Although A $\beta$  is associated with the disease state, APP cleavage occurs in normal healthy subjects, and A $\beta$  is found to be naturally present in the brain and CSF (Haass et al., 1992, Vigopelfrey et al., 1993). Consequently it is not the presence of A $\beta$  that causes toxicity, but rather the formation of amyloid fibrils and prefibrillar oligomers occurring at increased concentrations (Hardy and Selkoe, 2002).

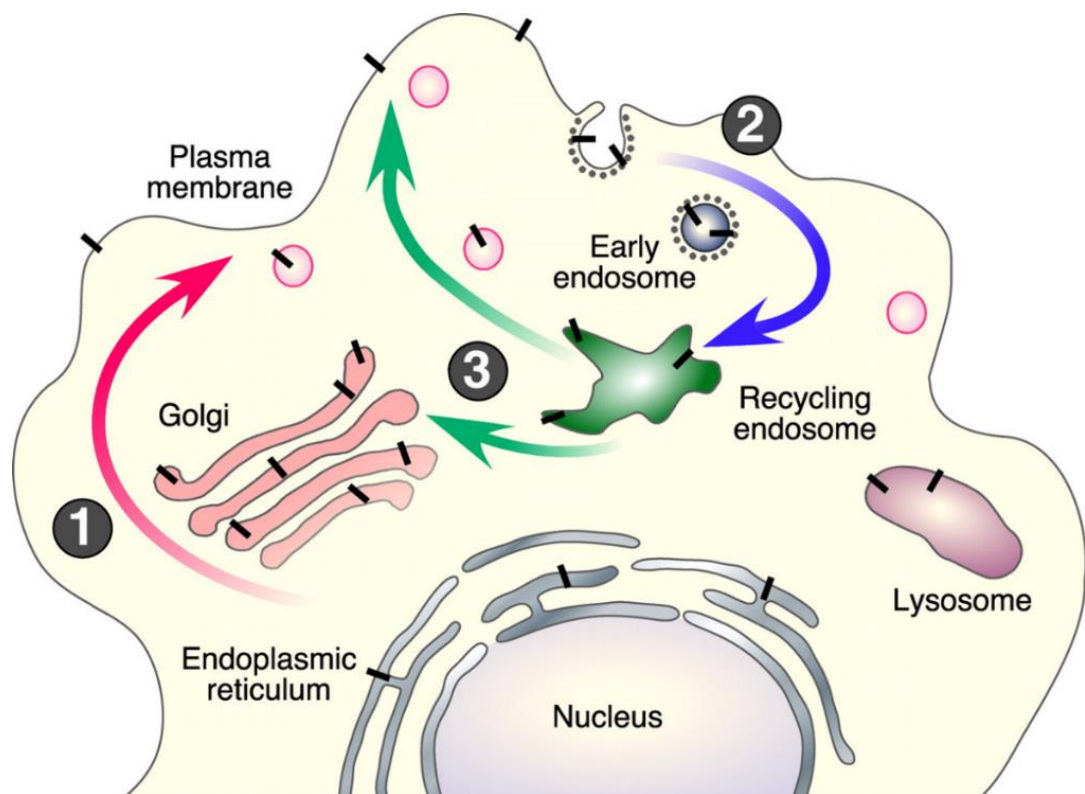


**Figure 1.14. Processing of APP**

*Step 1 - APP (black bars) matures through the secretory pathway where it reaches the cell surface. Step 2 – the protein is internalised. Step 3 – trafficking through the endocytic pathway brings APP back to the cell surface. Some APP is degraded in the lysosome. Non-amyloidogenic cleavage by  $\alpha$ -secretases occurs at the cell surface, whereas amyloidogenic cleavage and the production of A $\beta$  occurs in the endocytic organelles. Image taken from (Thinakaran and Koo, 2008) with permission from Elsevier.*

### 1.3. Cystatins

The cystatins are non-covalent reversible competitive inhibitors of papain-like cysteine proteases, which function through tight-binding to their target protease in an equimolar manner to form an inactive complex. Dissociation constants for these complexes are typically in the sub-nanomolar to nanomolar range (Barrett et al., 1984). Physiologically, the role of cystatins is to regulate endogenous protease activity and protect tissues from inappropriate proteolysis caused by the release of lysosomal enzymes following cell damage (Turk and Bode, 1991). Cystatins may also play a defensive role against microbial invasion (North et al., 1990).

There are three different families of cystatin, all retaining the common 'hot-dog' fold (Turk and Bode, 1991). Low molecular weight type I cystatins or "stefins" are single chain non-glycosylated intracellular proteins such as cystatin A and cystatin B (Grzonka et al., 2001). Members of the cystatin family (type II) have an average molecular weight of 13 kDa, and again generally lack glycosylation (with the exception of rat cystatin which is often N-glycosylated). These are extracellular inhibitors, and contain four cysteine residues that are involved in the formation of two characteristic disulphide bonds. Examples of type II cystatins include cystatins C, D, E, S, SN and SA (Rawlings and Barrett, 1990, Abrahamson et al., 2003). The third family of cystatins are the kininogens. These intravascular inhibitors consist of three cystatin-like domains, containing the characteristic type II cystatin disulphide bonds as well as others. Highly glycosylated, the kininogens are located only in the blood plasma and synovial fluid.

**TYPE I**  
(cystatin A and B)



**TYPE II**  
(cystatin C and chicken cystatin)



**TYPE III**  
(L- H - and T- kininogens)

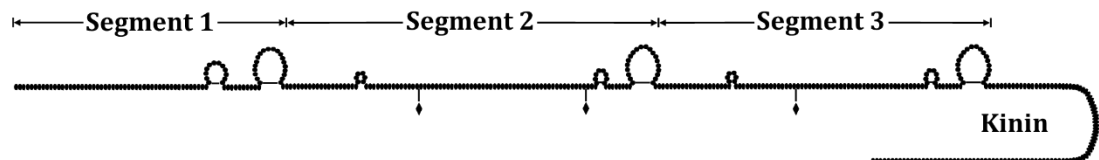


**Figure 1.15. Schematic of Cystatin Primary Structure**

*Line representation of three main cystatin families. Disulphide bonds represented by loops and sites of glycosylation represented by diamonds. The targeting sequence for secretion is shown in type II cystatins (O) with the cleavage site in red. Type III cystatins consist of several type-II-cystatin-like domains. H-kininogens have a longer C-terminal extension than is depicted here. Figure adapted from (Barrett, 1987) with permission from Elsevier.*

### 1.3.1. Cystatin C

Human cystatin C (hCC) is a cysteine protease inhibitor formerly known as  $\gamma$ -trace, which binds with high affinity to enzymes of the human C1 family of proteases such as cathepsins B, H and L (Janowski et al., 2001). Immunohistochemical analysis originally localised hCC to the neuroendocrine system (Grubb and Lofberg, 1982). However, expression and secretion of hCC is not tissue specific, all nucleated cells synthesise the protein (Mussap and Plebani, 2004). hCC is found ubiquitously in human biological fluids at relatively high concentrations as shown in Table 1.2 (Grubb and Lofberg, 1985); in cerebrospinal fluid, hCC is the dominating cysteine protease inhibitor, with a concentration of  $\sim 7 \mu\text{g/ml}$  (Abrahamson et al., 1986) which is  $0.52 \mu\text{M}$ . The protein is expressed as a 146 amino acid product containing a hydrophobic signal peptide, which is then cleaved to produce the mature protein consisting of 120 amino acids. A typical type II cystatin, hCC is not glycosylated and contains two disulphide bonds at the C-terminal end. hCC retains 50% sequence identity with three other human family 2 cystatins, cystatins S, SA and SN.

<b>Biological Fluid</b>	<b>Concentration (nM)</b>
Plasma	105 ± 30
Cerebrospinal fluid	545 ± 180
Urine	7.5 ± 0.5
Saliva	135 ± 70
Seminal plasma	3810 ± 600

**Table 1.2. Physiological Concentrations of hCC. Adapted from (Grubb and Lofberg, 1985).**

### 1.3.2. Biological role of hCC

hCC is a highly effective inhibitor of papain-like cysteine proteases such as cathepsin B, H, K, L and S, along with papain, dipeptidyl peptidase and ficin (Barrett et al., 1984), and consequently plays a critical role in the regulation of extracellular protein degradation. In almost all bodily fluids, including CSF, milk and seminal plasma, hCC is the controlling inhibitor for cathepsin B (Abrahamson et al., 1986), which has many roles including A $\beta$  clearance (Mueller-Steiner et al., 2006, Sun et al., 2008). Based on the dissociation constant, hCC is predicted to contribute to the physiological inhibition of any extracellular cysteine protease passing from the lysosomal system (Barrett et al., 1984). Moreover, hCC is also thought to play an important role in the endocytic pathway (D'Adamio, 2010), and is active in endosomes and lysosomes.

#### 1.3.2.1. C13 cysteine protease inhibitory activity

In addition to the C1 protease binding site commonly found in cystatins, hCC is unusual in that it also has an inhibitory site for legumain. This member of the C13 cysteine protease family (originally identified in plants) is a more recently discovered mammalian lysosomal endopeptidase, which shows restricted hydrolysis of asparaginyl bonds (Dando et al., 1999). hCC dimerisation prevents papain (C1) inhibition, however this is not the case for legumain as the inhibitor is still active as a dimer (Alvarez-Fernandez et al., 1999). The binding site is thought to be the  $\alpha$ -helix in conjunction with the loop around Asn39 (Alvarez-Fernandez et al., 1999), a region that is not altered by dimerisation (Janowski et al., 2001).

#### 1.3.2.2. Inflammation

At sites of inflammation, increased levels of protease and protease inhibitors have been observed, indicating that cystatins could play an important role in the inflammatory

response (Bobek and Levine, 1992). Monocyte and macrophage secretion of hCC is down-regulated by pro-inflammatory lipopolysaccharide and interferon- $\gamma$  (Warfel et al., 1987). Phagocytosis and superoxide anion release in human neutrophils are thought to be inhibited by the N-terminal tetrapeptide of hCC (Leung-Tack et al., 1990b) (Leung-Tack et al., 1990a), and hCC was found to have an effect on granulocyte locomotion (important for initiation and maintenance of inflammation) (Leung-Tack et al., 1990b). This activity is believed to be independent of its activity as a proteinase inhibitor.

### 1.3.3. Inhibition Mechanism

The mechanism of inhibition is similar for hCC and the more widely studied chicken cystatin (cC). Three regions have been identified as being involved in the interaction with target proteases and it is thought that hydrophobic interactions are involved, as all three identified regions contain many hydrophobic residues. The N-terminal 11 amino acid residues were shown early on to be important for high-affinity binding to papain (Abrahamson et al., 1987). Glycine 11 is evolutionarily conserved (Gly-9 in cC), and removal of the N-terminal region either before or after this residue through proteolytic cleavage leads to a reduction in binding affinity for both hCC and cC (Abrahamson et al., 1987, Bode et al., 1988, Lindahl et al., 1992). The NMR and X-ray structure of cC shows the flexibility of the N-terminal region, and removal of this region does not seriously alter the overall three-dimensional structure. It is therefore suggested that the reduction in activity upon truncation is due to loss of interactions involving the N-terminal, as opposed to a perturbation of the remainder of the binding surface. The other two identified regions are the two hairpin loop sections (Ekiel et al., 1997). Within the first loop is a highly conserved sequence among cystatins, which is QIVAG in hCC (Figure 1.16A). It is the constrained, energetically unfavourable geometry of the loop structure, where branched chain amino acids (valine) are enclosed within the very tight loop, which renders the chain resistant to cleavage by the protease while binding in the active site (Engh et al., 1993). It follows then that it is the relaxation of this constrained loop that provides the driving force for dimerisation (Staniforth et al., 2001).

### 1.3.4. Structure of hCC

Recently two crystal structures of monomeric hCC variants have been published; these are the first structures of hCC monomer to be solved. The first is of a stabilised mutant, which has two point mutations that allow the formation of an extra disulphide bond, stabilising the monomer (Kolodziejczyk et al., 2010). The second structure utilises a

mutation of V57 to asparagine in the hairpin loop L1 (Orlikowska et al., 2011), which is involved in providing the epitope that recognises target enzymes. It is thought that the first eleven residues of the N-terminal region are flexible, as no electron density was observed for this region. Both of these studies show a similar structure, indicating that the monomer has a typical cystatin fold consisting of (N)- $\beta$ 1- $\alpha$ - $\beta$ 2-L1- $\beta$ 3-AS- $\beta$ 4-L2- $\beta$ 5-(C) (Kolodziejczyk et al., 2010). This produces a five-stranded antiparallel  $\beta$ -sheet that wraps around the  $\alpha$ -helix (Orlikowska et al., 2011). Two disulphide bonds are located in the C-terminal sub-domain, between C73 and C83, and C97 and C117.

One of the characteristics of the cystatin superfamily is the formation of domain swapped dimers. As demonstrated by Ekiel & Abrahamson (1996), dimerisation of hCC can be induced by de-stabilising the protein using high temperature ( $> 65\text{ }^{\circ}\text{C}$ ), low pH (pH 3.0 - 4.0) or chemical denaturants (0.3 – 1.2 GuHCl). The optimal range of conditions is where the folded state still dominates but where the unfolded state of the protein is significantly more populated, equating to “pre-transitional” conditions in equilibrium unfolding curves. The dimer was first to be crystallised and the structure reveals a tight two-fold symmetry (Figure 1.16), retaining the secondary structure of the monomeric form.

Formation of the hCC dimer results from exchange of sub-domains between two monomers (Janowski et al., 2001). One of the molecules contributes a single  $\beta$ -strand and  $\alpha$ -helix, whereas the rest of the structure is provided by the other molecule. As this  $\alpha/\beta$  interface retains the structure of the monomer it is termed a closed interface. An open interface is formed through the new  $\beta$ L- $\beta$ L sheet that is created. It is thought that 3D domain swapped dimers only form where there is a high local hCC concentration.

Native hCC exists as a monomer, and it is in this state that it is functional; dimerisation causes a complete loss of inhibitory activity (Ekiel and Abrahamson, 1996). Considerable levels of extracellular hCC dimer are only found under pathological conditions (Abrahamson and Grubb, 1994) and wild-type hCC has not been found to form fibrils *in vivo* (Ekiel and Abrahamson, 1996). It is suggested that dimer is an essential intermediate in fibril formation (Wahlbom et al., 2007), as stabilised mutants, with an extra disulphide bond to prevent dimerisation, will not form amyloid fibrils. More convincingly, kinetic studies of cC in solution showed that assembly of this cystatin into tetramers and higher molecular weight species went through an obligatory dimerisation step (Sanders et al., 2004).

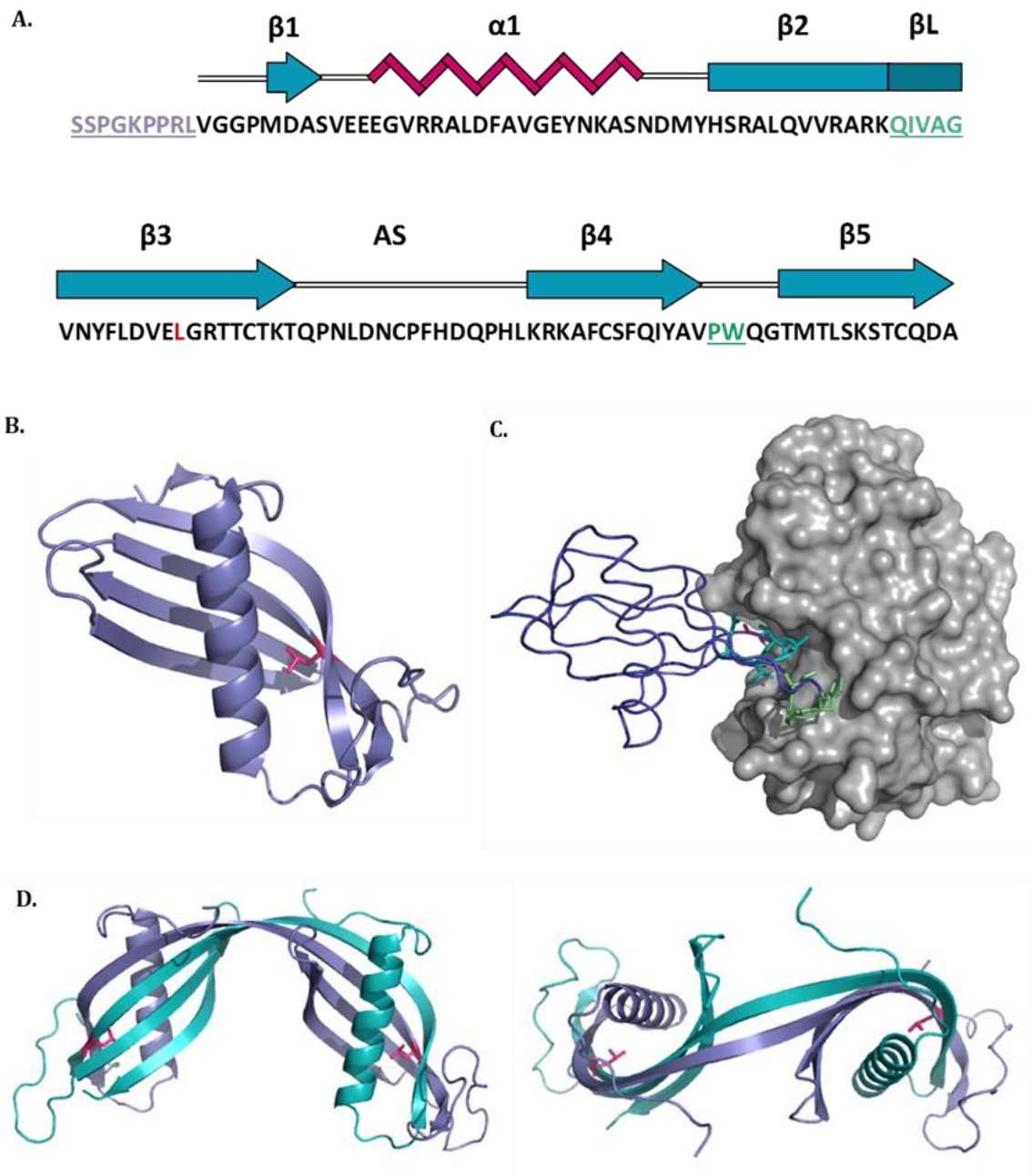


**Figure 1.16. Structure of hCC**

Primary and secondary structure of hCC (A) with regions involved in protease inhibition underlined in green and purple. The L68Q mutation is shown in pink throughout. Tertiary structure of monomeric form of variant hCC V57N (B) illustrating hot-dog fold with  $\alpha$ -helix enclosed in 5  $\beta$ -strands (PDB: 3NX0). An example of cysteine protease inhibition (C) showing cystatin B (blue) in complex with papain (grey) with the highly conserved primary binding site loop QVVAG (turquoise), secondary binding loop (green) and N-terminal residues weakly involved in binding (purple) (PDB: 1STF). The domain swapped dimer of hCC (D) highlights the closed interface formed between the swapped domains where an extended  $\beta$ -strand is formed encompassing the original strands 2 and 3 and the intervening loop  $\beta L$ .

### 1.3.5. L68Q Variant of hCC

The disease hereditary cystatin C amyloid angiopathy (HCCAA) is caused by the hCC L68Q variant (Ghiso et al., 1986). A point mutation changes the codon for residue 68 from CTG to CAG, substituting glutamine for leucine (Levy et al., 1989). Leu68 is positioned in strand  $\beta$ 3 of the  $\beta$ -sheet and so is part of the hydrophobic core of the protein (Janowski et al., 2001). Whilst not directly participating in amyloid-forming interactions, the mutation causes destabilisation of the monomer at the molecular  $\alpha/\beta$  interface, making the protein more prone to dimerisation. Both WT and L68Q hCC effectively inhibit cathepsin B with similar equilibrium constants for dissociation ( $K_d$ ), indicating that the variant is capable of folding into the correct conformation; the difference comes in their tendency to dimerise and form aggregates (Abrahamson and Grubb, 1994). Destabilisation in the hydrophobic core causes the variant to form dimers at temperatures  $\sim 25^\circ\text{C}$  lower than for the wild-type protein (Abrahamson and Grubb, 1994). At  $37^\circ\text{C}$ , dimerisation of L68Q hCC progresses to a significant extent as evidenced by the detection of dimers *in vivo*, and this is coupled with an aggregation process which leads to the formation of large insoluble cystatin aggregates. Levels of both WT and L68Q hCC are reduced in the cerebrospinal fluid in patients (to around one third of the normal level) (Palsdottir et al., 2006); this is likely due to a combination of the formation of aggregates and an impaired secretion of L68Q-hCC (Abrahamson and Grubb, 1994). The blood plasma of patients with the disease contains hCC dimers as well as monomers, whereas only monomeric hCC is found in healthy individuals (Palsdottir et al., 2006). A reduction in the total cysteine protease inhibition capacity of the CSF, caused by the existence of inactive dimers, could contribute to cerebral haemorrhages in HCCAA (Olafsson et al., 1990). As well as the L68Q mutation discussed previously, the variant found in amyloid deposits in HCCAA also has an N-terminal truncation of 10 residues when compared to normal hCC (Ghiso et al., 1986, Grubb and Lofberg, 1985). It is suggested that this truncation could be due to cleavage by leucocyte elastase (Abrahamson et al., 1991).

### 1.3.6. Cystatins and Disease

#### 1.3.6.1. Hereditary Cystatin C Amyloid Angiopathy

hCC was identified as the amyloid forming protein in the dominantly inherited disorder hereditary cystatin C amyloid angiopathy (HCCAA) by protein sequencing over 30 years ago (Cohen et al., 1983). This disease is systemic, as immunohistochemical

studies have indicated that hCC amyloid deposits are present in several tissues as well as the brain, for example salivary glands, the spleen and the skin (Abrahamson and Grubb, 1994). hCC is ubiquitous in body fluids, so it is perhaps not surprising to find that amyloid is deposited systemically. However, the highest plaque load is in the arterioles and arteries of the brain, causing the vessel walls to thicken and leading to brain haemorrhage (Palsdottir et al., 2006). This disease is found in Icelandic individuals, normally aged in their 20s or 30s.

#### 1.3.6.2. Kidney Function

Increased serum levels of hCC are an important biomarker in the detection of kidney failure. Measuring the glomerular filtration rate (GFR) is seen as the most effective measure of kidney function, with a reduced GFR corresponding to impaired kidney function (Stevens et al., 2006). As the GFR decreases the disease state will progress to kidney failure, eventually leading to premature death caused by cardiovascular disease. GFR is measured as the urinary or plasma clearance of a filtration marker, a process that is complex, expensive and difficult to do in routine clinical practice with exogenous markers. Serum levels of endogenous markers can be used to estimate the GFR without the need for a urine sample, as timed urinary collections have been found to be cumbersome and susceptible to error. As a non-glycosylated protein with a low molecular mass, hCC is freely filtered by the glomerulus before being reabsorbed and catabolised by the tubular epithelial cells. It is suggested that hCC may be a better filtration marker than the historical creatinine, with less variation between patients.

#### 1.3.6.3. Alzheimer's Disease

As will be discussed in greater detail later in the chapter, there is an increasing amount of evidence that there is a significant link between hCC and Alzheimer's disease. The co-localisation of hCC and A $\beta$  amyloid plaques has been identified in the brains of AD patients, as well as those with hereditary cerebral haemorrhage with amyloidosis – Dutch type (HCHWA-D) and sporadic cerebral amyloid angiopathy (CAA) (Haan and Roos, 1992, Levy et al., 2001, Deng et al., 2001, Vinters et al., 1990).

### 1.4. Interactions with A $\beta$

A $\beta$  is the major component of amyloid plaques in AD, with amyloid fibrils interspersed with non-fibrillar species (De Strooper and Annaert, 2000). These plaques also contain degenerating axons and dendrites, and are invaded and surrounded by microglia and

reactive astrocytes, indicating there is an inflammatory component in the process of neurodegeneration. There is significant evidence to show that aggregation of the peptide is modulated through interactions with various factors, some of which will also become incorporated into the plaques. These associated factors can be protein, lipid, metal ions or other molecules. Factors can be classed as inhibitory, either by solubilising the peptide, inhibiting fibril formation or dissolving already existing amyloid fibrils, or alternatively as enhancing where the associated molecule may initiate or exacerbate fibril formation and deposition (De Strooper and Annaert, 2000). Some of the associated proteins may play a role in the pathological pathways leading to amyloid deposition, and others may bind to the neuritic plaques in a secondary process after deposition (Sastre et al., 2004). The presence of protease inhibitors may reflect a role in the regulation of proteolytic degradation of plaque components. It is of great interest to identify the driving forces behind the interaction of these different factors, and any structural motifs necessary (McLaurin et al., 2000), in addition to determining the roles they play in the formation and deposition of amyloid (Wilhelmus et al., 2007), thereby providing information of potential sites that may be targeted in the development of a novel therapeutic.

Recent genome-wide susceptibility studies (GWAS) (Sleegers et al., 2010) and staged association studies (GERAD+) (Hollingworth et al., 2011) have suggested several novel susceptibility loci for Alzheimer's disease. The proteins identified, including an ATP binding cassette (ABC) transporter, clusterin and CD33 (a member of the sialic acid binding immunoglobulin-like lectins) have functions in the immune system, lipid processing and processes at the cell membrane such as endocytosis. Chaperones, including heat shock proteins, were also identified and are likely to play an important part in preventing A $\beta$  misfolding and facilitating protein refolding. Although significant advances have been made in this area with the creation of a website for "susceptibility" genes in AD, a clear genetic link between genes other than those encoding APP, the presenilins and ApoE is still difficult to establish.

#### **1.4.1. Albumin**

One of the known risk factors in AD is a reduction in serum albumin with age and in association with inflammation. Human serum albumin (HSA) binds 90-95% of A $\beta$  in blood plasma (Biere et al., 1996, Kuo et al., 2000) with a  $K_d$  of 5-10  $\mu$ M at a 1:1 stoichiometry (Kuo et al., 2000). It is proposed that the reduced concentration of HSA

in the CSF during AD, reducing the availability for albumin binding to A $\beta$ , could explain why A $\beta$  plaques are only observed in the extracellular space of the brain, rather than the peripheral tissue (Stanyon and Viles, 2012).

It is not yet known whether HSA binds to A $\beta$  monomer or oligomers: evidence exists to suggest both possibilities. As HSA is not found within amyloid plaques in brains from AD patients, it is thought that it does not interact or become incorporated with the fibril. However, it is known that HSA will significantly inhibit A $\beta$  fibril formation in a concentration-dependent manner (Stanyon and Viles, 2012). Through binding to albumin, A $\beta$  molecules are trapped in a non-fibrillar form and therefore are not available for fibril formation. It is proposed that HSA prevents formation of the nucleation seed, however has little effect on fibril elongation. An albumin plasma exchange schedule is currently showing promise in phase II clinical trials at reducing A $\beta$  levels in blood plasma (Boada et al., 2009), which in turn will reduce the levels of A $\beta$  in the CSF due to the ability of the peptide to cross the blood-brain barrier (Mackic et al., 1998).

#### 1.4.2. Amyloidogenic Proteins

Interestingly, a group of amyloidogenic proteins are known to associate with A $\beta$ . These proteins form amyloid fibrils *in vivo* and often cause amyloidogenic diseases themselves through destabilising mutations or intracellular processing. This group of proteins includes hCC, neuroserpin and transthyretin, prion protein, gelsolin and Bri2 (Li and Buxbaum, 2011).

##### 1.4.2.1. hCC and A $\beta$

One of the amyloidogenic proteins found to co-localise with A $\beta$  in several different disease states is hCC. In AD, human immunohistochemical studies show that hCC is mostly observed in amyloid deposits surrounding blood vessels but is also seen in some parenchymal deposits (Deng et al., 2001, Sastre et al., 2004). Cell culture work reveals intracellular localisation of hCC and  $\beta$ -APP in both human embryonic kidney HEK293 cells and mouse neuroblastoma N2a cells. Co-localisation of hCC with A $\beta$  has also been observed in the brains of transgenic mice over-expressing human APP (Tizon et al., 2010).

The co-localisation of hCC and A $\beta$  is not limited to AD. Cerebral amyloid angiopathy (CAA) is the deposition of amyloid in the blood vessel walls of the central nervous

system. As the protein deposited is often A $\beta$ , patients with AD have a higher propensity to CAA than age-related controls, with amyloid deposition in CAA leading to haemorrhage, stroke and eventual death. A third of patients with sporadic A $\beta$  CAA co-stained for hCC (Haan and Roos, 1992). In patients with HCHWA-D (hereditary cerebral haemorrhage with amyloidosis – Dutch type), the majority co-stained for hCC in A $\beta$ -staining blood vessels. Interestingly, when hCC is the key amyloidogenic protein, such as in HCCAA, there is no evidence for co-deposition with A $\beta$  despite probing with several anti-A $\beta$  antibodies (Haan and Roos, 1992, Vinters et al., 1990).

In humans, elevated levels of hCC are observed in susceptible parts of the brain (Deng et al., 2001), and in animal models there is evidence for a physiological response to the disease state whereby expression of hCC is increased (Steinhoff et al., 2001). Studies of transgenic mice overexpressing hCC to twice the normal levels shows inhibition of amyloid  $\beta$  deposition in transgenic mice expressing the Swedish mutant APP (Kaesler et al., 2007, Mi et al., 2007). It seems therefore, that co-localisation may be more than a simple consequence of circulatory proteins binding to a “sticky” surface. In addition to co-localisation with A $\beta$  and stimulation in AD, induction of TTR amyloidosis in the heart in mouse models is seen to lead to increased transcription of the hCC gene and other amyloidogenic proteins in the liver (Buxbaum, J. N., personal communication). This then leads to an increase in levels of circulatory hCC, which is shown to have benefits in reducing amyloid load. This physiological response adds up to a chaperone-like physiological role for these proteins in a range of amyloid diseases.

Genetic association studies have shown further that polymorphisms in the hCC gene, CST3, are linked with late onset AD (Beyer et al., 2001) and have led some to name CST3 as a strong candidate susceptibility gene for AD. The mutation of alanine to threonine at position –2 causes less efficient cleavage of the signal peptide, and consequently a reduction in secretion of the full length protein (Tizon et al., 2010), increasing the risk of AD for those homozygous for those with this polymorphism (Selenica et al., 2007). Other polymorphisms including the CST3 +73 G/A mutation (Crawford et al., 2000) or the CST3 –157 G/C polymorphism (Finckh et al., 2000) are also associated with late onset AD. As with many such studies, significant difficulties arise in reproducing these findings, presumably due to the variety of different risk factors for AD and also the difficulties in selecting suitable control groups. However these studies, in association with evidence for physiological and biochemical effects in

animal, cell and test tube models of AD, strengthen the proposal of a protective role for hCC in Alzheimer's disease.

In order to explain the observed effects, a number of possible hypotheses exist. One initial working model for hCC neuro-protection was that hCC is endocytosed by damaged neurons and targeted to the lysosome. At this stage, the neurons would have begun to accumulate lysosomal proteases, and hCC could act to inhibit some of these in order to protect the cell from excessive lysosomal dysfunction. If the damage is too great, or too persistent, the neurons may degenerate due to accumulation of neurofibrillary changes (Deng et al., 2001). In support of this theory is the observation that secreted cathepsin B from microglia can induce neuronal apoptosis (Kingham and Pocock, 2001). Investigations *in vitro* however favour a more direct salutary effect of hCC on A $\beta$ .

One of the first investigations of the interaction between hCC and A $\beta$  was investigated using an ELISA assay (Sastre et al., 2004). This indicated that the two proteins were binding with high affinity at physiological pH and temperature, with a dissociation constant ( $K_d$ ) in the nanomolar range. Addition of a monoclonal antibody 6E10 at concentrations of 5 nM was enough to block the binding of hCC to A $\beta$ . This antibody binds to the N-terminal end of the peptide (residues 1-17), suggesting that hCC also binds in this region. This study also suggested that the binding of hCC to A $\beta$  is highly concentration dependent.

The investigation by Sastre *et al.* (2004) demonstrated that hCC inhibited A $\beta$  fibril formation *in vivo* in a concentration-dependent manner through analysis by electron microscopy. It was suggested that the speed of aggregation of A $\beta$  is reduced by hCC through direct binding in a sub-stoichiometrical manner. hCC has since been reported to prevent the formation of protofibrils and oligomers of A $\beta$ , including toxic ADDLs, *in vitro* (Selenica et al., 2007). Since A $\beta$  oligomers are potentially causative in AD, this observation has important implications. The association of A $\beta$  with hCC was investigated using size-exclusion chromatography (SEC) and immunoprecipitation, which the authors suggest form a one-to-one equimolar complex. The result is somewhat ambiguous as the chromatography used is unable to resolve the species concerned. However, a mechanism was proposed in which hCC and A $\beta$  react rapidly to form high affinity one to one molar complexes, with the N-terminal region of A $\beta$  involved in the binding (Selenica et al., 2007). Upon prolonged incubation, these initial

complexes have less propensity than the monomeric A $\beta$  to produce higher species such as ADDLs, protofibrils or even fibrils. Instead larger, amorphous aggregates are produced without the structural characteristics of the aforementioned species and precipitate from solution.

There may therefore be as many as three separate ways in which hCC can carry out its protective role in AD. hCC has been shown to directly protect N2a neuroblastoma cells and rat hippocampal neurons from A $\beta$ -induced toxicity (Tizon et al., 2010). hCC could play an important neuroprotective role in AD (D'Adamio, 2010), consistent with hCC being a paracrine/autocrine factor involved in neurogenesis (Taupin et al., 2000). In addition, by increasing levels of hCC in the disease state, cathepsin activity could be inhibited both intracellularly in the cytosol and vesicles, and extracellularly, potentially leading to the rescue of neurons (Kaur et al., 2010). Thirdly, it has been proposed that in bodily fluids hCC acts as a carrier of soluble A $\beta$ , thereby preventing A $\beta$  aggregation and the formation of amyloid plaques (Tizon et al., 2010).

However, although it has been demonstrated that hCC can prevent A $\beta$  amyloid formation, a separate study by Sun *et al.* (2008) has suggested that hCC actually increases aggregation of A $\beta$ . In the early stages of AD there is an increase in levels of cathepsins, due to an increase in activity in the endocytic pathway. However, at the same time, hCC acts as an inhibitor for the cysteine protease cathepsin B, which, crucially, is involved in the degradation of A $\beta$  (Sun et al., 2008). Silencing the CST3 gene was shown to lower the levels of soluble A $\beta$ , as well as lowering the plaque load and relative abundance of A $\beta$ <sub>1-42</sub> in hAPP-J20 mice. These beneficial effects were not seen when the gene encoding cathepsin B (*CatB*) was also knocked out, indicating that inhibition of cathepsin B by hCC is used to regulate A $\beta$  degradation, and consequently levels of soluble A $\beta$ .

It is suggested that the disparity between these results, with both overexpression of hCC and silencing of the CST3 gene being able to reduce A $\beta$  plaque load is due to two separate mechanisms by which hCC regulates levels of soluble and insoluble A $\beta$  (Sun et al., 2008). Levels of soluble A $\beta$  could be regulated through degradation by cathepsin B, whereas levels of insoluble A $\beta$  could be regulated through direct binding of hCC to A $\beta$ .

#### 1.4.2.2. Transthyretin and A $\beta$

Transthyretin (TTR), otherwise known as pre-albumin, is a transporter of thyroid hormones from blood plasma into the CSF, of which it is the major component, as well as transport of retinol binding proteins in plasma (Hamilton and Benson, 2001). TTR is active as a homotetramer. There are several disease related mutations of TTR which lead to amyloidogenic diseases such as familial amyloid polyneuropathy and senile systemic amyloidosis. Most of these variants form normal tetrameric structures (Hornberg et al., 2000), and have normal function. It is therefore the increased propensity of the mutant proteins to dissociate and their ability to misfold that results in disease, not their inability to fold and function (Babbes et al., 2008, Du and Murphy, 2010). Although details of the disease mechanism remain unclear, it is thought to be associated with TTR aggregation causing toxic gain of function (Hammarstrom et al., 2001, Reixach et al., 2004, Sousa et al., 2001). TTR is secreted into the blood by the liver, whereas the choroid plexus secretes the protein into the CSF, suggesting different sources for amyloidogenic TTR (Babbes et al., 2008).

There is significant evidence to show that there is a functional interaction with A $\beta$ , and it is proposed that TTR could sequester A $\beta$  thereby inhibiting its aggregation and neurotoxicity (Schwarzman et al., 1994). Neuronal TTR transcription is increased in AD as well as Tg2576 transgenic mice which express the Swedish mutation of APP, and the increased levels of TTR in these mice is linked to neuroprotection (Stein et al., 2004, Stein and Johnson, 2002). Co-expression of TTR and A $\beta$  in *C. elegans* resulted in a significant reduction in amyloid deposits, and reversed the abnormal mobility seen in A $\beta$ -expressing worms (Link, 1995). In APP23 mouse models, over-expression of TTR suppressed both the behavioural and neuropathological abnormalities normally seen in these mice, whereas silencing the *ttr* gene accelerated the appearance of A $\beta$ -associated neuropathology (Choi et al., 2007, Buxbaum et al., 2008). In addition to these studies, TTR-A $\beta$  complexes have been isolated from both transgenic mouse and AD patient brains (Li et al., 2011). *In vitro* studies have demonstrated the inhibition of both A $\beta$ <sub>1-40</sub> and A $\beta$ <sub>1-42</sub> cytotoxicity through pre-incubation with TTR using a range of techniques (Mazurkolecka et al., 1995, Giunta et al., 2005, Costa et al., 2008, Li et al., 2011) and TTR has been shown to inhibit A $\beta$  fibrillisation at sub-stoichiometric ratios (Liu and Murphy, 2006). A reduced number of short aggregates with a similar linear morphology

to mature fibrils were formed, suggesting TTR suppresses aggregate growth but not the initial assembly.

Although it is clear that there is an interaction between WT TTR and A $\beta$ , there is conflicting evidence over which species of the respective proteins are interacting. Surface plasmon resonance (SPR) experiments have indicated that immobilised A $\beta$  monomers and fibrils will bind to both TTR monomer and tetramer; however, ELISA assays have suggested that binding is monomer specific (Buxbaum et al., 2008, Du and Murphy, 2010). Solution NMR, in conjunction with both liquid- and solid-phase assays have determined the binding of both A $\beta$  monomer and oligomers to variants of TTR with varying degrees of stability (Li et al., 2013). It is proposed that the A $\beta$  binding site involves amino acids in and around the T4 thyroxine binding site within the TTR tetramer; when this site is occupied by small molecules A $\beta$  binding is less effective. This corresponds to the binding region identified by Du *et al.* (2012) through site-directed mutagenesis and peptide array. Binding of the A $\beta$  monomer to TTR tetramer prevents A $\beta$  seed formation at sub-stoichiometric concentrations. Previous studies have suggested that in order for the A $\beta$  to bind, the TTR tetramer needs to dissociate to monomer, and that the binding of A $\beta$  actually causes this dissociation (Yang et al., 2013). A more recent analysis suggests that at physiological levels of monomer and tetramer, tetramer binding will dominate although binding constants for tetramer association are several orders of magnitude lower than that for monomers (Li et al., 2013). It is possible that this balance may change on the cell surface as the disease progresses as it is notable that TTR monomers interact with oligomeric A $\beta$  whereas tetrameric TTR interacts with monomeric A $\beta$ . As with hCC, tight binding was only observed when A $\beta$  was immobilised on either an ELISA plate or a chromatography column.

#### 1.4.2.3. Neuroserpin and A $\beta$

Another protein component of extracellular A $\beta$  amyloid plaques is the extracellular serine protease inhibitor neuroserpin (Kinghorn et al., 2006). As indicated by its name, neuroserpin is neuron-specific, therefore ideally placed to interact with A $\beta$ . Mutated versions of the inhibitor cause an inclusion body dementia known as familial encephalopathy with neuroserpin inclusion bodies (Davis et al., 1999). A specific binary complex is formed between A $\beta$ <sub>1-42</sub> and neuroserpin with a 1:1 stoichiometry (Kinghorn et al., 2006). The target serine protease of neuroserpin is tissue plasminogen activator;

inhibitory activity against the protease is irreversibly inactivated through neuroserpin binding to A $\beta$ . A distinctive characteristic of the serpin super-family is loop-sheet polymerisation, where homopolymers are formed at high temperatures; this is also inhibited through interaction with A $\beta$ . It is therefore proposed that this region is involved in the interaction i.e.  $\beta$ -strand A. The binding area in A $\beta$  is likely to be in the N-terminal or middle region, however this is difficult to determine due to the promiscuity of serpin interactions. A $\beta$  fibril formation is inhibited through interaction with neuroserpin, and there is a reduction in cytotoxicity in both cell culture and *in vivo* *Drosophila* models (Kinghorn et al., 2006), suggesting neuroserpin could play a neuro-protective role in AD. Aggregation of A $\beta$  is accelerated with the addition of neuroserpin, however the species formed have a distinctly different appearance to mature fibrils (small amorphous aggregates) and so it is proposed these are off-pathway non-toxic oligomers.

#### 1.4.3.4. Prion and A $\beta$

In contrast to the other systems discussed here, the direct high affinity interaction between A $\beta$  and cellular prion protein (PrP<sup>C</sup>) is thought to mediate A $\beta$  toxicity (Lauren et al., 2009, Gimbel et al., 2010). Although A $\beta$  amyloid plaques can form in PrP knockout mice, neurotoxicity and AD pathology do not develop. PrP<sup>C</sup> is GPI-anchored to the cell membrane and acts as a receptor for A $\beta$  oligomers, facilitating synaptic dysfunction, however PrP<sup>C</sup> is not the only cell surface molecule that binds A $\beta$  oligomers (Lauren et al., 2009). Amyloid plaques from AD patient brains have been found to contain both A $\beta$  and PrP<sup>C</sup> (Zou et al., 2011, Ferrer et al., 2001). PrP<sup>C</sup> is thought to bind selectively to A $\beta$  oligomers with nanomolar affinity (Lauren et al., 2009), inhibiting fibril formation by trapping the A $\beta$  in a  $\beta$ -sheet rich toxic oligomeric form (Younan et al., 2013). PrP<sup>C</sup> has three domains that are associated with different activities. The N-terminal domain contributes to extracellular copper binding (Viles et al., 1999), whilst the unstructured central domain has been associated with maintaining the structural integrity of myelin via binding to an unknown receptor (Baumann et al., 2007). The globular C-terminal domain is GPI-anchored to the plasma membrane. The A $\beta$ -binding site on PrP<sup>C</sup> has been mapped to the natively unstructured N-terminal by solution NMR (Younan et al., 2013) which corresponds to regions previously identified by site-directed spin labelling and SPR (Chen et al., 2010).

## 1.5. Overview of Thesis

The overall aim of this project was to characterise the interaction between A $\beta$  and hCC. A role for hCC in the pathology of AD has been suggested by the genetic linkage of the hCC gene with late onset AD and the observation of co-localisation of hCC and A $\beta$  in amyloid deposits in AD brain. It has been suggested that hCC plays a neuro-protective role in AD due to direct inhibition of A $\beta$  oligomer and fibril formation. Uncovering the details of this association, and comparing the mechanism of inhibition with other systems could lead to the development of a novel therapeutic intervention.

Previous work has identified that the interaction between hCC and A $\beta$  may not be a simple monomer-monomer interaction as had been proposed in the literature. An alternative hypothesis that the amyloidogenic propensity of inhibitory proteins might not be coincidence by looking not only at hCC monomers but also the different species populated during fibrillisation. This required a more in-depth study of the fibrillisation pathway which is described in Chapter 4 along with an initial characterisation of the fibrils formed by this protein by limited proteolysis.

The initial stages of this project were devoted to the development of a protocol to produce recombinant A $\beta$ <sub>1-40</sub> using a ubiquitin tag, which is described in detail in Chapter 3. Chapter 5 then investigates the interaction of A $\beta$  with hCC and begins with an analysis of the kinetics of fibrillisation of A $\beta$  in the presence of its inhibitor. The reactions are monitored using fluorescence assays, EM and analytical size exclusion chromatography experiments. Finally the interaction of the two species is examined using NMR <sup>15</sup>N-HSQC spectroscopy.

## **Chapter Two: Materials and Methods**

This chapter includes details of common experimental procedures throughout the work presented in this thesis. Further details of the materials and methods that are relevant to specific experiments are found in each chapter.

### **2.1. Buffers and Reagents**

All reagents were purchased from Fisher, Melford or Sigma-Aldrich, unless stated otherwise. Deionised water (18.2Ω) from an Elga Purelab 611 Classic UVF was used throughout all experiments and buffers were prepared as described in Sambrook et al. (1989) and filtered through a 0.2 μm filter. 1 mM sodium azide (NaN<sub>3</sub>) was added to all buffers, except those used for bacterial growth or cell assays.

### **2.2. DNA Manipulation**

#### **2.2.1. Expression Vectors**

##### **2.2.1.1. Wild type and L68Q hCC**

Wild type hCC cloned into the pIN-III-ompA periplasmic expression system was provided by Dr Adham Elshawaihde. Expression was carried out in *E. coli* BL21 strain for which an efficient purification had been established (Elshawaihde, 2012). Previous work had removed the rare codons found in genes for human proteins to allow expression in this strain. Site-directed mutagenesis was carried out on the wild type plasmid to produce the L68Q variant.

##### **2.2.1.2. His<sub>6</sub>Ub-Aβ<sub>1-40</sub> and GST-YUH1**

GST-tagged YUH1 cloned into pGEX-6p-1 and His<sub>6</sub>Ub-Aβ<sub>1-40</sub> cloned into pET28a were provided by Dr Maho Yagi-Utsumi (Okazaki Institute for Integrative Bioscience). Expression of both constructs was carried out in *E. coli* Rosetta (DE3) pLysS.

#### **2.2.2. Plasmid Extraction**

Plasmid DNA was extracted from 5 ml overnight growths using a QIAprep Spin Miniprep kit (Qiagen) according to the manufacturer's protocol. The plasmid was eluted using sterilised H<sub>2</sub>O, quantified and stored at -20°C.

#### **2.2.3. Primer Sequences**

The primer sequences used for sequencing purposes and for the production of the L68Q mutation in hCC are shown in Table 2.1.

Primer	Sequence	T <sub>m</sub> (°C)	Notes
hCC-F	GCTAGAGAGGCTTTACAC	51.2	Forward sequencing primer
hCC-R	CCTGAACGTCGGAACGCATTG	71.8	Reverse sequencing primer
L68Q-F	TGGACGTGGAGCAGGGCCGAACCAC	71.2	Forward mutagenesis primer
L68Q-R	GTGGTTCGGCCCTGCTCCACGTCCA	71.2	Reverse mutagenesis primer

**Table 2.1 Primer Sequences**

#### 2.2.4. Quantification of DNA

DNA concentration was calculated by measuring the absorbance at 260 nm using a Varian Cary 50-Bio UV-Visible spectrophotometer. An absorbance reading of 1 was taken as being equivalent to a nucleotide concentration of 50 µg/ml. Protein contamination was calculated using the ratio  $A_{260}/A_{280}$ . If this was greater than 1.7 then DNA samples were taken as being free from contamination.

#### 2.2.5. Competent Cells

##### 2.2.5.1. Preparation of Competent Cells

The *E. coli* strain XL10 Blue was routinely used for plasmid production and mutagenesis experiments. The strain BL21 was used for expression of hCC (both wild-type and L68Q mutant). The strain Rosetta (DE3) pLysS was used for expression of GST-YUH1 and His<sub>6</sub>Ub-Aβ<sub>1-40</sub>.

An LB agar streak plate was produced using non-competent cells from glycerol cell stocks and incubated overnight at 37°C. A single colony was used to inoculate 5ml of LB and incubated overnight at 37°C with shaking at 200 r.p.m. 10 ml of LB was inoculated with 200 µl of the overnight culture and grown at 37°C with shaking until OD<sub>600</sub> = 0.6 and then incubated on ice for 5 minutes. After centrifugation at 1,663 x g at 4°C for 10 minutes, the pellet was re-suspended in 3.3 ml of RF1 buffer and incubated on ice for 30 minutes. After further centrifugation at 1,663 x g at 4°C for 10 minutes, the pellet was re-suspended in 1 ml RF2 buffer and incubated on ice for 30 minutes. The sample was frozen at -80°C in 200 µl aliquots.

RF1 Buffer pH 5.8    30 mM KCH<sub>3</sub>CO<sub>2</sub>, 100 mM RbCl, 10 mM CaCl<sub>2</sub>, 50 mM MnCl<sub>4</sub>,  
15% glycerol

RF2 Buffer pH 6.5    10 mM MOPS, 10 mM RbCl, 75 mM CaCl<sub>2</sub>, 15% glycerol

### **2.2.5. Site-Directed Mutagenesis**

Site-directed mutagenesis was performed using a Quikchange Mutagenesis Kit (Qiagen) to the manufacturer's instructions.

### **2.2.6. Transformations**

1.5 µl of plasmid DNA was added to 200 µl of competent cells in a 14 ml polypropylene Falcon tube on ice and incubated for 30 minutes. The cells were heat shocked at 42°C for 90 seconds and then incubated on ice for 2 minutes. 800 µl of non-selective LB was added and incubated at 37°C with shaking for 90 minutes. Aliquots of 100 µl, 10 µl and 1 µl (diluted in fresh LB) were plated out on selective plates and grown overnight at 37°C.

### **2.2.7. DNA Sequencing**

Sequencing was carried out by the Core Genomic Centre, Medical School, University of Sheffield, Sheffield, UK.

## **2.3. Growth Media and Solutions**

### **2.3.1. Luria-Bertani Media**

Per litre of deionised water:

tryptone	10 g
yeast extract	5 g
NaCl	10 g

The solution was adjusted to pH 7.0, made up to 1 litre with deionised water and sterilised by autoclaving. Antibiotic was added after cooling. If LB-agar was required, 28 g Nutrient Agar (Oxoid Ltd, UK) was made up to 1 litre with deionised water and autoclaved.

### **2.3.2. M9 Minimal Media**

Per litre of deionised water:

Na <sub>2</sub> HPO <sub>4</sub>	6 g
KH <sub>2</sub> PO <sub>4</sub>	3 g
NaCl	0.5 g

The solution was adjusted to pH 7.4 and the volume made up to 1 litre before sterilisation by autoclaving.

The following were added to the media immediately before use (per litre):

trace elements	650 µl	(autoclaved)
glucose	2g	
10 mg/ml thiamine	0.1 ml	
0.5 mg/ml (NH <sub>4</sub> ) <sub>2</sub> SO <sub>4</sub>	2 ml	(Cambridge Isotope Laboratories)
1 M MgSO <sub>4</sub>	1 ml	(autoclaved)
1 M CaCl <sub>2</sub>	0.1 ml	(autoclaved and added last)

All solutions were 0.2 µm filter-sterilised before use except where autoclaved as indicated. The flask was swirled immediately to disperse precipitate; if precipitate did not disperse then the preparation was abandoned.

#### 2.3.2.1. Trace Elements

Per 100 ml deionised water:

CaCl <sub>2</sub> .2H <sub>2</sub> O	550 mg
MnSO <sub>4</sub> .H <sub>2</sub> O	140 mg
CuSO <sub>4</sub> .5H <sub>2</sub> O	40 mg
ZnSO <sub>4</sub> .H <sub>2</sub> O	220 mg
CoCl <sub>2</sub> .6H <sub>2</sub> O	45 mg
Na <sub>2</sub> MoO <sub>4</sub> .2H <sub>2</sub> O	26 mg
H <sub>3</sub> Bo <sub>4</sub>	40 mg
KI	26 mg

The above were added to 70 ml of deionised water and the pH adjusted to 8.0 before adding:

EDTA	500 mg
------	--------

The pH was again adjusted to 8.0 before adding:

FeSO <sub>4</sub> .7H <sub>2</sub> O	375 mg
--------------------------------------	--------

The solution was made up to 100 ml with deionised water before autoclaving.

### **2.3.3. Antibiotic Solutions**

#### **2.3.3.1. Ampicillin**

100 mg/ml ampicillin sodium salt was dissolved in water to produce a 1000 x stock solution, and 0.2  $\mu\text{m}$  filter-sterilised. Aliquots were stored at  $-20^{\circ}\text{C}$ , then gently thawed and added to growth media to a final concentration of 100  $\mu\text{g}/\text{ml}$  as required.

#### **2.3.3.2. Kanamycin**

15 mg/ml kanamycin was dissolved in water to produce a 1000 x stock solution and 0.2  $\mu\text{m}$  filter-sterilised. Aliquots were stored at  $-20^{\circ}\text{C}$ , then gently thawed and added to growth media to a final concentration of 15  $\mu\text{g}/\text{ml}$  as required.

#### **2.3.3.3. Chloramphenicol**

25 mg/ml chloramphenicol was dissolved in ethanol to produce a 1000 x stock solution. Aliquots were stored at  $-20^{\circ}\text{C}$ , then gently thawed and added to growth media to a final concentration of 25  $\mu\text{g}/\text{ml}$  as required.

#### **2.3.4. Isopropyl- $\beta$ -D-galactosidase (IPTG)**

120 mg/ml isopropyl- $\beta$ -D-galactosidase was dissolved in water to produce a 1 M stock solution, and 0.2  $\mu\text{m}$  filter-sterilised. Fresh solution was added to growth media as required to induce protein over-expression.

## 2.4. Protein Expression and Purification

### 2.4.1. Protein Characteristics

Predicted extinction coefficients (calculated from the primary sequence of the protein using ProtParam on the ExPASy Proteomics Server (Gasteiger et al., 2005)) and molecular weights obtained from mass spectrometry are shown in Table 2.2.

<b>Protein</b>	<b>Extinction Coefficient at 280 nm (M<sup>-1</sup> cm<sup>-1</sup>)</b>	<b>Molecular Weight (Da)</b>
<b>hCC</b>	11 050	13,344
<b>hCC L68Q</b>	11 050	13,362
<b>GST-YUH1</b>	62 700	52,313.8
<b>His<sub>6</sub>Ub-A<math>\beta</math><sub>1-40</sub></b>	2 600	16,364.5
<b>A<math>\beta</math><sub>1-42</sub></b>	1 490	4,514.6
<b>A<math>\beta</math><sub>1-40</sub></b>	1 490	4,329.8

**Table 2.2. Predicted Protein Characteristics**

### 2.4.2. Cystatin C

#### 2.4.2.1. Over-expression

Single colonies of *E. coli* BL21 were used to inoculate 10 ml of LB broth. Cultures were grown overnight aerobically at 37°C. 10 ml of each starter culture was used to inoculate 600 ml of M9 minimal media. The total growth was 4.8 litres. Cultures were grown at 37°C with shaking at 200 r.p.m. Cell growth was monitored by measuring the OD<sub>600</sub>, and expression cultures were induced with 75  $\mu$ M IPTG when OD<sub>600</sub> = 0.4 – 0.6 and grown for 5 hours.

#### 2.4.2.2. Periplasmic Extraction

Cells were harvested by centrifugation at 18,592 g (4°C) for 10 minutes and the pellets re-suspended in 14 ml 20% sucrose, 0.2 M Tris pH 8.0. The suspension was centrifuged at 48,384 x g (20 °C) for 15 minutes and pellets re-suspended in 28 ml of cold 2 mM EDTA pH 8.0. Phenylmethylsulphonyl fluoride (PMSF) was added immediately to give a final concentration of 1 mM. After re-suspension, the sample was centrifuged at 48,384 x g at 4 °C for 15 minutes. The supernatant was recovered and protease inhibitors (EDTA-free, 1 tablet per 50ml), 0.1 mg/ml DNase and 20 mM MgCl<sub>2</sub> were

added. The sample was dialysed into cold 10 mM sodium phosphate buffer pH 7.0 to remove small molecules.

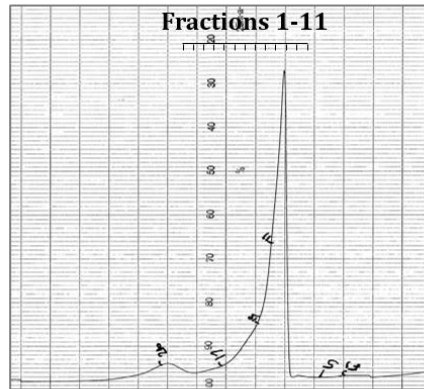
#### 2.4.2.3. Cation Exchange Chromatography

Cold periplasmic extract was loaded onto a 100 ml SP-Sepharose (Pharmacia) cation exchange column, which had been equilibrated with cold 10 mM sodium phosphate buffer pH 7.0, at a rate of 2 ml/min. The column was washed with 10 mM sodium phosphate pH 7.0 until  $A_{280}$  of the eluent reached the baseline. 10 mM sodium phosphate buffer pH 7.0, 0.2 M NaCl was used to elute hCC, and 5 ml fractions collected. Any remaining bound protein was eluted with sodium phosphate buffer pH 7.0, 1 M NaCl. Fractions were analysed by SDS-PAGE and those containing hCC were pooled and stored at  $-20^{\circ}\text{C}$ .

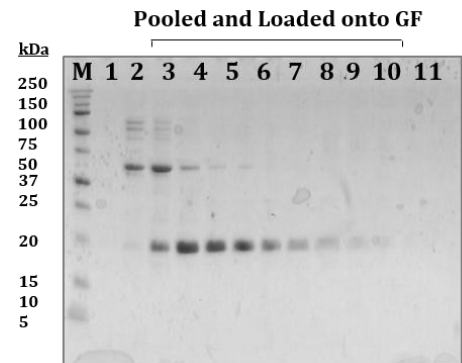
#### 2.4.2.4. Size-Exclusion Chromatography

The pooled sample was concentrated to a volume of 10 ml using an Amicon ultra-filtration stirred-cell device in conjunction with a Millipore regenerated cellulose membrane with a molecular weight cut-off of 10,000 Da and filtered using a 0.2  $\mu\text{m}$  filter. The sample was loaded onto a 400 ml preparative Superdex 75 gel filtration column (GE Healthcare), which had been equilibrated with 10 mM sodium phosphate buffer pH 6.0, 0.1 M NaCl. Buffer was run through the column at a rate of 3 ml/min and 6 ml fractions collected. The fractions were analysed using SDS-PAGE and any containing hCC were pooled. The average yield of hCC was 1-2 mg per litre of cell growth.

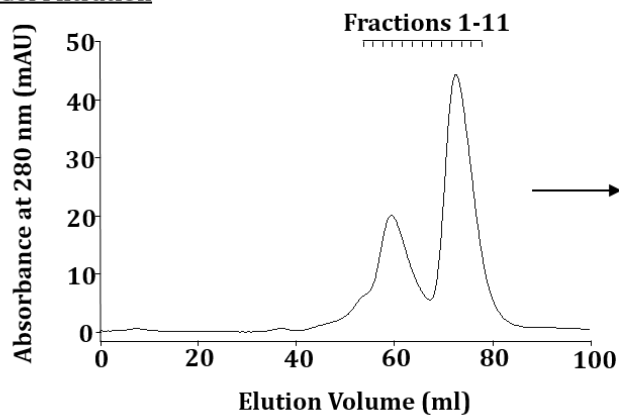
**A. SP-Sephrose**



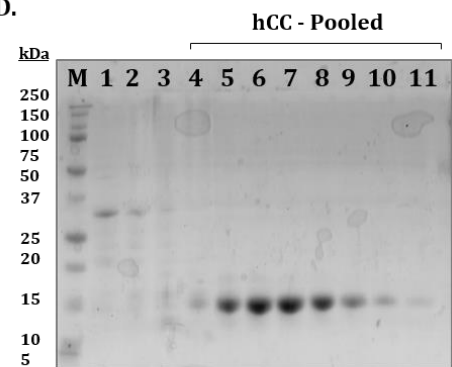
**B.**



**C. Gel Filtration**



**D.**



**E. SEC-HPLC**

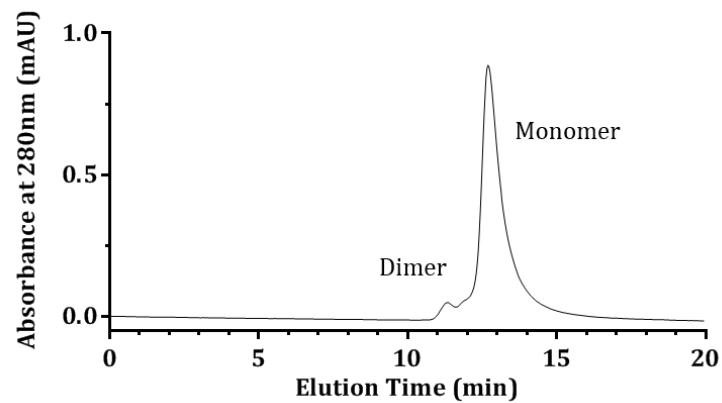


**Figure 2.1. Purification of hCC**

*Elution profile (A) of hCC from SP-sepharose ion exchange chromatography. SDS-PAGE (B) of ion exchange fractions 1-11. Elution profile (C) of size exclusion chromatography and SDS-PAGE (D) analysis for fractions 1-11. SEC-HPLC trace (E) showing purity and oligomeric state of purified hCC.*

## 2.5. Protein Procedures

### 2.5.1. SDS Polyacrylamide Gel Electrophoresis

All electrophoresis was carried out using a Bio-Rad Mini Protean II apparatus.

#### 2.5.1.1. SDS-PAGE Buffers

4x Upper Buffer	0.5 M Tris HCl pH 6.8, 0.4% (w/v) SDS
4x Lower Buffer	1.5 M Tris HCl pH 8.8, 0.4% (w/v) SDS
Running Buffer	25 mM Tris HCl pH 8.3, 190 mM glycine, 0.1% (w/v) SDS
2x Loading Buffer	100 mM Tris HCl pH 6.8, 200 mM DTT, 4% (w/v) SDS, 0.2% (w/v) bromophenol blue, 30% (v/v) glycerol. 200µl aliquots were frozen at -20°C and defrosted as required.
Stain	45% (v/v) methanol, 10% (v/v) acetic acid, 0.25% (w/v) Coomassie Brilliant Blue R250
De-Stain	45% (v/v) methanol, 10% (v/v) acetic acid

#### 2.5.1.2. Gel Preparation

4% stacking gels were cast above 16% resolving gels as described below:

16% Resolving gel (per gel):

2.5 ml 4x Lower Buffer

4 ml 40% acrylamide (acrylamide: bisacrylamide ratio 37.5:1) (Bio-Rad)

Make up to 10 ml and shake before adding:

100 µl 10% (w/v) ammonium persulphate (APS)

10 µl N, N, N', N'-tetramethylethylenediamine (TEMED) (Bio-Rad)

4% Stacking gel (per gel):

2.5 ml 4x upper buffer

1.1 ml 40% acrylamide (acrylamide: bisacrylamide ratio 37.5:1) (Bio-Rad)

Make up to 10 ml and shake before adding:

100 µl 10% (w/v) ammonium persulphate (APS)

10 µl N, N, N', N'-tetramethylethylenediamine (TEMED) (Bio-Rad)

Samples were typically prepared with a 1:1 ratio of 2x loading buffer to protein solution, and 5 – 20 µl were loaded depending on the sample concentration. Samples

were not heated prior to loading, as this has been observed to promote oligomerisation of cystatins (Dr Rosie Staniforth, personal communication). A $\beta$ <sub>1-40</sub> is also prone to aggregation, therefore A $\beta$  samples were not heated either. Gels were run with 1x running buffer at 180 V for 55 minutes. Gels were then stained on a rotating platform for 1 hour, and de-stained until clear bands could be seen.

### 2.5.1.3. SDS-PAGE Molecular Weight Marker

Bio-Rad pre-stained Precision Plus Protein Dual Xtra Standards were used, with typical mass values as below:

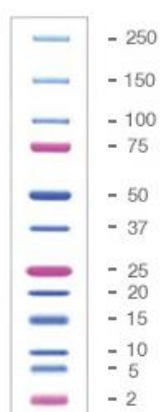


**Figure 2.2. Precision Plus Protein Dual Xtra Standards (Bio-Rad)**

## 2.5.2. Tricine SDS Polyacrylamide Gel Electrophoresis

### 2.5.2.1. Tricine SDS-PAGE Buffers

Gel Buffer	3 M Tris HCl pH 8.45 0.3% (w/v) SDS
Anode Buffer	0.2 M Tris HCl pH 8.9
Cathode Buffer	0.1 M Tris HCl pH 8.25, 0.1 M tricine, 0.1% (w/v) SDS
2x Loading Buffer	100 mM Tris/HCl pH 6.8, 200 mM DTT, 4% (w/v) SDS, 0.2 % (w/v) bromophenol blue, 30 % (v/v) glycerol. 200 $\mu$ l aliquots were frozen at -20°C and defrosted as required.
Stain	45% (v/v) methanol, 10% (v/v) acetic acid, 0.25% (w/v) Coomassie Brilliant Blue R250
De-Stain	45% (v/v) methanol, 10% (v/v) acetic acid

### 2.5.2.2. Gel Preparation

A 4% stacking gel was cast above a 10% spacer gel and a 16.5% separating gel as described below:

16.5% Separating gel (per gel):

- 1.3 g glycerol
- 3.3 ml gel buffer
- 4.1 ml 40% acrylamide (acrylamide: bisacrylamide ratio 19:1) (Bio-Rad)
- 800 µl 2% bisacrylamide

Make up to 10 ml and shake before adding:

- 100 µl 10% (w/v) ammonium persulphate (APS)
- 10 µl N, N, N', N'-tetramethylethylenediamine (TEMED) (Bio-Rad)

10% Spacer gel (per gel):

- 1.65 ml gel buffer
- 493 µl 40% acrylamide (acrylamide: bisacrylamide ratio 37.5:1) (Bio-Rad)
- 43.5 µl 2% bisacrylamide

Make up to 5 ml and shake before adding:

- 55 µl 10% (w/v) ammonium persulphate (APS)
- 5.5 µl N, N, N', N'-tetramethylethylenediamine (TEMED) (Bio-Rad)

4% Stacking gel (per gel):

- 1.25 ml gel buffer
- 4.1 ml 40% acrylamide (acrylamide: bisacrylamide ratio 37.5:1) (Bio-Rad)
- 110 µl 2% bisacrylamide

Make up to 10 ml and shake before adding:

- 50 µl 10% (w/v) ammonium persulphate (APS)
- 5 µl N, N, N', N'-tetramethylethylenediamine (TEMED) (Bio-Rad)

Samples were typically prepared with a 1:1 ratio of 2x loading buffer to protein solution, and 5 – 20 µl were loaded depending on the sample concentration. Anode buffer was added to the outer chamber (positive electrode) and cathode buffer was added to the inner chamber (negative electrode) of the gel apparatus. Gels were run at 180 V for 55 minutes. The gels were then stained on a rotating platform for 1 hour, and de-stained until clear bands could be seen.

### **2.5.3. Determination of Protein Concentration**

The concentration of protein was determined by measuring the UV absorption spectra at 280 nm using a Varian Cary 50-Bio UV-Visible spectrophotometer. Protein concentration was calculated using the Beer-Lambert law:

$$A = \epsilon l c$$

where A is the absorbance, c is the concentration (M),  $\epsilon$  is the molar extinction coefficient ( $M^{-1} \text{ cm}^{-1}$ ) and l is the pathlength (cm).

### **2.5.4. Protein Concentration and Buffer Exchange**

An Amicon ultra-filtration stirred-cell was used in conjunction with the appropriate molecular weight cut-off (MWCO) filter to concentrate large volumes (greater than 15 ml). For smaller volumes a Vivaspin centrifugal concentrator (Generon) was used for both concentration and buffer exchange. The MWCO was normally 10 kDa, however for purification of hCC oligomers 100,000 Da and 1,000,000 Da MWCO Vivaspin centrifugal concentrators with a volume of 0.5 ml were used. Buffer exchange was achieved either through dialysis using Spectra/Por dialysis tubing with a 6 – 8 kDa MWCO or with repeated rounds of concentration and dilution into the required buffer.

### **2.5.5. Analytical Size Exclusion Chromatography**

Protein samples were tested for purity by size exclusion high-pressure liquid chromatography (SEC-HPLC). 20  $\mu\text{l}$  samples were analysed using a Shodex KW803 column and KW-G guard column (Shodex, Japan) with a Perkin Elmer Series 200 HPLC system equipped with a UV-visible absorbance detector. Specific HPLC experiments are discussed further in the appropriate chapters.

## **2.6. Spectroscopic Techniques**

### **2.6.1. Fluorescence Spectroscopy**

Thioflavin T (ThT) fluorescence measurements were taken on either a Cary Eclipse fluorimeter (Varian, UK) or a Fluostar Omega plate-reader (BMG Labtech, UK). In the fluorimeter, spectra were recorded at time-points with an excitation wavelength of 442 nm. Emission spectra were recorded from 400-600 nm and emission values at 482 nm were plotted as a function of time to follow the rate of fibril formation. On the plate-reader single readings were taken rather than the whole spectrum, with an excitation

wavelength of 442 nm and an emission wavelength of 482 nm. Further details on specific fluorescence experiments are provided in the relevant chapters.

### **2.6.2. Nuclear Magnetic Resonance (NMR)**

NMR spectra were recorded on a Bruker DRX spectrometer operating at 600 MHz controlled using XWinNMR (Bruker) and NMR data was processed using Felix (Accelrys). Experiments are discussed in further detail in the appropriate chapter.

### **2.6.3. Transmission Electron Microscopy (TEM)**

Carbon-coated copper grids (Agar Scientific) were glow-discharged with 3x 15 second pulses using a Cressington 208 glow-discharge unit. Samples were adsorbed on a freshly glow-discharged grid for 1 minute and blotted. Grid was washed shortly in two drops of water and two drops of 0.75% uranyl formate and blotted between each wash; grid was held in the final drop of 0.75% uranyl formate for 20 seconds and dried with gentle vacuum suction after blotting. A Philips CM-100 electron microscope, operating at 100 kV and equipped with a 1024 x 1024 pixel Gatan CCD camera, was used to record micrographs.

## Chapter Three: Purification of A $\beta$ <sub>1-40</sub> Using a Ubiquitin Tag

### 3.1. Introduction

A $\beta$  is a difficult protein to produce and work with due to its hydrophobicity, low solubility and propensity to aggregate; it has been rightly described as the ‘peptide from hell’ (Zagorski et al., 1999). Synthetic methods of peptide production often lead to high degrees of variability within different preparations causing discrepancies between results due to the presence of minor impurities. These can include salts, metals, truncated products and partial racemisation. Finder et al. (2010) demonstrated that synthetic A $\beta$ <sub>1-42</sub> is less toxic *in vivo* and to cultured rat primary cortical neurons than recombinant A $\beta$ <sub>1-42</sub>, in addition to lengthening fibrillogenesis *in vitro*. It is therefore highly desirable to produce large quantities of the peptide recombinantly, to allow us to model physiological conditions as accurately as possible. Moreover a recombinant system allows easy isotopic labelling for NMR purposes, greatly reducing the cost of these experiments as such peptides are expensive to purchase. The quality of the expression and purification methods still affect the process significantly, with some authors reporting large variations between samples while others claim high reproducibility, with A $\beta$ <sub>1-40</sub> and A $\beta$ <sub>1-42</sub> alike (Hortschansky et al., 2005, Hellstrand et al., 2009).

There are a number of expression systems for both A $\beta$ <sub>1-42</sub> and A $\beta$ <sub>1-40</sub> reported in the literature, some of which are listed in Table 3.1. Most of these use a protein tag to increase the solubility of the A $\beta$  and allow expression of high levels of protein in *E. coli*. This fusion tag is then cleaved at a specific protease site that has been incorporated into the construct, producing A $\beta$  peptide. In most instances the peptide is separated from the cleavage mixture by reverse-phase HPLC. The purity of the resulting peptide is established by a variety of methods including MALDI-TOF MS, SDS-PAGE and NMR.

The system used in this thesis was first described in Lee et al. (2005) for the purification of A $\beta$ <sub>1-42</sub>, and since then has been shown to also be successful for the purification of A $\beta$ <sub>1-40</sub> (Utsumi et al., 2009). The peptide is expressed with an ubiquitin tag, increasing the solubility and stability of the A $\beta$ <sub>1-40</sub> and allowing high levels of protein to be expressed and purified. The addition of this larger protein also makes the peptide less susceptible to hydrolysis by proteolytic enzymes. As bacteria do not contain ubiquitin, and therefore do not contain de-ubiquitinating enzymes, this is an ideal system for

protein expression and purification. Ubiquitin has also been used as a tag for A $\beta$  purification in conjunction with GroES and trigger factor (Shahnawaz et al., 2007, Thapa et al., 2008), however in these instances ubiquitin is used to allow specific cleavage of the A $\beta$  from the fusion protein rather than to aid expression.

Reference	Yield (mg/l growth)	Fusion Construct	Final Purification Step	Analysis
Finder et al. (2010)	22	His <sub>6</sub> -(NANP) <sub>19</sub> -TEV protease recognition site-A $\beta$	RP-HPLC	MALDI-TOF MS, RP-HPLC, protein sequencing
Hortschansky et al. (2005)	0.7-0.8 mg/g cells	His <sub>6</sub> -MBP-TEV protease recognition site-A $\beta$	RP-chromatography	SDS-PAGE, RP- HPLC, MS, protein sequencing
Shahnawaz et al. (2007)	15	His <sub>6</sub> -GroES-ubiquitin- A $\beta$	RP-HPLC	SDS-PAGE, MALDI-TOF MS
Thapa et al. (2008)	8	His <sub>6</sub> -trigger factor- ubiquitin-A $\beta$	RP-HPLC	PAGE, MALDI-TOF MS
Nagata-Uchiyama et al. (2007)	-	Lysozyme-linker- enterokinase cleavage site-A $\beta$	RP-HPLC	MALDI-TOF MS
Macao et al. (2008)	4	No tag; co-expressed with His <sub>6</sub> -tagged affibody ligand Z <sub>A<math>\beta</math>3</sub> ; exogenous initiating M	SEC	NMR, SDS-PAGE, SEC, MS
Walsh et al. (2009)	14	No tag; exogenous initiating M	Anion-exchange chromatography; SEC	SDS-PAGE, RP- HPLC, LC-MS, MALDI-TOF MS, protein sequencing
<b>Utsumi et al. (2009)</b>	<b>4</b>	<b>His<sub>6</sub>-ubiquitin-A<math>\beta</math></b>	<b>RP-HPLC</b>	<b>SDS-PAGE, RP- HPLC, N-terminal sequencing, NMR</b>
Garai et al. (2009)	4	His <sub>6</sub> -IFABP-linker- Factor Xa cleavage site-A $\beta$	RP-HPLC	SDS-PAGE, ESI-MS

**Table 3.1. Production Strategies for A $\beta$ <sub>1-40</sub>. Adapted from Finder et al. (2010).**

In the initial protocol the cleavage products were separated using reverse-phase HPLC to produce pure A $\beta$ <sub>1-40</sub>, however attempts to reproduce this proved unsuccessful. Several different purification methods were tried with mixed success before an effective system was established. This chapter describes the development of this system, with the final protocol for the production of A $\beta$ <sub>1-40</sub> shown in section 3.3.5.

## **3.2. Materials and Methods**

### **3.2.1. His<sub>6</sub>Ub-A $\beta$ <sub>1-40</sub> Construct**

The plasmid pET28a containing the His<sub>6</sub>Ub-A $\beta$ <sub>1-40</sub> construct was kindly provided by Dr Maho Yagi-Utsumi (Okazaki Institute for Integrative Bioscience). The construct consists of the gene encoding A $\beta$ <sub>1-40</sub> with the ubiquitin gene positioned at the 5'-end. This means that the A $\beta$ <sub>1-40</sub> is expressed with His<sub>6</sub>Ub at the N-terminal. The six histidines allow easy purification of the fusion protein by Ni<sup>2+</sup> affinity chromatography, and the ubiquitin tag increases the solubility and stability of the A $\beta$ <sub>1-40</sub> peptide. The tag is cleaved using the yeast hydrolase YUH1, which cuts specifically at the C-terminal end of the ubiquitin. The pGEX-6p-1 plasmid for GST-YUH1 was also provided by Dr Maho Yagi-Utsumi. The enzyme is expressed with a GST tag to aid purification by glutathione affinity chromatography.

### **3.2.2. Expression and Purification of GST-YUH1**

#### **3.2.2.1. Buffers**

Binding Buffer	50 mM Tris-HCl pH 8.0, 1 mM EDTA, 1 mM DTT
Glutathione Elution Buffer	50 mM Tris-HCl pH 8.0, 1 mM EDTA, 1 mM DTT, 20 mM reduced glutathione
Dialysis Buffer	50 mM Tris-HCl pH 8.0, 0.2 mM DTT

#### **3.2.2.2. Expression**

Single colonies of *E. coli* Rosetta were used to inoculate 5 ml of LB broth and the cultures were grown overnight aerobically at 37°C. Each starter culture was used to inoculate 1 litre of LB containing 50 µg/ml ampicillin and 25 µg/ml chloramphenicol. The cultures were grown at 37°C with shaking at 200 r.p.m. Cell growth was monitored by measuring the OD<sub>600</sub>, and expression cultures were induced with 0.5 mM IPTG when OD<sub>600</sub> = 0.7 – 0.9 and grown for 3 hours before harvesting.

### 3.2.2.3. Preparation of Cell Extract

The cells were harvested by centrifugation at 18,592 x g (4°C) for 10 minutes and the pellets re-suspended in binding buffer (40 ml per 1 litre of cell culture). The suspension was ruptured by sonication on ice for 5 x 2 minutes and the insoluble pellet isolated by centrifugation at 26,000 x g for 30 minutes at 4°C. The supernatant was recovered and pooled.

### 3.2.2.4. Glutathione Affinity Chromatography

Cold cell extract was loaded onto a 100 ml glutathione column (GE Healthcare) equilibrated with cold binding buffer at a flow rate of 2 ml/min. To ensure maximal binding, the flow-through was loaded onto the same column 3-4 times and then washed with binding buffer to prevent non-specific binding until the  $A_{280}$  reached the baseline. GST-YUH1 was eluted using elution buffer at a flow rate of 1 ml/min and 2 ml fractions collected. The fractions were analysed by SDS-PAGE and those containing GST-YUH1 were pooled, dialysed into dialysis buffer and stored at -20°C as 1 ml aliquots.

### 3.2.3. Expression and Purification of His<sub>6</sub>Ub-A $\beta$ <sub>1-40</sub>

#### 3.2.3.1. Buffers

Binding Buffer	50 mM Tris-HCl pH 8.0, 150 mM NaCl
Wash Buffer	50 mM Tris-HCl pH 8.0, 150 mM NaCl, 50 mM imidazole
Elution Buffer	50 mM Tris-HCl pH 8.0, 150 mM NaCl, 500 mM imidazole
Urea Buffer	50 mM Tris-HCl pH 8.0, 150 mM NaCl, 8 M urea
Dialysis Buffer	10 mM Tris-HCl pH 8.0, 1 mM EDTA

#### 3.2.3.2. Expression

The pET28a plasmid was transformed into *E. coli* Rosetta (DE3) pLysS and single colonies were grown overnight in 5 ml LB broth containing 15  $\mu$ g/ml kanamycin and 25  $\mu$ g/ml chloramphenicol at 37°C with shaking at 200 r.p.m. Each overnight culture was used to inoculate 1 litre of LB broth containing 15  $\mu$ g/ml kanamycin and 25  $\mu$ g/ml chloramphenicol and cultures were grown at 37°C with shaking at 200 r.p.m. until an OD<sub>600</sub> of 0.6 was reached. Expression of His<sub>6</sub>Ub-A $\beta$ <sub>1-40</sub> was induced by the addition of 0.5 mM IPTG, and cells were incubated for a further 3 hours before harvesting.

### 3.2.3.3. Preparation of Cell Extract

Cells were harvested by centrifugation at 18,592 x g (4°C) for 10 minutes and the pellets re-suspended in binding buffer (40 ml per 1 litre of cell culture) containing 1 mM PMSF. The suspension was ruptured by sonication on ice for 5 x 2 minutes and the insoluble pellet isolated by centrifugation at 26,000 x g for 30 minutes at 4°C. The supernatant was recovered and pooled. His<sub>6</sub>Ub-Aβ<sub>1-40</sub> was purified from both the supernatant and the insoluble pellet.

### 3.2.3.4. Ni<sup>2+</sup>-NTA Affinity Chromatography (Supernatant)

The cold cell extract was loaded onto a 20 ml Ni<sup>2+</sup>-NTA super-flow column (Qiagen) equilibrated with cold binding buffer at a rate of 2 ml/min. The column was washed with binding buffer until A<sub>280</sub> of the eluent reached the baseline, and then washed with wash buffer, again until the baseline was reached. His<sub>6</sub>Ub-Aβ<sub>1-40</sub> was eluted with elution buffer and collected in 2 ml fractions. Fractions were analysed by SDS-PAGE and those containing His<sub>6</sub>Ub-Aβ<sub>1-40</sub> were pooled and dialysed into dialysis buffer before storage at 4°C.

### 3.2.3.5. Ni<sup>2+</sup>-NTA Affinity Chromatography (Pellet)

The cell pellet was washed twice with binding buffer by centrifugation at 26,000 x g for 15 minutes at 4°C, and then re-suspended in urea buffer at room temperature (40 ml per 1 litre of culture). The suspension was centrifuged at 26,000 x g for 30 minutes at 4°C to remove the insoluble pellet, and the supernatant was immediately loaded onto a 20 ml Ni<sup>2+</sup>-NTA super-flow column (Qiagen) equilibrated with urea buffer at a rate of 2 ml/min. The column was washed with binding buffer until A<sub>280</sub> of the eluent reached the baseline, and then washed with wash buffer, again until the baseline was reached. His<sub>6</sub>Ub-Aβ<sub>1-40</sub> was eluted with elution buffer at a flow rate of 1 ml/min and collected in 2 ml fractions. Fractions were analysed by SDS-PAGE and those containing His<sub>6</sub>Ub-Aβ<sub>1-40</sub> were pooled and dialysed against dialysis buffer before storage at 4°C.

## 3.2.4. Hydrolysis of His<sub>6</sub>Ub-Aβ<sub>1-40</sub>

### 3.2.4.1. Original Method

His<sub>6</sub>Ub-Aβ<sub>1-40</sub> and GST-YUH1 were incubated in 10 mM Tris-HCl pH 8.0, 1 mM EDTA, 2 mM DTT at 37°C for 1-2 hours. The molar ratio of His<sub>6</sub>Ub-Aβ<sub>1-40</sub> and GST-YUH1 was 100:1.

#### 3.2.4.2. Final Adapted Method

In this method, both the ratio of fusion protein and hydrolase, and the volume of the reaction, is crucial due to the size of the column used. 5 ml of His<sub>6</sub>Ub-A $\beta$ <sub>1-40</sub> (154  $\mu$ M) was incubated with 40  $\mu$ l of GST-YUH1 (35  $\mu$ M) in 10 mM Tris-HCl pH 8.0, 1 mM EDTA, 2 mM DTT for 1-2 hours at 37°C.

#### 3.2.5. Separation of A $\beta$ <sub>1-40</sub> from the Ubiquitin tag

##### 3.2.5.1. Method 1: by Reverse-Phase Chromatography

The reaction mixture was acidified with 0.1% (v/v) TFA to a pH of 2-4 and passed through a 0.2  $\mu$ m filter. The solution was loaded onto a Grace Vydac Everest C18 column which had been equilibrated in 0.1 % (v/v) TFA, 2% (v/v) acetonitrile. Bound polypeptides were eluted with a linear acetonitrile gradient up to 80% over 40 minutes, and fractions were collected and lyophilised. After re-suspension in 10 mM HCl pH 2.0, the fractions were analysed by tricine SDS-PAGE.

##### 3.2.5.2. Method 2: by Size-Exclusion Chromatography

###### *Native Conditions (analytical)*

20  $\mu$ L samples were loaded onto a Shodex KW803 column (Shodex, Japan) equilibrated in 10 mM sodium phosphate buffer pH 6.0, 100 mM NaCl and eluted over 20 minutes at a flow rate of 1 ml/min.

###### *Denaturing Conditions (analytical)*

After acidification, 20  $\mu$ l samples were loaded onto an analytical BioSep SEC-S3000 column (Phenomenex) equilibrated in varying concentrations (0-50% (v/v)) of acetonitrile in 0.1% (v/v) TFA and eluted over 20 minutes at a flow-rate of 1 ml/min. A preparative column (Biosep SEC-S3000) was also employed with a loading volume of 100  $\mu$ l and eluted over 40 minutes with a flow-rate of 3.7 ml/min.

###### *Denaturing Conditions (scale-up)*

The His<sub>6</sub>Ub-A $\beta$ <sub>1-40</sub> solution was concentrated to 1.5 ml (510  $\mu$ M) before the hydrolysis reaction. After incubation with 5.10  $\mu$ M GST-YUH1 at 37°C for 2 hours, 1 ml of 40% (v/v) acetonitrile in 0.1% (v/v) TFA was added and the pH was checked (should be between 2 and 4). After centrifugation at 13,000 x g at 4°C for 15 minutes to remove any precipitate, the sample was loaded onto a 100 ml Superdex 75 gel filtration column (GE Healthcare) which had been equilibrated in 40% (v/v) acetonitrile in 0.1% (v/v)

TFA. The peptide was eluted at a flow rate of 1 ml/min and 2 ml fractions were collected and lyophilised. The fractions were analysed by tricine SDS-PAGE to identify those containing A $\beta$ <sub>1-40</sub>.

#### **3.2.5.1. Method 3: Purification by Ni<sup>2+</sup>-NTA Affinity Chromatography**

The cleavage reaction was immediately loaded onto a 20 ml Ni<sup>2+</sup>-NTA super-flow column (Qiagen) which had been equilibrated with wash buffer diluted 50x in water (i.e. 1 mM Tris-HCl pH 8.0, 3 mM NaCl, 1 mM imidazole). The mixture was manually poured on top of the Ni<sup>2+</sup> column and allowed to drip through with the upper lid open and no buffer flow. When the sample level reached 1-2 mm from the top of the column, buffer flow was started at 1 ml/min. Fractions were collected in eppendorf tubes according to elution profile. GST-YUH1 elutes immediately, followed very closely by A $\beta$ . His<sub>6</sub>Ub-A $\beta$ <sub>1-40</sub> was eluted using elution buffer. Fractions were analysed by SDS-PAGE and those containing A $\beta$ <sub>1-40</sub> were pooled and lyophilised.

#### **3.2.6. Preparation of Monomeric A $\beta$ <sub>1-40</sub>**

The lyophilised peptide film was re-suspended in HFIP to a concentration of 1 mg/ml and any salt was removed by centrifugation at 13,000 x g for 30 minutes at 4°C. The supernatant was removed and aliquoted in 200  $\mu$ l aliquots. HFIP was removed by evaporation under N<sub>2</sub> and samples were lyophilised again to remove any trace HFIP, and stored at -20°C.

### 3.3. Results

Both GST-YUH1 and His<sub>6</sub>Ub-A $\beta$ <sub>1-40</sub> were purified successfully with yields of 29 mg per 1 litre of cell culture and 8 mg per 1 litre of cell culture (supernatant only) respectively.

#### 3.3.1. Cleavage of His<sub>6</sub>Ub-A $\beta$ <sub>1-40</sub>

GST-YUH1 activity was analysed by tricine SDS-PAGE of the products of the hydrolysis reaction. Figure 3.1 shows the expected molecular weights of the various proteins which had been previously established by mass spectrometry (Dr Maho Yagi-Utsumi, personal communication). The tricine SDS-PAGE gel indicated the successful cleavage of His<sub>6</sub>Ub-A $\beta$ <sub>1-40</sub> to produce His<sub>6</sub>Ub and A $\beta$ <sub>1-40</sub>. The shift of the largest band in lane 1 at ~ 15 kDa to ~12 kDa in lane 3 shows the cleavage of His<sub>6</sub>Ub-A $\beta$ <sub>1-40</sub> to produce His<sub>6</sub>Ub with no uncleaved His<sub>6</sub>Ub-A $\beta$ <sub>1-40</sub> remaining. The A $\beta$ <sub>1-40</sub> produced by this reaction can be clearly seen with a band at ~7 kDa. Tricine SDS-PAGE also demonstrated that the cleavage efficiency was the same whether incubated for 1 or 2 hours at 37°C (data not shown), with no uncleaved protein remaining in the sample.

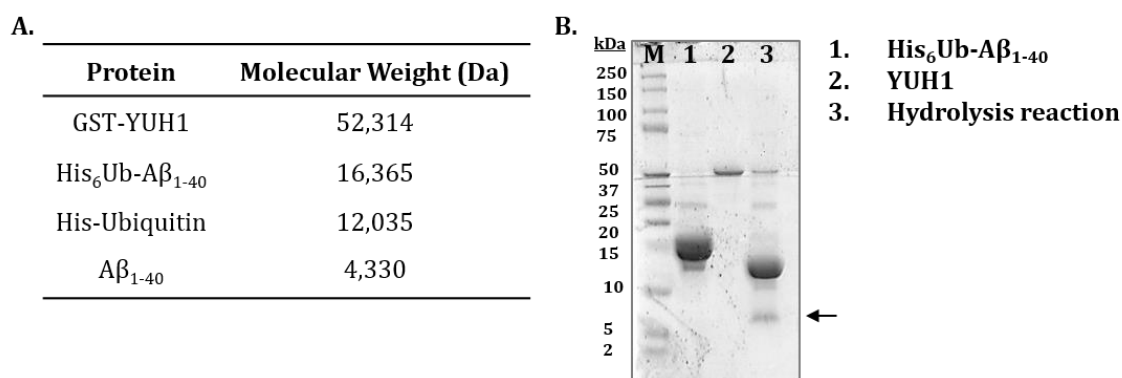


**Figure 3.1. Hydrolysis Reaction**

Table of relevant protein molecular weights (A) obtained by mass spectrometry (provided by Dr Maho Yagi-Utsumi (Okazaki Institute for Integrative Bioscience)). Tricine SDS-PAGE (B) showing purified His<sub>6</sub>Ub-A $\beta$ <sub>1-40</sub> (lane 1; band at ~ 15 kDa) and purified GST-YUH1 (lane 2; band at ~ 50 kDa). Lane 3 shows the hydrolysis reaction after incubation at 37°C for 2 hours. The A $\beta$ <sub>1-40</sub> band can be clearly seen at ~ 7 kDa (arrow) with a band at ~12 kDa corresponding to His<sub>6</sub>Ub after removal of the A $\beta$ <sub>1-40</sub> peptide.

#### 3.3.2. Separation of A $\beta$ <sub>1-40</sub> Peptide from Ubiquitin

##### 3.3.2.1. Method 1: Reverse Phase – HPLC

Reverse-phase HPLC is commonly used in the literature for the purification of A $\beta$ ; using acetonitrile as the mobile phase reduces association with the column and the

formation of aggregates, problems which are often encountered when using aqueous buffer. After hydrolysis at 37°C for 2 hours, the cleavage reaction was run down an analytical Vydac C18 column (Grace) in a 2-80% acetonitrile gradient. Pure samples of GST-YUHI, His<sub>6</sub>Ub-Aβ<sub>1-40</sub> and commercial recombinant Aβ<sub>1-40</sub> (rPeptide, Georgia USA) were used for comparison (Figure 3.2). The peak for commercial Aβ<sub>1-40</sub> (~37 min) showed considerable peak tailing indicating that the peptide could be associating weakly with the column under the conditions used. The trace for the cleavage products shows several small peaks, none of which are easily identifiable, suggesting a lack of separation.

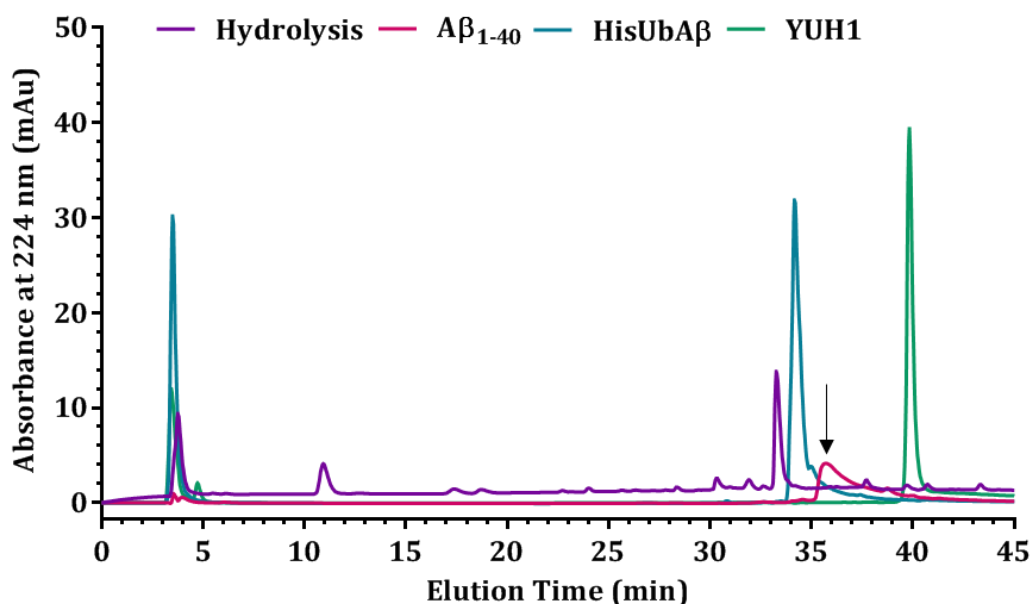


**Figure 3.2. Separation of Hydrolysis Products by Reverse-Phase HPLC**

*Analytical RP-HPLC elution profiles of commercial Aβ<sub>1-40</sub> (pink), His<sub>6</sub>Ub-Aβ<sub>1-40</sub> (blue), GST-YUHI (green) and the hydrolysis reaction (purple) in a 0-80% acetonitrile gradient in 0.1% TFA. The arrow indicates the commercial Aβ<sub>1-40</sub> peak at ~36 min, however there is no corresponding peak in the hydrolysis sample.*

A similar column on a preparative scale showed better separation of peaks (data not shown). However, attempts to analyse the peaks by tricine SDS-PAGE failed indicating that the eluted sample was too dilute. In order to continue down the reverse-phase route, it would be necessary to concentrate the injected sample further and increase its volume. It was evaluated that within soluble limits, the eluted samples would be too dilute for further work-up. A different method would be desirable for the amounts of peptide required.

### 3.3.2.2. Method 2: Size Exclusion Chromatography

#### *HPLC*

As shown in Figure 3.3, running the cleavage products on SEC-HPLC in 10 mM sodium phosphate pH 6, 150 mM NaCl greatly reduced the number of peaks and allowed different species to be identified upon comparison with the standards. As A $\beta$  is essentially unfolded, the increase in hydration leads to a higher radius of gyration ( $R_g$ ) which can be predicted to be as much as 3 times that of a folded protein (Semisotnov et al., 1996). This means that the A $\beta_{1-40}$  runs with an apparent molecular weight higher than would be expected, and so the retention time is similar to that of the His-ubiquitin, even though the latter is 12 kDa compared to A $\beta_{1-40}$  at 4 kDa.

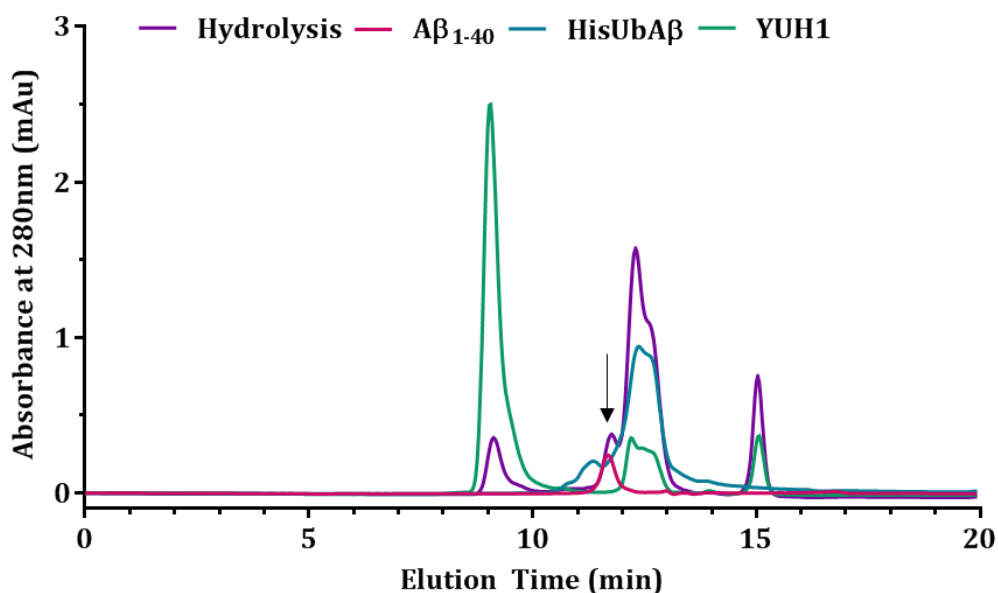
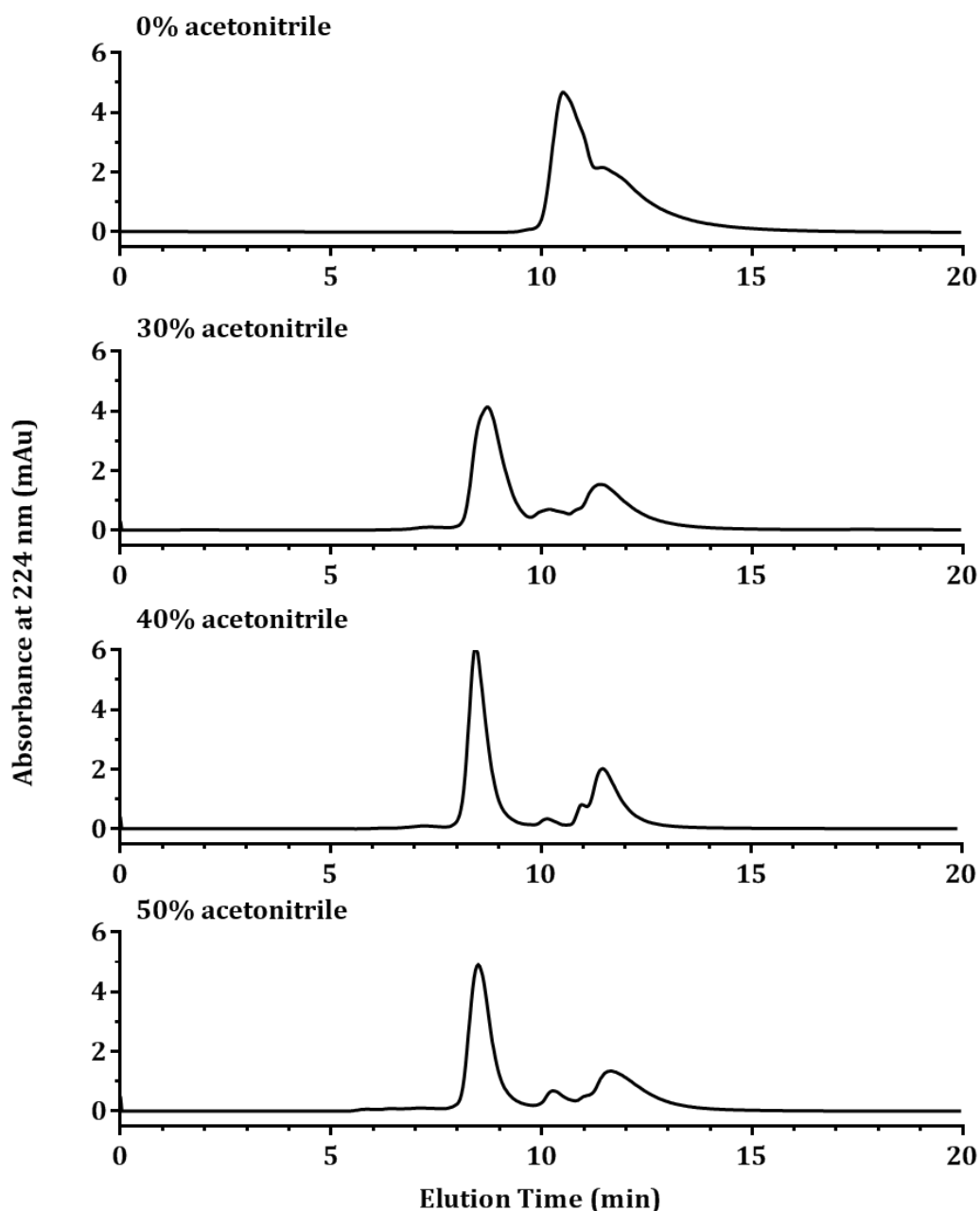


**Figure 3.3. Separation of Hydrolysis Products by Size-Exclusion HPLC**

*Analytical SEC-HPLC elution profiles of commercial A $\beta_{1-40}$  (pink), His<sub>6</sub>Ub-A $\beta_{1-40}$  (blue), GST-YUH1 (green) and the hydrolysis reaction (purple) in 10 mM sodium phosphate pH 6.0, 100mM NaCl. The arrow indicates the A $\beta_{1-40}$  at ~11.5 min.*

It was therefore decided to try running the size-exclusion column in acetonitrile, an unusual system. By unfolding all of the other proteins in the sample, it was hoped that the proteins would run in accordance to their molecular weight, therefore allowing the A $\beta$  to be purified. Analytical tests indicated that the best separation was achieved at 40% acetonitrile where proteins eluted with the sharpest peaks (Figure 3.4), so all further experiments were performed at this concentration.



#### 3.4. SEC-HPLC of His<sub>6</sub>Ub-Aβ<sub>1-40</sub> in Varying Concentrations of Acetonitrile

*Analytical SEC-HPLC elution profiles of His<sub>6</sub>Ub-Aβ<sub>1-40</sub> in 0%, 30%, 40% and 50% (v/v) acetonitrile in 0.1% TFA.*

As illustrated in Figure 3.5, separation of the hydrolysis products and production of pure Aβ<sub>1-40</sub> was achieved by SEC-HPLC on both an analytical and a semi-preparative scale. However, even the semi-preparative column available had an injection limit of 100 μl of sample, meaning that in order to obtain a large enough yield of peptide (>10 mg), too many elution runs would be necessary for an efficient protein production. Further methods were investigated.

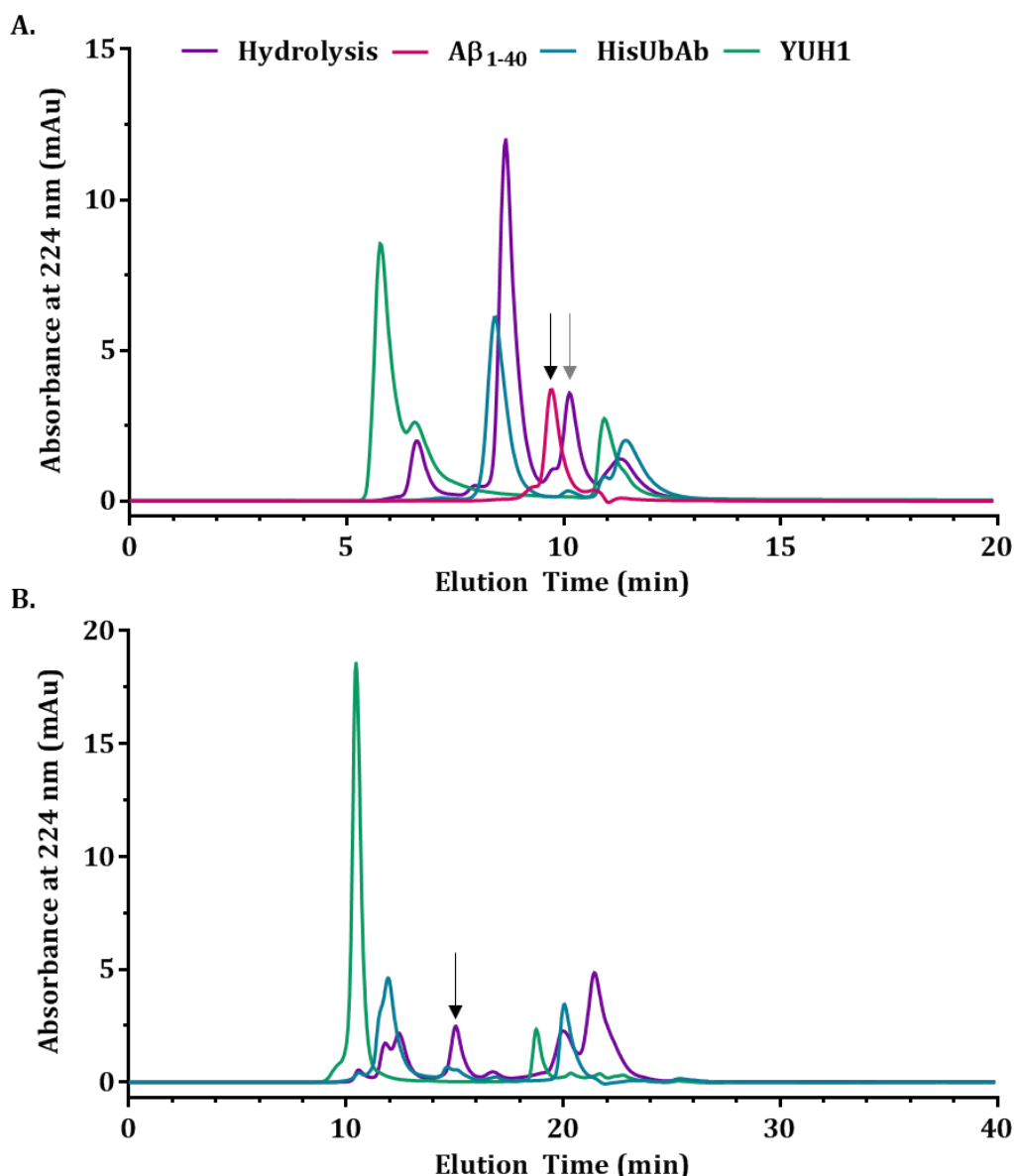


**Figure 3.5. Separation of Hydrolysis Products by SEC-HPLC in 40% Acetonitrile**

Analytical (A) and semi-preparative (B) SEC-HPLC elution profiles of commercial Aβ<sub>1-40</sub> (pink), His<sub>6</sub>Ub-Aβ<sub>1-40</sub> (blue), GST-YUH1 (green) and the hydrolysis reaction (purple) in 40% acetonitrile in 0.1% TFA. The black arrow indicates the Aβ<sub>1-40</sub> peak at ~9.5 min (A) and ~15 min (B), however it is also thought that the peak immediately to the right of this in the analytical profile (grey arrow) could also be Aβ<sub>1-40</sub>.

### Low Pressure Size-Exclusion Chromatography

In an attempt to scale-up the SEC-HPLC experiment and obtain a greater yield of peptide, a more standard liquid chromatography system was used to carry out the size-exclusion chromatography. The hydrolysis products were loaded onto a 100 ml Superdex 75 column (GE Healthcare) in 40% acetonitrile:water (v/v) and 0.1% TFA then 4 ml fractions were collected. As shown in Figure 3.6, SDS-PAGE indicated that

partial separation was achieved, with most of the His<sub>6</sub>Ub being removed from the sample. In order to achieve complete separation, it would be necessary to use a column of double the length (or two columns in tandem). Although this method had only limited success in isolating A $\beta$ <sub>1-40</sub> from the hydrolysis mixture, it has proved to be successful both in purifying A $\beta$  from mixtures where the contaminating protein has a higher molecular weight, and in buffer-exchanging the peptide into 40% acetonitrile to remove salt and other contaminants and allow easy lyophilisation.

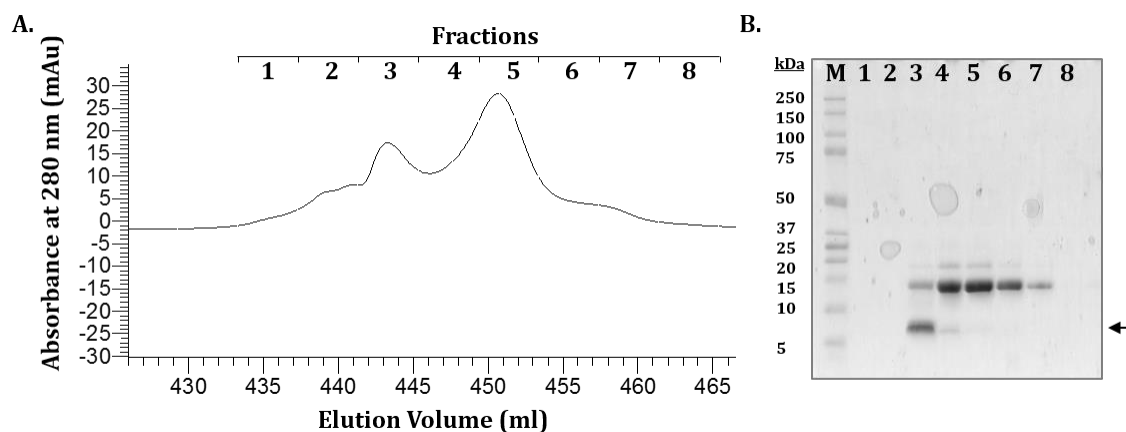


**Figure 3.6. Size-Exclusion Chromatography and SDS-PAGE Analysis**

*Elution profile (A) of size-exclusion chromatography of hydrolysis products in 40% acetonitrile in 0.1% TFA using a Superdex 75 column (GE Healthcare). 4 ml fractions were collected and fractions 1-8 were analysed by SDS-PAGE (B). Fractions 3 and 4 show the presence of A $\beta$ <sub>1-40</sub> (band at ~ 7 kDa) but the band at ~ 13 kDa indicates that His<sub>6</sub>Ub is still present.*

### 3.3.2.3. Method 2b: Separation by Aggregation of A $\beta$ <sub>1-40</sub>

Due to mixed success with chromatography, a completely different method for separating out the A $\beta$  was trialled. By incubating the cleavage mixture in conditions in which A $\beta$  is known to fibrillise, it was hoped that the A $\beta$  would form fibrils which could then be harvested by centrifugation, re-dissolved using hexafluoroisopropanol (HFIP) eventually producing a pure sample of A $\beta$ <sub>1-40</sub>. A $\beta$  is known to form fibrils at either low pH or neutral pH with the addition of salt. Taking the peptide through the pH region 4.0 to 6.0 is undesirable, as this causes the A $\beta$  to precipitate (Zagorski et al., 1999). Initially low pH conditions were chosen in which neither salt nor buffer were present, allowing easy lyophilisation of the dissociated peptide. Evidence from the literature suggests that at a peptide concentration of 100  $\mu$ M significant amounts of fibril will have formed after 24 hours at 37°C (Stine et al., 2003). After incomplete separation by SEC in 40% acetonitrile, fractions containing A $\beta$ <sub>1-40</sub> were pooled and

lyophilised before re-suspension in 10 mM HCl pH 2.0. Incubation of the cleavage products in these conditions for 9 days produced small protofibrils, as shown by TEM in Figure 3.7, however further incubation did not lead to mature fibrils. Centrifugation at 13,000 x g for 30 minutes caused pelleting of the protofibrils, allowing analysis by SDS-PAGE after dissolution in HFIP. This indicated that the A $\beta$  had been effectively isolated in the insoluble fraction, however attempts to repeat this were unsuccessful.

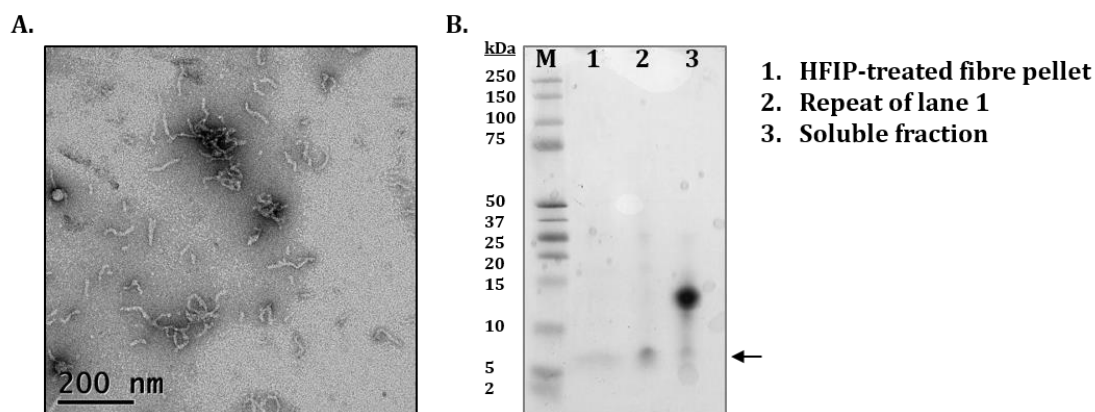


**Figure 3.7. Isolation of A $\beta$ <sub>1-40</sub> by Fibrillisation at pH 2.0**

*Electron micrograph of A $\beta$ <sub>1-40</sub> protofibrils (A) formed by incubation of hydrolysis products at pH 2.0. Fibrils were separated from soluble species by centrifugation at 13,000 x g for 30 minutes. Samples were analysed by SDS-PAGE (B); lanes 1 and 2 indicate that the fibril pellet contained only A $\beta$ <sub>1-40</sub> (band at ~ 7 kDa indicated by arrow) whereas the His<sub>6</sub>Ub remained in the soluble fraction (lane 3; band at ~ 13 kDa). Some soluble A $\beta$ <sub>1-40</sub> was still present.*

A purification technique described by Garai et al. (2009) involved the addition of 100 $\mu$ M ZnCl<sub>2</sub> to A $\beta$ <sub>1-40</sub> incubated in Tris pH 7.4, 100mM NaCl at room temperature with agitation, resulting in the formation of fibrils overnight. Utilisation of this method would allow the production of fibrils over a short time period. Fibrils were produced after 24 hours as confirmed by TEM. After harvesting by repeated cycles of centrifugation and washing with EDTA to remove the ZnCl<sub>2</sub>, the fibrils were dissolved with HFIP and lyophilised. Analysis by SDS-PAGE showed a pure sample of A $\beta$ <sub>1-40</sub> (Figure 3.8). The process was then performed on a large scale, however in this case the SDS-PAGE showed that the sample was not pure as larger bands corresponding to His<sub>6</sub>Ub and GST-YUH1 were present (data not shown). Ensuring removal of all the zinc from the sample is a major problem with this purification method, as even residual amounts of the metal will affect the fibrillisation kinetics.

Further development of this method should include testing these conditions without the addition of the zinc, as A $\beta$ <sub>1-40</sub> readily forms fibrils at pH 7.4 without the addition of the

metal. This will eradicate the necessity of removing the zinc. Methods trialled in parallel were successful first and were more readily adaptable to purifying the more challenging A $\beta_{1-42}$ , therefore aggregation methods were not pursued further.

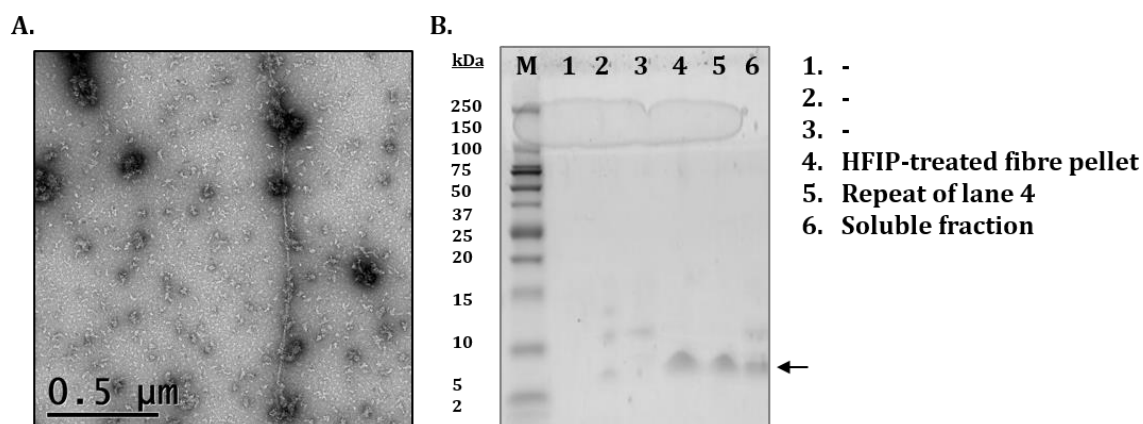


**Figure 3.8. Isolation of A $\beta_{1-40}$  by Fibrillisation at pH 7.4 with 100  $\mu$ M ZnCl<sub>2</sub>**

*Electron micrograph (A) of A $\beta_{1-40}$  fibrils and large molecular weight species formed by incubation of hydrolysis products at pH 7.4 with the addition of 100  $\mu$ M ZnCl<sub>2</sub>. Fibrils were separated from soluble species by centrifugation at 13,000  $\times$  g for 30 minutes and analysed by tricine SDS-PAGE (B).*

#### 3.3.2.4. Method 3: Ni<sup>2+</sup>-NTA Affinity Chromatography

The addition of a histidine tag allows efficient purification of the fusion protein by Ni<sup>2+</sup>-NTA affinity chromatography in a one-step process. This histidine tag can also be exploited in the purification of the A $\beta_{1-40}$  peptide from the cleavage mixture; by running the sample down the Ni<sup>2+</sup>-NTA column again, the His<sub>6</sub>-ubiquitin will bind to the column, allowing the A $\beta_{1-40}$  to flow through the column. The small amount of GST-YUH1 that remains can either be removed by running the sample through a GST affinity column, or a size-exclusion chromatography column. Initial trials indicated that in aqueous buffer the A $\beta_{1-40}$  would adhere to the column beads and be lost; running the column in 40% acetonitrile proved moderately successful but had difficulties with the solvent stripping the nickel from the column when trying to reproduce the experiment.

Finally my colleague Dr Fernando Macedo Jr. attempted a further modification of this method and was successful in purifying A $\beta_{1-40}$  using the Ni<sup>2+</sup>-NTA column. While the A $\beta_{1-40}$  will stick to the column when run in buffer, the addition of low concentrations (1 mM) of imidazole to the running buffer prevents non-specific binding of the A $\beta$ . The peptide is still slightly retarded by the column, meaning that the GST-YUH1 elutes first and removing the need for separate purification for the hydrolase. The His<sub>6</sub>Ub will bind

to the  $\text{Ni}^{2+}$  and only be removed by the addition of higher concentrations of imidazole (100 mM). Analysis of the fractions by SDS-PAGE showed the presence of pure  $\text{A}\beta_{1-40}$ . Fractions were pooled, lyophilised and re-suspended in HFIP. Centrifugation at 13,000 x g removed any salt that would not dissolve in the solvent, and the HFIP was evaporated under a stream of nitrogen gas before lyophilisation to remove any residual traces of solvent.

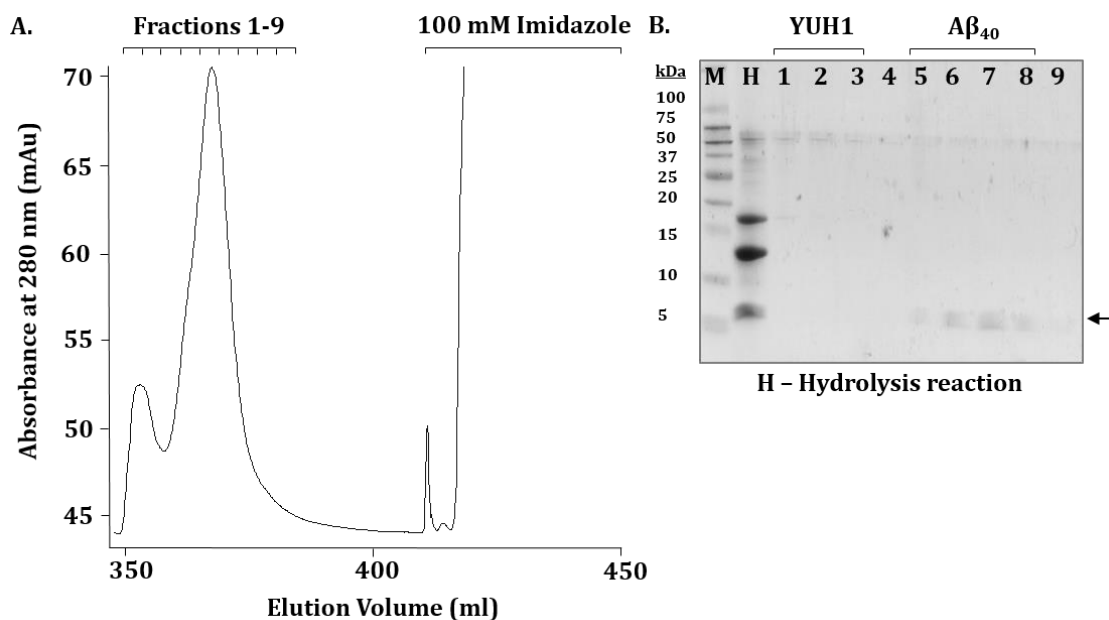


**Figure 3.9.  $\text{Ni}^{2+}$ -NTA Chromatography of Hydrolysis Reaction**

*Elution profile (A) from  $\text{Ni}^{2+}$ -NTA chromatography of hydrolysis products in 1 mM imidazole. Fractions were collected until the elution trace reached the baseline. Bound  $\text{His}_6\text{Ub-A}\beta_{1-40}$  was then eluted using 100 mM imidazole. Tricine SDS-PAGE of fractions 1-9 (B) indicated that uncleaved  $\text{His}_6\text{Ub-A}\beta_{1-40}$  was still present in the initial hydrolysis reaction (band at ~16 kDa). Pure  $\text{A}\beta_{1-40}$  was seen in fractions 5-8.*

After purification by  $\text{Ni}^{2+}$ -NTA affinity chromatography, SDS-PAGE indicated that a pure sample of  $\text{A}\beta_{1-40}$  had been produced. However analysis of the sample by SEC-HPLC (Figure 3.10) revealed that, although the peptide was pure, there was a large peak at 49 minutes thought to correspond to contaminating buffer salts such as imidazole. As imidazole absorbs strongly at 280 nm this makes it impossible to quantify the yield of protein through measuring the absorbance of the sample at 280 nm. It is also not known what effect the imidazole will have on fibrillisation and peptide interaction with hCC, making it necessary to remove the imidazole, and any other contaminating buffer salts, from the sample. The method chosen for this was size-exclusion chromatography in 40% (v/v) acetonitrile in 0.1% TFA, as this had been shown to be successful in purification of  $\text{A}\beta$  in the previous section.

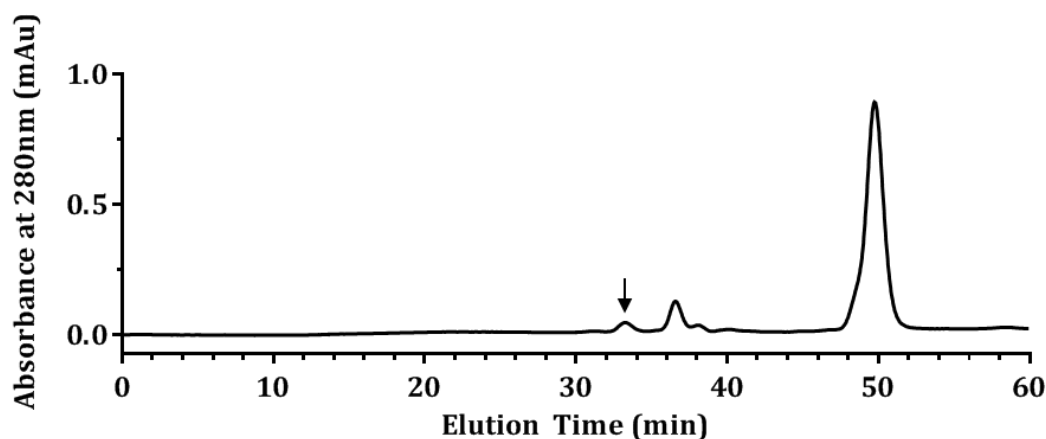


**Figure 3.10. Analytical SEC of Purified A $\beta$ <sub>1-40</sub>**

*Elution profile of purified A $\beta$ <sub>1-40</sub> analysed by size-exclusion chromatography in 50 mM sodium phosphate pH 7.4, 150 mM NaCl with the absorbance measured at 280 nm. The arrow indicates the A $\beta$ <sub>1-40</sub> peak at ~33 minutes. The large peak at 49 minutes is thought to correspond to contaminating imidazole that has not been removed from the sample by the purification process.*

### **3.3.3. Characterisation of the Purified Peptide after SEC**

After purification using a preparative Superdex 75 gel filtration column (GE Healthcare) carried out in 40% acetonitrile, the peptide was characterised by SEC-HPLC and mass spectrometry. Fibril formation by the purified A $\beta$ <sub>1-40</sub> was then compared to a commercial preparation from rPeptide (Georgia, US). The lyophilised peptide was re-suspended in 10 mM NaOH before being diluted 1:1 with 100 mM sodium phosphate pH 7.4, 300 mM NaCl. The pH was adjusted with HCl to give a final 1 ml sample in 50 mM sodium phosphate pH 7.4, 150 mM NaCl.

#### **3.3.3.1. SEC-HPLC**

Initially the sample of purified A $\beta$ <sub>1-40</sub> was analysed using analytical SEC in 50 mM sodium phosphate pH 7.4, 150 mM NaCl with the absorbance read at 280 nm, as shown in Figure 3.11A. Comparison with a commercial sample identified the A $\beta$ <sub>1-40</sub> peak as being at 33 minutes, however there were several other peaks present after this one. In both the commercial and the purified sample a small peak was observed at ~13 minutes, potentially corresponding to a small amount of oligomeric A $\beta$  being present in the sample.

To try and identify whether the extra peaks in the purified sample were truncated forms of A $\beta$ , or buffer components that had not been removed by the purification process, the

same samples were analysed by SEC in an identical manner, except reading the absorbance at 224 nm. Measuring the absorbance at this wavelength identifies the peptide bond, rather than the aromatic residues that absorb at 280 nm, of which A $\beta$  has very few. Again this identified the A $\beta$  peak in the same position at 33 minutes, with a reduction in the number of extra peaks with only one remaining. This could indicate that the majority of extra peaks are from buffer components. The height of the A $\beta$  peak in the purified sample was comparable to that of the commercial sample, indicating that they were at a similar concentration of 0.1 mg/ml, and allowing quantification of the purified peptide.

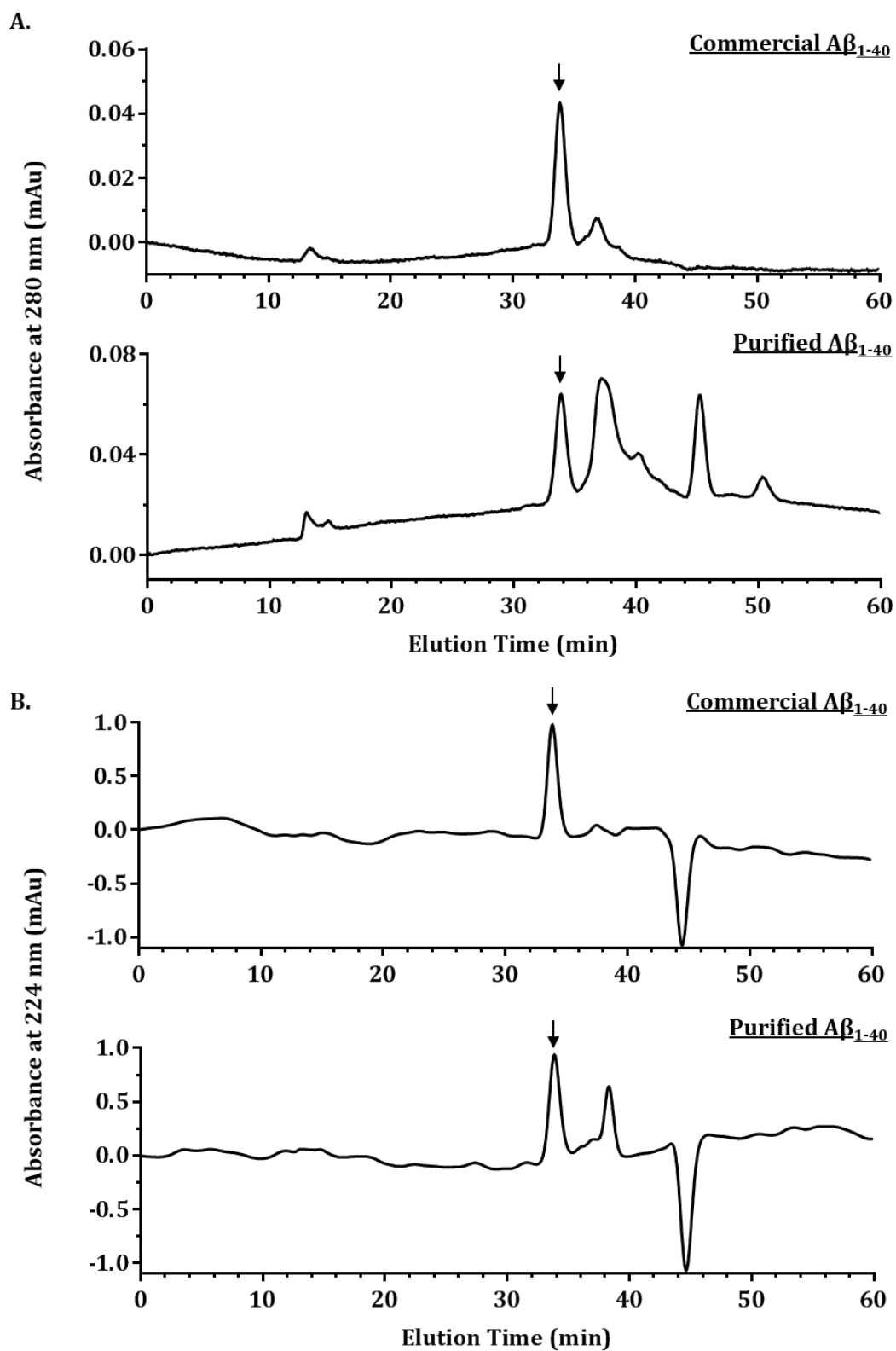


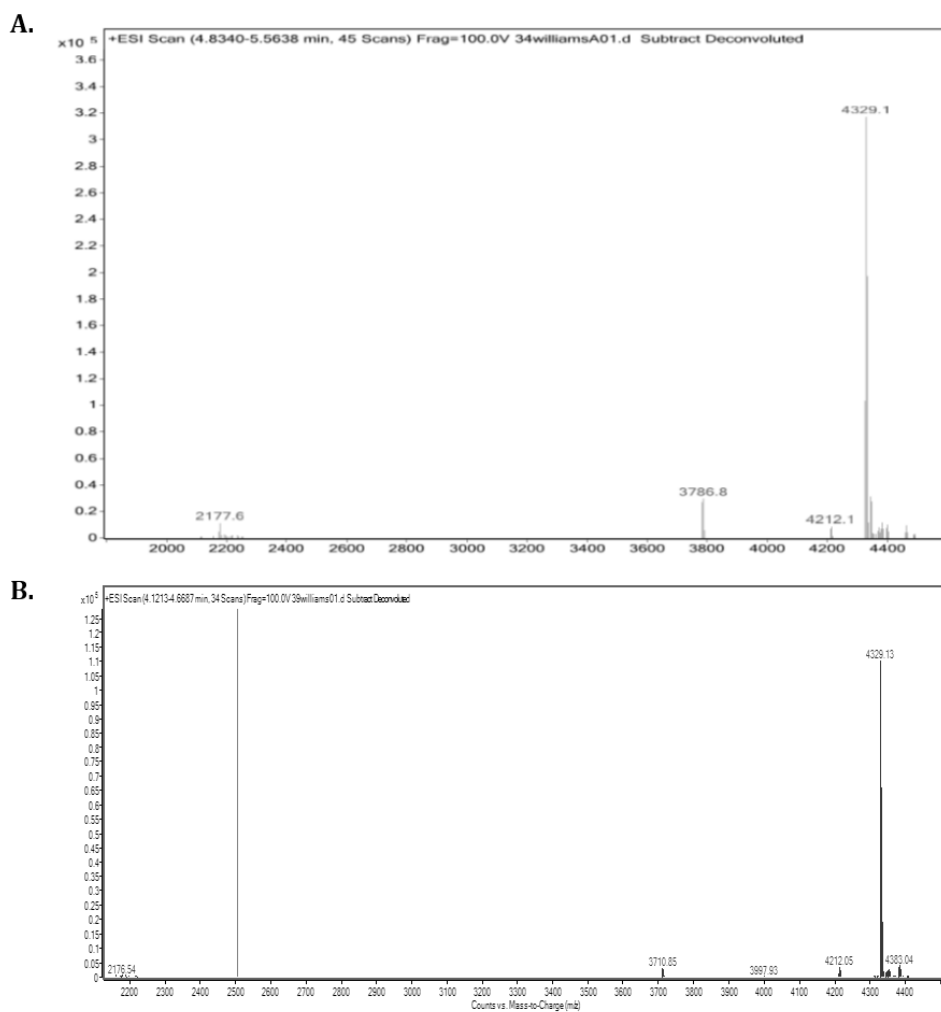
**Figure 3.11. SEC-HPLC Analysis of Purified  $A\beta_{1-40}$**

*Elution profiles of SEC-HPLC commercial and purified  $A\beta_{1-40}$  monitoring the absorbance at 280 nm (A) and at 224 nm (B) with the arrow indicating the  $A\beta_{1-40}$  peak.*

### 3.3.3.2. Mass Spectrometry

Figure 3.12 shows analysis by ESI-MS, which indicated that A $\beta$ <sub>1-40</sub> had been produced with a mass of 4329.1 Da which compares well with the predicted mass of 4329.8 Da, given the accuracy of the instrument is low ( $\pm 1$  Da). This also confirmed that there had been no oxidation of methionine 35, which is a common problem with preparation of A $\beta$ .

There were two extra masses in the MS data, both of which could be attributed to truncated forms of the peptide. Loss of the N-terminal aspartic acid gives rise to a peptide with a mass of 4212 Da which could be attributed to inefficient cleavage by the GST-YUH1. The second truncated peptide has lost the last 6 residues. The peak of 2177.6 did not correspond to any fragment masses within the A $\beta$  peptide sequence. Although the peaks for the two identified truncates are a lot smaller than that of the full length peptide, this cannot be used for quantification purposes as peak heights are dependent on how well the ions fly, not how much of each species is present. It is possible that these peptide fragments correspond to the extra peak observed in the SEC (Figure 3.11), in which case they would constitute a significant proportion of the sample, however this is very unlikely as the analytical Superdex 200 column does not have the resolving power to distinguish between peptides with only 6 residues difference. MS analysis of a sample of commercial A $\beta$ <sub>1-40</sub> also indicated the presence of small truncated peptides, demonstrating that the purified peptide had a similar purity to the commercial product.



Mass (Da)	Calculated Mass (Da)	$\Delta$ mass (Da)	Residues
4329.1	4329.8	0.7	1-40
4212.1	4212.12	0.02	2-40
3786.8	3784.86	-1.94	1-34

**2-40**

**DAEFRHDSGYEVHHQKLVFFAEDVGSNKGAIIGLMVGGVV**

**1-34**

**Figure 3.12. Mass Spectrometry Analysis of Purified A $\beta$ <sub>1-40</sub>**

*ESI-MS analysis of a sample of purified (A) and commercial (B) A $\beta$ <sub>1-40</sub> showing identification of peptide masses. The table shows a comparison between the experimental masses and the calculated mass for the identified peptides. Truncated peptides are indicated on the A $\beta$ <sub>1-40</sub> primary structure.*

### 3.3.4. Fibrillisation

Having produced a pure sample of A $\beta$ <sub>1-40</sub>, as confirmed by HPLC and mass spectrometry, it was then desirable to compare the fibrillisation of the peptide with a commercial preparation. The lyophilised peptides were resuspended in 10 mM NaOH before being diluted 1:1 with 100 mM sodium phosphate pH 7.4, 300 mM NaCl. The pH was adjusted with HCl to give a final 1 ml sample in 50 mM sodium phosphate pH 7.4, 150 mM NaCl and the fibrillisation time-course at 37°C was followed by ThT fluorescence. This amyloid-specific dye shows an increase in fluorescence upon binding to amyloid fibrils, allowing the fibril formation to be followed over a period of time. Figure 3.13 shows the data obtained from both samples which followed a sigmoidal curve, thought to correspond to an initial lag phase and an exponential elongation phase which eventually reaches an equilibrium plateau.

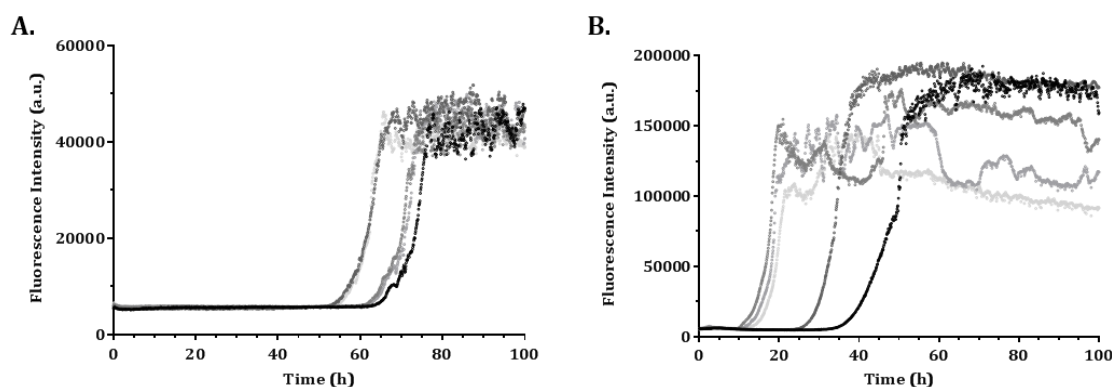


**Figure 3.13. Fibrillisation of A $\beta$ <sub>1-40</sub>**

*ThT fluorescence curves (5 replicates) showing fibrillisation of purified (A) and commercial (B) A $\beta$ <sub>1-40</sub> incubated in 50 mM sodium phosphate pH 7.4, 150 mM NaCl at 37°C.*

The purified sample had a lag phase of ~ 60 hours, compared to the average lag time of ~30 hours that was obtained for the commercial sample. There is a considerable difference in the final ThT intensity for the two samples, with the commercial sample having approximately three times the fluorescence of the purified A $\beta$ . This could indicate that less fibrils are being produced from the latter peptide, or that one of the contaminants observed in the SEC is quenching the ThT fluorescence. Each experiment consisted of 5 replicates. In the commercial sample there was a large variation between the replicates, however the curves obtained from the purified sample are a lot more reproducible.

### 3.3.5. Overview of Final Purification

Figure 3.14 illustrates the final protocol used for the purification of A $\beta$ <sub>1-40</sub>. After purification of the ubiquitin tagged peptide using Ni<sup>2+</sup>-NTA affinity chromatography, the tag is removed using the specific ubiquitin hydrolase for 1-2 hours. Separation of the A $\beta$ <sub>1-40</sub> peptide is achieved using the Ni<sup>2+</sup>-NTA column and the A $\beta$ <sub>1-40</sub> is then denatured and monomerised in HFIP. Removal of any residual buffer components and contaminants is then achieved by gel filtration (Superdex 75) under denaturing conditions, in 40% acetonitrile:water and 0.1% TFA. The purified peptide is then lyophilised, treated with HFIP and further lyophilised before storing at -20°C.

### 3.4. Conclusions

The properties that make A $\beta$  so significant in neurodegenerative diseases, and therefore so interesting to study, are the very same properties that make this peptide so difficult to work with. Recombinant production of A $\beta$  is no exception. Problems start with expression in *E. coli*, low solubility and propensity to degrade makes the addition of a tag appear necessary. This does lead to high expression levels, and a good yield of fusion protein, however then comes the issue of removing this tag and purifying out the peptide without it precipitating, aggregating or sticking to any surface it comes into contact with. The purification detailed here allows the production of a pure sample of A $\beta$ <sub>1-40</sub> in high enough yields to be used for NMR purposes, however this was not achieved in time to be used for the interaction studies with hCC (Chapter 5).

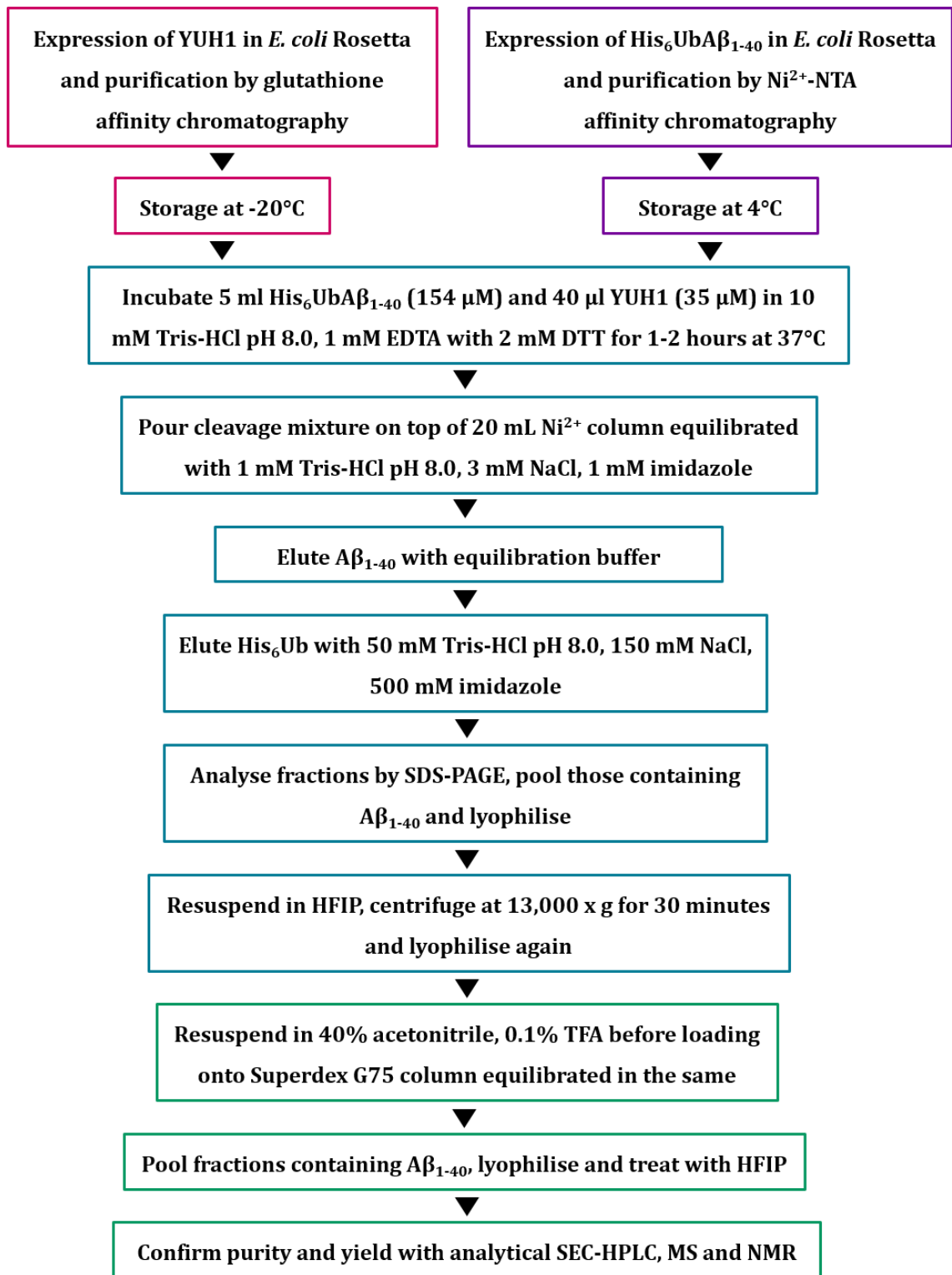


Figure 3.14. Outline of the optimised protocol for A $\beta$ <sub>1-40</sub> purification

## Chapter Four: Structural Studies of Cystatin C

### 4.1. Introduction

Although the L68Q variant of hCC will readily aggregate *in vivo* (Abrahamson and Grubb, 1994), as will type I family member cystatin B (Zerovnik et al., 2002), wild-type hCC requires drastic conditions for fibril assembly demonstrating high stability (Ekiel and Abrahamson, 1996, Nilsson et al., 2004). The fibrillisation mechanism of cystatin B has been extensively studied, however there is minimal information available on the assembly pathway of hCC.

The current structural model for hCC amyloid formation is that this protein oligomerises via a mechanism known as runaway domain swapping (Figure 4.1). Stabilised mutants containing disulphide bridges across the domain swapping interface, and thereby unable to domain swap, have a drastically reduced ability to produce both dimers and amyloid fibrils under fibrillising conditions (Nilsson et al., 2004). Although the prevention of amyloid formation in this manner has been suggested to mean that dimerisation is an obligatory intermediate in the fibrillisation pathway, the behaviour observed could also be attributed to a general stabilisation of the protein through the insertion of new disulphide bonds, rather than the specific inhibition of domain swapping. In addition to amyloid fibrils, hCC will also form donut-shaped oligomers which are thought to be on-pathway intermediates. Again, mutants stabilised against domain swapping will not form these oligomeric structures (Wahlbom et al., 2007).

Limited proteolysis has recently been used to develop a structural model for cystatin B fibrils (Davis, 2013) through probing with three different proteases elastase, proteinase K and endoproteinase Lys-C. Rapid hydrolysis of the N-terminal  $\alpha$ -helix, in conjunction with previously observed hydrogen-deuterium exchange data (Morgan et al., 2008) suggests that the native-like helix is not present in the fibril structure and that unfolding of this  $\alpha$ -helix is essential for fibril formation. Limited proteolysis identified a protease-resistant fragment extending from residues 27 to 80, suggesting that the fibril core is composed of native-like  $\beta$ -strands 2, 3 and 4 and leading to the proposal of a new non-native structural model with the cystatin B forming a  $\beta$ -strand arc (Figure 4.1). A comparison with the proteolytic pattern of hCC fibrils could be used to determine structural similarities between these family members, and establish whether the

extensive structural work that has already been carried out on cystatin B can be related to the amyloidogenic disease-causing hCC.

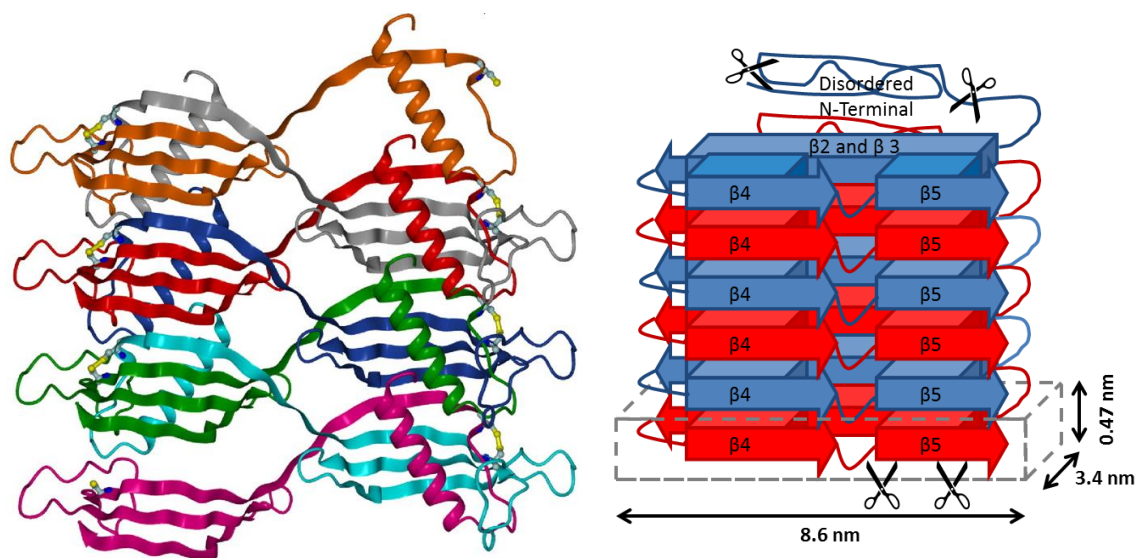


**Figure 4.1. Current models of Cystatin Fibril Structures**

*The suggested working models for hCC (left) and cystatin B (right) amyloid fibril structures. hCC is assumed to polymerise via a runaway domain swapping model (Wahlbom et al., 2007). Cystatin B is modelled here to account for hydrogen-exchange protection data and proteolysis protection, fitting both EM and AFM size restrictions. This model allows access to  $\beta$ -strand 5, which has been shown to be susceptible to proteolysis, without major remodelling of the fibril structure required upon its removal. The N-terminal is disordered and not included in the fibril core. Images taken from (Wahlbom et al., 2007) and (Davis, 2013).*

This chapter describes ThT assays and electron microscopy exploring the formation of amyloid fibrils and oligomeric intermediates by hCC. Different methods of separating these species will be discussed, in addition to their stability in different conditions, in the attempt to produce samples of both species for structural characterisation by limited proteolysis. Finally a preliminary limited proteolysis experiment of hCC fibrils is described, providing some insights into the structure of these fibrils and the validity of using the established models to describe hCC fibrils.

## 4.2. Materials and Methods

### 4.2.1. hCC Fibril Formation

hCC was buffer-exchanged into either 10 mM glycine pH 2.0 or 50 mM sodium acetate pH 4.0, 100 mM NaCl. The sample was incubated at either 225  $\mu$ M or 22.5  $\mu$ M at 48°C with constant stirring with a micro-stirrer (at approx. 100 r.p.m.).

#### **4.2.2. ThT Fluorescence**

10  $\mu$ M ThT was added to hCC fibrillation samples, which were incubated in a Cary Eclipse fluorimeter (Varian, UK). Emission scans were taken from 400 – 500 nm every 15 minutes with an excitation wavelength of 442 nm at a PMT voltage of 800 V. The emission at 482 nm was plotted using GraphPad Prism 6.04.

#### **4.2.3. SEC-HPLC**

Samples were analysed using an analytical Superdex 200 column (GE Healthcare) run in fibrillation buffer conditions at 0.5 ml/min for 60 minutes. Absorbance was measured at 280 nm.

#### **4.2.4. Purification of Oligomeric Species**

The protocol used for purification of hCC oligomers was adapted from that established in Wahlbom et al. (2007). After incubation at 48°C for the appropriate amount of time, hCC oligomer samples were inserted into a 0.5 ml Vivaspin filter device (Sartorius, UK) with a 1,000 kDa molecular weight cut off (MWCO) and centrifuged at 6,442 x g for 15 minutes to remove any fibrillar material or large amorphous aggregates from the sample. The flow-through was then loaded onto a 0.5 ml Vivaspin with a 100 kDa MWCO and centrifuged at 6,442 x g for 15 minutes. The sample retained at the top of the Vivaspin was diluted to the original volume with buffer and centrifuged again. This cycle was repeated three times to remove any monomeric hCC or lower molecular weight species from the solution and the volume of the retentate adjusted to the initial volume with buffer at the end. This method was also used for buffer-exchanging oligomers. All centrifugation steps were carried out at 4 °C.

#### **4.2.5. Purification of Fibrils**

hCC fibril samples were centrifuged at 13,000 x g for 30 minutes at 4°C. The supernatant was removed and the fibrils re-suspended in the original volume of buffer. This cycle was repeated three times to remove any monomeric and oligomeric hCC present in the sample.

##### **4.2.5.1. Incubation of Fibrils in Different Conditions**

5  $\mu$ l samples of hCC fibrils at 225  $\mu$ M protein concentration were incubated in a range of conditions as shown in Table 4.1. Conditions were altered through the addition of stock solutions to the samples in 50 mM sodium acetate pH 4.0, 100 mM NaCl.

<b>Condition</b>	<b>hCC Fibril Sample</b>	<b>Solution Added</b>	<b>Incubation Time (min)</b>
<b>pH 1.0</b>	4 $\mu$ l	1 $\mu$ l 1 M HCl	15
<b>pH 7.0</b>	4 $\mu$ l	1 $\mu$ l 150 mM NaOH	15
<b>pH 14.0</b>	4 $\mu$ l	1 $\mu$ l 5 M NaOH	15
<b>20% TFE</b>	4 $\mu$ l	1 $\mu$ l TFE	15
<b>Sonication</b>	5 $\mu$ l	-	10
<b>85 °C</b>	10 $\mu$ l	-	10
<b>1.2 M GuHCl</b>	4 $\mu$ l	1 $\mu$ l 6M GuHCl	15
<b>6 M GuHCl</b>	15 $\mu$ l	5.7 mg GuHCl	10
<b>0.4 M NaCl</b>	3 $\mu$ l	2 $\mu$ l 1M NaCl	15
<b>1 M NaCl</b>	10 $\mu$ l	0.5 mg NaCl	10

**Table 4.1. Buffer Conditions for Fibril Stability Tests**

#### **4.2.6. Limited Proteolysis**

This technique uses very low concentrations of protease to hydrolyse peptide bonds in unprotected regions. Limited proteolysis rarely occurs within regular secondary structure, with proteinases requiring sites with high chain mobility for proteolytic activity. Regions in the fibril core can be identified as they will be shielded from proteolytic activity.

##### **4.2.6.1. Sample Preparation**

hCC fibrils were produced by incubation of the monomeric protein at 225  $\mu$ M in 50 mM sodium acetate pH 4.0, 150 mM NaCl for 4 weeks and purified as described above. During the purification process fibrils were buffer-exchanged into 10 mM Tris-HCl pH 8.0 and diluted to a protein concentration of 75  $\mu$ M.

##### **4.2.6.2. Limited Proteolysis Reaction**

The protocol for the limited proteolysis experiment was taken from Davis (2013) and an overview is depicted in Figure 4.2. Elastase from porcine pancreas was used for proteolysis reactions at a 1:1000 protease to cystatin ratio (by mass). Elastase digestion

was carried out in 10 mM Tris-HCl pH 8.0 at 25 °C and quenched using a final concentration of 100 µM PMSF. Protease and inhibitor were purchased from Sigma Aldrich and stored frozen at -20 °C. Fresh aliquots from the same preparation were used for each digestion to maintain activity and reproducibility. Samples were taken at 5 time-points over 24 hours, and analysed by tricine SDS-PAGE and in-line C18 RP-HPLC ESI-TOF-mass spectrometry.

The reaction sample was equilibrated at 25 °C for 5 minutes before addition of the protease. An initial time-point sample was immediately removed and quenched with PMSF. An aliquot of 20 µl was removed and added to 20 µl loading buffer for SDS-PAGE analysis and the remaining sample was centrifuged at 13,000 x g for 15 minutes to pellet the digested fibrils. The supernatant (containing soluble peptide fragments) was retained and the insoluble fibril pellet washed by centrifugation with fresh reaction buffer. The final pellet was re-suspended in an equal volume of 6 M guanidine hydrochloride to dissolve the fibrils and allow the fragments to be analysed. The aliquots were frozen in liquid nitrogen as soon as possible after processing, with storage on ice up until this point, and then stored at -20 °C. Each time-point was treated in an identical manner and a soluble protein digest, again treated the same, was used as a control. Elastase and elastase with PMSF controls are described in Davis (2013) so these were not repeated.

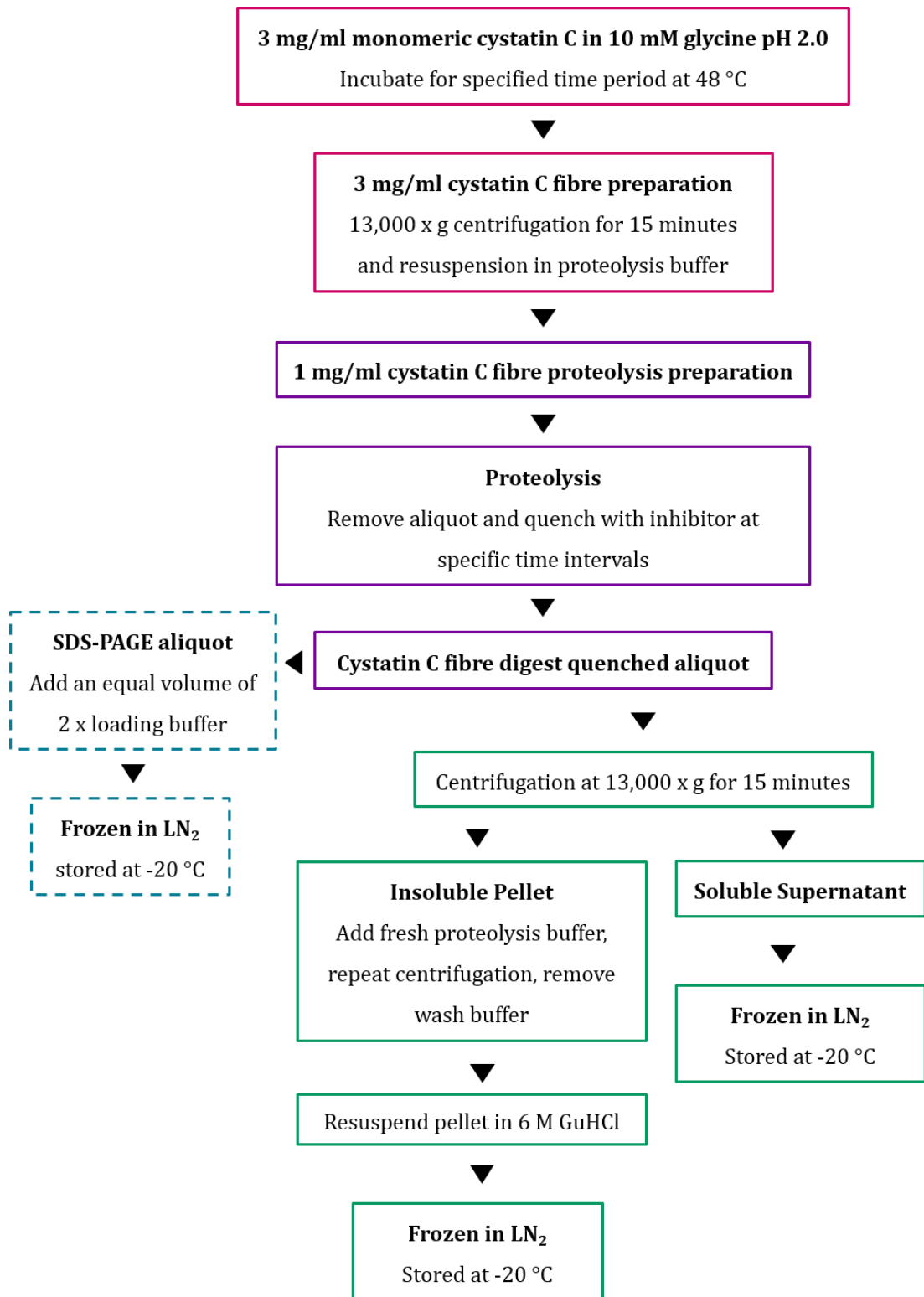


**Figure 4.2. Limited Proteolysis Sample Preparation**

*A flow chart depicting method of sample preparation for limited proteolysis. The SDS-PAGE sample is suggested to be optional as its use was limited in fragment analysis. Adapted from (Davis, 2013).*

#### 4.2.6.3. Elastase

Elastase is a serine proteinase that hydrolyses small hydrophobic amino acids with straight side chains such as alanine, valine, leucine, glycine and serine, unless preceded immediately by proline (Atlas 1970, Thompson and Blout 1973, Gold and Shalitin 1975). Isoleucine and threonine were also included according to (Rietschel et al., 2009) resulting in forty-eight specific cleavage sites throughout the soluble hCC structure from the primary sequence alone, as illustrated in Figure 4.3.

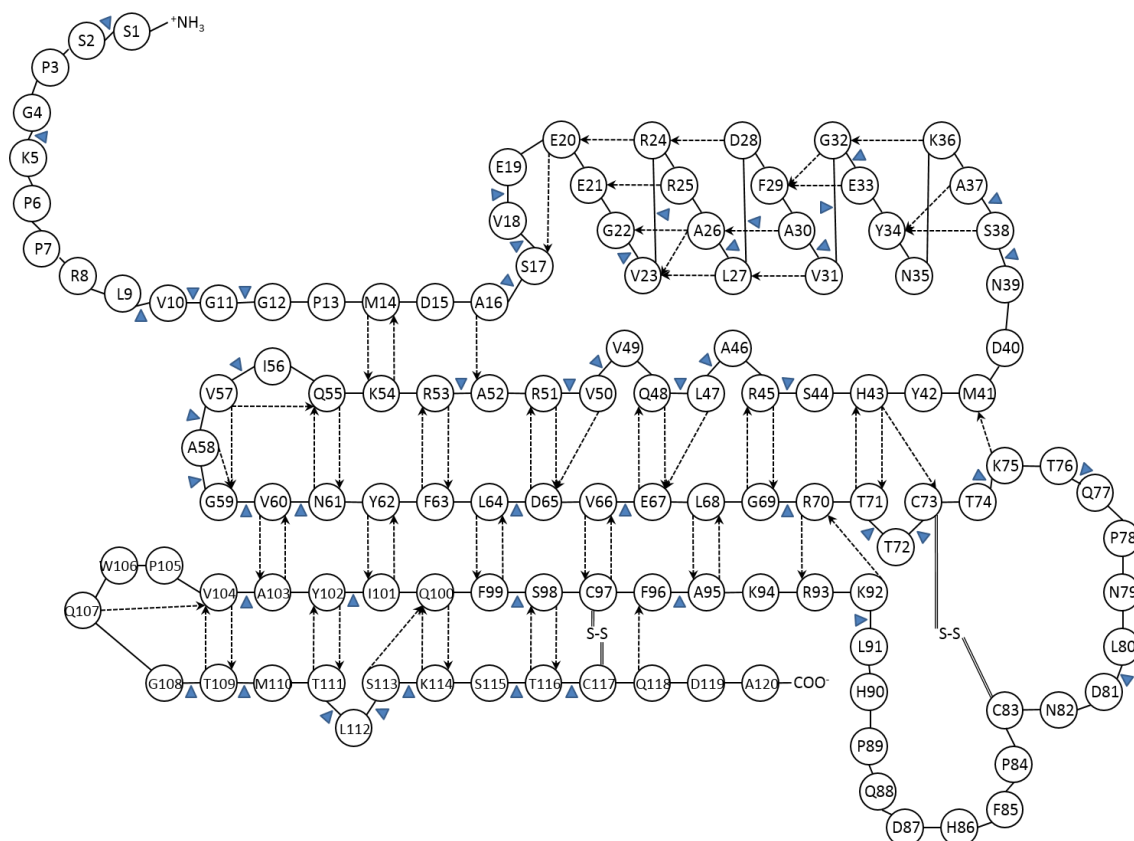


**Figure 4.3. Topology Map of hCC with Predicted Elastase Cut Sites**

*Predicted elastase hydrolysis sites (blue triangles) based on the primary sequence of hCC.*

Elastase was chosen for its wide coverage of the protein primary sequence, its activity under physiological conditions and the ease of quenching. In addition, and perhaps most importantly, these experiments have demonstrated that porcine elastase does not cleave the soluble protein readily suggesting that hCC monomer is also a potent inhibitor of serine proteinases (under most conditions) as well as its natural target the cysteine proteinases. In this way, fragments resulting from the proteolysis reactions can be traced to only fibrils or other oligomers of hCC. The observation of proteolysis also validates

the hypothesis that the population of active soluble hCC monomers is negligible in the hydrolysis reactions.

hCC is a natural substrate of leukocyte elastase *in vivo*, leading to a truncation between residues 10 and 11, however the activity of the porcine pancreatic elastase that was used is thought to be different to that of leukocyte elastase (Bode et al., 1989), as confirmed by the absence of this truncation from both monomer and fibril digests.

#### 4.2.6.4. Reverse Phase HPLC-ESI-MS and Mass Fragment Identification

Samples from the hydrolysis reaction were loaded onto a Grace Vydac Everest C18 reverse-phase column equilibrated with 5% acetonitrile, 0.1% formic acid and eluted using a linear acetonitrile gradient up to 50% over 40 minutes, then a 50-95% acetonitrile gradient over 5 minutes at 0.2 ml/min. Masses were detected by a Micromass LCT electrospray-ionisation time-of-flight instrument (Waters Corporation, Manchester) in positive ion mode. Masslynx 3.5 software was used to identify masses present and FindPept (ExPASy) (Artimo et al., 2012) was used to determine protein fragment identities by matching the predicted and actual masses. The analysis methodology is shown in Figure 4.4.

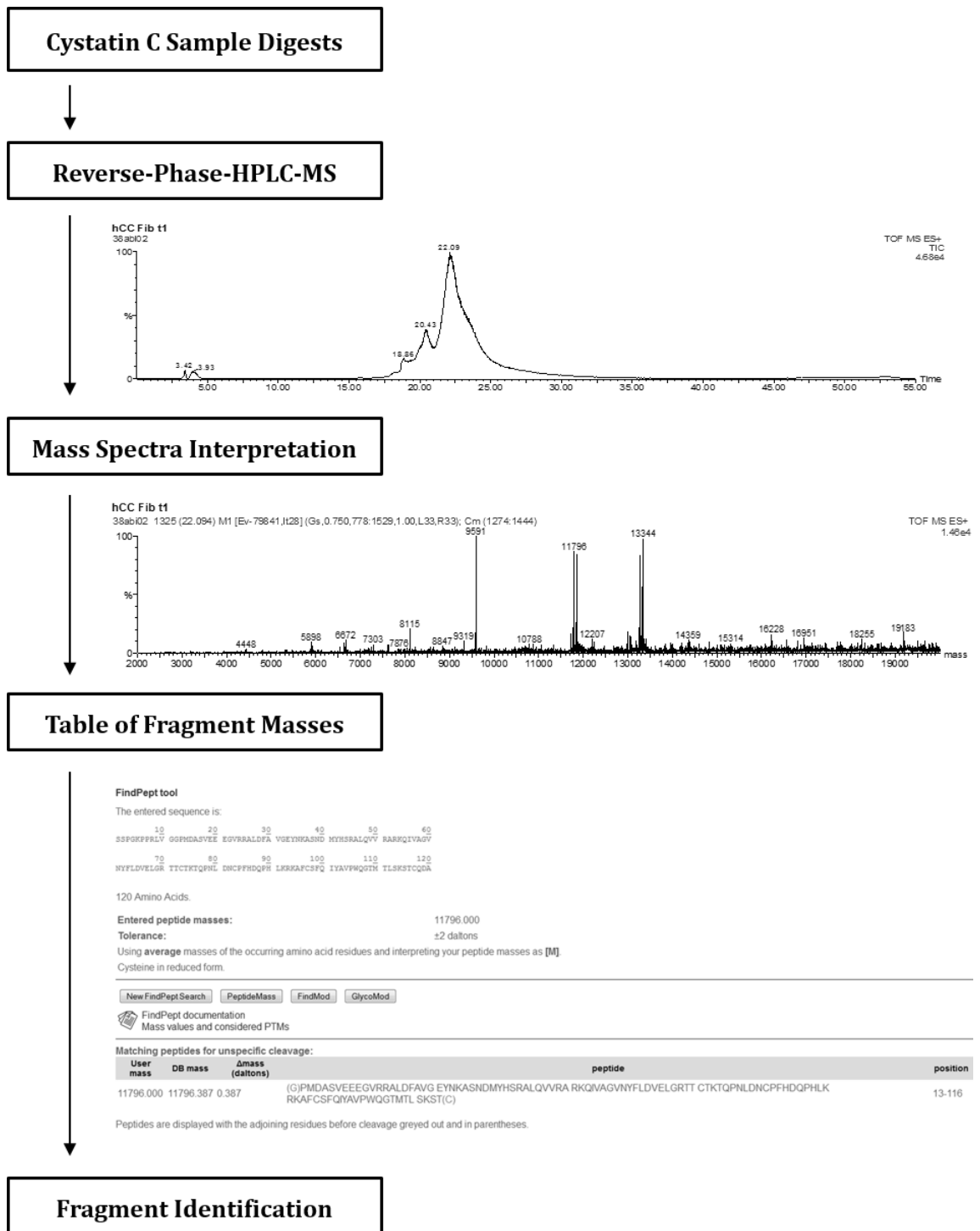


**Figure 4.4. Limited Proteolysis Fragment Analysis**

*Flow-chart illustrating analysis of limited proteolysis fragments by mass spectrometry and identification using FindPept (Artimo et al., 2012). Mass entropy peaks that were considered to be within the noise of the experiment were not used for identification purposes. Adapted from (Davis, 2013).*

## 4.3. Results and Discussion

### 4.3.1. Fibrillisation of hCC

Incubation of hCC in 10 mM glycine pH 2.0 or 50 mM sodium acetate pH 4.0, 100 mM NaCl at a concentration of 225  $\mu$ M resulted in the formation of amyloid fibrils as monitored by an increase in ThT fluorescence. The kinetic profiles of these reactions followed the classic sigmoidal curve that is characteristic of amyloid formation, and is consistent with the nucleation polymerisation model of fibril assembly.

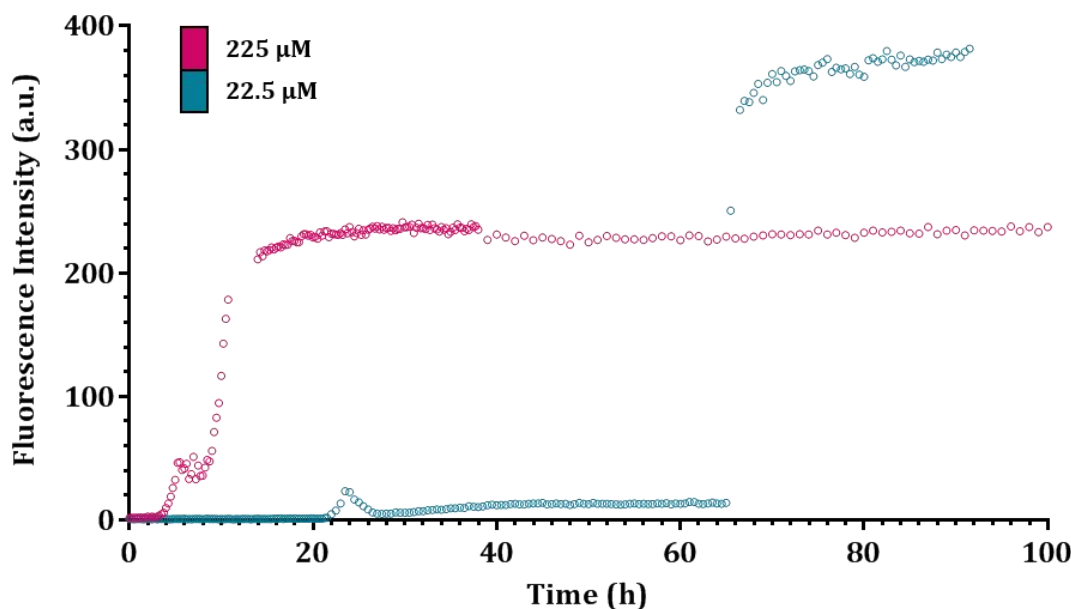
#### 4.3.1.1. Incubation at pH 4.0

Figure 4.5 shows that when incubated at pH 4.0, hCC forms fibrils within 20 hours. Fluorescence intensity begins to increase after 3 hours, with a small peak forming before a significant increase is observed after 8 hours. This is a distinctly shorter lag phase than is reported in the literature, where an exponential increase in fluorescence was not detected until 3 weeks of incubation (Wahlbom et al., 2007). Intriguingly, a small peak in fluorescence intensity was also observed before the elongation phase in a similar sample with a lower protein concentration of 22.5  $\mu$ M. The latter experiment was performed at a different time to the initial experiment, suggesting that this peak could correspond to the formation of ThT-positive species prior to fibril elongation. Other studies also observe an initial small increase in fluorescence intensity before the exponential phase of the reaction (Wahlbom et al., 2007), suggesting that this is not just an artefact of this specific experiment.

The reactions underwent agitation by constant stirring to induce fibrillogenesis. Although the samples in the Wahlbom study were also subject to constant agitation, the method of agitation is not described. A change in motion could lead to faster formation of nucleating species or increased fragmentation of existing fibrils, consequently causing fibril assembly to be quicker. Fragmentation of fibrils leads to an increase in the number of extension sites that are available for elongation, therefore increasing the rate of fibril assembly. In such a case the lag phase is often defined by the length of time it takes for the initial filaments to multiply and fragment, thereby allowing detection, rather than the formation of the initial nucleating species.

Another difference in these two experiments is that the study described here monitors ThT fluorescence in a continuous assay, where the dye is added at the start of the experiment and the whole sample is incubated and monitored. In a discontinuous assay,

the ThT is not present in the aggregating sample. Instead an aliquot is removed at specific time-points and added to a solution of ThT before analysis. Most of the published fluorescence studies of hCC fibrillisation have use the discontinuous method of analysis. It is therefore possible that the presence of ThT in the sample is enhancing fibril formation, although the opposite is usually observed.



**Figure 4.5. Fibrillisation of hCC at pH 4.0**

*hCC fibril formation monitored by ThT fluorescence intensity incubated in 50 mM sodium acetate pH 4.0, 100 mM NaCl at 48°C with agitation at protein concentrations of 225 μM and 22.5 μM*

#### 4.3.1.2. Incubation at pH 2.0

At pH 2.0, fibril formation occurred after approximately 200 hours, with an initial lag phase of 30 hours (Figure 4.6). As this sample was incubated at 48 °C for an extended period of time, low levels of evaporation were noted, especially towards the end of the experiment (> 200 hours), potentially leading to increases in ThT fluorescence that are unrelated to amyloid formation. The noise in this data could be attributed to the reduced fluorescence intensity of ThT at low pH.

In a similar fashion to the pH 4.0 experiments, the lag phase is decreased in comparison to previous work. A study by Nilsson et al. (2004) reports that significant amounts of fibril were produced after 7 days, with the exponential increase in fluorescence being observed after 4 days, and a plateau reached after 21 days. Previous experiments within the Staniforth lab following an agitated reaction by ThT fluorescence and TEM show a

lag phase of 12 days, with significant amounts of fibril observed after 2 weeks (Elshawaihde, 2012). Again, a small increase in intensity was observed early in the time-course in both these studies, which could indicate the formation of small ThT-positive species before the formation of mature amyloid (Nilsson et al., 2004, Elshawaihde, 2012).

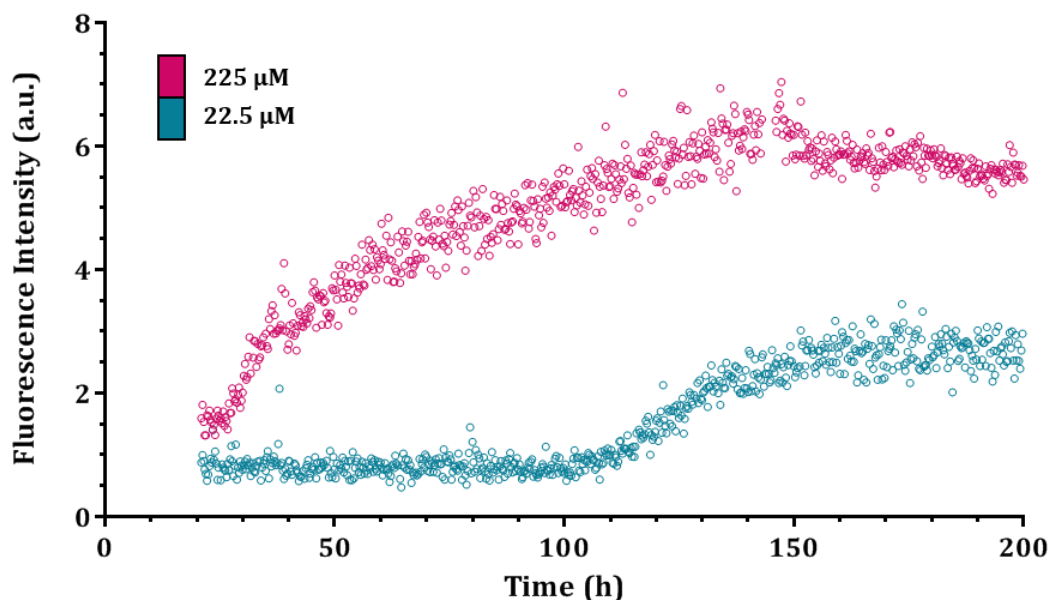


**Figure 4.6. Fibrillisation of hCC at pH 2.0**

*hCC fibril formation monitored by ThT fluorescence intensity incubated in 10 mM glycine pH 2.0 at 48°C with agitation at protein concentrations of 225 µM and 22.5 µM.*

#### 4.3.1.3. Concentration Dependence

hCC fibril formation was also investigated at lower protein concentrations. Difficulties in producing large amounts of the protein meant that carrying out experiments at the established concentration of 225 µM considerably limited experimental progress. Therefore establishing fibrillisation conditions at lower protein concentrations was very desirable, and has already shown to be successful in the cystatin B system where fibrils readily form at protein concentrations of 30 µM.

Figure 4.5 shows the fibrillisation of hCC at 22.5 µM at pH 4.0. Reducing the concentration 10-fold increases the lag time to 65 hours, still considerably quicker than the reported time of 15 days at the higher concentration. There is a very small increase in ThT intensity from 30 hours, suggesting that low levels of amyloid fibrils could be

being formed from this time onwards. Alternatively, on-pathway pre-fibrillar intermediates are forming that bind ThT and cause a small increase in fluorescence.

Samples produced at 225  $\mu\text{M}$  are often very cloudy, with large clumps of fibrils observed in the TEM. Comparison of the samples at the two different concentrations indicated that large masses of fibrils were present in the 225  $\mu\text{M}$  reaction, while the fibrils in the 22.5  $\mu\text{M}$  were more disperse. Fibrillisation at the lower concentration gives a higher fluorescence amplitude, almost double that of the 225  $\mu\text{M}$  sample. It seems unlikely that the amount of fibril produced was greater in the dilute sample, rather that there is an alternative explanation for the increase in ThT intensity. It was noted that many of the fibrils had oligomers associated with the surface of the fibril, potentially preventing the ThT molecules from binding to the fibril. Differences in fibril morphology could also lead to differences in ThT intensity.

At pH 2, lowering the concentration 10-fold again causes an increase in lag phase from 30 hours to 100 hours, as can be seen in Figure 4.6. In contrast to the pH 4.0 sample, the more dilute sample does not show a greater amplitude, suggesting that fewer fibrils are being formed.

The increase in the lag phase at lower concentrations of hCC indicates that the creation of nuclei is a concentration-dependent process, unlike other cystatins reported in the literature (Sanders et al., 2004, Skerget et al., 2009). The nucleation polymerisation model of fibril assembly indicates that this should be the case, consistent with the hypothesis that this is the mechanism by which hCC forms amyloid fibrils. However the fact that the rate increase is not obviously proportional to the change in concentration, with a 10-fold increase in hCC concentration leading to only a 3-fold change in lag time, suggests that secondary nucleation events are important. Fragmentation is likely to be a key effect given the dependence on agitation discussed above and the fact that this phenomenon would explain why the process may occur faster than expected at low concentrations of protein. Although it was not possible to fit a curve to the data to determine kinetic parameters unambiguously, the elongation rate at pH 4.0 appears superficially to be maintained at the lower concentrations. This is not consistent with the nucleation polymerisation model, which predicts that the rate of fibril elongation will increase with increased protein concentrations. However, without further replication of these data, and curve-fitting to establish kinetic parameters, subtle differences in elongation rate cannot be established from the experiments shown here.

The low levels of fibril that were produced at pH 2.0 when the protein concentration was 22.5  $\mu\text{M}$  makes these conditions unlikely to be viable for further experimentation. However, incubation at the lower concentration at pH 4.0 was promising, with less clumping of fibrils and fewer oligomeric species present.

#### 4.3.1.4. pH Dependence

It has been established that hCC will form amyloid fibrils in two different pH conditions. Although there were difficulties with obtaining a curve fit in order to establish the kinetic parameters of fibril assembly, from Figure 4.7 it is clear to see that fibril formation occurs faster at pH 4.0, with a lag phase of approximately 8 hours compared to 30 hours at pH 2.0 at 225  $\mu\text{M}$  protein concentration. There also appears to be a difference in elongation rate, as the pH 4.0 sample has a much steeper curve than the pH 2 sample. This suggests that both nucleus formation and fibril elongation are pH dependent. A similar pattern is seen at the lower protein concentration of 22.5  $\mu\text{M}$ , where again the lag phase is increased in the pH 2 sample. It also appears as though the rate of elongation is reduced at the lower pH, again consistent with what is observed at 225  $\mu\text{M}$ .

The kinetics of fibril formation and the effect of pH are likely to reflect the changes in the stability of key intermediates or transition states on route to fibril formation, as well as potential for self-association. hCC has a predicted pI of 8.75 (Keeley, 2008), therefore will carry a net positive charge at pHs below this. At low pH the high positive charge, caused by protonation of aspartates and glutamates, leads to destabilisation of the protein by electrostatic repulsion and can induce unfolding. At the slightly higher pH 4.0, the charge will be slightly more neutral due to deprotonation of these acidic amino acid side-chains. This will therefore favour self-association due to a reduction in the repulsive forces present at pH 2.0 between highly positively charged protein molecules, creating a faster lag phase and increase in the rate of fibrillisation as observed.

At pH 2.0 it is thought ~50% of the hCC molecules will be in an intermediate state which is extensively unfolded, as demonstrated by an 80% loss in CD signal (Keeley, 2008). This means that the formation of amyloid-competent structure may be too slow to favour fibrillisation, leading to an extended lag phase and slower rate of fibril formation in these conditions. At pH 4.0, it is expected that the folded state of the protein will still dominate, yet the stability of the molecule will be sufficiently

compromised to allow structural conversions via the unfolded state on a measurable timescale. As with other cystatins, conditions which are “pre-denaturing” seem to be favoured, however neither the unfolding rates nor stabilities ( $\Delta G$ ) of cystatin C have been determined under different pH conditions.

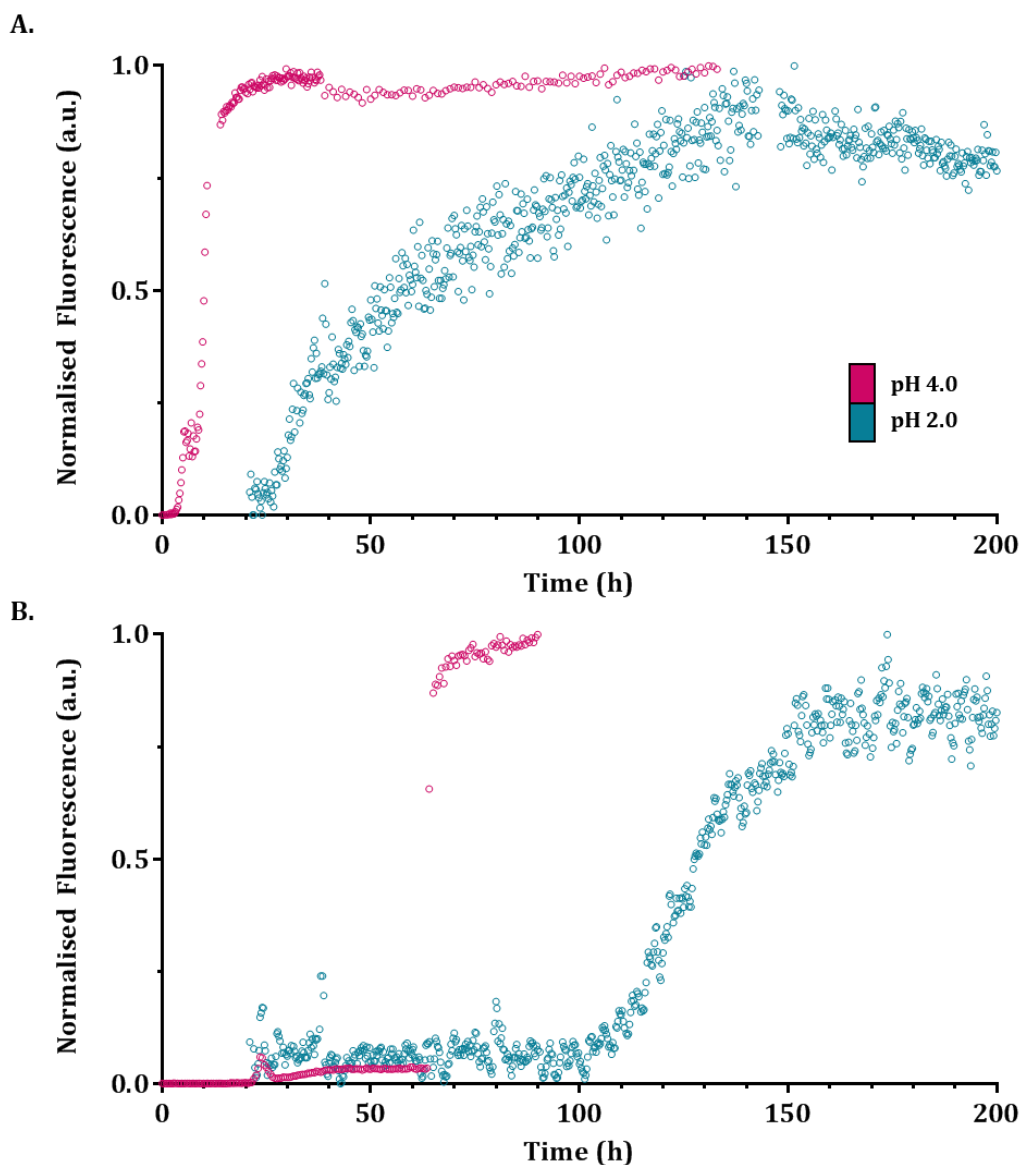


**Figure 4.7. pH Dependence of hCC Fibril Formation**

*Comparison of hCC fibril formation at pH 2.0 and pH 4.0 monitored by ThT fluorescence intensity at protein concentrations of (A) 225  $\mu\text{M}$  and (B) 22.5  $\mu\text{M}$ .*

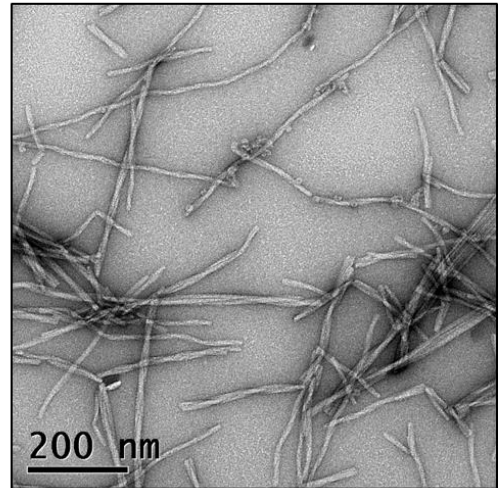
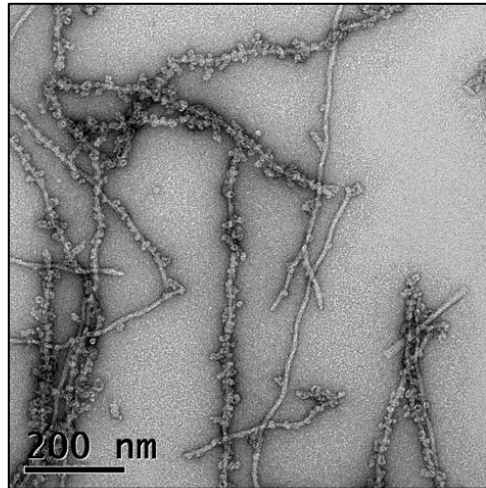
#### 4.3.1.5. Electron Microscopy

Transmission electron microscopy was used to confirm the formation of amyloid fibrils in the aggregation conditions described above, in addition to providing information about the differences in species morphology. Incubation of 225  $\mu\text{M}$  hCC at pH 4.0 led

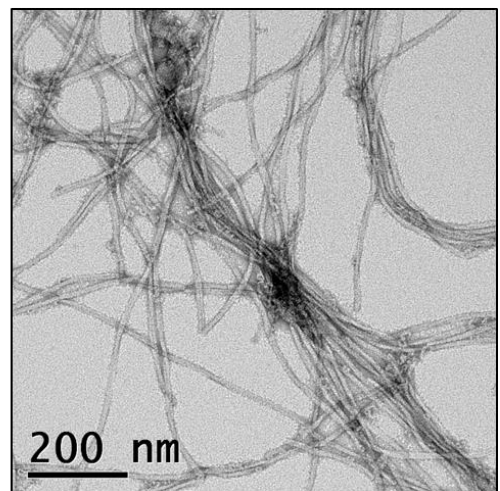
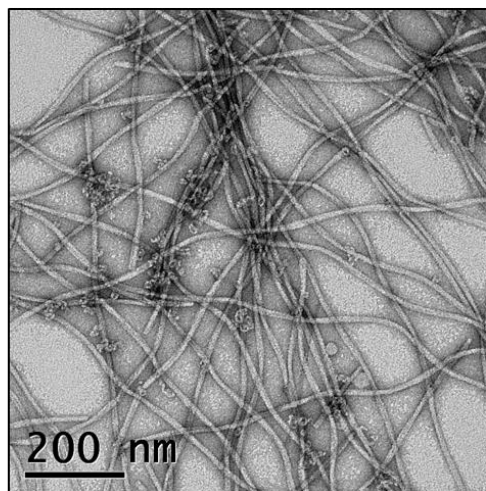
to the production of long unbranched amyloid fibrils as shown in Figure 4.8. These often bundle together to form large heavily stained masses of fibrils through lateral association (data not shown). There appear to be two different populations of amyloid fibril, as many of the fibrils have associated circular oligomeric species along the length of the fibril. An alternative population of fibrils shows no association with these oligomers. This implies a difference in morphology between the two populations in which, although not observable by TEM, an alternative surface has been exposed. This could lead to an interaction with oligomers, potentially through exposed hydrophobic residues. The observation of two different populations in the same sample indicates two different nucleation events. Still at pH 4.0, but with a lower protein concentration of 22.5  $\mu\text{M}$ , hCC again forms long unbranched amyloid fibrils. Although there is some lateral association between small groups of fibrils, the large clumps are absent from this preparation. There are also fewer oligomers present in the sample, and they do not appear to coat the fibrils in the same manner as is seen in the 225  $\mu\text{M}$  sample. At the lower concentration the fibrils have an almost 'wavy' appearance. There is also evidence of twisted fibrils, which appear to be composed of two (or more) amyloid fibrils wrapped around each other. The formation of amyloid fibrils does not appear to be concentration dependent, as mature fibrils are observed in both of the preparations. Oligomers are produced at both concentrations, indicating that this is not a process that depends on high concentrations of hCC.

Figure 4.9A shows that hCC has also formed amyloid fibrils at pH 2.0 at both protein concentrations. These fibrils are much straighter than those formed at pH 4.0, with a considerable reduction in the amount of fibrils produced at 22.5  $\mu\text{M}$ . Again there is evidence of twisted fibrils. The samples produced in the ThT assays appear to consist entirely of amyloid, there are very few oligomers present and there is no coating of the fibrils. However in previous preparations at pH 2.0 oligomers are formed and can be observed along the length of the fibrils, as well as free in solution (Figure 4.9B). The majority of these preparations were in the absence of ThT. This could indicate that ThT has an effect on the process of oligomer formation at pH 2.0, preventing their production by favouring the formation of species which then go on to produce fibrils.

**225  $\mu$ M**



**22.5  $\mu$ M**



**Figure 4.8. Electron Microscopy of hCC Fibrils at pH 4.0**

*Electron micrographs of hCC fibrils formed at protein concentrations of 225  $\mu$ M and 22.5  $\mu$ M at the end of the ThT time-course. Images were taken at 21,000 magnification.*

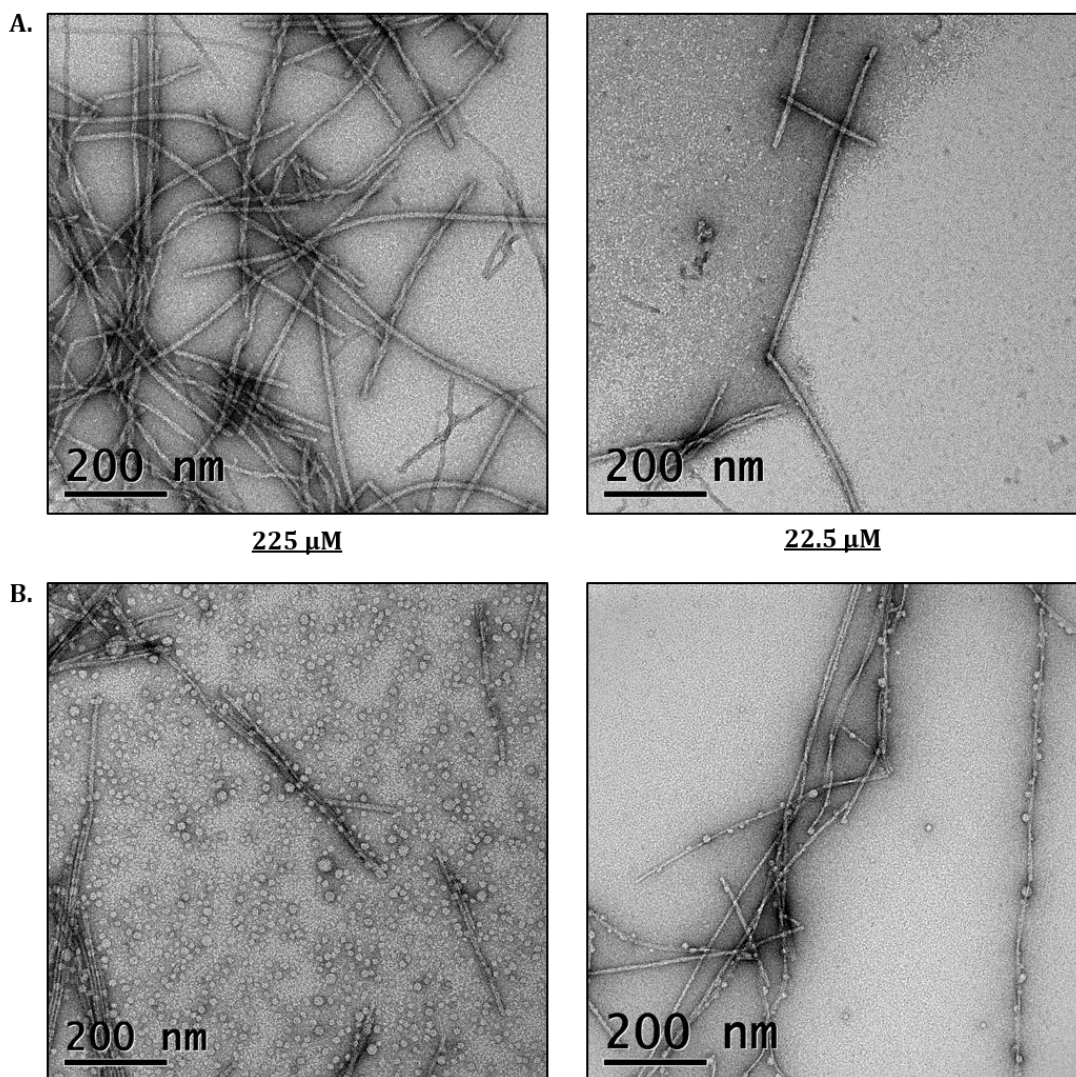


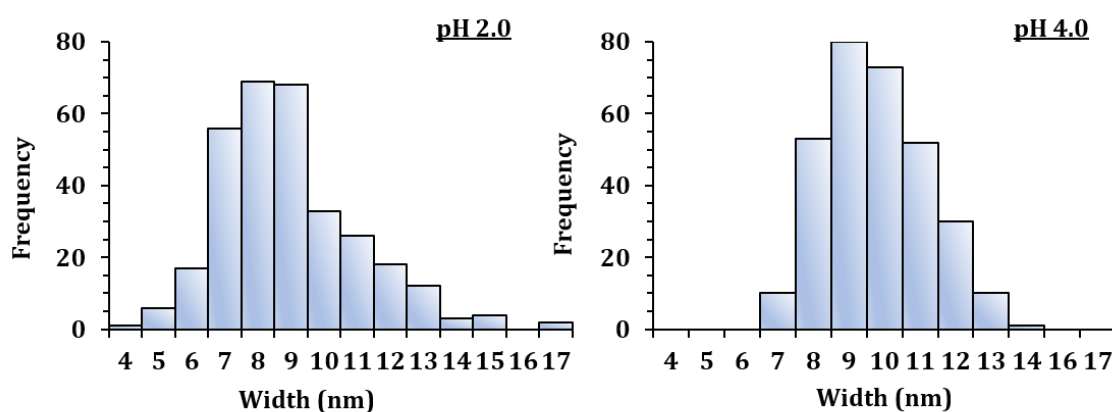
**Figure 4.9. Electron Microscopy of hCC Fibrils at pH 2.0**

*Electron micrographs of ThT end-points at pH 2 (A) at protein concentrations of 225  $\mu$ M and 22.5  $\mu$ M. A different preparation formed at 225  $\mu$ M is also shown (B), indicating the production of oligomeric species. This sample was taken after 3 weeks of incubation at 48°C with stirring, in the absence of ThT. The two images were taken from different parts of the EM grid. All images were taken at 21,000  $\times$  magnification.*

#### 4.3.1.6. Fibril Measurements

hCC fibrils formed at both pH 2.0 and pH 4.0 were measured to determine the width of the fibril and establish whether there were any major differences in morphology. Figure 4.10 shows histograms of these measurements and the calculated average fibril widths. In both of these conditions certain preparations show extensive lateral association of the fibrils, often into dense tangled clumps that prevent accurate width estimates; such fibrils were excluded from this study. Fibrils produced at pH 2.0 from different

preparations had an average width of 9.5 nm ( $\pm 2.0$  nm SD,  $n = 315$ ) with a minimum and maximum of 4.8 nm and 17.9 nm respectively. Fibrils produced at pH 4.0 from different preparations had an average width of 10.3 nm ( $\pm 1.4$  nm SD,  $n = 309$ ) with a minimum and maximum of 7.5 and 14.3 nm respectively. At both pHs, no single preparation showed obvious deviation in width or morphology. There is a large distribution of fibril widths from the samples produced at pH 2.0, with the largest width measured (17.9 nm) being almost 4 times greater than the smallest (4.8 nm). Cystatin B fibrils have an average width of 8.6 nm ( $\pm 1.4$  nm SD,  $n = 237$ ).



Conditions	Average Width (nm)	Number of Fibres Measured	Maximum Width (nm)	Minimum Width (nm)
pH 2.0	9.5 $\pm$ 2.0	105	17.9	4.8
pH 4.0	10.3 $\pm$ 1.4	103	14.3	7.5

**Figure 4.10. Fibril Width Measurements**

*Electron micrographs of different fibril preparations were measured using Digital Micrograph 3 software (Gatan, UK). Each fibril was measured 3 times at different points. The histograms show the distribution of width measurements at pH 2.0 and pH 4.0 and average width measurements are shown with the standard deviation.*

#### 4.3.1.7. L68Q Variant

The increased propensity of L68Q to aggregate caused expression and purification of this mutant to be challenging. Expression of the protein at 30°C, a temperature which normally produces lower yields of wild-type protein anyway, produced 1.5 mg of L68Q from 4.8 L of *E. coli*. Expression of L68Q at 37°C produced undetectable amounts of protein, suggesting that the expressed OmpA-protein is not soluble and has gone into inclusion bodies rather than being exported to the periplasm.

Incubation of L68Q in the purification buffer (10 mM sodium phosphate pH 6, 100 mM NaCl) at 4°C, which are the standard storage conditions, led to the formation of amyloid fibrils over ~2 weeks. This highlights the increased aggregation-propensity of this mutant, as wild-type hCC is stable in these conditions for extended periods of time, even years. The L68Q sample was viewed by TEM, which indicated that amyloid fibrils had formed as shown in Figure 4.11. These appear to have a slightly different morphology to those of the wild-type protein, with a highly twisted appearance and are substantially associated in a lateral manner to form large bundles. Small amounts of oligomer were also present, with a similar morphology to those produced by wild-type hCC at pH 2.0. The oligomers appeared highly stable as they remained in solution for an extended period of time, which could have important physiological implications. Analysis by SEC-HPLC indicated that monomeric and dimeric protein was still present, indicated that not all the protein had been converted to amyloid. That L68Q can form fibrils at relatively low concentrations (40  $\mu$ M), at pH 6 and in the fridge (reasonably mild conditions) whilst WT must be incubated at low pH and 48°C demonstrates the amyloidogenic potential of the L68Q variant as well as highlighting the experimental difficulties in working with this mutant compared to other cystatin family members.

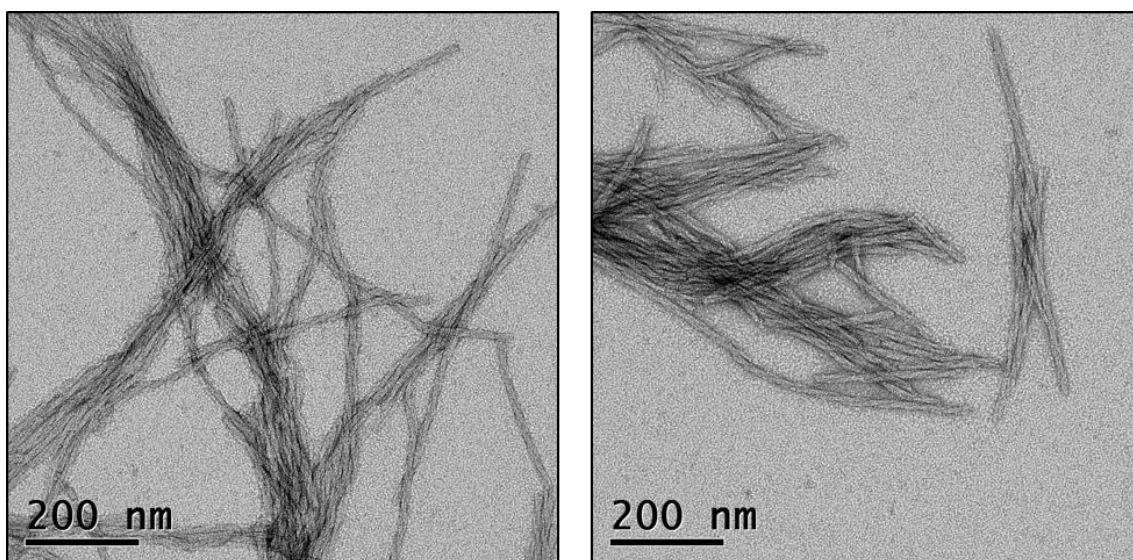


**Figure 4.11. TEM of L68Q Fibrils**

*Electron micrographs of L68Q fibrils formed at pH 6.0. Images taken at 21,000 x magnification.*

### 4.3.2. Oligomeric Intermediates

As previously mentioned, hCC forms oligomeric species as part of the aggregation process at both pH 2 and pH 4.0. As it is hypothesised that intermediates could be the toxic species in amyloidogenic diseases, these are important structures to study.

#### 4.3.2.1. Formation of Oligomers at pH 4.0

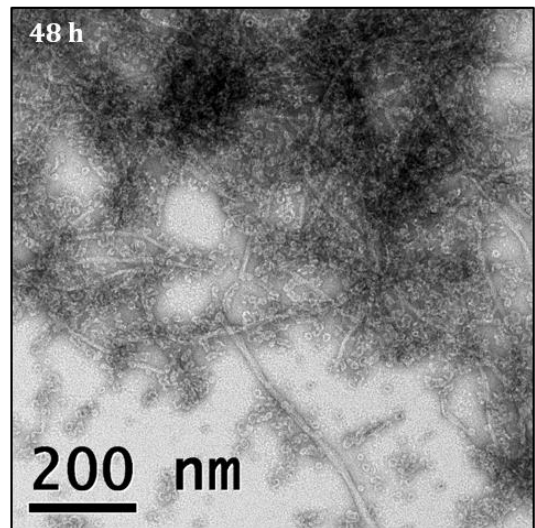
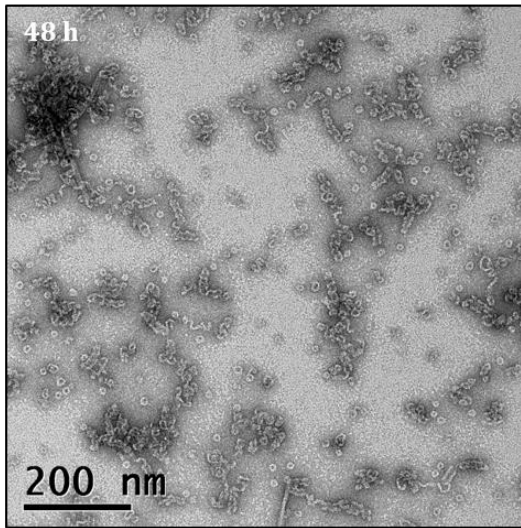
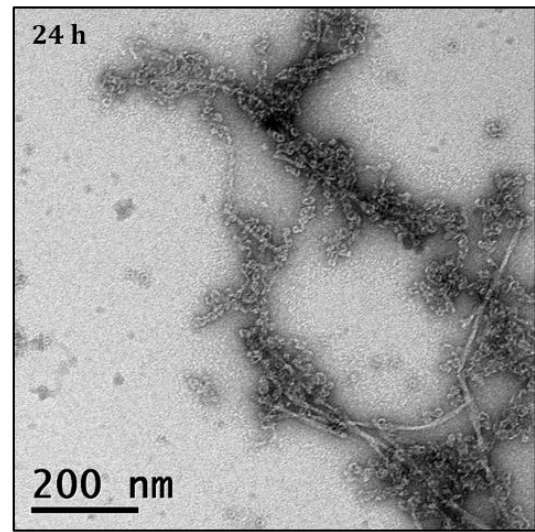
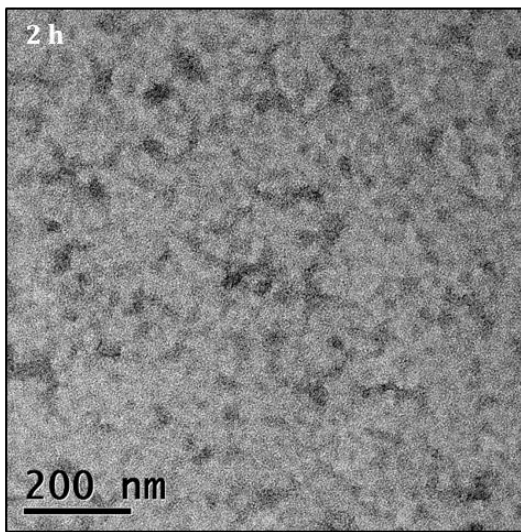
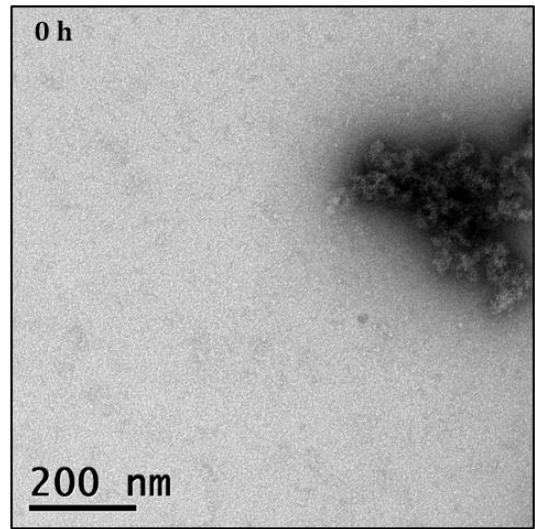
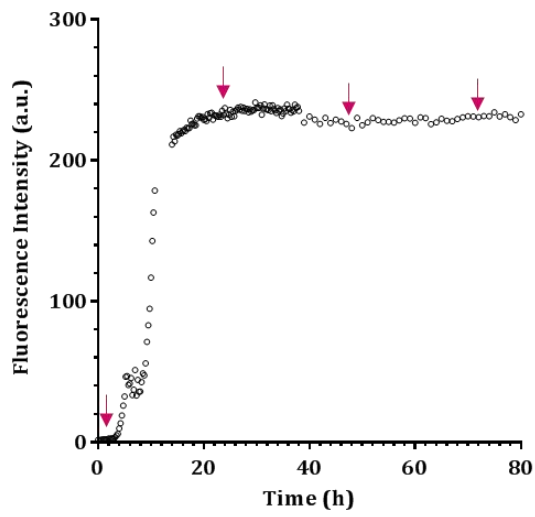
TEM of fibrillation samples formed from 225  $\mu\text{M}$  at pH 4.0 indicates that, as well as amyloid fibrils, there are also large amounts of non-fibrillar, oligomeric species present. These species are circular, or spherical often with a ring-like morphology. It is proposed that oligomers are transient on-pathway intermediates, assembling before protofibrils and subsequent amyloid formation. Intriguingly the hCC oligomers are present in solution after the formation of amyloid fibrils, indicating that they may not be on-pathway intermediates (and are definitely not transient) but rather that these structures could denote a secondary end-point to hCC aggregation.

hCC amyloid fibrils produced at pH 4.0 fall into two distinct populations, those with associated oligomers and those without. The prevalence of these coated fibrils, and their presence in different preparations of hCC amyloid, makes it unlikely that they are an artefact from grid preparation for electron microscopy whereby oligomers may just happen to fall on the surface of the fibril. As well as associating with the fibrils there are also many oligomers present in solution, indicating that their stability is not dependent on the association with the amyloid fibril. TEM of the sample produced at a lower concentration of the protein showed that very few oligomers were present, and not many were associated with the fibrils. This could indicate that oligomer formation is concentration-dependent, and the formation of fibril is favoured over that of oligomer at low concentrations.

It is possible that in the hCC system, amyloid fibrils are exerting a surface effect to catalyse the formation of stable oligomeric species in a secondary nucleation mechanism and that once formed these species are remaining associated with the fibril structure. If this were the case then following the reaction over time would show the production of fibrils before oligomers. Alternatively, instead of catalysing oligomer formation, the fibril surface could be acting to stabilise the oligomers once formed, preventing their further aggregation into mature fibrils. This would require the formation of fibrils and oligomers simultaneously for the fibrils to act as a surface. It

would also mean that the rate of oligomer and fibril formation is different, again suggesting that the oligomers are not on-pathway to amyloid formation.

To gain further insight into oligomer formation, the fibrillisation reaction of hCC at pH 4.0 was followed by transmission electron microscopy as shown in Figure 4.12. Unfortunately the TEM time-course was undertaken before the ThT time-course, hence the lack of time-points during the elongation phase. Although it has been suggested in the literature that oligomers can be seen as early as after 1 hour of incubation (Wahlbom et al., 2007), early time-points indicated that oligomers were not present for the first 2 hours; many had formed by 24 hours. A few fibrils were present after 24 hours, however it was not until 48 hours that larger amounts were seen. In addition to being free in solution, the oligomers appear to interact with the amyloid fibrils, as they can be observed associated along the length of the fibril. After 1 week, many annular oligomers are still present, however there are also some spherical species that lack the donut-like appearance. After 3 weeks, although there are fewer oligomers free in solution, they are still present in the large clumps of associated fibrils. In these conditions, the fibrils appear very 'sticky' and there is a lot of lateral association, with smaller aggregates coating the fibrils and causing large clumps to form. These large clumps make it difficult to resolve distinct structures under EM, except at the very edges.



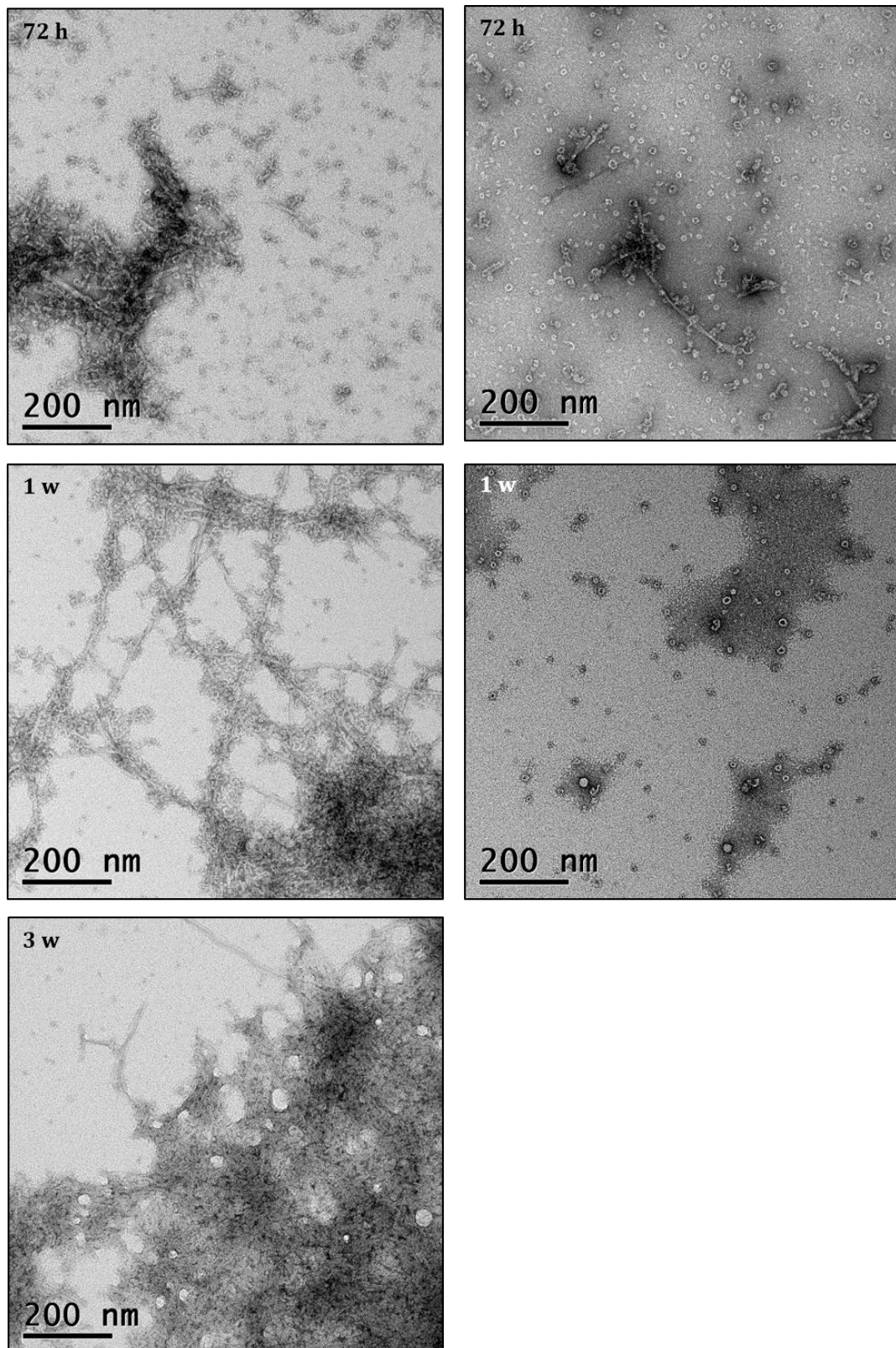


**Figure 4.12. TEM Time-Course of hCC Fibrillisation at pH 4.0**

*TEM time-course of the fibrillisation of 225  $\mu$ M hCC at pH 4.0 and 48°C over 3 weeks. A graph showing the change in ThT fluorescence in these conditions is used to indicate the points at which EM was performed (pink arrows). Images were taken at 21,000 x magnification.*

#### 4.3.2.2. Formation of Oligomers at pH 2.0

hCC also forms non-fibrillar oligomers when incubated at pH 2.0. These species are also circular, or spherical, but they are lacking the annular appearance, and therefore potentially the central water-filled pore, that is seen at pH 4.0. Either the change in pH causes the formation of structures with a different morphology, or these are similar structure which have associated differently with the EM grid. The spherical species produced have a very homogenous morphology, although there is a wide range of sizes. Again these structures appear to associate with the amyloid fibrils that are present in the sample. Although these oligomers have been previously observed in preparations within the Staniforth group (Elshawaihde, 2012), no description of them has been found in the literature.

Figure 4.13 shows a TEM time-course of hCC incubated at pH 2.0. This indicates the formation of small aggregates after 1 week, some of which have an annular appearance. However, although the sample was analysed for several weeks, very few amyloid fibrils were observed, even after an extended period of time, and the appearance of amorphous aggregate after 1.5 months suggests that the protein has aggregated but not formed amyloid fibrils. Oligomeric aggregates are still observed after 2 months, highlighting the stability of these structures and suggesting that they do not assemble further to form larger aggregates. Intriguingly these species have lost their annular appearance.

The formation of amyloid by hCC appears to be quite variable, as occasional preparations were incubated that did not lead to the formation of fibrils. This is highlighted in this time-course, where all of the time-points were taken after ThT assays indicate that amyloid fibrils should have formed. The production of amorphous aggregates in these preparations indicates that there is a fine balance between the formation of amyloid and non-fibrillar aggregates in this system. Amorphous aggregates were not observed when hCC was incubated at 22.5  $\mu$ M at pH 2.0, however this experiment has not been repeated so it is impossible to categorically say that amorphous aggregation could not occur in these conditions.

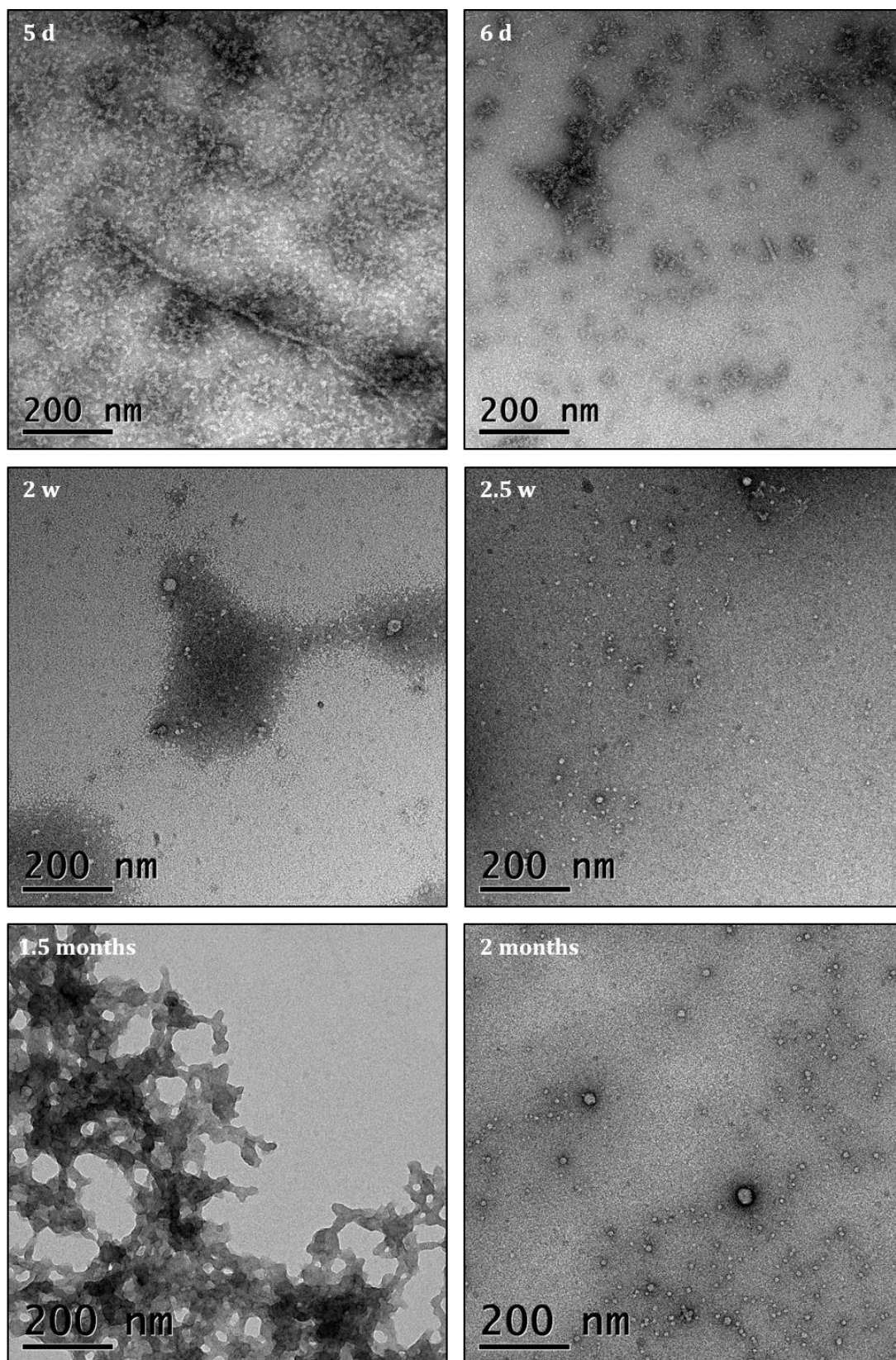


**Figure 4.13. TEM Time-course of hCC Fibrillisation at pH 2.0**

*TEM time-course of hCC fibrillisation at pH 2.0 and 48°C over 2 months. Images were taken 21,000 x magnification.*

### 4.3.2.3. Association of Oligomers and Fibrils

There appears to be a high degree of association between the oligomers and fibrils, with the oligomers coating the fibrils in both pH conditions. In the ThT time-course at pH 4.0 there appear to be two distinct populations of fibril grouped together, with some having no associated oligomers and some being completely covered. In order to try and determine the nature of the interaction between the two species, samples were incubated under different conditions (Table 4.2) and observed by TEM (Figures 4.14 – 4.17), whilst also demonstrating the stability of the two species in these conditions. The conditions were chosen to investigate extremes of pH, high salt environments and the presence of denaturants, as well as mechanical perturbations such as sonication and high temperatures.

Condition	Fibrils	Free Oligomers	Associated Fibrils
<b>pH 1.0</b>	***	*	**
<b>pH 7.0</b>	**	-	*
<b>pH 14.0</b>	*	*	**
<b>20% TFE</b>	**	-	**
<b>Sonication</b>	***	-	**
<b>85°C</b>	-	-	***
<b>1.2 M GuHCl</b>	**	*	**
<b>6 M GuHCl</b>	**	**	*
<b>0.5 M NaCl</b>	***	-	**
<b>1 M NaCl</b>	-	-	***

**Table 4.2. Incubation of hCC Fibrils in Different Conditions**

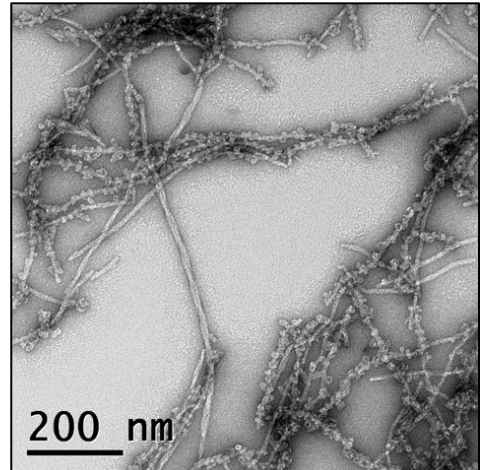
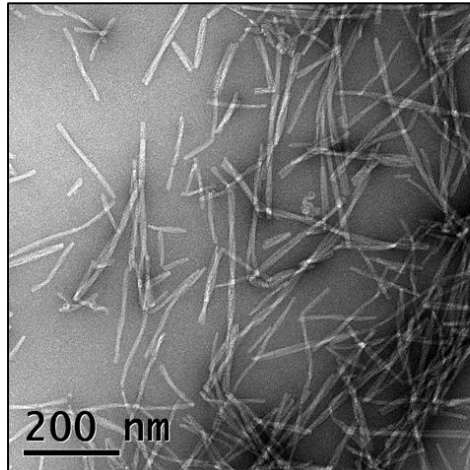
Amyloid fibrils and oligomers were observed in all of the preparations described above, highlighting the stability of both of these structures in extreme environments. In very few of the samples were free oligomers observed, only at pH 1.0 and pH 14.0 and in the presence of 6 M GuHCl, demonstrating that there is a strong association with the amyloid fibrils which is not easily broken by alterations in environment. Figure 4.14 shows electron micrographs of the samples incubated with different concentrations of salt (0.5 M and 1 M NaCl). When incubated with 0.5 M NaCl short straight fibrils are observed, in addition to long fibrils coated with oligomers. With the increase in salt

concentration to 1 M, the fibrils remain highly associated with the oligomers, with very few plain fibrils observed. This reinforces the idea that the interaction between the oligomers and the fibrils may be hydrophobic in nature.

In the presence of 1.2 M GuHCl (Figure 4.15), both types of fibril (with and without associated oligomers) were present, however at the higher concentration of 6 M guanidine there were many oligomers free in solution and not associated with the fibrils. Many short fibrils were also observed, potentially indicating the start of the dissociation of the long fibrils in the presence of the denaturant. Amyloid fibrils are not generally resistant to 6 M guanidine, a property that is exploited later in the limited proteolysis experiment. It is likely that here as well substantial amounts of protein are solubilised, but the species persisting the longest reveal something about the nature of the interactions between the oligomers and the fibrils. An aged sample could also infer some resistance to the denaturing effect through the formation of cross-links between tyrosine side chains within the fibril as has been observed for A $\beta$  and  $\alpha$ -synuclein (Souza et al., 2000, Yoburn et al., 2003). Both the fibrils and oligomers are much more stable than hCC dimer and monomer in guanidine, as the latter species unfolds at a concentration of 1.3 M and does not retain its structure (Keeley, 2007).

The addition of 20% 2,2,2-trifluoroethanol made little alteration to the morphology and abundance of the species observed (Figure 4.16), as did sonication for 10 minutes and heating to 85°C for 10 minutes. Sonication is regularly used to fragment fibrils for seeding experiments in many different systems, and leads to the formation of very short fibrils which are not observed here. The sonication applied to this sample could be less harsh therefore than typically used. Altering the pH of the fibril sample (Figure 4.17) to extremely acidic (pH 1.0) and extremely basic (pH 14.0), as well as neutral (pH 7.0) demonstrated that both species, the fibrils and oligomers, were stable in all of these conditions. Incubation at pH 1.0 shows some dissociation of oligomers from the fibril surface, potentially leading to the uncoiling of these oligomeric structures. The stability of the fibrils in these different conditions could have useful implications for future experiments, but unfortunately, did not highlight conditions for the separation of oligomers and fibrils of hCC.

**0.5 M NaCl:**



**1 M NaCl:**

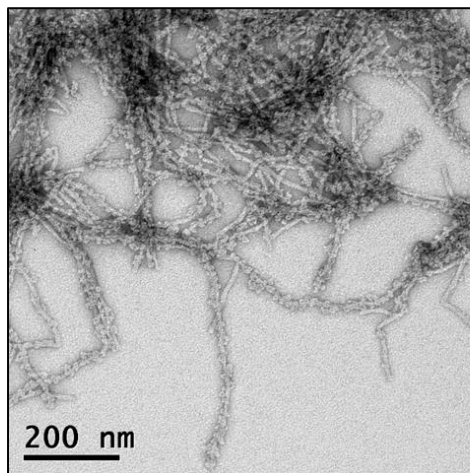
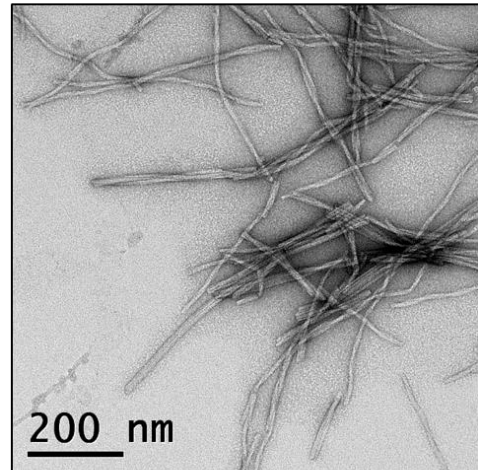
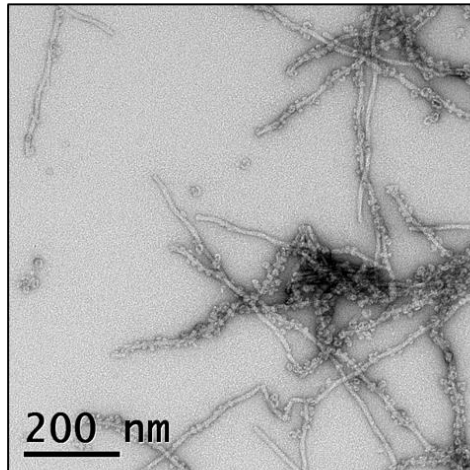


**Figure 4.14. Incubation of hCC Fibrils at Different Ionic Strengths**

*Electron micrographs of amyloids fibrils formed at pH 4.0 in different concentrations of salt. Images were taken at 21,000 x magnification.*

**1.2 M GuHCl:**



**6 M GuHCl:**

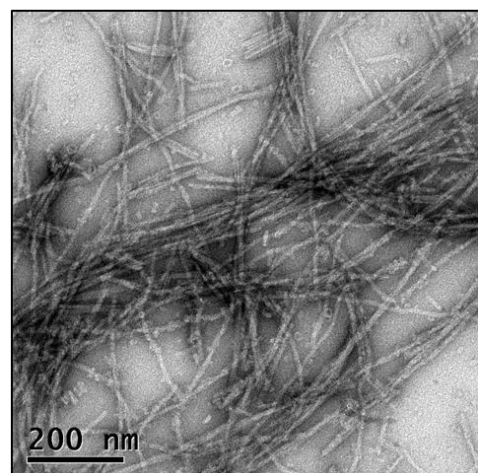
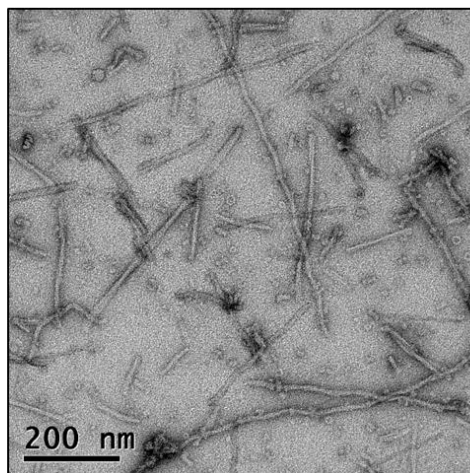
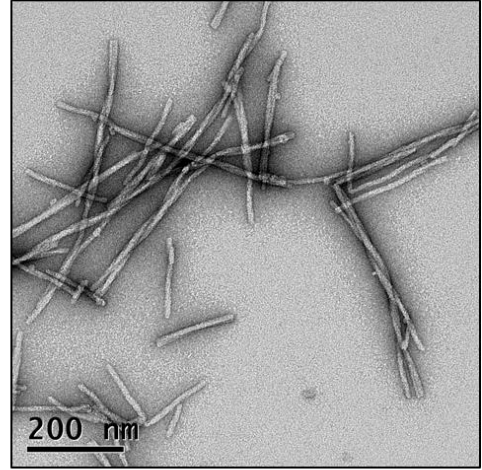
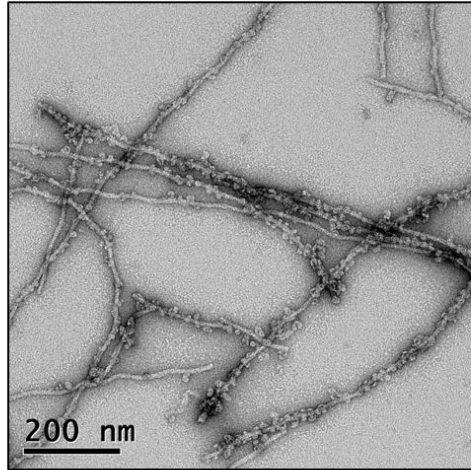


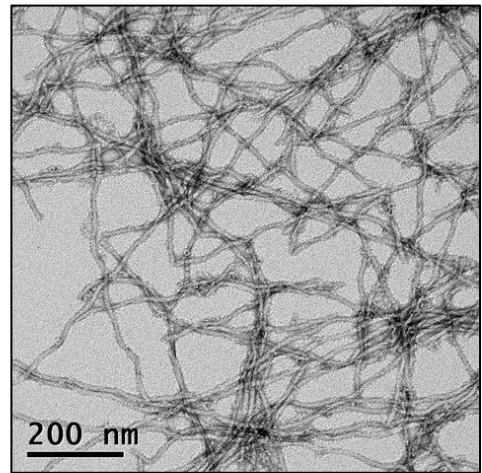
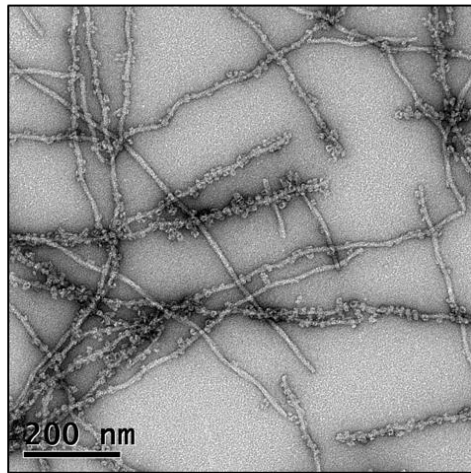
**Figure. 4.15. Incubation of hCC Fibrils in Denaturant**

*Electron micrographs of hCC fibrils formed at pH 4.0 in different concentrations of denaturant. Images were taken at 21,000 x magnification.*

**20% TFE:**



**Sonicated:**



**85°C:**

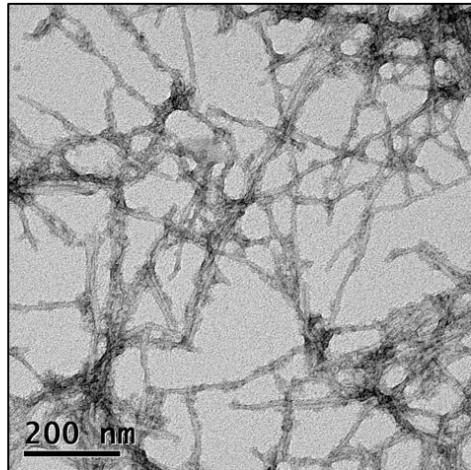
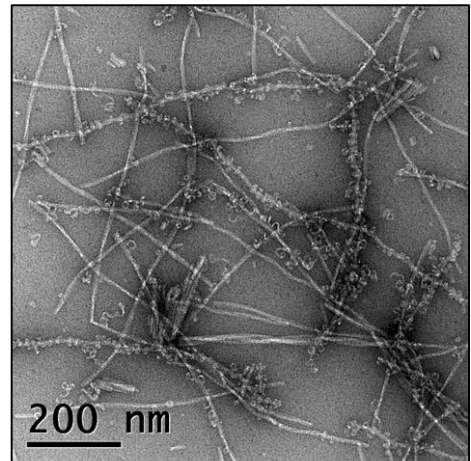
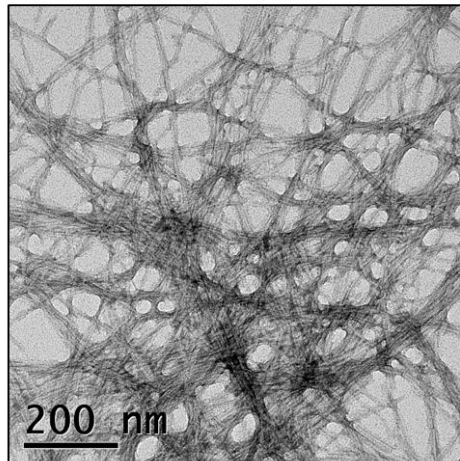


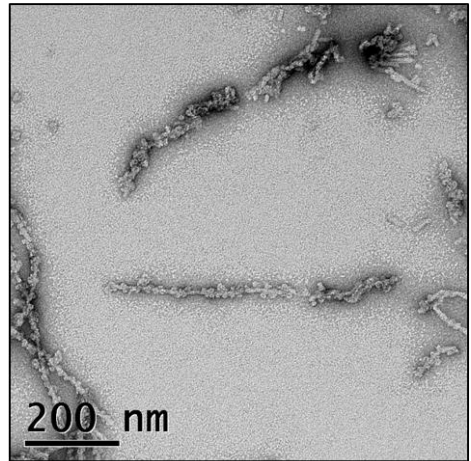
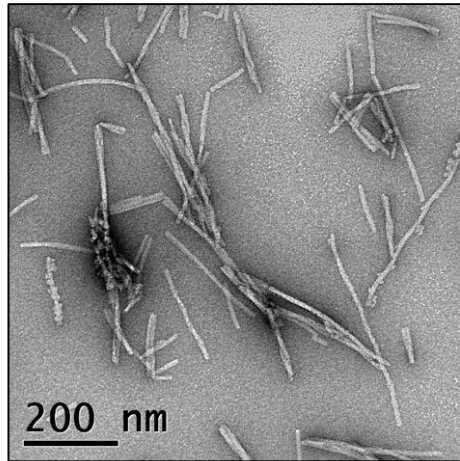
**Figure 4.16. Incubation of hCC Fibrils – Mechanical Perturbations**

*Electron micrographs of hCC fibrils formed at pH 4.0 in different conditions: 20% trifluoroethanol, after sonication for 10 minutes and after incubation at 85°C for 10 minutes. Images were taken at 21,000 x magnification.*

**pH 1.0:**



**pH 7.0:**



**pH 14.0:**

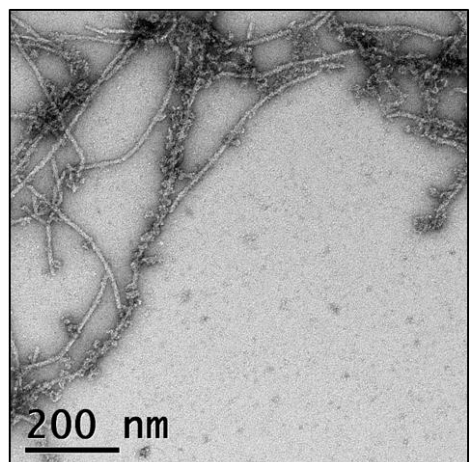
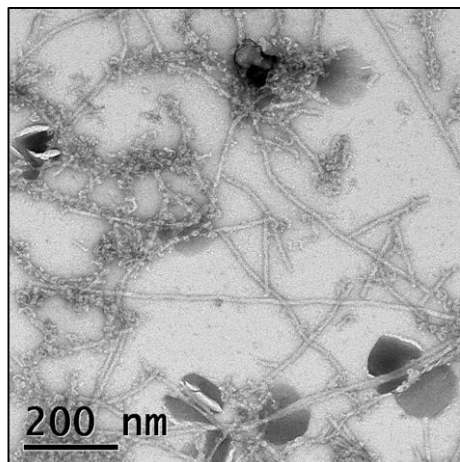


**Figure 4.17. Incubation of hCC Fibrils at Different pH**

*Electron micrographs of hCC fibrils formed at pH 4.0 in acidic, neutral and basic pH. Images were taken at 21,000 x magnification.*

#### 4.3.2.4. Purification of Oligomers

As most oligomer preparations contained fibrous species as well as potentially monomeric hCC it was important to establish a protocol for the separation of these species. Initial trials using centrifugation to pellet the fibrils, thereby leaving a pure sample of oligomers, proved unsuccessful as supernatant still contained fibrils even after several rounds of centrifugation. There were also a lot of oligomers left in the pellet, both associated with the fibril and free in solution. However, ultrafiltration, the method of oligomer purification used by Wahlbom et al. (2007), proved successful and by using two centrifugal filtration devices with PES membrane filters with different molecular weight cut-offs, pure samples of oligomer were produced. This suggests that the oligomers being purified have a molecular weight of between 100 and 1,000 kDa, which corresponds to species containing approximately 7-70 hCC molecules, however this can only ever be a rough estimate of size and will also be selecting for species within this range. The disadvantage of this protocol is that it does not allow the purification of fibrils as they got caught in the filtration membrane and attempts to re-suspend these proved unsuccessful.

#### 4.3.2.5. Oligomer Morphology by TEM

TEM analysis of purified oligomer preparations from hCC incubations at pH 2.0 and pH 4.0 are shown in Figure 4.18. These demonstrated that there was a difference in structural morphology depending on the pH of the sample. Those formed at pH 4.0 have an annular appearance which could be due to a bi-concave disc or hollow sphere morphology. Alternatively this could correspond to a hollow pore with a hole in the centre. Also present in the TEM images were small protofibrillar-like threads which are potentially curling up (or uncurling) to produce the oligomeric structures. At pH 2.0, although the structures do not have a donut-like morphology they are still circular in appearance. In both the samples, the majority of the oligomers observed have a uniform morphology, however there is a large variation in size.

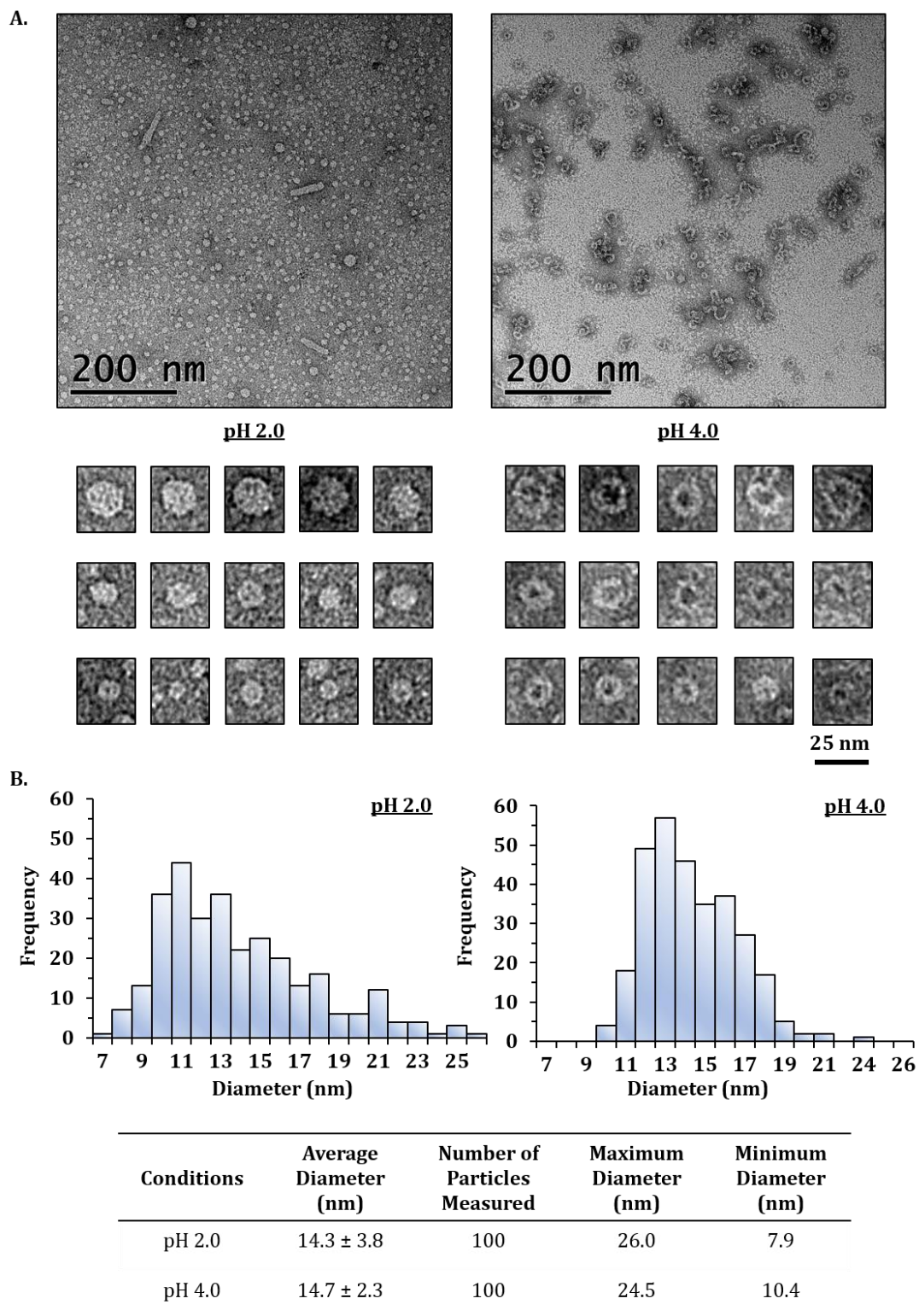


**Figure 4.18. Oligomer Measurements**

Electron micrographs (A) of purified hCC oligomers produced at pH 2.0 and pH 4.0. Images were taken at 28,500 x magnification and close-ups of oligomers were scaled by a factor of 4. Histograms (B) displaying the distribution of diameters of the oligomers measured using Digital Micrograph. Each particle was measured three times and the average diameter is shown with the standard deviation.

The diameter of oligomers produced at both pH 2.0 and pH 4.0 was measured from electron micrographs of different preparations in these conditions. Oligomers formed at pH 2.0 have an average diameter of 14.3 nm (SD +/- 3.8 nm, n = 300). There is a very large distribution of sizes, ranging from 7.91 nm to 26 nm. This distribution will be skewed as small species do not have the resolution to allow accurate measurements to be taken. Interestingly, the oligomers formed at pH 4.0 had a very similar average diameter of 14.7 nm (SD +/- 2.3 nm, n = 300). This is consistent with the oligomer diameter measured by Wahlbom et al. (2007) of 13.4 nm (SD +/- 1.9 nm, n = 916).

It is possible that the species being formed at the different pHs are the same and that the differences in appearance are a by-product of the process of preparing the samples for TEM. A difference in charge could cause a different surface of the structure to adhere to the grid, and cause an alternative morphology to be observed. Observing samples by TEM will not necessarily give an indication of all of the species present in that sample, as some molecules will not bind to the grid. The drying process can also introduce artefacts into the sample, as the appearance of a dried structure on a surface may be quite different to that same species in solution.

#### *4.3.2.6. Characterisation of Oligomers by PAGE and SEC*

Characterisation of these oligomers has proved challenging, partly due to the difficulties of producing large quantities of hCC. Attempts to analyse oligomeric samples and determine whether monomeric hCC was present by native-PAGE proved unsuccessful, with large amounts of smearing occurring on the gel and no distinct bands. Analysis by SDS-PAGE was equally ineffective, again with no distinct bands forming and just a large smear of protein observed on the gel. Characterisation by SEC was also unsuccessful.

#### *4.3.2.7. Stability of Oligomers*

One of the properties of oligomeric intermediates is their transient nature and ability to form larger structures, which causes great problems for studying these species. It was therefore desirable to establish the stability of these species under physiological conditions. An advantage of purifying the oligomers by ultrafiltration is that it allows easy buffer exchange and concentration within the ultrafiltration device. The oligomers were buffer exchanged into water and viewed by TEM. The oligomers produced at pH 4.0 retained their structure after this process, although amorphous aggregate was

observed in the sample. However, in this experiment the oligomers at pH 2.0 did not remain and only amorphous aggregate was produced, potentially indicating that these species are less stable than those produced at pH 4.0. A previous experiment in which a combination of fibrils and oligomers produced at pH 2.0 had been incubated in H<sub>2</sub>O had indicated that both of these species were stable in water for several days.

The oligomers produced by hCC are different to many that have been described in the literature as they appear to be stable for extended periods of time (several months) and do not immediately go on to form fibrils, a property that could be exploited for structural studies by hydrogen-deuterium exchange and limited proteolysis. If these species are related to the toxic species found *in vivo* and responsible for the disease state, then this high stability could be a crucial property in extended toxicity. Oligomers do not appear to form amyloid fibrils, as both species are observed in solution for several weeks. The presence of fibrils coated with oligomers could indicate a stabilisation, or segregation, of these species by the fibrils. Alternatively the oligomers could be a stable off-pathway intermediate, or species that have a much slower rate of fibril formation.

### **4.3.3. Limited Proteolysis of hCC Fibrils with Elastase**

#### **4.3.3.1. Sample Preparation**

After incubation in pH 4.0 fibrillisation conditions for several weeks, hCC fibrils were centrifuged and re-suspended in 10 mM Tris-HCl pH 8.0. This process was repeated several times in an attempt to disrupt the large clumps of fibril that had been produced, and to try and remove any oligomers that remained in solution. The sample was incubated for several days at pH 8.0 and viewed by EM to check that the fibrils remained stable in these conditions (Figure 4.19). TEM of the sample after proteolysis was also performed which showed that the fibrils had remained intact through the experiment and retained their structural morphology. This project has been hindered due to problems with producing a pure sample of hCC fibrils without oligomers present.

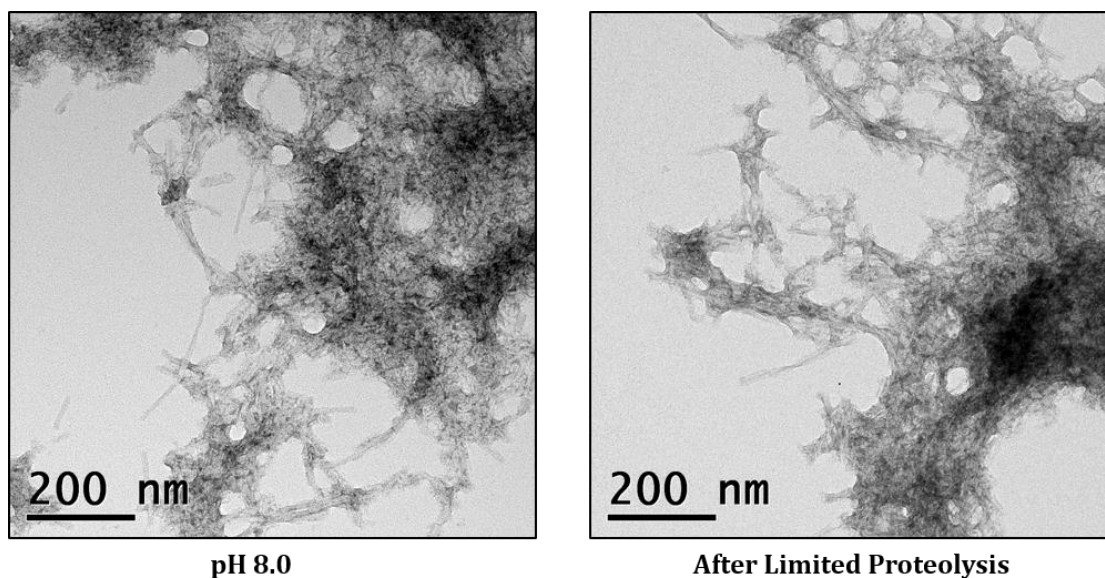


**Figure 4.19. TEM of Limited Proteolysis**

*Electron micrographs showing hCC fibril sample after incubation in 10 mM Tris-HCl pH 8.0 for 48 hours and the same sample after limited proteolysis with elastase.*

#### 4.3.3.2. hCC Monomer Digest

Mass spectrometry analysis of the proteolysis of monomeric hCC indicated that there was no digestion of the monomer at 0.5, 1 and 4 hours. After 24 hours a small amount of proteolytic activity was detected; it is possible that some digestion is occurring at the earlier times, but that the concentration of protein fragments generated were not enough to be detected by mass spectrometry. These digested fragments constituted only a minor part of the sample, shown by a small peak in the reverse-phase HPLC used to separate the fragments before mass spectrometry. None of the fragments produced involved hydrolysis at any of the predicted elastase cut sites, a limitation that was used in order to analyse the data from the fibril digest. This reveals that, as with cystatin B, inhibitors of cysteine proteinases are efficient inhibitors of serine proteinases such as elastase when folded and soluble. Consequently any fragments identified from the fibril digests with elastase cannot come from soluble hCC, particularly at time-points prior to 24 hours.

#### 4.3.3.3. hCC Fibril Digest: Analysis

The fibrils used for this experiment were shown to be highly associated into large clumps by electron microscopy, potentially making it difficult for the protease to access all regions of the structure. This high level of association makes it difficult to determine the morphology of the fibrils tested, and also if there are any oligomeric structures

present in the clumps of amyloid. Replication of the results presented here would be necessary for any definitive conclusions to be drawn, however the data produced could still provide novel insights into the structure of hCC amyloid fibrils.

A further complication with this system is the presence of two disulphide bonds in the hCC molecule. These extend from C73 to C83 in the AS loop, and from C97 to C117 between strands four and five. Analysis of the limited proteolysis experiment by mass spectrometry was carried out without the addition of DTT, which acts as a reducing agent to break the disulphide bonds. This meant that the fragment masses obtained relate to peptides with the disulphides retained, leading to some difficulties with identification of these peptides. The experimental conditions will not inherently break these disulphide bonds, as indicated by the observed mass of the full length protein (13,344 Da) in comparison to the predicted mass (13,347 Da). The difference of 3 Da can be attributed to the loss of the four hydrogen atoms required to make the disulphide bonds (to within the 1 Da accuracy of the MS machine) thereby suggesting that these bonds have remained intact throughout the process. Peptide fragments were therefore identified with the assumption that the disulphides had not been broken; any suggested fragments that would have required the breaking of these bonds were discarded. The initial analysis was conducted making the assumption that elastase would only cut at its preferred hydrolysis sites predicted from the primary sequence.

It was important to establish a protocol for identifying separated individual fragments which are held together only by the disulphide linkage and do not follow on from each other in sequence. However, it was difficult to find software designed to take into account disulphide bridges satisfactorily when assigning mass data to specific protein fragments. The closest program identified was ProteinProspector MS-Bridge (University of California, San Francisco, US). This program uses the predicted elastase cut sites to link together fragments and determine if any correspond to the experimental mass. It is possible to define the type of linkage required, in this case a disulphide bond, however it is not possible to define which residues the linkage occurs between. The program also assumes that two identical fragments can be linked, as if all disulphides had been reduced and then allowed to reform.

A separate program created by Dr Jeremy Craven (University of Sheffield) was used to calculate the molecular weight of all possible fragments within the protein sequence. All those that could potentially be linked through the two disulphide bonds were combined

to create a database of all the fragments that could possibly be generated through proteolysis of hCC. A search for a specific mass with a limit of two peptides linked resulted in identification of ~100 pairs of fragments. Extending the search to allow three peptides to be linked led to ~1000 possibilities for each specific mass searched for. It is therefore essential to be able to narrow down the search in order to identify these linked fragments.

If the assumption is made that elastase can only work at its predicted cut sites, the amount of fragment matches generated is significantly reduced. The second disulphide bond (C97 to C117) is thought to be the more stable, and most likely to be retained within the molecule. This bond was kept intact and all the potential fragments based on the predicted hydrolysis sites within strands 4 and 5 were calculated. Subtraction of each of these from the generated peptide masses from the MS data gave the mass of the fragment that would have to be attached through the disulphide bond to produce the experimental mass. These were then analysed using FindPept (via ExPASy website, Artimo et al., 2012) to produce many linked pairs of fragments used here for analysis. Re-analysing the samples by MS after incubation in reducing conditions to break the disulphides and then comparing the obtained masses with the linked fragments identified would then allow confirmation that these linked fragments are indeed present.

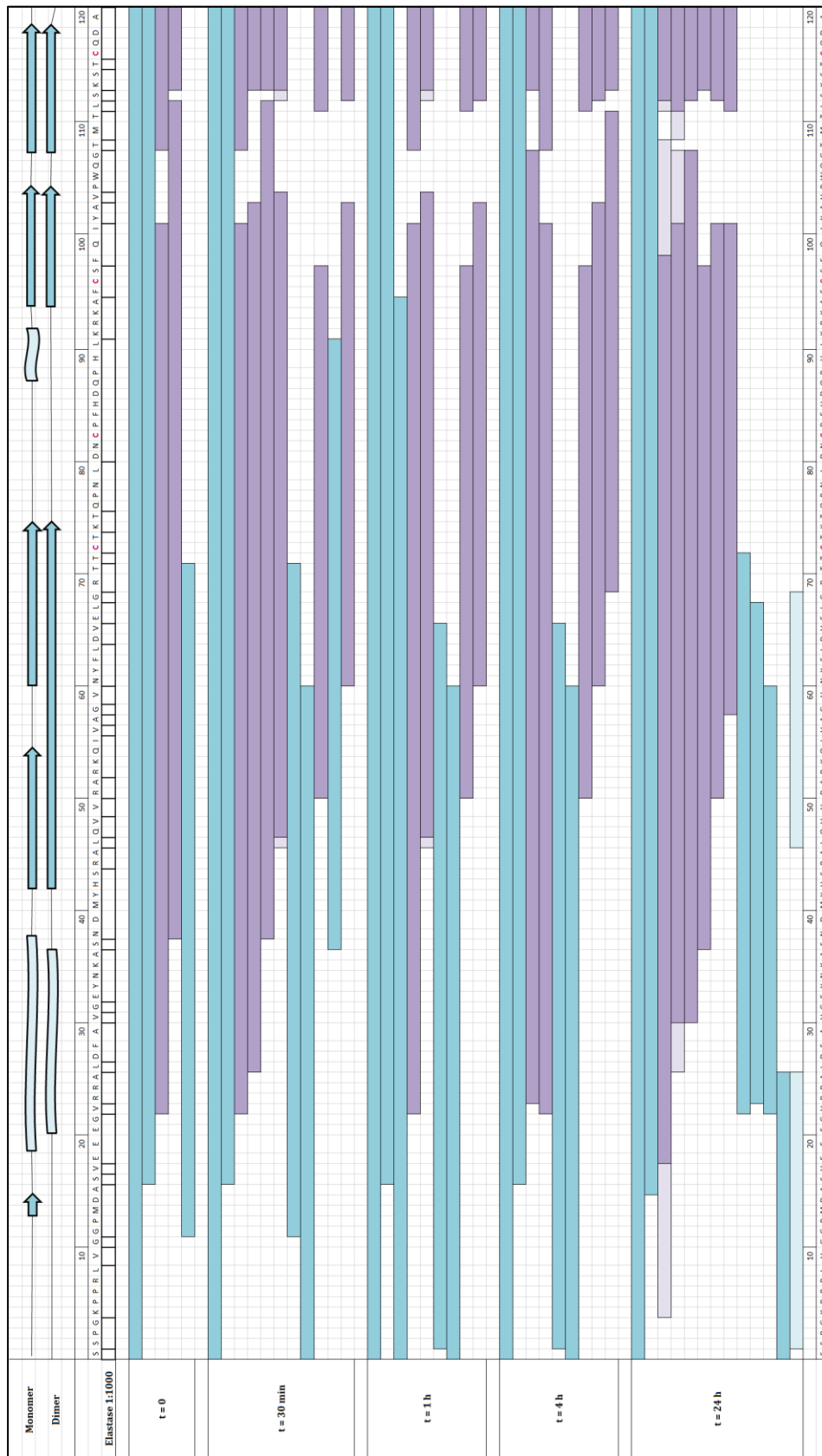
#### *4.3.3.4. hCC Fibril Digest: Pattern of Resistance*

Table 4.3 shows the experimental masses obtained from the digest at each of the five time-points and the identified fragment for each of them. These fragments were then combined to produce a digestion map as shown in Figure 4.20. The predicted sites of elastase hydrolysis are indicated in conjunction with the amino acid sequence and the secondary sequences for both the monomer and the dimer.

Digest Time (h)	Fragment Mass (Da)	Fragment Identity	
0	11796	17-120 (0.7)	
	10383	23-101 + 109-120 (1.2)	
	9319	39-112 + 114-120 (0.4)	
	6702	12-71 (1.5)	
0.5	11796	17-120 (0.7)	
	10383	23-101 + 109-120 (1.2)	
	9983	24-103 + 114-120 (1.2)	
	9319	39-112 + 114-120 (0.4)	
	8086	48-109 + 112-120 (0.8); 47-109 + 113-120 (0.8)	
	6702	12-71 (1.5)	
	6469	1-60 (0.7)	
	6197	38-91 (0.0)	
	5898	61-103 + 113-120 (0.4)	
	1	12129	11-113 + 116-120 (1.3)
11796		17-120 (0.7)	
10383		23-101 + 109-120 (1.2)	
8086		48-109 + 112-120 (0.8); 47-109 + 113-120 (0.8)	
7132		2-66 (1.1)	
6469		1-60 (0.7)	
5898		61-103 + 113-120 (0.4)	
4		11796	17-120 (0.7)
		10551	24-108 + 114-120 (0.0)
		10383	23-101 + 109-120 (1.2)
	7132	2-66 (1.1)	
	6469	1-60 (0.7)	
	5898	61-103 + 113-120 (0.4)	
	5660	70-111 + 114-120 (0.4)	
	24	11868	16-120 (1.6)
		11396	19-109 + 112-120 (0.2)
		10367	31-101 + 110-120 (0.8); 27-108 + 112-120 (0.7)
9808		31-108 + 113-120 (0.1)	
6742		51-101 + 113-120 (0.7)	
5934		59-101 + 112-120 (1.3)	
5186		24-68 (1.1)	
4290		23-60 (0.1)	
2679		1-26 (0.0)	
2590		2-26 (1.9); 47-69 (2.0)	

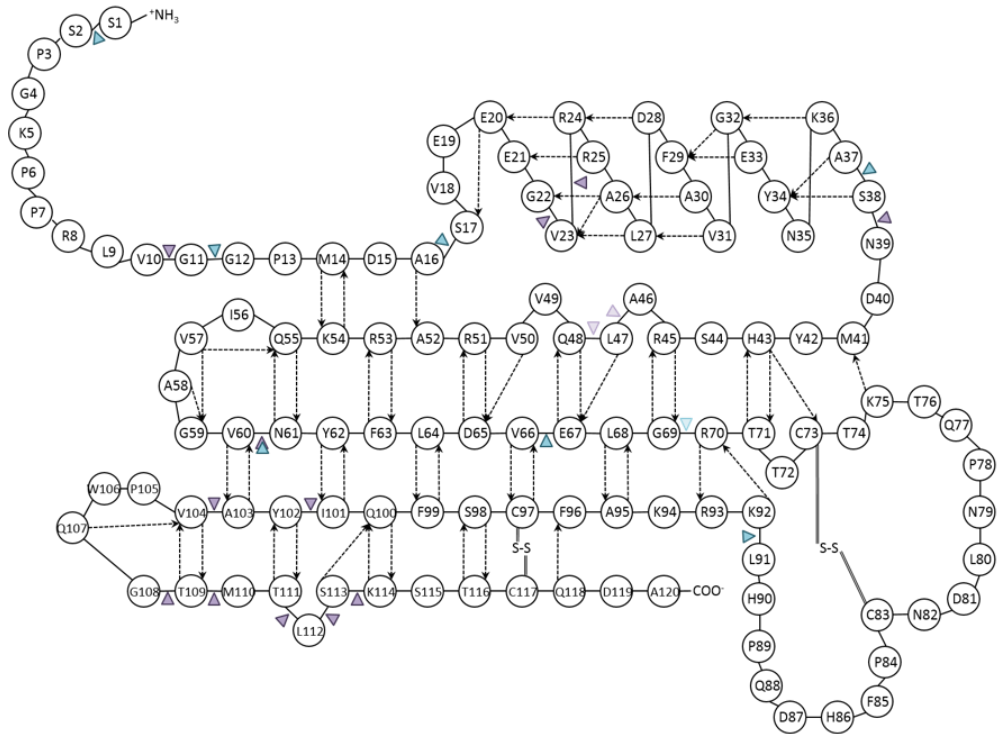
**Table 4.3. Fragments Observed from Elastase Digest of hCC Fibril**

*The bracketed figure in the fragment identity column is the mass unit variance between the experimental and predicted fragment mass.*



**Figure 4.20. Digestion Map of hCC Fibrils at Predicted Cut Sites.** Fragments resulting from the digestion of hCC with elastase at a protease to protein ratio of one to a thousand. The analysis carried out uses elastase predicted sites and allows cleavage into disulphide linked peptides. Blue fragments are single length peptides whereas purple fragments are linked via a disulphide bond. Pale blue or purple illustrates ambiguities in assignments where several possibilities exist for the same mass as defined by mass spectrometry.

**0-4 h:**



**24 h:**

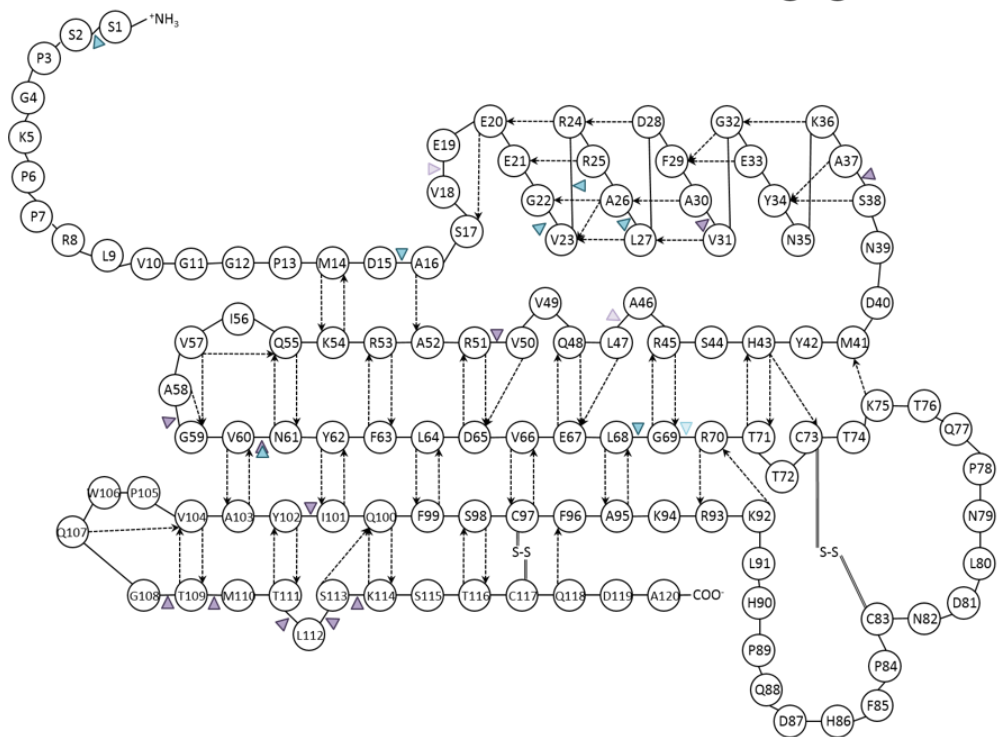


**Figure 4.21. hCC Topology Identifying Positions of Hydrolysis**

Cleavage positions observed at the first 4 time-points of 0, 0.5, 1 and 4 hours are identified (**top**) as well as additional sites observed after 24 hours (**bottom**). Blue triangles indicate cut sites from analysis of the full length protein and purple triangles indicate linked fragments where two separate peptides are joined through a disulphide bond, with lightened triangles of each colour indicating ambiguous cut sites. Hydrogen bonding is shown using dashed arrows.

Very similar fragments were observed at the 0.5, 1 and 4 hour time-points, however after 24 hours further proteolysis at different sites was observed. Figure 4.21 shows topology maps of the monomeric hCC structure at 4 and 24 hours with the identified cut sites indicated. The blue triangles indicate cut sites from analysis of the full length protein, whereas the purple triangles indicate linked fragments where two separate peptides are joined through a disulphide bond.

Many peptide fragments were obtained from the limited proteolysis of hCC fibrils with elastase, more than had been previously observed for the digestion of cystatin B fibrils with the same enzyme, indicating that hCC fibrils are more susceptible to proteolysis by elastase than its type I family member. The previous work led to the generation of a defined cystatin B fibril core from residues 24-80, which is resistant to proteolysis by both elastase and proteinase K. With the hCC data it is impossible to define a resistant core in this manner, as proteolysis is observed over the majority of the protein structure. Importantly, as the analysed samples result solely from the pelleted species that had been washed repeatedly, fragments identified are an integral part of a fibril structure or tightly associated with it. This suggests that, although the local structure may be less stable, the “nicked” structure may be more resistant to dissociation and solubilisation.

Alternatively, and especially considering the heterogeneity of the sample, digestion patterns could be being observed from several different fibril morphologies with different protected regions. If the association of oligomers to amyloid fibrils in hCC samples is due to differences in morphology, and which part of the molecule is exposed to the surface as discussed previously, then this indicates that different morphologies do occur with these fibril samples and are quite likely to lead to different digestion patterns.

A further possibility is that the hCC fibrils are less stable in these conditions than those formed by cystatin B, either leading to faster remodelling of the fibril or the recycling of molecules within the population. In this case the molecules being recycled would have to be oligomeric species or unfolded/misfolded protein, due to the inhibitory activity of folded hCC monomer. For this hypothesis to be correct, the cleaved species must then be able to precipitate and resist solubilisation during washes. Several small polypeptides were observed in the hCC fibril digest after 24 hours; it is possible that these fragments were unable to diffuse away and have remained associated with the large clumps of amyloid that were observed by TEM, therefore not constituting part of the fibril core.

This is not seen extensively with cystatin B where it was noted that the proteases used rapidly cleaved soluble protein fragments, as indicated by large amounts of small polypeptides being detected in the soluble fraction of the cystatin B fibril digests (Davis, 2013).

#### 4.3.3.5. hCC Fibril Digest: Position of Loop 1 in the Fibrils

A series of fragments involve hydrolysis between V60 and N61, an observation that is strengthened due to identification of peptides from either side of this cleavage position (i.e. both halves of the molecule). It is possible that although hydrolysis has occurred and the peptides are no longer joined, the two fragments remain incorporated in the fibril and are unable to diffuse away. Proteolysis at this position is intriguing as loop 1 forms the main component of the inhibitory activity of hCC, meaning it is unlikely that the molecule has remained monomer-like as this would cause inhibition of the elastase and not lead to hydrolysis at this position. Therefore this could suggest that the molecule includes an extension of the loop between  $\beta$ -strands 2 and 3 as is seen in the domain swapped dimer. This proposal is central to existing models of cystatin amyloids, but in the cystatin B models (Figure 4.22 A&B) this region of the protein is at the core of the structure and is highly protected from both H/D exchange and proteolysis (Morgan et al., 2008, Davis, 2013).

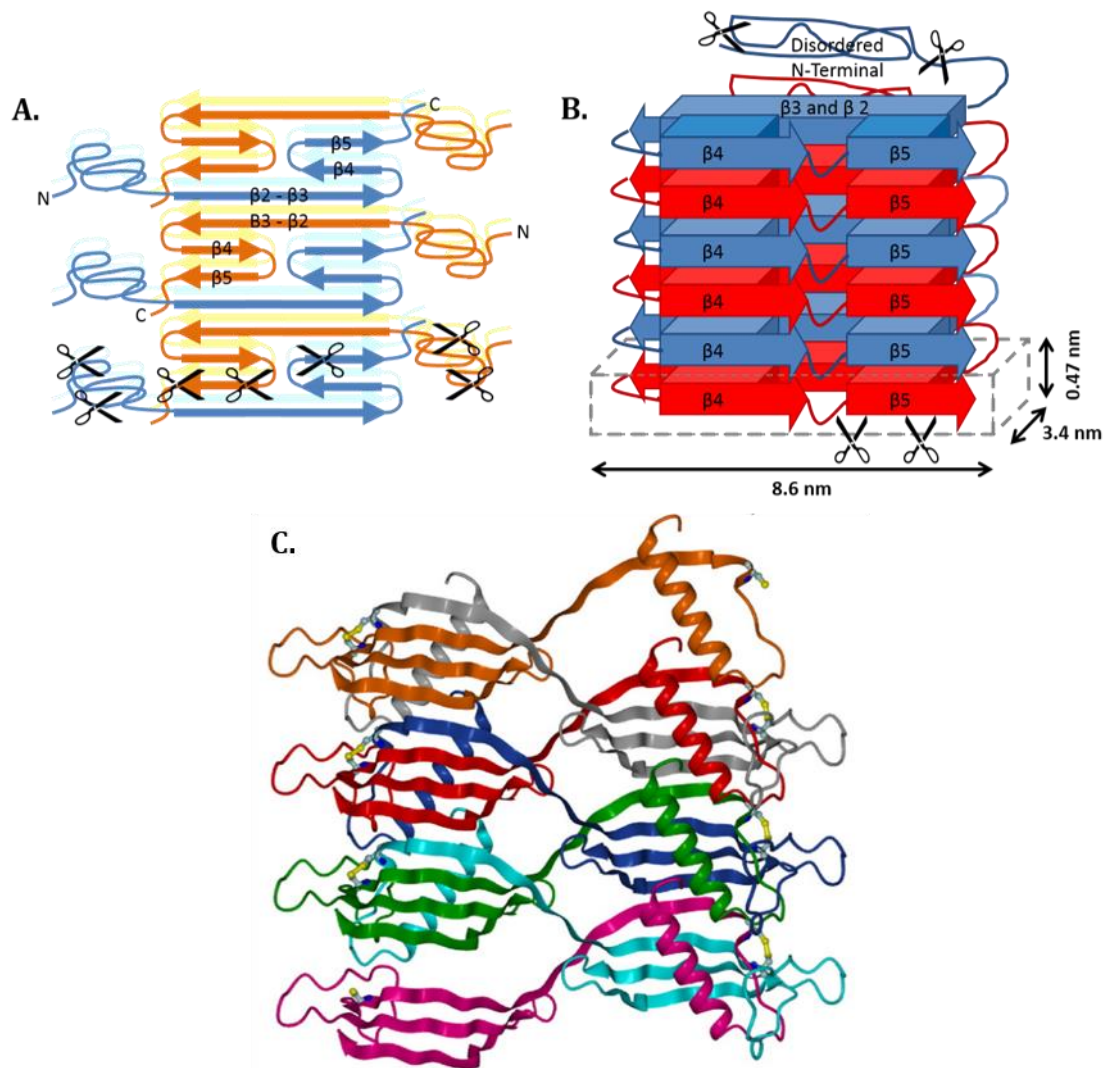


**Figure 4.22. Models of Cystatin Fibril Structure.** In **A & B**, models of cystatin B amyloid where regions which are protected from hydrogen-exchange in the fibrils are modelled as  $\beta$ -strands and incorporated into simple models that take into account the dimensions of the fibrils measured using TEM, AFM and mass-per-unit-length. In **A**, the dimer-like strands are arranged as flattened dimers stacked on top of each other, with a second “stack” or sheet sandwiched on the first to shield hydrophobic residues, uncovered by removal of the helix, from the solvent. In **B**, the model is further modified to incorporate the observation that fibrils are intact after removal of the C-terminal 20 residues. A parallel in-register  $\beta$ -arc is proposed. Image taken from (Davis, 2013). In **C**, the runaway domain swapping model proposed for hCC amyloid fibrils. Cystatin molecules swap from one fold to another using an extended loop between strand 2 & 3. The length of this loop is in reality a lot shorter than described here by the authors and would require local unfolding and complex 3D packing to achieve a stable structure. Image taken from (Wahlbom et al., 2007).

One of the current models of the formation of hCC fibrils is through propagated or ‘runaway’ three-dimensional domain swapping as shown in Figure 4.22C. In this model the loop between strands 2 and 3 is extended, forming a long  $\beta$ -strand which associates with strands 3, 4 and 5 from another hCC molecule. This molecule then domain swaps in a similar manner with yet another hCC molecule, resulting in an open-ended chain of intertwined identical protein subunits. Compared with the dimer structure, the central region does not have the same degree of hydrogen bonding that is normally observed in a  $\beta$ -strand and is thought to be more flexible. Indeed, given the very restricted length of the original loop, it is likely that considerable unzipping of the strand-strand interactions may have to occur in order to adopt a runaway domain swapping structure. This local unfolding may therefore be the source of the weakness or protease sensitivity exhibited by this region of the protein. This proteolysis pattern also indicates a slightly different fibril structure compared with cystatin B, as proteolysis was not seen at all around this region.

#### 4.3.3.6. hCC Fibril Digest: Loop 2 in the Fibril

Several linked fragments were observed, with hydrolysis occurring at a range of positions between Y102 and K114. This suggests that strand 5 and the end of strand 4 are vulnerable to proteolysis, and therefore are unlikely to be protected within the fibril. If the position of  $\beta$ -strands is conserved in the fibril, as is suggested by H/D exchange studies of its intracellular counterpart cystatin B, then this loop may protrude from the surface of a flattened  $\beta$ -sheet structure and become susceptible to proteolysis (Figure 4.23). Compared with cystatin B however, this cystatin is vulnerable to proteolysis in a similar way across the structure whereas cystatin B showed some resistance at the C-terminal at early time points, consistent with H/D protection data (Davis, 2013).

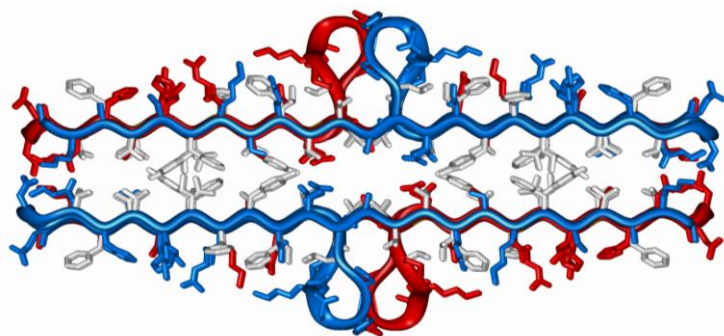


**Figure 4.23. Loop Protrusion.** Model showing the protrusion of the loop between strands 4 and 5 in the cystatin B domain swapped dimer viewed from the top, with blue and red indicating the two molecules.

#### 4.3.3.7. hCC Fibril Digest: the N-Terminal

At the early time-points proteolytic activity is observed at the N-terminal, which increases after 24 hours. Localised unfolding is often required for the polypeptide chain to enter the active site of the protease, making it difficult for proteinases to cleave in structured regions. This observation therefore supports the hypothesis that although the N-terminal is  $\alpha$ -helical in the monomer it is unstructured in the fibril. It is thought that the N-terminal is not incorporated into the amyloid fibril structure and therefore would be readily available for proteolytic activity. The C-terminal also appears vulnerable to protease activity from the start of the experiment, which is not observed for cystatin B. In the latter system digestion of C-terminal is not observed until 4 hours at a ratio of 1:1000 protease to cystatin B, with extensive proteolysis of both termini after 24 hours.

#### 4.3.3.8. hCC Fibril Digest: Alternative Analysis

The analysis described above made the assumption that elastase has only cut at preferred sites predicted from the primary sequence of hCC and the known activity of the enzyme. However it is probable that hydrolysis also occurred at alternative sites as has been shown in other limited proteolysis studies. Fragments identified without the aforementioned constraint produced a digestion map as shown in Figure 4.24, which again highlights regions that are more sensitive to proteolysis. However this means that fragments from the C-terminal cannot be considered here due to the presence of the disulphide bond. This analysis also does not include potential linked fragments, as the number of matches generated was excessive as discussed earlier. Several fragments were identified, which together with Figure 4.20, underline similar regions across the molecule that are sensitive to proteolysis. The only area which is novel here is a clearly defined a cut site after D87 which reoccurs under several conditions. Unlike the different fragments identified in Figure 4.20 no matching “partner” fragments from the C-terminal were observed, where it becomes credible that a nicked protein molecule remains stable within the fibril structure. It seems unlikely that the whole of strands 4 and 5 have been lost, as these fragments would suggest, and is more likely that the nicked fragments identified earlier in the C-terminal region are present.

#### 4.3.3.9. hCC Fibril Digest: Conclusions

The regions of hCC that have been identified as being susceptible to proteolysis in the amyloid fibril show some similarities with the model of cystatin B fibril structure, such

as the exclusion of the N-terminal and the disorder of this region. However, other identified regions are strikingly different, such as region between strands 2 and 3, indicating that there are differences between the fibril structures of the two proteins, and that the cystatin B model would need further adaptation before it could be directly applied to hCC.

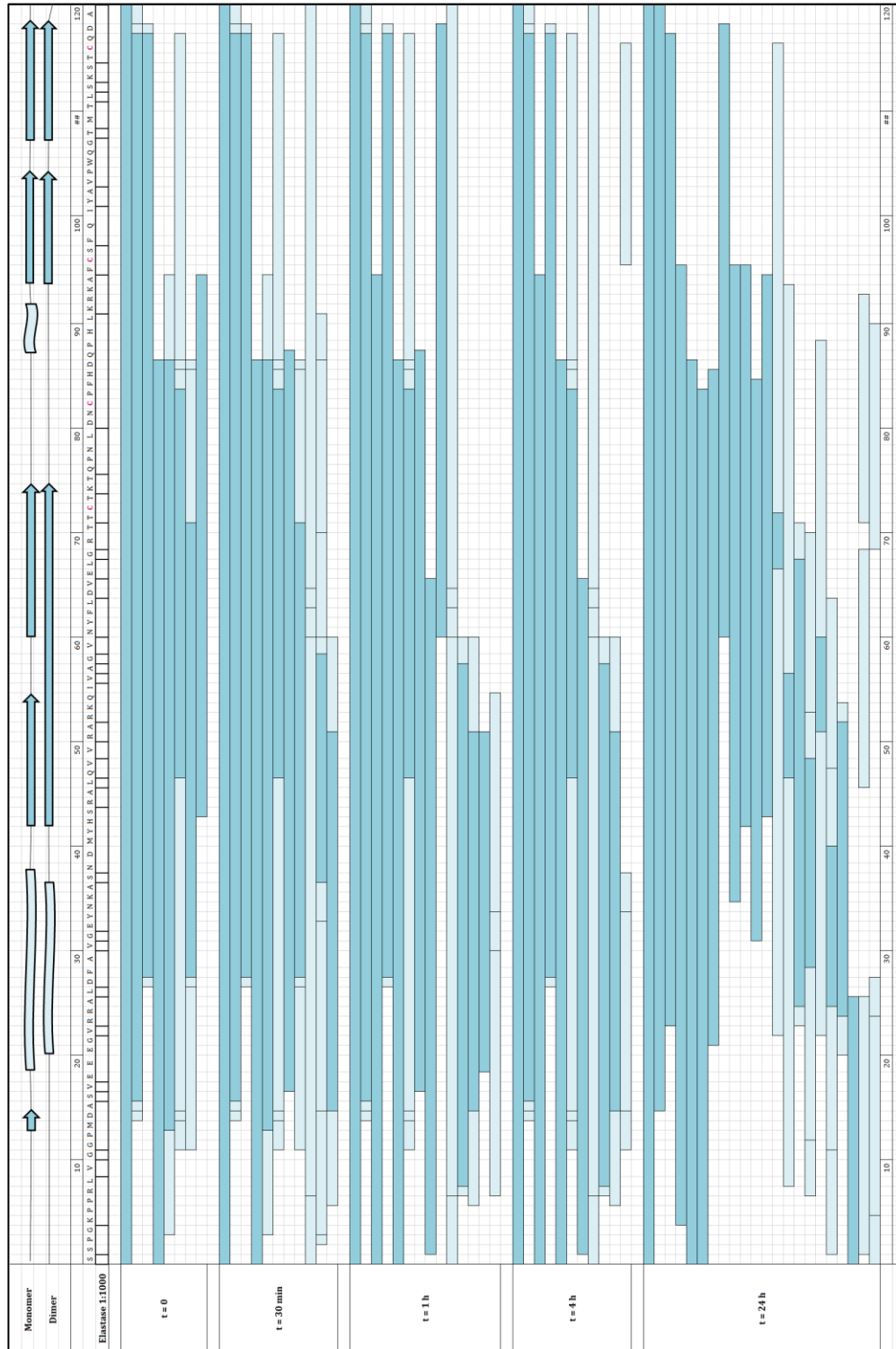


**Figure 4.24. Digestion Map of hCC Fibrils with no constraints on possible cut sites. Fragments assigned to the observed masses without the restriction to elastase preferred cutting sites. The possibility of cleavage between 2 cysteines linked by a disulphide bond is not included here as it leads to too many possibilities for each mass.**

## Chapter Five: Interaction of Cystatin C and A $\beta$ <sub>1-42</sub>

### 5.1. Introduction

It is well established that Alzheimer's disease is characterised by the aggregation of A $\beta$  peptide into extracellular amyloid plaques and that it is either this, or the formation of toxic soluble oligomeric intermediates, that leads to major neurodegeneration and the consequent pathology. As previously discussed, the aggregation of A $\beta$  can be modulated by many different factors including the amyloidogenic proteins transthyretin, neuroserpin and hCC. In addition to these, several small molecules such as epigallocatechin gallate have been also been identified that work to prevent A $\beta$  toxicity. Although these factors often have a similar effect by reducing the toxicity of A $\beta$ , there appear to be several different mechanisms by which they do this, as illustrated in Figure 5.1. Perhaps it is unsurprising that nature has developed alternative methods of inhibiting fibrillogenesis at different stages. A greater understanding of these mechanisms, and how to control them, could lead to development of a therapeutic strategy against AD.

Binding to A $\beta$  monomer in a 1:1 complex prevents formation of nucleating species thus inhibiting fibril formation at the earliest possible juncture. As nucleus formation is the rate-limiting step, and is a highly concentration dependent process, a slight decrease in the amount of protein present can lead to a significant reduction in the rate of amyloid assembly (Jarrett and Lansbury, 1993). Stabilisation of the nucleus, or inhibition of monomer addition may also prevent fibril formation. Other factors cause dissolution of mature fibrils into smaller aggregates which are not resistant to proteolysis and therefore can be cleared by the body. Binding to on-pathway oligomeric intermediates often induces a remodelling event, thereby forming non-toxic oligomers. In some cases the interacting molecule acts as a catalyst, inducing the production of non-toxic species without itself being incorporated into the final product.

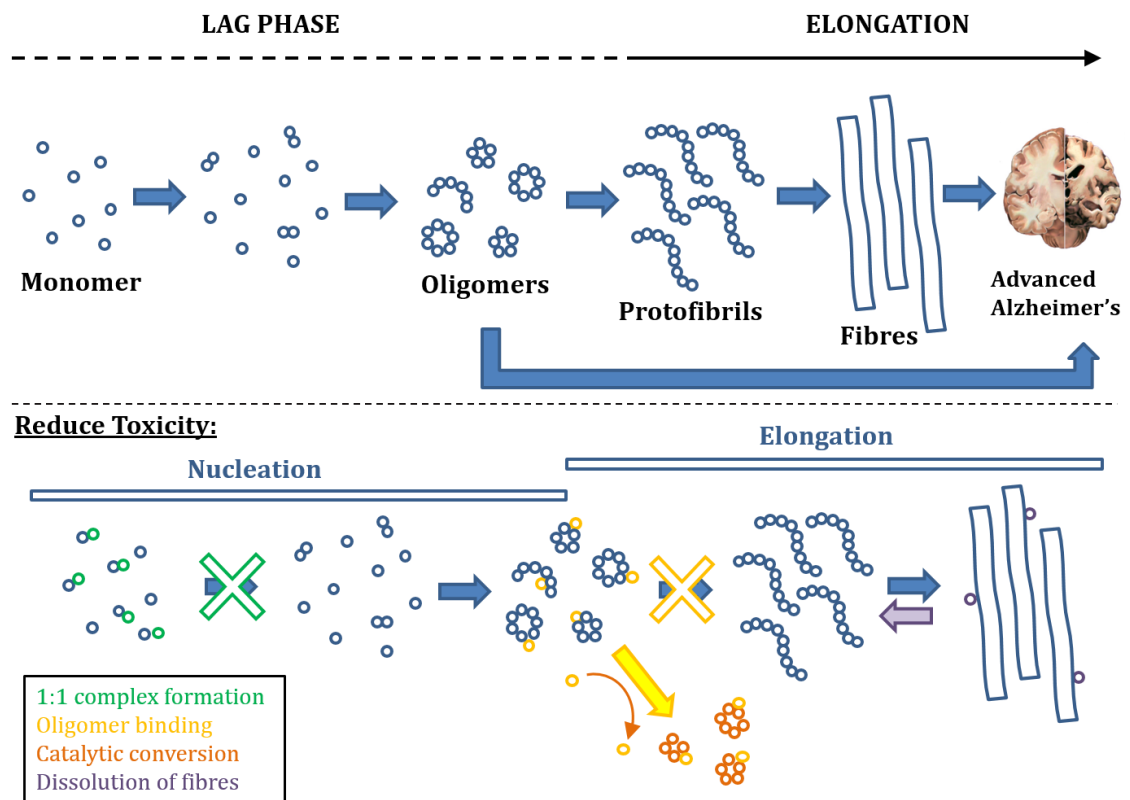


**Figure 5.1. The Aggregation of A $\beta_{1-42}$  and Different Methods of Modulation**

Schematic illustrating the assembly pathway of A $\beta_{1-42}$  into amyloid fibrils, from the formation of a nucleus through the production of oligomeric species before the assembly of protofibrils and finally mature fibrils, demonstrating the presence of both fibrils and oligomers in advanced AD. Mechanisms of reducing A $\beta_{1-42}$  toxicity at different points in the aggregation process are highlighted such as the formation of a 1:1 complex (green), binding to oligomers (yellow), catalytic conversion (orange) and dissociation of amyloid (purple).

### 5.1.1. hCC and A $\beta$

The discovery that cystatins co-deposited with A $\beta$  within parenchymal and vascular amyloid deposits in the brains of AD patients led to the hypothesis that this family of proteins could play an important role in preventing neurodegeneration in AD. In recent years, a collection of studies using cell assays, mouse models and *in vitro* assays have been used to investigate this hypothesis and have led to the proposal that hCC in particular plays a neuroprotective role in AD. It is thought that hCC exerts this neuroprotective effect on A $\beta$  through several routes including the inhibition of cysteine proteases, induction of autophagy and direct inhibition of amyloid fibril formation (section 1.4.1). It is upon the latter mechanism that this chapter will focus.

Historically it has been suggested that hCC is working as a chaperone and stabilising monomeric A $\beta$ . Analysis by ELISA demonstrated a specific, saturable and high affinity binding of hCC to both A $\beta_{1-40}$  and A $\beta_{1-42}$ , as the authors were able to fit the obtained data to a binding curve with a rectangular hyperbola as shown in Figure 5.2A (Sastre et al., 2004). This experiment also indicated a nanomolar dissociation constant for both peptides. The study demonstrated that fibril formation by both A $\beta_{1-40}$  and A $\beta_{1-42}$  is inhibited *in vitro* by the presence of hCC, causing the production of amorphous aggregates rather than mature fibrils. This effect is dose dependent and TEM estimated that substoichiometric amounts of hCC will prevent A $\beta_{1-40}$  fibril formation, as when 22  $\mu$ M A $\beta_{1-40}$  was incubated with 3.75  $\mu$ M hCC no fibrils were observed. However ratios close to 1:1 hCC to A $\beta$  were required to completely inhibit the formation of A $\beta_{1-42}$  amyloid fibrils (15  $\mu$ M hCC for 22  $\mu$ M A $\beta_{1-42}$ ) in a 10  $\mu$ l volume. Co-immunoprecipitation experiments with deletion mutants of APP and *in vitro* binding assays with GST-A $\beta$  mapped the binding site of hCC to the extracellular N-terminal region of A $\beta$ .

Selenica et al. (2007) used western blotting and gel filtration to probe the effect of adding hCC to preparations of A $\beta_{1-42}$  ADDLs and protofibrils. The authors propose that hCC is decreasing the formation of both small and large A $\beta_{1-42}$  oligomers, as supported by a reduction in the amount of A $\beta$  trimers, tetramers and high molecular weight oligomers (38-98 kDa) observed by SDS-PAGE when A $\beta_{1-42}$  was incubated in the presence of equimolar hCC (Figure 5.2B). They also report an increase in the amount of precipitate formed in the presence of hCC; TEM showed that this precipitate was composed of large protein aggregates with very few oligomers or amyloid fibrils present. SEC-HPLC was used to demonstrate a decrease in the formation of A $\beta_{1-42}$  protofibrils when both equimolar and 2 x concentrations of hCC was added to the incubation mixture. Radio-labelled  $^{125}$ I-hCC was used in conjunction with a Sephadex G-50 gel filtration column (Amersham) to detect the hCC-A $\beta_{1-40}$  complex that forms after incubation of the two proteins for 35 minutes. A shift in the radioactive peak was observed as seen in Figure 5.2C and was thought to correspond to a complex with a molecular weight of 17 kDa, leading to the proposal that hCC (13 kDa) and A $\beta_{1-40}$  (4 kDa) form a 1:1 molar complex. These data are difficult to interpret, given the lack of resolution of Sephadex G-50 and the non-standard behaviour of oligomeric species upon gel filtration. The nature of any complex formed in solution is still open to debate.

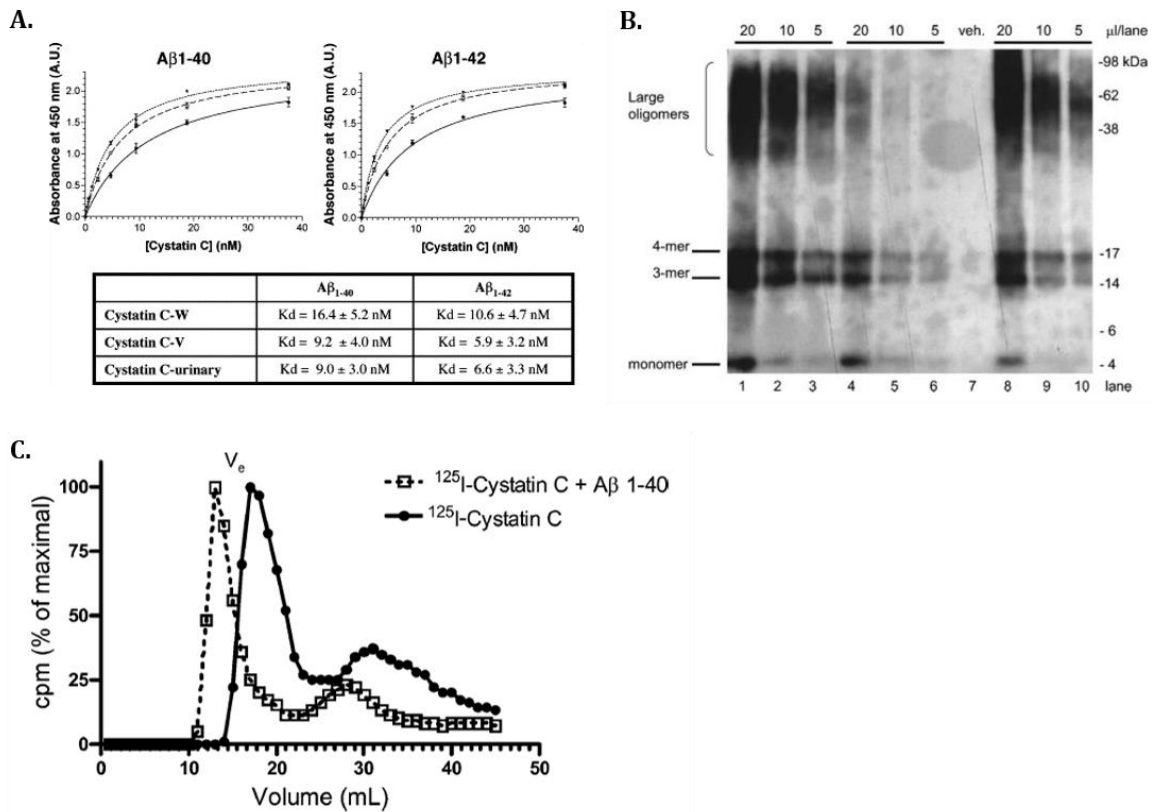


**Figure 5.2. The Interaction between hCC and Aβ in the Literature**

The binding of hCC to Aβ was studied by ELISA (A) with the image taken from Sastre et al. (2004) with permission from Elsevier. Different concentrations of wild-type (solid line, solid circles), L68Q variant (dashed line, open squares) and urinary hCC (dotted line, solid triangles) were incubated for 3 h at 37°C with Aβ<sub>1-40</sub> or Aβ<sub>1-42</sub> coated wells. Anti-hCC antibody was used to detect bound hCC, and the means and standard deviations were calculated from three independent experiments. A western blot of Aβ<sub>1-42</sub> oligomers with and without hCC (B) was taken from Selenica et al. (2007) with permission. SDS-PAGE of the oligomeric preparations was analysed using the anti-Aβ monoclonal antibody 6E10. Lanes 1-6 show different volumes of the supernatants of mixtures in the absence (lanes 1-3) and presence (lanes 4-6) of equimolar hCC after 24 h incubation. Lanes 8-10 represent different volumes of the supernatants of mixtures with preformed Aβ-oligomers to which 100 μM has been added and incubated for a further 24 h. Lane 7 (veh.) is a control of the incubation solution with no proteins present. The elution profile (C) of gel filtration of 0.6 nM <sup>125</sup>I-labelled hCC (solid circles) and a solution of 0.6 nM <sup>125</sup>I-labelled hCC in the presence of a slight molar excess of Aβ<sub>1-40</sub> (open squares) was also taken from Selenica et al. (2007). The shift in the peak of radioactivity to a volume thought to correspond to a molecular mass of ~17 kDa is explained as the formation of an equimolar complex between <sup>125</sup>I-labelled hCC (13 kDa) and Aβ<sub>1-40</sub> (4 kDa).

Although the interaction between hCC and A $\beta$  has been studied through several different methods, there is very little information available about the structural details of this association. NMR spectroscopy enables residue-specific information about protein structure, stability and interactions to be easily obtained. The use of NMR has proven successful in both the transthyretin and the PrP systems in determining a binding site upon the formation of a complex with A $\beta$ . hCC is an ideal candidate for NMR studies as it is small, with a molecular weight of ~13.5 kDa, and the majority of the backbone residues have already been successfully assigned (Ekiel et al., 1997).

As described above, it has been proposed that there is a single binding site in this interaction, with a dissociation constant in the nanomolar range. The binding of hCC prevents further aggregation of A $\beta$  into amyloid fibrils, and rather diverts the assembly pathway to the formation of amorphous aggregates. However, preceding NMR studies have failed to identify formation of this 1:1 complex (Keeley, 2007, Elshawaihde, 2012), suggesting that this is not a simple monomer-monomer interaction as was previously thought.

Establishing the molecular mechanism of how this process works would then allow a comparison of this with other A $\beta$ -modulating systems to discover if there is a general mechanism for *in vivo* protection which could potentially lead to the identification of a therapeutic peptide. This chapter describes the biophysical characterisation of the interaction between hCC and A $\beta$  using fluorescence assays, electron microscopy and size-exclusion chromatography. An NMR HSQC titration and time-course of hCC with A $\beta$ <sub>1-42</sub> to monitor complex formation is also described.

## **5.2. Materials and Methods**

### **5.2.1. Preparation of Monomeric A $\beta$ <sub>1-42</sub>**

1 mg aliquots of HFIP-treated A $\beta$ <sub>1-42</sub> were purchased from rPeptide (Georgia, USA) and stored at -20°C. Before dissolution each vial was allowed to equilibrate at room temperature for 10 minutes to prevent condensation on opening. The lyophilised peptide was re-suspended in 1 ml of cold HFIP to produce a 1 mg/ml solution and sonicated for 10 minutes in a DECON Ultrasonics sonicator bath (Sussex, UK) to ensure complete dissolution. The clear solution was transferred into sterile micro-centrifuge tubes to produce 0.1 mg aliquots. HFIP was removed by evaporation under N<sub>2</sub> and any remaining traces removed by lyophilisation. The peptide was stored as a thin clear film at -20°C.

### **5.2.2. A $\beta$ <sub>1-42</sub> Fibril Formation**

#### **5.2.2.1. Fluorimeter**

Each 0.1 mg aliquot of HFIP-treated A $\beta$ <sub>1-42</sub> was allowed to equilibrate to room temperature before the addition of 20  $\mu$ l DMSO (peptide concentration 10 mM). The sample was sonicated for 10 minutes before the addition of 1 ml of 50 mM sodium phosphate pH 7.4, 150 mM NaCl to bring the final peptide concentration to 22  $\mu$ M (0.1 mg/ml) with the addition of 10  $\mu$ M ThT, and a final DMSO concentration of 2% (v/v). The sample was split between 4 fluorescence cuvettes (250  $\mu$ l in each) and placed in a Cary Eclipse (Varian, UK) fluorimeter pre-heated to the required temperature. The excitation wavelength was 442 nm and emission was monitored at 482 nm. Samples were incubated both with and without stirring.

#### **5.2.2.2. Plate Reader**

Each 0.1 mg aliquot of HFIP-treated A $\beta$ <sub>1-42</sub> was allowed to equilibrate to room temperature before the addition of 20  $\mu$ l DMSO (peptide concentration 10 mM). The sample was sonicated for 10 minutes before being further aliquoted depending on the number of experiments being performed. Buffer and hCC solutions were produced at the correct concentration and pre-incubated at 30°C, so they could be added directly to the A $\beta$ <sub>1-42</sub>, preventing the peptide from forming low molecular weight species before the addition of hCC. After the addition of 10  $\mu$ M ThT, 100  $\mu$ l samples were added to 96

half-well plates (Corning) and incubated in a Fluostar Omega (BMG Labtech, UK) at 30°C with continual shaking at 300 r.p.m. Each experiment consisted of 5 replicates in each condition and each experimental series was performed 3 times with a different peptide stock. The excitation wavelength was 440 nm and fluorescence emission was measured at 485 nm. For the experiments investigating the addition of hCC at different times throughout the reaction, 10 µl aliquots of 100 µM hCC were added to 90 µl of 11 µM Aβ<sub>1-42</sub> at each of the time-points to produce a 100 µl sample of 10 µM hCC and 10 µM Aβ<sub>1-42</sub>.

### 5.2.2.3. Curve Fitting

In order to compare the effect of different doses of hCC on Aβ<sub>1-42</sub> fibril assembly, kinetic parameters such as  $t_{lag}$ ,  $t_{50}$  and  $k_{app}$  were extracted through fitting to a sigmoidal growth curve (Nielsen et al., 2001) with the equation

$$Y = y_i + m_i x + \frac{y_f + m_f x}{1 + e^{-\left[\frac{x-x_0}{\tau}\right]}}$$

where Y is the fluorescence intensity, x is the time, and  $x_0$  is the time of 50% the maximal fluorescence ( $t_{50}$ ). The lag time of the reaction is given by  $x_0 - 2\tau$  and the apparent rate constant ( $k_{app}$ ) can be calculated by  $1/\tau$ . Each replicate curve was fitted using GraphPad Prism 6.04 and the values extracted from each were averaged to give a final value for each of the parameters. The fit for each replicate curve is shown in Figure 5.3.

One-way ANOVA and Tukey's test for mean comparison were used to determine significant differences between the calculated kinetic parameters in the presence of different concentrations of hCC.

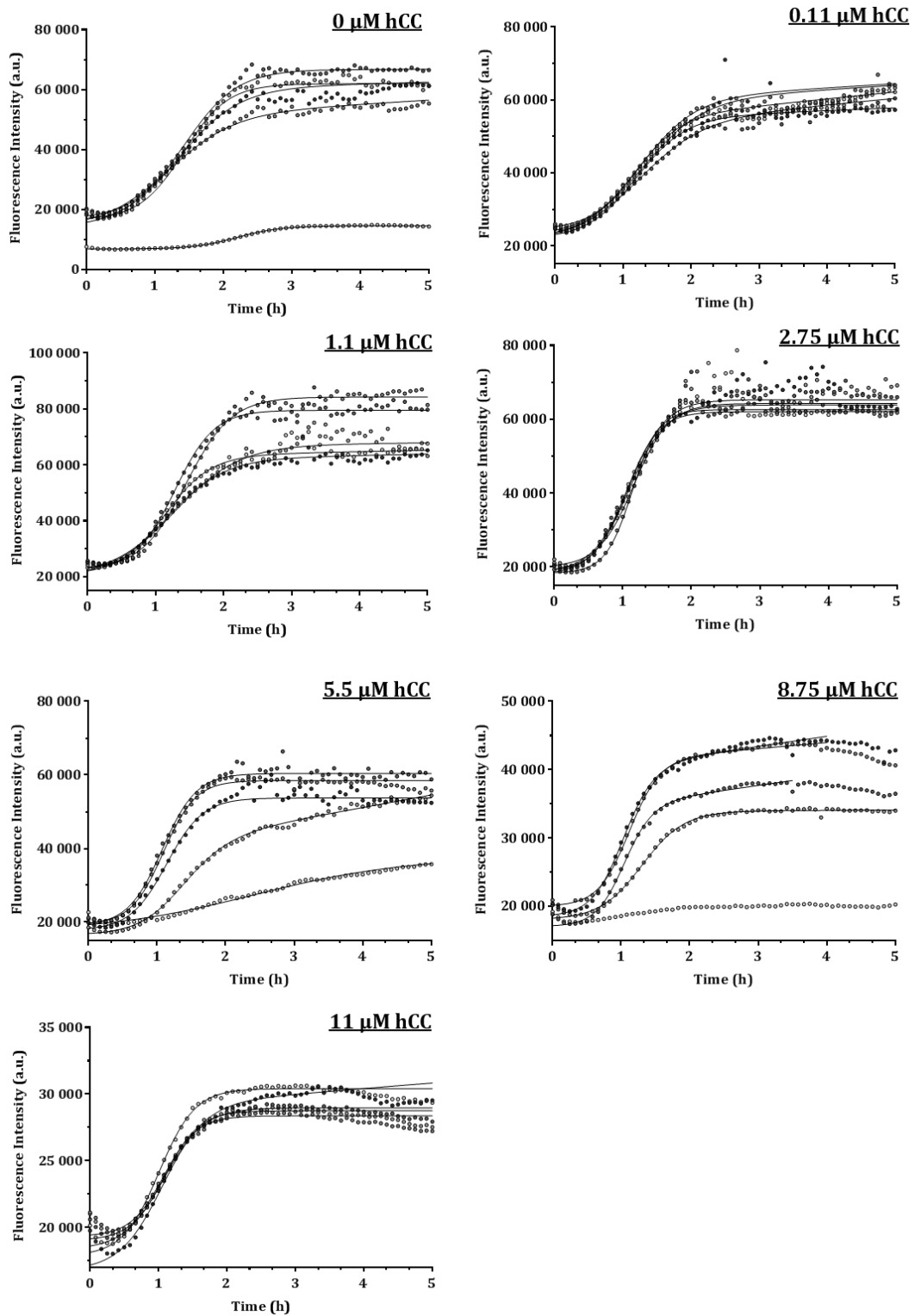


**Figure 5.3. Curve Fitting**

Each replicate data set from a series of ThT fluorescence time-courses of  $A\beta_{1-42}$  fibrillisation in the presence of different molar concentrations of hCC was fitted to a sigmoidal curve and parameters were extracted. The y-scale or amplitudes vary from graph to graph but are shown to report on the variability of this parameter within individual sets of time-courses.

### **5.2.3. Preparation of hCC Species**

#### **5.2.3.1. Domain Swapped Dimer**

75  $\mu$ M hCC in 10 mM sodium phosphate pH 6.0, 100 mM NaCl was incubated for 30 minutes at 68 °C before loading onto a preparative Superdex 75 gel filtration column (GE Healthcare) equilibrated in 50 mM sodium phosphate pH 7.4, 150 mM NaCl. 6 ml fractions were collected and those containing dimeric hCC were pooled and quantified by measuring the absorbance at 280 nm, before immediate use in ThT assays.

#### **5.2.3.2. Oligomer**

hCC was incubated in 15 mM sodium acetate pH 4, 100 mM NaCl at 48°C with agitation for 48 hours. Oligomers were purified by repeated rounds of ultrafiltration. 50 – 200  $\mu$ L samples were added to a 1,000 kDa Vivaspin and centrifuged for 10 minutes at 9.8 k x g at 4°C to remove any fibrils and amorphous aggregates from the solution. The flow-through was removed and added to a 100 kDa Vivaspin and centrifuged for 10 minutes at 9,800 x g at 4 °C to remove any monomeric hCC from the sample. This final step was repeated 3 times with the retentate volume being made up to the original volume with 50 mM sodium phosphate pH 7.4, 150 mM NaCl each time. After the final spin the retentate volume was adjusted to the original volume with buffer, removed and placed in a clean eppendorf. Preparations were examined by electron microscopy to determine the morphology of the oligomers produced and check that there were no fibrils present.

### **5.2.4. Analytical Size Exclusion Chromatography (SEC)**

20  $\mu$ l samples of A $\beta$ <sub>1-42</sub> incubated in the absence or presence of equimolar hCC were analysed using either a Shodex KW-803 (Shodex, Japan) or a Superdex 200 (GE Healthcare) gel filtration column respectively. The columns were equilibrated in 50 mM sodium phosphate pH 7.4, 150 mM NaCl. The Shodex column has a protein exclusion limit of 700 kDa and is made of a silica hydrophilic polymer. The Superdex column has a protein exclusion limit of 1,300 kDa, with a separation range between 10 and 600 kDa, and a matrix of cross-linked agarose and dextran.

### 5.2.5. Nuclear Magnetic Resonance Spectroscopy

$^{15}\text{N}$ -labelled hCC was expressed and purified as described in section 2.4.2. Before the NMR experiments, the purity and monomeric state of the protein was established through analysis by mass spectrometry and SEC-HPLC.

#### 5.2.5.1. Preparation of $A\beta_{1-42}$

Lyophilised HFIP-treated  $A\beta_{1-42}$  was purchased from rPeptide. 1 mg  $A\beta_{1-42}$  was dissolved in 1 ml HFIP and sonicated for 10 minutes in a DECON Ultrasonics sonicator bath (Sussex, UK). The solution was split into 0.1 mg aliquots and HFIP was evaporated under a stream of  $\text{N}_2$ . Samples were lyophilised to remove any residual HFIP and stored at  $-20\text{ }^\circ\text{C}$ .

Monomeric  $A\beta_{1-42}$  for subsequent experiments was prepared by dissolving 0.22 mg of HFIP-treated  $A\beta$  in 450  $\mu\text{l}$  of cold 20 mM Tris, with sonication for 10 minutes, before the addition of 60  $\mu\text{l}$  of cold deuterium oxide ( $\text{D}_2\text{O}$ ). The pH was adjusted to pH 7.5 with the addition of TFA ( $\sim 45\text{ }\mu\text{l}$  1% TFA) and the final volume brought to 600  $\mu\text{l}$  with cold 2 mM azide to produce 15 mM Tris-TFA pH 7.5, 10%  $\text{D}_2\text{O}$ . The concentration of  $A\beta$  was quantified by measuring the absorbance at 280 nm, and where necessary adjusted to 50  $\mu\text{M}$  by the addition of 15 mM Tris-TFA pH 7.5, 10%  $\text{D}_2\text{O}$ . A 1D  $^1\text{H}$  spectrum was recorded at 278 K.

#### 5.2.5.2. NMR Spectroscopy

In solution, proteins do not have a fixed, rigid structure. Instead they are dynamic molecules that can adopt a number of different conformations. The probability of a particular structural state being populated is dependent on the stability of that conformation. NMR can give an indication of the state of this population as data is recorded on a vast number of molecules. NMR can also provide valuable information on the exchange rate between a free and ligand-bound form of a protein, as the amides involved in the binding process will experience variations in chemical shift due to changes in their local environment. If the rate of chemical exchange between two states is fast then a single peak will be observed at a position reflecting an average of the two conformations and their relative populations. Alternatively, if the two states are in slow exchange, then two discrete peaks will be observed as the binding and release is slower than the acquisition time. A new peak will form at a different resonance frequency in line with the chemical shift of the bound form, while the peak for the unbound form will

remain in the original position. As the titration continues, the peak of the unbound form should decrease in height as the peak of the bound form increases. Finally, if the two states exchange at an intermediate rate, with the binding and release occurring on a similar time-scale to the chemical shift time-scale, then the peaks will generally broaden or disappear as the line-widths broaden.

All NMR spectra described in this chapter were recorded on a Bruker DRX spectrometer operating at 600 MHz with a cryogenically cooled probe, and controlled using XWinNMR (Bruker). Spectra were processed and analysed using Felix 2004 (Accelrys) with in-house macros. All heteronuclear single quantum coherence (HSQC) experiments were acquired using 1024 increments in the proton dimension and 512 increments in the nitrogen dimension. The spectral widths of the proton and nitrogen dimensions were 7507.5 Hz and 2128.6 Hz respectively.

#### 5.2.5.3. $^1\text{H}$ - $^{15}\text{N}$ HSQC Spectrum of hCC

An HSQC experiment measures the chemical shifts of the proton and nitrogen nuclei of every bonded  $^{15}\text{N}$ -H pair by modulating each proton signal with the signal of the attached nitrogen. After processing to deconvolute the two frequencies, a two-dimensional plot is generated with a peak for every amide at the intersection of the proton and nitrogen chemical shifts. Factors that alter the chemical environment of an amide can be detected by changes in the HSQC spectrum, as the chemical shift of each nucleus is directly related to its chemical environment. As each amino acid contains a backbone amide, each peak in the HSQC spectrum will correspond to a specific residue within the protein structure. It is important to know which amide, and therefore residue, corresponds to which peak in the spectrum to allow changes in chemical environment to be mapped onto the protein structure. This is achieved through a process known as resonance assignment. A backbone assignment for hCC has previously been determined at the required experimental conditions of 15 mM Tris-TFA pH 7.5, 278 K (Keeley, 2007). This assignment was based on a published assignment for 200  $\mu\text{M}$  hCC in 50  $\mu\text{M}$  sodium phosphate pH 6.0, which was recorded at 303 K (Ekiel et al., 1997).

In order to establish that the movement of an amide peak is relevant and due to changes in chemical environment, rather than the slight drift that is generally associated with HSQC titrations, a minimal chemical shift change is required which can be calculated by computing an average line width at 50% height for 4-5 peaks. Any peak that moves by at least 2 times this average line width is considered to have a significant chemical

shift change. The value used here was 0.11 ppm for proton and 0.41 ppm for nitrogen chemical shift. Weighted average chemical shift differences were calculated using the formula

$$\Delta_{\text{avg}}(\text{HN}) = [(\Delta\text{H})^2 + (\Delta\text{N}/10)^2]^{1/2}$$

where  $\Delta\text{H}$  and  $\Delta\text{N}$  are chemical shift differences for  $^1\text{H}$  and  $^{15}\text{N}$  respectively and 10 is the estimated ratio of chemical shift changes for the two nuclei (Elshawaihde, 2012).

#### 5.2.5.4. Titration of Monomeric $\text{A}\beta_{1-42}$ into $^{15}\text{N}$ -labelled hCC

A 500  $\mu\text{l}$  sample of 50  $\mu\text{M}$   $^{15}\text{N}$ -labelled monomeric hCC in 15 mM Tris-TFA pH 7.5, 10%  $\text{D}_2\text{O}$  was placed in an NMR tube and initial 1D and 2D spectra were obtained at 278 K to use as a reference. At each stage of the titration either 100  $\mu\text{l}$  or 200  $\mu\text{l}$  of monomeric  $\text{A}\beta$ , produced as described above, was added to the hCC sample. The solution was gently inverted and spun to produce a homogenous sample. At each titration interval, two 1D spectra were recorded either side of a 2D HSQC spectrum. Four titration points were used to give molar ratios of 1:0.4, 1:0.8, 1:1 and 1:1.2 hCC to  $\text{A}\beta$ .

#### 5.2.5.5. Time-course of $\text{A}\beta_{1-42}$ with $^{15}\text{N}$ -labelled hCC

$^{15}\text{N}$ -labelled hCC was buffer exchanged into 2 mM azide to produce a 50  $\mu\text{M}$  solution in 500  $\mu\text{l}$  and lyophilised. 500  $\mu\text{l}$  of 50  $\mu\text{M}$  monomeric  $\text{A}\beta_{1-42}$  was produced as described above and added to the lyophilised hCC before sonication for 10 minutes. This produced a sample of 50  $\mu\text{M}$  hCC and 50  $\mu\text{M}$   $\text{A}\beta_{1-42}$  in 15 mM Tris-TFA pH 7.5, 10%  $\text{D}_2\text{O}$ . The sample was incubated at 303 K for 24 hours and 1D and 2D HSQC spectra were obtained.

### 3. Results

#### 5.3.1. A $\beta$ <sub>1-42</sub> Fibrillisation

A $\beta$ <sub>1-42</sub> fibril formation was monitored using ThT fluorescence. The changes in ThT fluorescence upon A $\beta$  fibrillisation followed a characteristic sigmoidal curve consistent with the nucleation-dependent elongation model of amyloid assembly.

Conditions for the formation of A $\beta$ <sub>1-42</sub> fibrillisation were established that were reproducible, both between experiments and between the replicates within each experiment, to allow comparison of data from different systems. Initially experiments were performed in a Cary Eclipse fluorimeter (Varian, UK); later experiments were carried out in a Biotech Omega fluorescence plate-reader (BMG Labtech, UK). Different protein concentrations were investigated, as shown in Figure 5.4. There is a greater variation between the individual replicate curves obtained from the cuvette method than from the plate-reader. The mean of these replicates was plotted, and normalisation of these curves allowed a comparison between the different data sets. This demonstrated that data obtained from the plate-reader experiments showed similar curves to those obtained with the fluorimeter, with a lag phase of 20-30 minutes and reaching an equilibrium plateau at 3 hours. It could be suggested that halving the peptide concentration from 22  $\mu$ M to 11  $\mu$ M should lead to a variation in the lag phase and elongation rate of the reaction, consistent with the nucleation-dependent model. However, this was not observed. In a similar fashion, Hasegawa et al. (1999) comment that although they observe a concentration-dependent increase in final equilibrium levels, the time taken to proceed to this equilibrium level was unchanged at comparable concentrations of A $\beta$ <sub>1-42</sub>.

Transmission electron microscopy was also carried out in order to analyse the morphology of A $\beta$ <sub>1-42</sub> fibrils produced in different systems and at different peptide concentrations. Figure 5.5 shows examples of electron micrographs of these different preparations after 24 hours. TEM confirmed that mature fibrils had formed in all of the samples. The fibrils are long, straight and unbranched, with an average fibril width of  $9.4 \pm 1.3$  nm ( $n = 105$ ). There appeared to be very little structural variation between preparations in addition to the similarities in kinetics therefore data from both experimental set-ups (fluorimeter and plate-reader) are shown throughout this chapter.

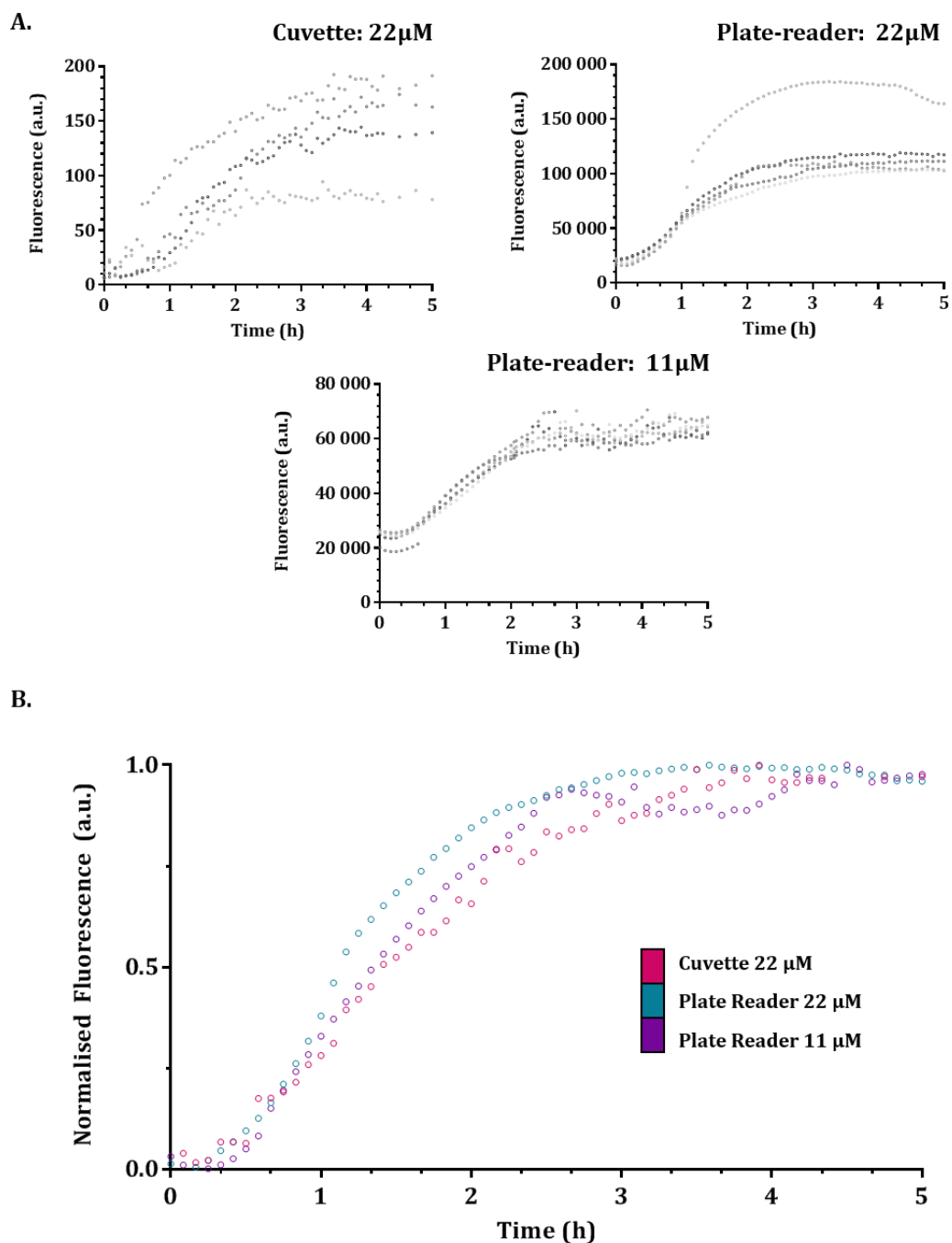
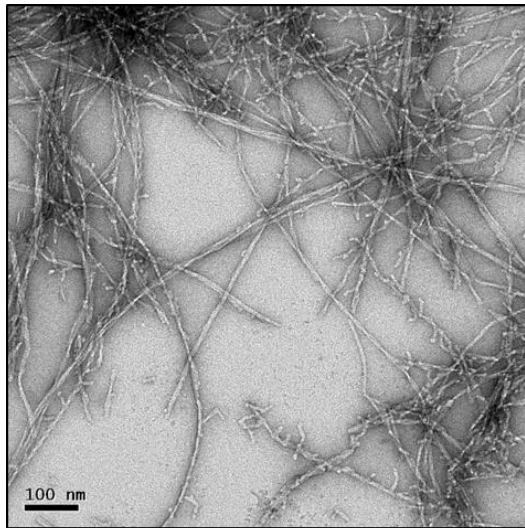
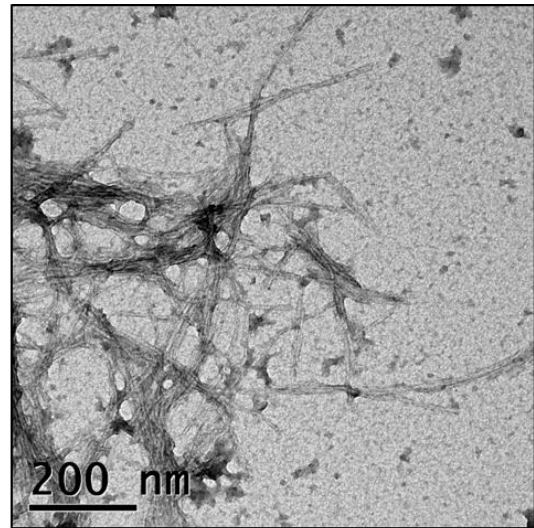


**Figure 5.4. Fibrillisation of  $A\beta_{1-42}$  using Different Systems**

*ThT* fluorescence curves (A) showing  $A\beta_{1-42}$  fibrillisation reactions in different systems.  $A\beta_{1-42}$  was incubated at either 22  $\mu\text{M}$  or 11  $\mu\text{M}$  in 50 mM sodium phosphate pH 7.4, 150 mM NaCl in a Varian Cary fluorimeter at 25°C or an Omega plate-reader at 30 °C with agitation. The increase in fluorescence intensity at 482 nm was monitored over several hours. The mean of 4 or 5 replicates from each experiment was plotted and curves were normalised to allow comparison between the different systems (B), indicating a similar lag time and elongation rate.



**Cuvette: 22 $\mu$ M Quiescent**



**Cuvette: 22 $\mu$ M Agitated**

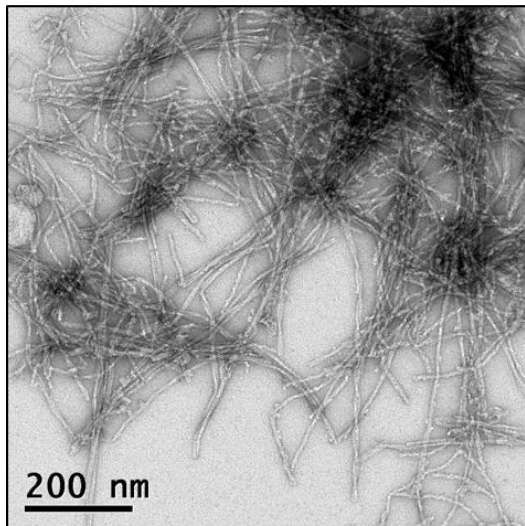


**Plate-reader: 22 $\mu$ M Agitated**

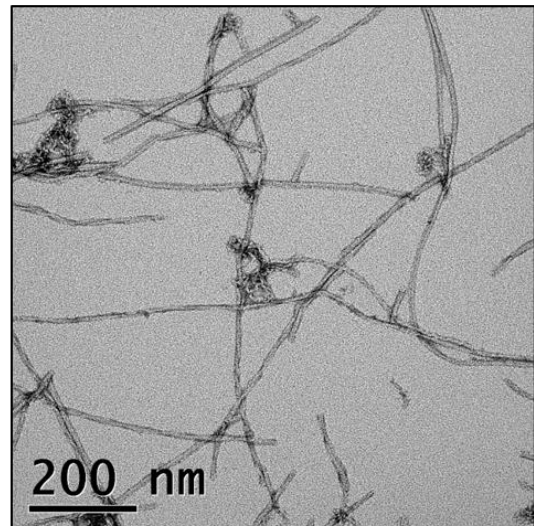


**Plate-reader: 11 $\mu$ M Agitated**

**Figure 5.5. TEM of A $\beta$ <sub>1-42</sub> Fibrillisation using Different Systems**

*A $\beta$  fibrils produced in different systems and at different protein concentrations in 50 mM sodium phosphate pH 7.4, 150 mM NaCl show a similar structural morphology after 24 hours. All images were taken at 21,000 x magnification.*

### 5.3.2. Addition of hCC to A $\beta$ <sub>1-42</sub> Fibrillisation

#### 5.3.2.1. ThT Time-course

It has previously been proposed that ratios of 1:1 hCC to A $\beta$ <sub>1-42</sub> are required to completely inhibit the formation of amyloid fibrils by A $\beta$ <sub>1-42</sub> (Sastre et al., 2004). However, substoichiometric amounts of hCC (0.3  $\mu$ M) have been shown to protect both N2a neuroblastoma cells and rat primary hippocampal neurons from A $\beta$ -induced cell death when incubated with 30  $\mu$ M A $\beta$ <sub>1-42</sub>. The kinetics of A $\beta$ <sub>1-42</sub> fibrillisation were measured in the presence of different molar ratios of hCC in the standard conditions described earlier, with an A $\beta$ <sub>1-42</sub> concentration of 11  $\mu$ M, as shown in Figure 5.6. Each curve is the average of 5 replicates with error bars displaying the standard error of the mean (SEM) to give an indication of the spread of the data. Different concentrations of hCC were tested ranging from 22  $\mu$ M (twice the concentration of A $\beta$ <sub>1-42</sub>) to 0.11  $\mu$ M (100 times less than the concentration of A $\beta$ <sub>1-42</sub>). Equimolar concentrations of hCC caused a large reduction in ThT fluorescence, suggesting that the amount of fibril being produced was significantly less in the presence of hCC. The intensity of the hCC + A $\beta$  curve is about 25% of the A $\beta$  curve in the absence of hCC, suggesting a reduction in fibril production of about 75%. hCC concentrations of 8.75  $\mu$ M and 5.5  $\mu$ M caused a reduction in ThT fluorescence of 62% and 25% respectively. In all cases however there is still a small amount of fibril being formed; a molar ratio of 1:2 A $\beta$  to hCC will inhibit A $\beta$  fibril formation completely. Smaller ratios of hCC do not appear to have an effect on A $\beta$  aggregation with the curves showing similar lag time, elongation rate and amplitude. When incubated alone in these conditions, hCC did not form fibrils and there was no increase in ThT fluorescence.

The calculated lag time for A $\beta$  fibrillisation was 0.4 hours (or 24 minutes), with a  $t_{50}$  of 1.3 hours and an apparent rate constant of 2.5 h<sup>-1</sup> (7 x 10<sup>-4</sup> s<sup>-1</sup>). As seen in Figure 5.7, one-way ANOVA and Tukey's test indicated that there are no significant differences between either the lag time, the  $t_{50}$  or the  $k_{app}$  when hCC is added to A $\beta$ <sub>1-42</sub> fibrillisation in a 1:1 ratio. However small changes in  $k_{app}$  were observed in the presence of 2.25  $\mu$ M, 5.5  $\mu$ M and 8.75  $\mu$ M hCC with values of 4.13 h<sup>-1</sup>, 3.75 h<sup>-1</sup> and 4.21 h<sup>-1</sup> respectively (11.4 x 10<sup>-4</sup> s<sup>-1</sup>, 10.4 x 10<sup>-4</sup> s<sup>-1</sup> and 11.7 x 10<sup>-4</sup> s<sup>-1</sup>).

Fibril elongation is limited in a dose dependent manner, with both 8.75  $\mu$ M and 11  $\mu$ M hCC (1:0.75 and 1:1 molar ratios of A $\beta$  to hCC respectively) having a significant inhibitory effect on aggregation and majorly reducing the fibril load. These are not

saturation conditions, where each cystatin molecule is binding to an A $\beta$  molecule or complex, as this would work at very low concentrations of hCC. If the mechanism involves native, folded hCC monomer binding to monomeric A $\beta$ <sub>1-42</sub> as described by the literature, then this would imply a high dissociation constant.

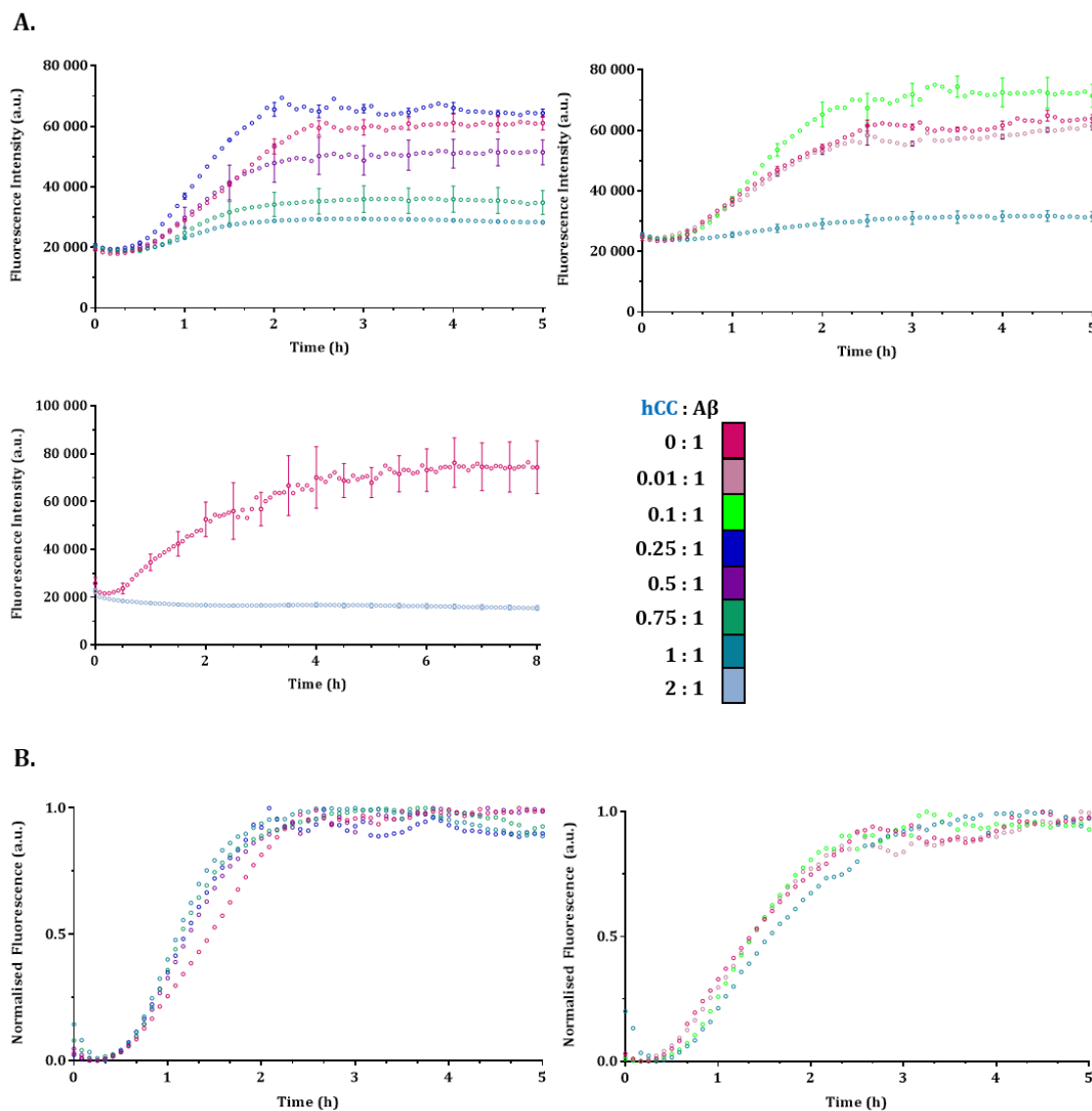
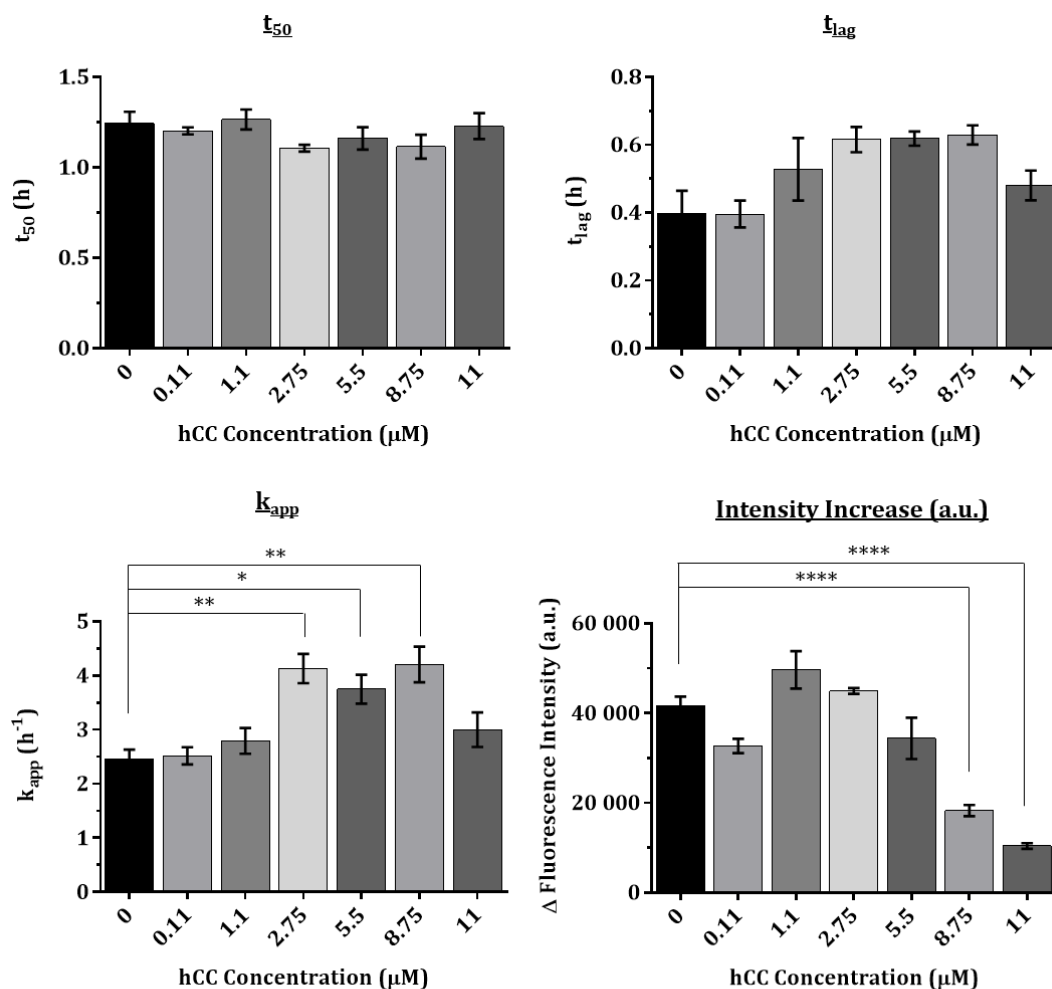


**Figure 5.6. Incubation of A $\beta$ <sub>1-42</sub> in the Presence of hCC**

*ThT fluorescence time-courses (A) of A $\beta$ <sub>1-42</sub> fibrillisation at 11  $\mu$ M with the addition of different molar ratios of hCC. Each curve is the average of 5 replicates, with error bars indicating the standard error of the mean (SEM). Different experimental series performed at different times and with different protein stocks are shown for comparison. Curve amplitudes were normalised to 1 (B) to allow initial comparison of lag phase and elongation rate.*



hCC Concentration ( $\mu\text{M}$ )	$t_{50}$ (h)	$t_{lag}$ (h)	$k_{app}$ ( $h^{-1}$ )	Intensity Increase (a.u.)
0	1.24	0.40	2.46	41 628
0.11	1.20	0.40	2.52	32 682
1.1	1.27	0.53	2.80	49 638
2.75	1.11	0.62	4.13	44 937
5.5	1.16	0.62	3.75	34 380
8.75	1.12	0.63	4.21	18 267
11	1.2	0.48	3.0	10 412

**Figure 5.7. Calculated Kinetic Parameters**

Box-plots displaying kinetic parameters  $t_{50}$ ,  $t_{lag}$  and  $k_{app}$ , as well as the increase in fluorescence intensity, for  $A\beta_{1-42}$  fibrillisation reactions in the presence of different molar concentrations of hCC. Each value is the average of 5 replicates. Significant differences were calculated using one-way ANOVA and Tukey's test and those with  $\alpha \leq 0.05$  (\*),  $\alpha \leq 0.01$  (\*\*) and  $\alpha \leq 0.0001$  (\*\*\*\*) are indicated.

### 5.3.2.2. Electron Microscopy

Although changes in ThT fluorescence suggested that hCC was inhibiting A $\beta$ <sub>1-42</sub> fibril production, this reduction in intensity could be attributed to other factors such as changes in morphology or the production of alternative species which also bind ThT. TEM was used to study the structural morphology of the structures produced at the end of the incubation of A $\beta$ <sub>1-42</sub> in the presence of an equimolar concentration of hCC. Figure 5.8 shows electron micrographs of different preparations of A $\beta$ <sub>1-42</sub> and hCC in the same conditions after at least 24 hours of incubation. In the absence of hCC, A $\beta$ <sub>1-42</sub> produces long straight unbranched fibrils with an average width of  $9.4 \pm 1.3$  nm (n=105) (Figure 5.5). Very few oligomeric species were present, and a large amount of amorphous aggregate was not observed. The fibril morphology was maintained in different preparations, with samples consistently forming amyloid fibrils.

When A $\beta$ <sub>1-42</sub> was incubated in the presence of equimolar hCC several species were observed with very different morphologies. Short curly protofibril-like structures appeared in several preparations, in some cases highly associated and clumped together. These were often thinner and more fragile-looking than the mature fibrils, however in some cases these structures appeared to be a similar width to the fibrils produced in the absence of hCC. The curved structures and highly associative nature of these species made it difficult to extract measurements from the electron micrographs, especially the smaller structures which often lacked the contrast required. A small number of annular oligomers were also occasionally observed. A large amount of amorphous aggregate was often observed, suggesting that the short protofibrillar species could be further associating to form large unstructured aggregates under these experimental conditions. As would be expected from the small increase in ThT fluorescence, the presence of a small amount of mature fibril was regularly noted. If this reaction is followed over an extended period of time (months) the formation of high quantities of mature fibrils was still not observed. Instead a large amount of amorphous aggregate is present. It is tempting to speculate that these protofibrillar species accumulate further to produce large aggregates, especially considering the presence of large clumps in the sample after only 24 hours. The lack of fibrils suggests these species are no longer thermodynamically favoured, and that the protofibrillar species formed are in a kinetically trapped state.

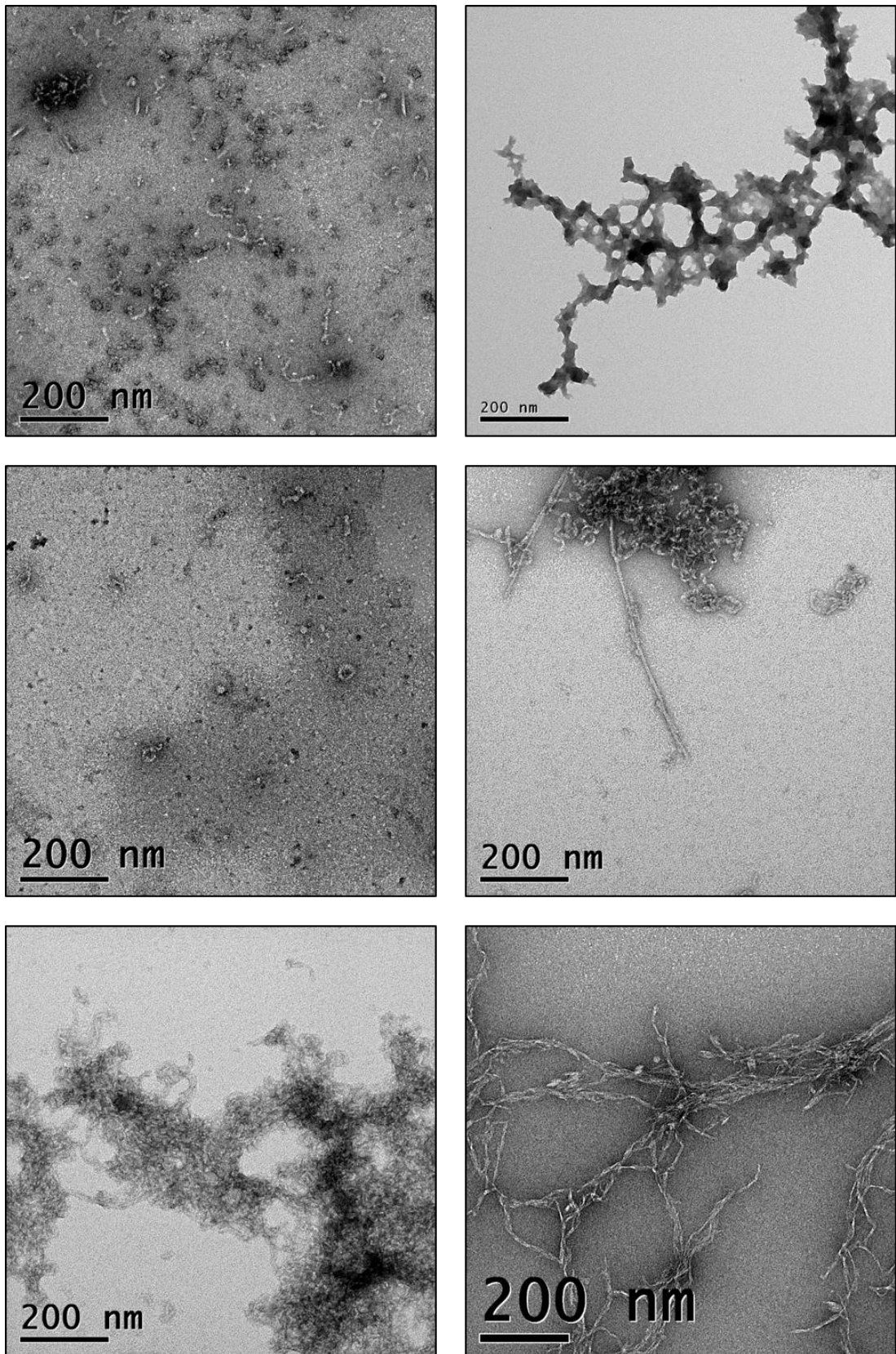


**Figure 5.8. TEM of Incubation of  $A\beta_{1-42}$  in the Presence of hCC**

*Electron micrographs of examples of different preparations of  $A\beta_{1-42}$  and hCC in a 1:1 equivalence after at least 24 hours. Images taken at 21,000 x magnification.*

### 5.3.3. Time-course of A $\beta$ <sub>1-42</sub> and hCC

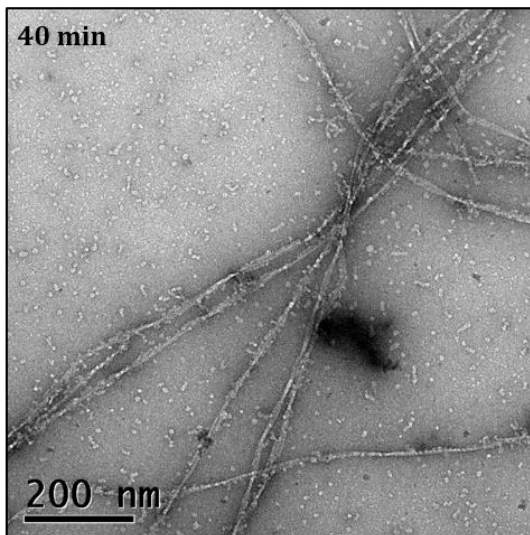
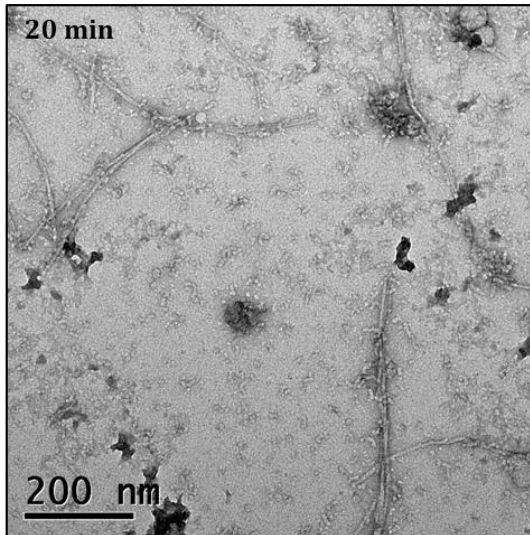
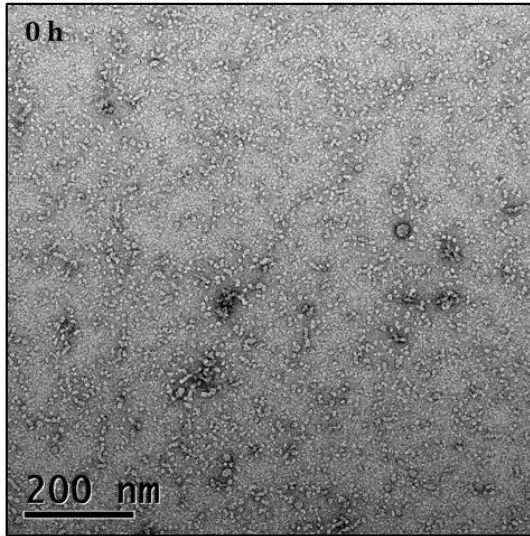
A time-course of the aggregation reaction of A $\beta$ <sub>1-42</sub> was monitored by TEM and SEC in the presence and absence of equimolar concentrations of hCC.

#### 5.3.3.1. Electron Microscopy

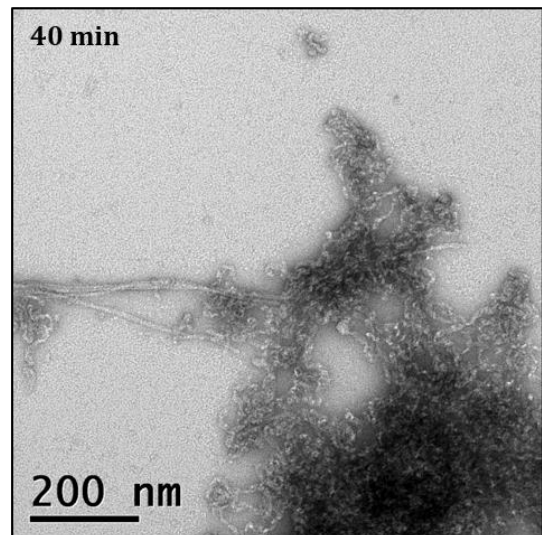
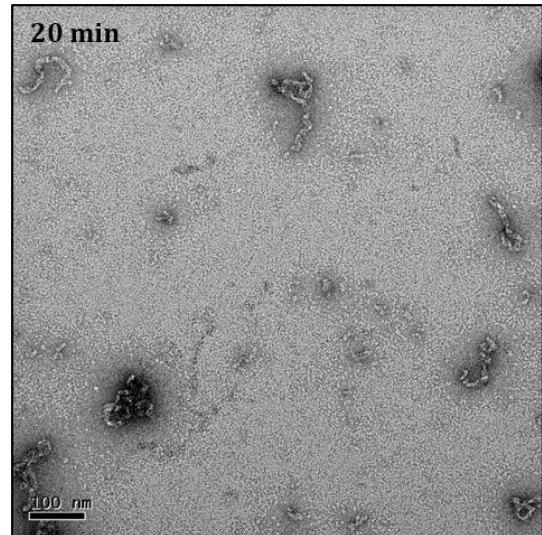
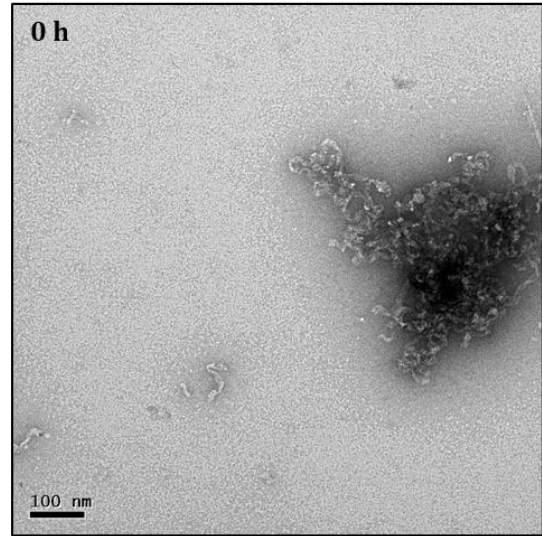
As seen in Figure 5.9, TEM indicated that small oligomeric species were forming in the A $\beta$  sample very early on, within the time that was taken for the sample to be put on an EM grid. A repeat of this experiment by my colleague Sirwan Al-Jaf indicated that if the sample is put on the grid immediately after buffer is added to the A $\beta$ -DMSO mixture then no oligomers are present, however small oligomeric species had formed within 20 minutes. A small population of amyloid fibrils were observed as early as 20 minutes, with more appearing at 40 minutes. This supports the ThT data, where fibril elongation begins after approximately 30 minutes. After 2 hours there are large amounts of mature fibril present in the sample with very few oligomers observed.

In the presence of hCC, small protofibrillar species appear very early on in the time-course. These structures are larger and more elongated than those seen in the A $\beta$  sample, and remain throughout the reaction. By the end of the time-course large quantities of the protofibrillar species are present and are associating to form large clumps. A few amyloid fibrils begin to appear after 40 minutes, as was seen in the A $\beta$  sample, again at the point at which an increase in intensity is seen in the ThT reaction. However, large amounts of mature fibril are not observed in the presence of hCC. This suggests that the hCC is preventing the formation of fibrils, rather than the formation of oligomeric intermediates. The structures that have assembled, and are maintained over the time-course, look quite different from those observed in the A $\beta$  sample, suggesting that the cystatin is not stabilising an intermediate on-pathway to fibril formation, but rather diverting the A $\beta$  down a different assembly pathway.

A $\beta$ <sub>1-42</sub>



A $\beta$ <sub>1-42</sub> + hCC 1:1



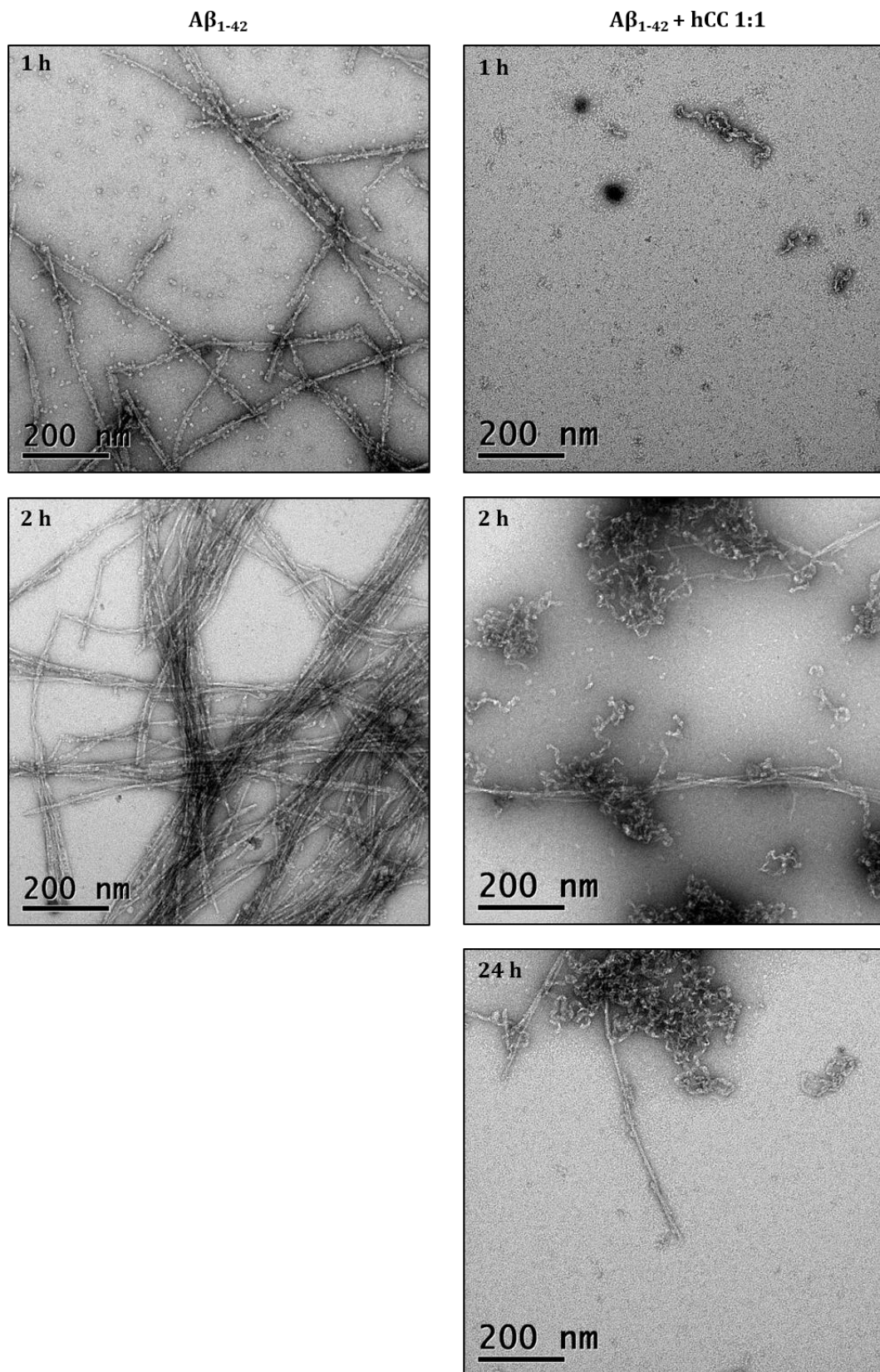


**Figure 5.9. Electron Microscopy Time-Course**

*TEM images following the aggregation of  $A\beta_{1-42}$  in the presence and absence of equimolar hCC over 24 hours. All images were taken at 21,000 x magnification.*

### 5.3.3.2. Size Exclusion Chromatography

The aggregation of A $\beta$ <sub>1-42</sub> was monitored in both the absence and presence of hCC by performing SEC in fibrillisation conditions. Following the A $\beta$  fibrillisation reaction alone showed a decrease in monomer peak height corresponding to the formation of large oligomers and mature fibrils, as more monomeric protein became incorporated (Figure 5.10). Monomeric A $\beta$  was still present in the solution after 2 hours, and there was still a very small peak present even after 24 hours, however the majority of the protein has been converted into aggregated structures. The equilibrium of this reaction means that a small amount of monomeric A $\beta$ <sub>1-42</sub> is often observed in such experiments, as has previously been reported by (Walsh et al., 1997). From previous experiments using A $\beta$ <sub>1-40</sub>, which is more stable and less prone to aggregation, 22  $\mu$ M A $\beta$ <sub>1-42</sub> should give a peak height of 0.047 mAU; the peak height observed in the time-course, also of 22  $\mu$ M A $\beta$ <sub>1-42</sub>, is 0.035 mAU which is 75% of the predicted height. This suggests that 25% of the A $\beta$  in the solution has already been converted into other species. The broadening of this peak is thought to be due to the formation of higher molecular weight species.

Although SEC can provide valuable insight into the formation of large molecular weight species in the fibrillogenesis of A $\beta$ , its usefulness in the identification of low molecular weight species can be limited. The amphipathic nature of the A $\beta$  peptide means that it can form both hydrophobic and/or electrostatic interactions with the column matrix under non-denaturing conditions.

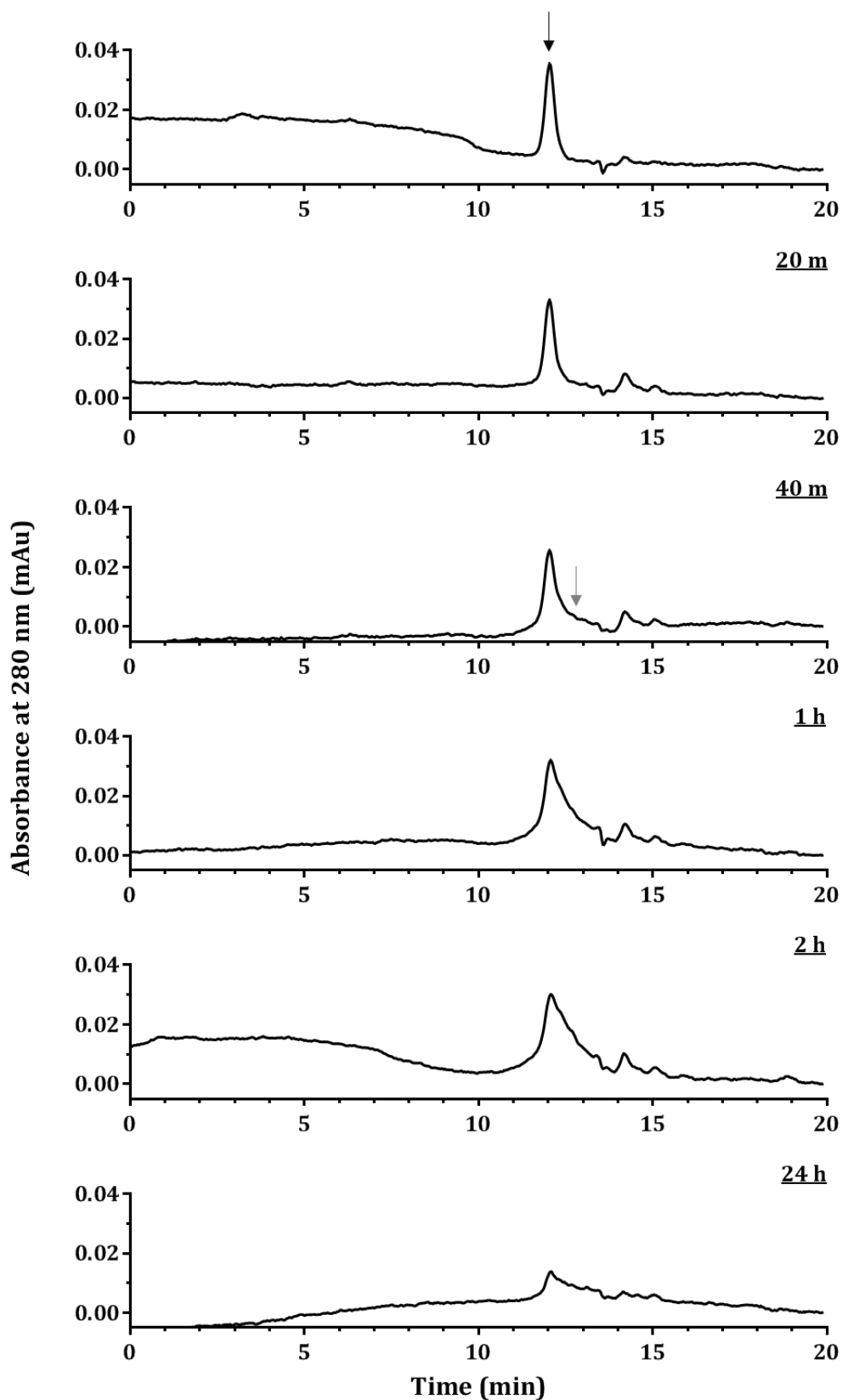


**Figure 5.10. SEC Time-course of Fibrillisation of  $A\beta_{1-42}$**

*SEC elution profiles of  $A\beta_{1-42}$  fibrillisation over 24 hours. The monomer peak is shown at 12 minutes (black arrow) and the broadening of this peak is highlighted (grey arrow).*

Figure 5.11 shows elution traces obtained by monitoring the fibrillisation of A $\beta$ <sub>1-42</sub> in the presence of equimolar hCC by SEC. Surprisingly, a significant reduction in hCC concentration is not observed when monitoring the reaction over 24 hours, implying that the cystatin is not being incorporated into the species that are assembling. However, the height of the hCC peak at the start of the reaction is reduced by 25% compared to a hCC sample in the absence of A $\beta$  (Figure 5.12), indicating that this proportion of hCC could already be bound to the A $\beta$  before the start of the HPLC time-course. This calculation takes into account the small amount of hCC dimer that is present in the time-course sample. This could mean that the A $\beta$  is binding to a minority species in the cystatin sample, therefore the majority of the molecules will be unaffected by the presence of the A $\beta$  and there will not be any major changes in apparent hCC concentration over the time-course. Alternatively, if the cystatin is working as a catalyst and converting A $\beta$  oligomeric intermediates into alternative, non-toxic conformations, then again there would be no change in the apparent 'free hCC' concentration.

Analysis of the time-course by SEC also shows the appearance of two small peaks near the exclusion volume of the column. Initially only a single peak is observed with an elution time of 13 minutes which increases in intensity as time progresses over the first 40 minutes. This peak remains at a constant height over the next two hours but is very much reduced after 24 hours. After 40 minutes a second peak appears at 11 minutes, which remains for the next two time-points (1 and 2 hours) but then is no longer present by 24 hours. It is likely that both of these peaks correspond to the formation of different populations of oligomeric species through the aggregation process. In the final time-point these peaks are greatly reduced or not present, which could indicate that these species have been incorporated into the aggregates observed by TEM.

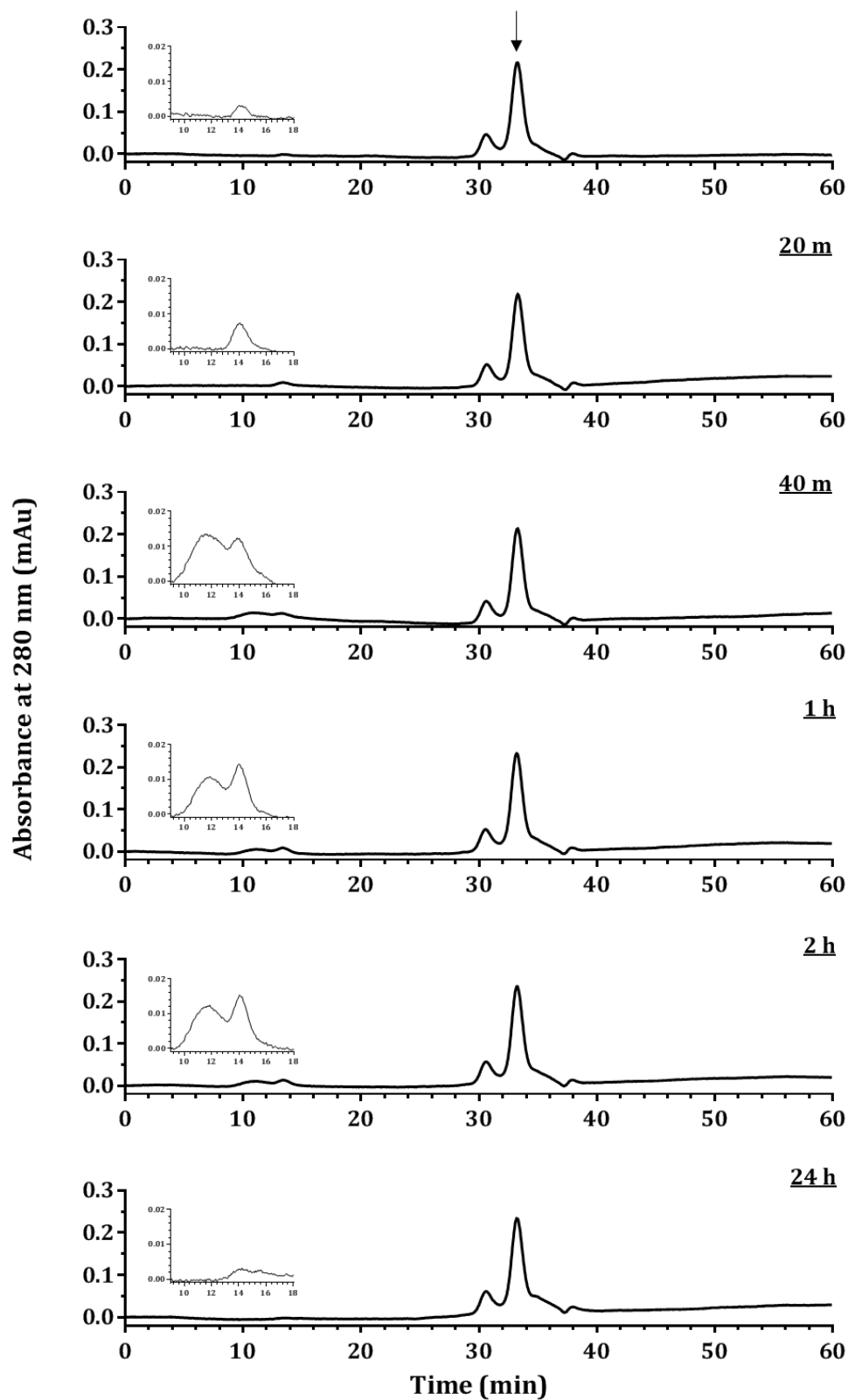


**Figure 5.11. SEC Time-course of  $A\beta_{1-42}$  Fibrillisation in the Presence of hCC**

*SEC elution profiles of  $A\beta_{1-42}$  fibrillisation in the presence of equimolar hCC over 24 hours. The arrow indicates the hCC monomer peak, and the formation of high molecular weight oligomers is followed in the inset graphs.*

Figure 5.12 shows the height of a selection of the peaks observed throughout the two time-courses. Following the time-course of  $A\beta_{1-42}$  and hCC in this way highlights that the concentration of hCC, both monomer and dimer, that is in solution (peaks at 30 and 33.5 minutes) is remaining constant. The formation of oligomeric species (peaks at 11 and 13 minutes) increases over the 40 minutes of the reaction, which is before a large increase in ThT fluorescence is observed. The concentration of these species remains constant until 2 hours, however they are no longer present after 24 hours, suggesting their incorporation into larger aggregates.

In the  $A\beta_{1-42}$  time-course the broadening of the monomer peak, monitored by measuring the peak height at an elution time of 12.6 minutes increases over the first hour before plateauing, in a similar fashion to the oligomer peaks observed in the  $A\beta$  and hCC time-course. Although a small decrease in the height of the  $A\beta$  monomer peak (12 minutes) is observed over the first hour, a large reduction is not seen until 24 hours incubation. This is consistent with variations in the lag time of individual time-courses shown in Figure 5.6 where not all samples show plateauing of the ThT signal after 2 hours. Expanding the time-course to include more time-points between 2 and 24 hours would establish a greater understanding of the changes in  $A\beta$  monomer levels throughout this reaction.

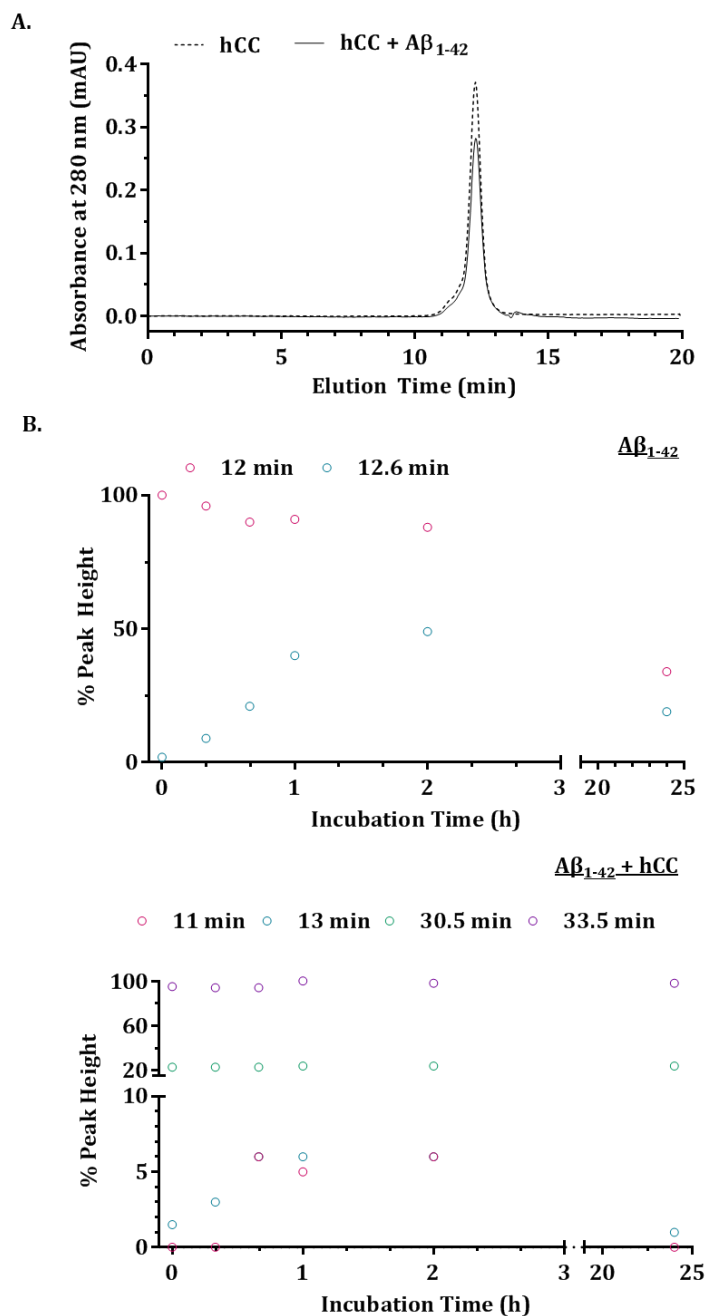


**Figure 5.12. Peak Heights from SEC-HPLC Time-course**

A comparison of the elution profiles (A) of 22  $\mu\text{M}$  hCC in the presence (solid line) and absence (dashed line) of equimolar A $\beta_{1-42}$  showing a reduction in peak height at 12 minutes of 25%. The height of specific peaks from the time-course elution profiles in Figures 5.10 and 5.11 were measured and plotted against the reaction time-point (B). The A $\beta_{1-42}$  monomer peak at 12 minutes (pink) and the broadening of this peak at 12.6 minutes (blue) were plotted for the A $\beta_{1-42}$  time-course as a percentage of the largest peak height to show the height of the peaks in comparison to each other. The two oligomer peaks at 11 minutes (pink) and 13 minutes (blue) were plotted for the A $\beta_{1-42}$  and hCC time-course, in addition to the hCC dimer peak at 30.5 minutes (green) and the hCC monomer peak at 33.5 minutes (purple). Again the peak heights were plotted as a percentage of the largest peak heights.

### 5.3.4. Comparison of Different Species

The species that are formed through the interaction of  $A\beta_{1-42}$  and hCC are short, thin and curved with a different structural morphology to that of mature fibrils. There are many examples of different soluble species produced by  $A\beta_{1-42}$  described in other studies; at least 10 are described in Benilova et al. (2012). Images from the experiments described here were compared to electron micrographs of protofibrils and ADDLs from the literature to establish any similarities in morphology as shown in Figure 5.13. It is difficult to compare species using only TEM, as alternative structures and conditions can associate differently with the copper grids used to mount the samples. Some species will stick well to the surface and be easily observed, whereas others will not bind. This means that the observations are skewed in favour of certain species.

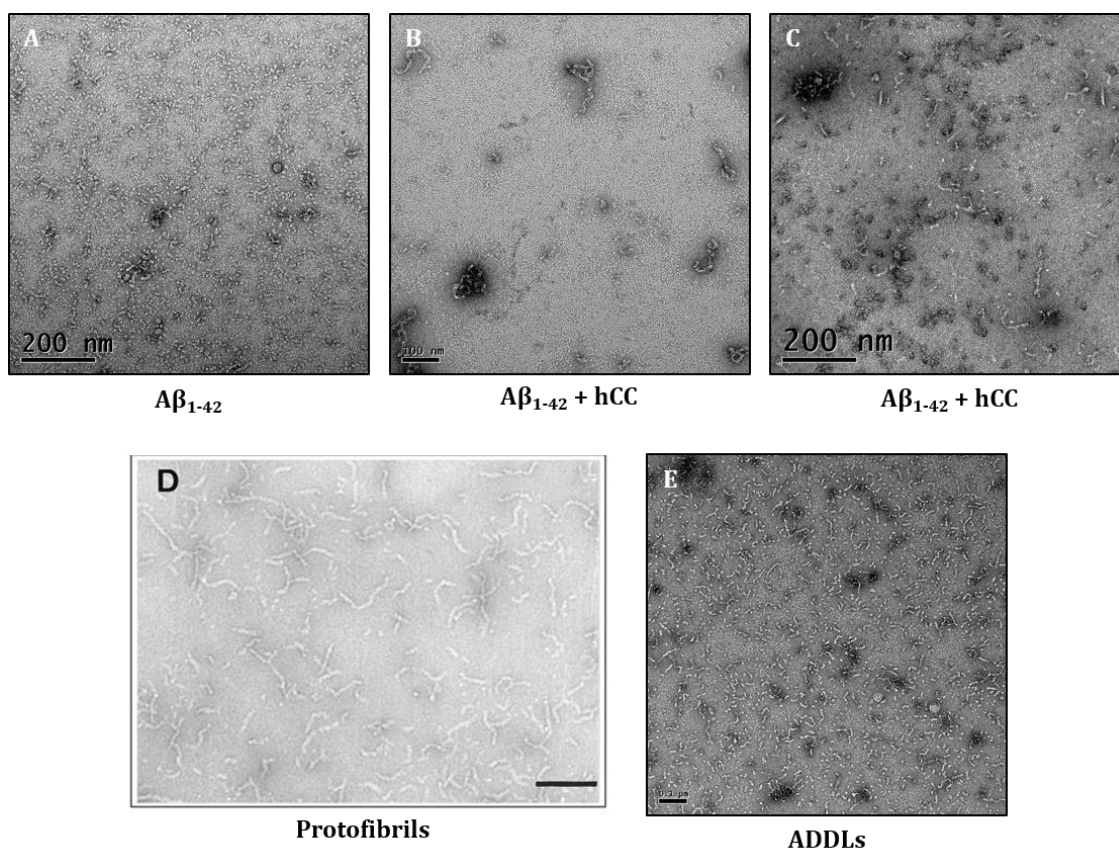


**Figure 5.13. Comparison of Different Species by TEM**

Electron micrographs of  $A\beta_{1-42}$  incubated in the absence (A) and presence (B and C) of equimolar hCC. The image of  $A\beta_{1-42}$  protofibrils purified by SEC (D) was taken from (Walsh et al., 1997) with a scale bar of 100 nm and the image of ADDLs produced by incubating  $A\beta_{1-42}$  in 50 mM sodium phosphate pH 7.4, 150 mM NaCl at 4°C for 24 hours was kindly provided by Sirwan Al-Jaf. Images A, B and C were taken at 21,000 x magnification.

A $\beta$  protofibrils have been previously described as unbranched, rod-like structures that are less than 200 nm in length, with a diameter of 4-8 nm (Walsh et al., 1997, Walsh et al., 1999). This is a similar width to the species under investigation, however the protofibrils are less curly and associated. It is thought that A $\beta$  aggregates through a series of transient intermediates to then form protofibrils, which act as a core for fibril elongation. Walsh et al. (1997) report that protofibril levels are at their peak after 8 hours, as measured by SEC, and that these levels are greatly reduced by 24 hours. Although the structures produced from the incubation of A $\beta$ <sub>1-42</sub> in the presence of hCC have a protofibrillar appearance, they remain in solution and their levels are not greatly reduced after 24 hours, as observed by TEM.

Under specific conditions it is known that A $\beta$ <sub>1-42</sub> forms a population of structures known as A $\beta$ -derived diffusible ligands (ADDLs). These species are thought to be responsible for cytotoxicity in AD and have been well characterised. A preparation of ADDLs was produced by my colleague Sirwan Al-Jaf by incubating 100  $\mu$ M A $\beta$ <sub>1-42</sub> in 50 mM sodium phosphate pH 7.4, 150 mM NaCl at 4°C for 24 hours. These structures were characterised by SDS-PAGE and TEM, and were also used for comparison purposes with the species formed after the incubation of A $\beta$ <sub>1-42</sub> with hCC. These latter species have a very different morphology to the ADDLs, which are a lot smaller and less elongated. The spherical species observed in the ADDL preparation are absent from the A $\beta$ <sub>1-42</sub> and hCC sample.

Although it was attempted to probe the structure of the different morphologies using the antibodies A11 and OC, this was unsuccessful. These antibodies recognise different structural motifs often observed in aggregated structures. The A11 antibody recognises a common structural epitope in prefibrillar oligomers, whereas the OC antibody recognises fibrils and fibrillar oligomers (Kayed et al., 2007). None of the samples tested showed any binding to A11 which was unexpected as ADDLs have been shown previously to bind to this antibody (Benilova et al., 2012). However this sample did show a positive result for the OC antibody, indicating that the species that had been produced were fibrous. It is therefore likely that the reaction had proceeded too far and mature fibrils had formed. The A $\beta$  monomer sample also showed binding to the OC antibody, again suggesting that fibrous structures had formed. Although there was a reduction in binding of OC to the A $\beta$  species that had been produced in the presence of hCC compared to the A $\beta$  alone sample, without successful controls further conclusions

could not be drawn. It has been reported that the species formed upon the incubation of 100  $\mu\text{M}$   $\text{A}\beta_{1-42}$  in the presence of 34  $\mu\text{M}$  hCC showed a significant reduction in binding to the A11 antibody compared to oligomers produced from the incubation of  $\text{A}\beta$  alone (Tizon et al., 2010). The species formed in the presence of hCC were added to rat primary hippocampal neurons and a significantly lower toxicity was observed than for oligomers formed by  $\text{A}\beta$  in the absence of hCC. This demonstrates that the species produced by the incubation of  $\text{A}\beta$  in the presence of hCC causes a reduction in toxicity of the  $\text{A}\beta$ .

### 5.3.5. Addition at Different Time-Points

In order to establish the species in the aggregation reaction to which the hCC was binding, equimolar hCC was added at different points throughout  $\text{A}\beta$  fibrillisation and the reaction monitored by ThT fluorescence. These points were chosen to be at the start of the elongation phase, at the mid-point of the elongation phase, and at the plateau.

The addition of hCC after both 20 minutes and 1 hour showed a 20% and 55% reduction respectively in ThT fluorescence intensity when compared to the control reaction. This is less than the reduction of 75% observed when equimolar hCC is added at the start of the reaction, however demonstrates that hCC still has an effect on  $\text{A}\beta$  fibrillisation at these time-points and suggests that the hCC-binding species are still present. The addition of hCC after 2 hours shows no difference in ThT fluorescence compared to the control. This suggests that hCC needs to be present early on in the reaction to have an effect, and that after 2 hours the reaction is too advanced for the hCC to have an effect. This could also suggest that hCC does not dissolve pre-formed mature  $\text{A}\beta$  fibrils, but rather has an effect on their formation. Analysis of the latter sample by SEC after 24 hours incubation and after 1 week shows a reduction in hCC concentration. It was thought that this could correspond to the hCC associating with the fibrils after their formation, or that the hCC itself is aggregating. Surprisingly, TEM at both of these time-points did not show large amounts of mature amyloid fibrils, but rather amorphous aggregates. This could mean that there is a slow dissociation of the amyloid fibrils by the hCC over an extended time period, or that the species being produced are ThT-positive. Further study would be required to validate these results.

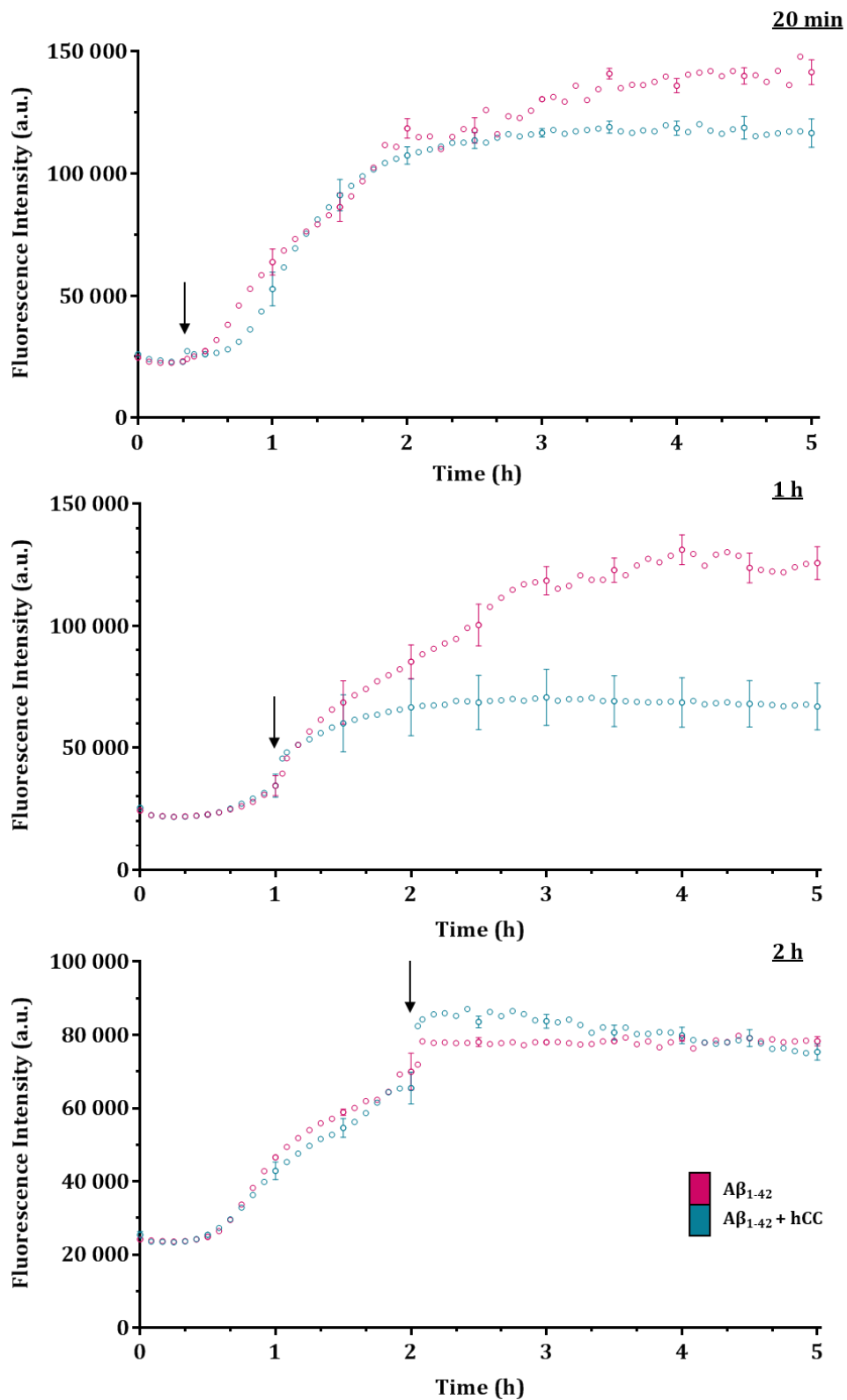


**Figure 5.14. Addition of hCC at Different Points**

*Equimolar hCC was added to  $A\beta_{1-42}$  at time points of 20 minutes, 1 hour and 2 hours during the fibrillation reaction as indicated by the arrows. Each curve is the average of 5 replicate reactions with error bars displaying the standard error of the mean.*

### 5.3.6. Addition of Different Species

Different species of hCC such as dimer and stable high-molecular-weight oligomers were produced and characterised and their ability to modulate A $\beta$  fibrillisation was examined using ThT fluorescence. An investigation into the effect of cystatin B on A $\beta$  fibril formation has indicated that tetramers of the wild-type cystatin will completely inhibit fibrillisation by A $\beta$ , as demonstrated by ThT and TEM, whereas the monomer, dimer and higher oligomeric species do not have an inhibitory effect (Skerget et al., 2010). Similarly, non-native species of transthyretin and neuroserpin are believed to be more effective inhibitors, presumably as this favours exposure of the active binding site (Du and Murphy, 2010, Chiou et al., 2009).

#### 5.3.6.1. Dimer

Figure 5.15 shows the change in ThT fluorescence when the hCC dimer preparation was incubated with 11  $\mu$ M A $\beta_{1-42}$  at two different dimer concentrations, 11  $\mu$ M and 5.5  $\mu$ M. The addition of the dimer has a dramatic effect on the lag time of the reaction. At a molar ratio of 1:1 hCC (subunit) to A $\beta$ , there is a 33% reduction in fluorescence intensity, however this effect is not seen at the lower concentration of dimer. This indicates that the addition of hCC dimer to A $\beta$  has a different effect on the assembly pathway than was observed for the hCC monomer and is more reminiscent of other proteins such as transthyretin. In the monomer experiments the lag phase, and consequently the nucleation process, was not affected by the presence of the hCC. With the dimer experiments the increase in the lag phase suggests that dimeric hCC is affecting the formation of nucleating species and delaying the formation of amyloid fibrils. This implies that this form of hCC is binding differently and because its modulation of the process is kinetic rather than thermodynamic, is probably not becoming incorporated into the aggregated species. TEM indicated the formation of protofibrillar species and amorphous aggregate when A $\beta_{1-42}$  and hCC dimer were incubated at a 1:1 molar ratio, similar to the sample in which hCC oligomers/fibrils were incubated with A $\beta_{1-42}$  (Figure 5.16). The lack of fibrillar species despite the high ThT signal may be due to precipitation of these species or adsorbance to the plate. Cell studies and *in vivo* work do show the localisation of the two proteins to surfaces so it is reasonable to imagine this may happen on the microplates used.

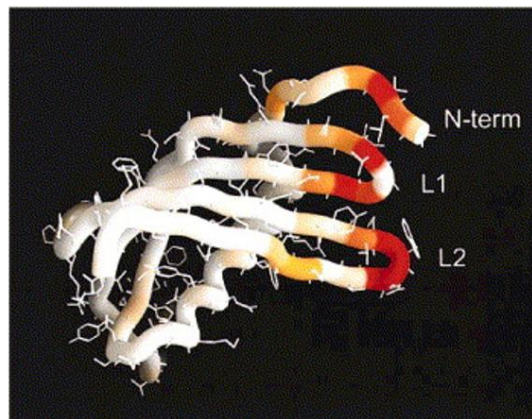
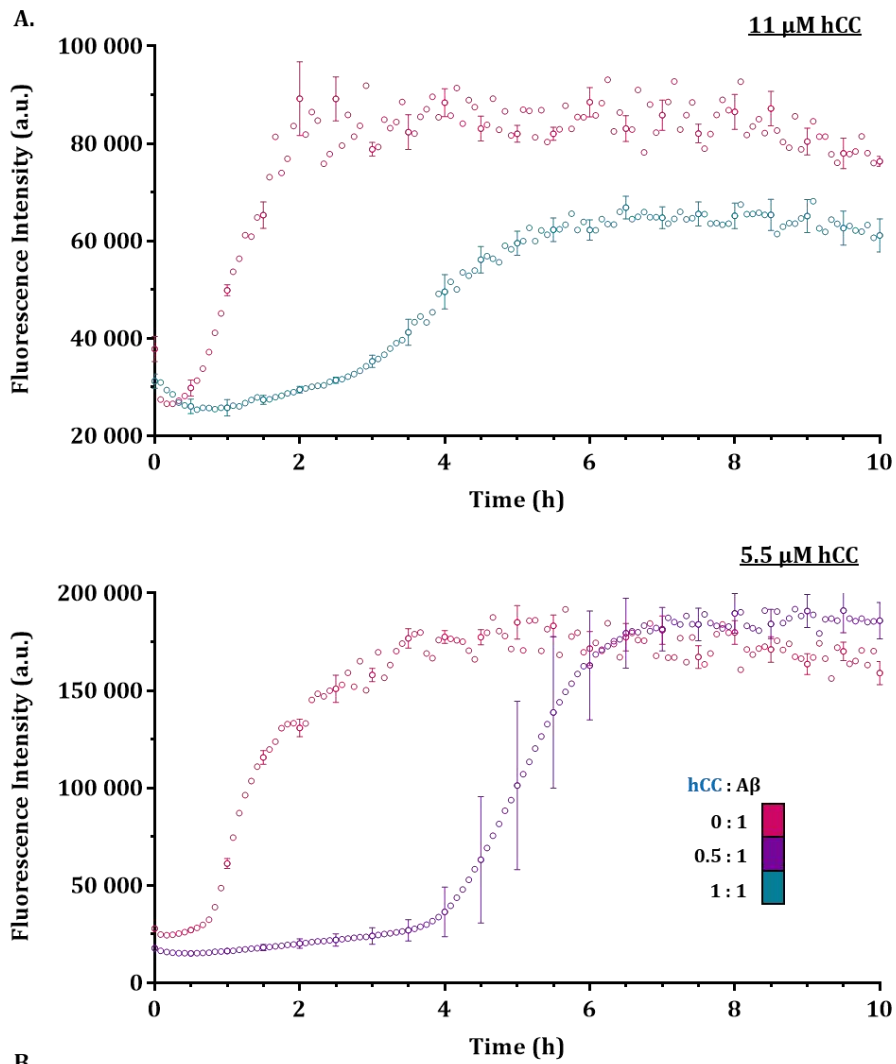


**Figure 5.15. Addition of hCC Dimer**

*ThT fluorescence time-courses (A) of  $A\beta_{1-42}$  fibrillisation at 11  $\mu\text{M}$  with the addition of different molar ratios of hCC dimer. Each curve is the average of 4 or 5 replicate reactions with the standard error of the mean indicated by the error bars. The structure of hCC is also shown (B) indicating the position of chemical shift changes upon dimerisation. Changes are graded with red being the biggest change, then orange then yellow. Figure taken from (Ekiel et al., 1997).*

### 5.3.6.2. Implications for the Structural Nature of the Interaction

The remarkable difference between the monomer and dimer interaction with A $\beta$  suggests strongly that differences in the surfaces of these molecules must be responsible. The surface of the dimer and the monomer are essentially identical in all regions of the molecule except for the loops involved in protease binding, as exhibited by small changes in chemical shift (Ekiel et al., 1997) (Figure 5.15). It is thus highly likely that a similar interface must be involved in binding A $\beta$ . Given the discussion above, where hydrophobic surfaces buried within a molecule may need to become exposed to allow binding, it is likely that local unfolding of this region is necessary to promote efficient inhibition of A $\beta$  fibrillisation. The hydrophobic nature of this region of the protein, which is necessary for binding proteases, makes it an ideal surface for interactions with the A $\beta$  peptide.

### 5.3.6.3. Oligomers

hCC oligomers were produced as discussed in Chapter 4; unfortunately significant amounts of amyloid fibrils remained in the sample, even after centrifugation. The method of purification should ensure that monomeric hCC is not present in the solution, however there were still a significant amount of oligomeric species associated with the fibrils. Although the hCC sample has a high ThT signal by itself, this remains stable through the experiment time, therefore it was assumed that any increase in fluorescence was due to the aggregation of A $\beta$ <sub>1-42</sub>.

Despite the absence of small molecular weight species, this oligomer sample still has an effect on A $\beta$ <sub>1-42</sub> fibrillisation as can be seen in Figure 5.17. When incubated with the hCC sample, there was a 54% reduction in ThT fluorescence at a molar ratio of 5:1 hCC to A $\beta$ , and a reduction of 38% at equimolar concentrations. The significance of this is difficult to ascertain given the difference in behaviour between monomers and dimers. The appearance of the time-courses are closer to the monomer suggesting the stabilisation of an alternative species which is not ThT-positive. It is likely that the structure of oligomers is relatively flexible and able to bind readily to A $\beta$ , in a non-specific albumin-like manner. All hCC concentrations were calculated as monomer-equivalent (i.e. using the extinction coefficient and molecular weight of the monomer). It was not possible to fit the data in the presence of hCC due to the shape of the curves exhibiting too many unresolvable phases.

When examining the end-point of the incubation with 1:1  $A\beta_{1-42}$  to hCC oligomers by TEM, no amyloid fibrils were observed as seen in Figure 5.16. Instead a large amount of amorphous aggregate was seen, as well as small protofibrils. As suggested above for the dimer sample, it is likely that the fibrillar species giving rise to the ThT signal are precipitating or adhering to the micro-plate, and were therefore not in the sample added to the carbon grids.

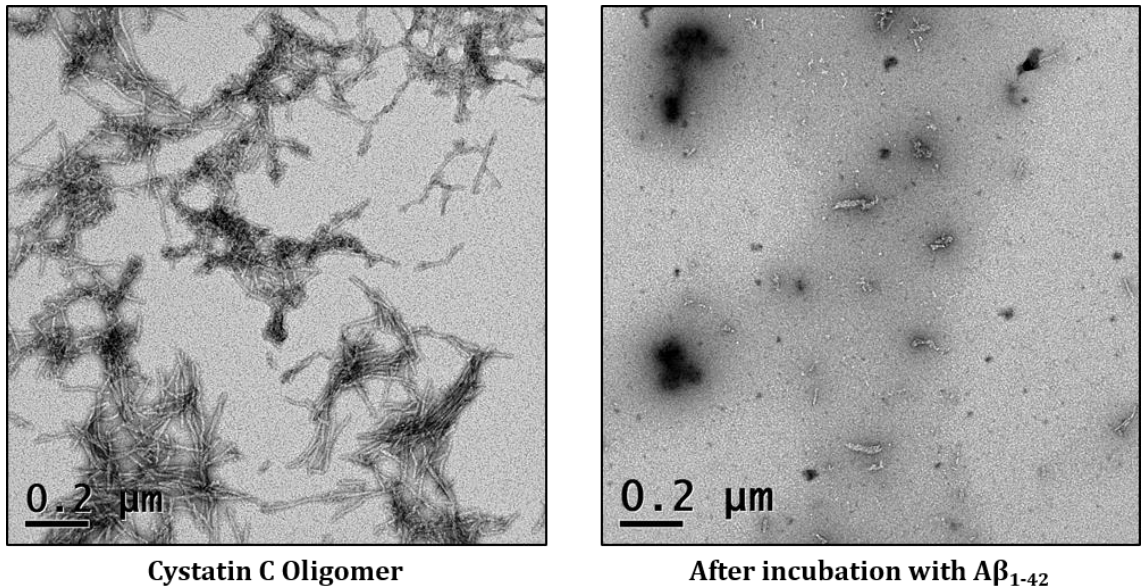


**Figure 5.16. TEM of hCC Oligomer with  $A\beta_{1-42}$**

*Electron micrographs showing the hCC oligomer sample (left) and the same sample after incubation with  $A\beta_{1-42}$  (right). Images were taken at 11,500 x magnification.*

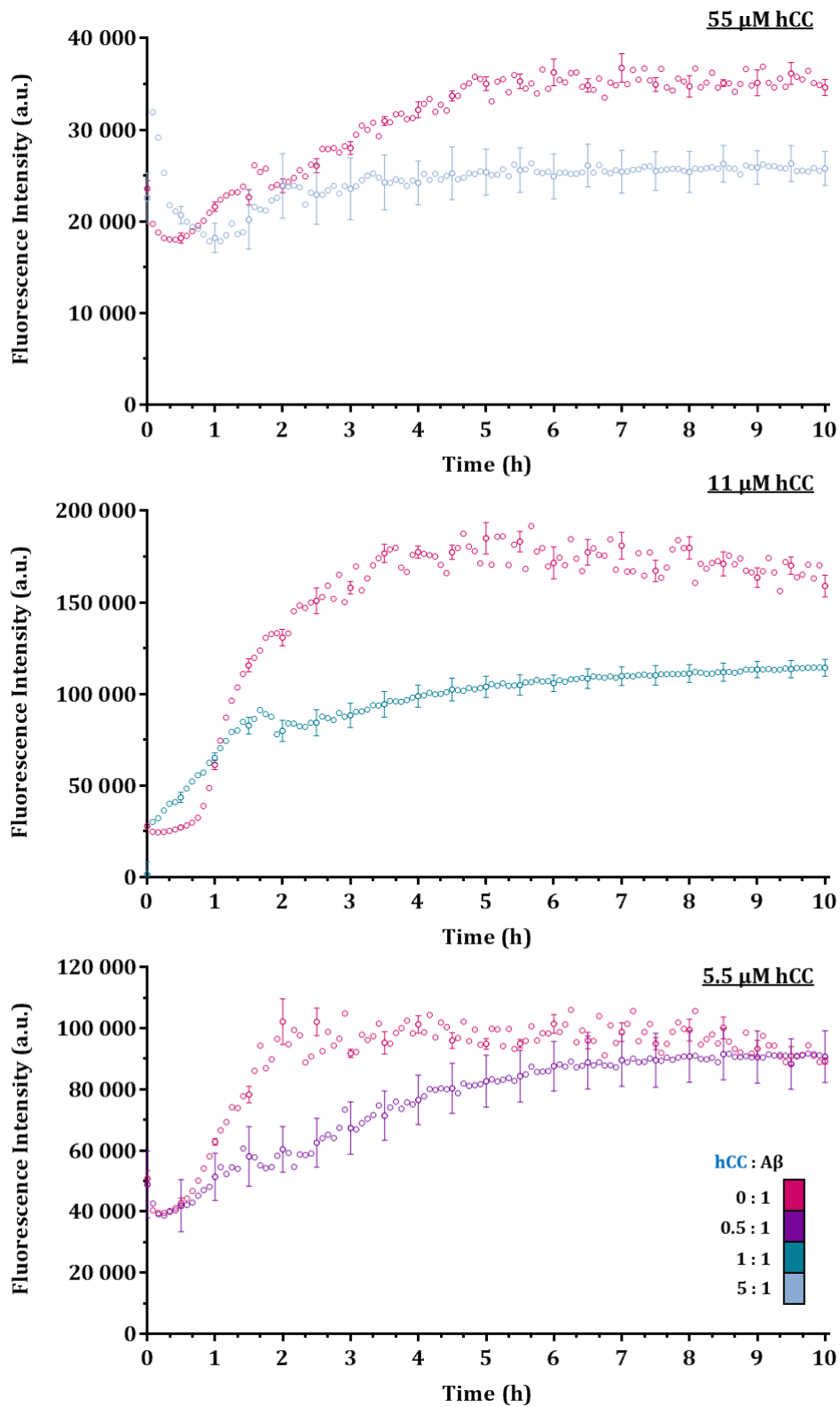


**Figure 5.17. Addition of hCC Oligomer**

*Molar ratios of 0.5:1 (purple), 1:1 (turquoise) and 5:1 (blue) hCC oligomer to  $A\beta_{1-42}$  were incubated and monitored by ThT fluorescence. Each curve is the average of 4 or 5 replicate reactions with the standard error of the mean indicated by the error bars.*

### 5.3.7. NMR Spectroscopy

The nature of the interaction between hCC and A $\beta$ <sub>1-40</sub> has been investigated by previous members of the lab through HSQC titration experiments (Keeley, 2007, Elshawaihde, 2012). These studies have shown that there are no major chemical shift changes when A $\beta$ <sub>1-40</sub> is titrated into a sample of hCC up to 1:1.2 equivalences, suggesting there is no tight binding event between the two proteins in their monomeric state. This was unexpected, as it has been reported that hCC forms a tight complex with monomeric A $\beta$ <sub>1-40</sub> as established by ELISA (Sastre et al., 2004). Given probable structural changes on the ELISA plate, experiments were designed to stimulate complex formation in solution by incubation for longer time periods, altering the conditions and increasing the concentration of the proteins as far as possible.

#### 5.3.7.1. A $\beta$ <sub>1-42</sub> Monomer Titration

An HSQC titration experiment has also been used previously to monitor the nature of the interaction between hCC and monomeric A $\beta$ <sub>1-42</sub> (Elshawaihde, 2012). hCC titration experiments with oligomeric A $\beta$ <sub>1-42</sub> and A $\beta$ -GM1 (ganglioside) were also carried out. In all three of these experiments there were no major chemical shift changes, however minor changes in amide cross-peak intensity were observed which could be mapped to the N-terminal  $\alpha$ -helix region of the protein.

#### *HSQC Spectrum of hCC*

The initial <sup>1</sup>H spectrum of 50  $\mu$ M hCC in 15 mM Tris-TFA pH 7.5 at 278 K shows a wide dispersion of amide proton resonances (6-10 ppm) and up-field aliphatic proton peaks (below 0 ppm) indicating that hCC is folded. This is reflected in the HSQC spectrum where the amide chemical shifts are also well dispersed (Figure 5.18). The distribution of amide peaks corresponds well with the established assignment in these conditions (Keeley, 2007). As even small changes in the chemical environment are reflected in the HSQC spectrum, this validates the reproducibility of the sample preparation. There is no evidence for the characteristic peak shifts that are associated with dimerisation in either the 1D or 2D spectra, indicating that the protein is in the required monomeric state. Out of 120 residues, 87 were successfully assigned; those that were excluded were either not present, very weak or significantly overlapped.

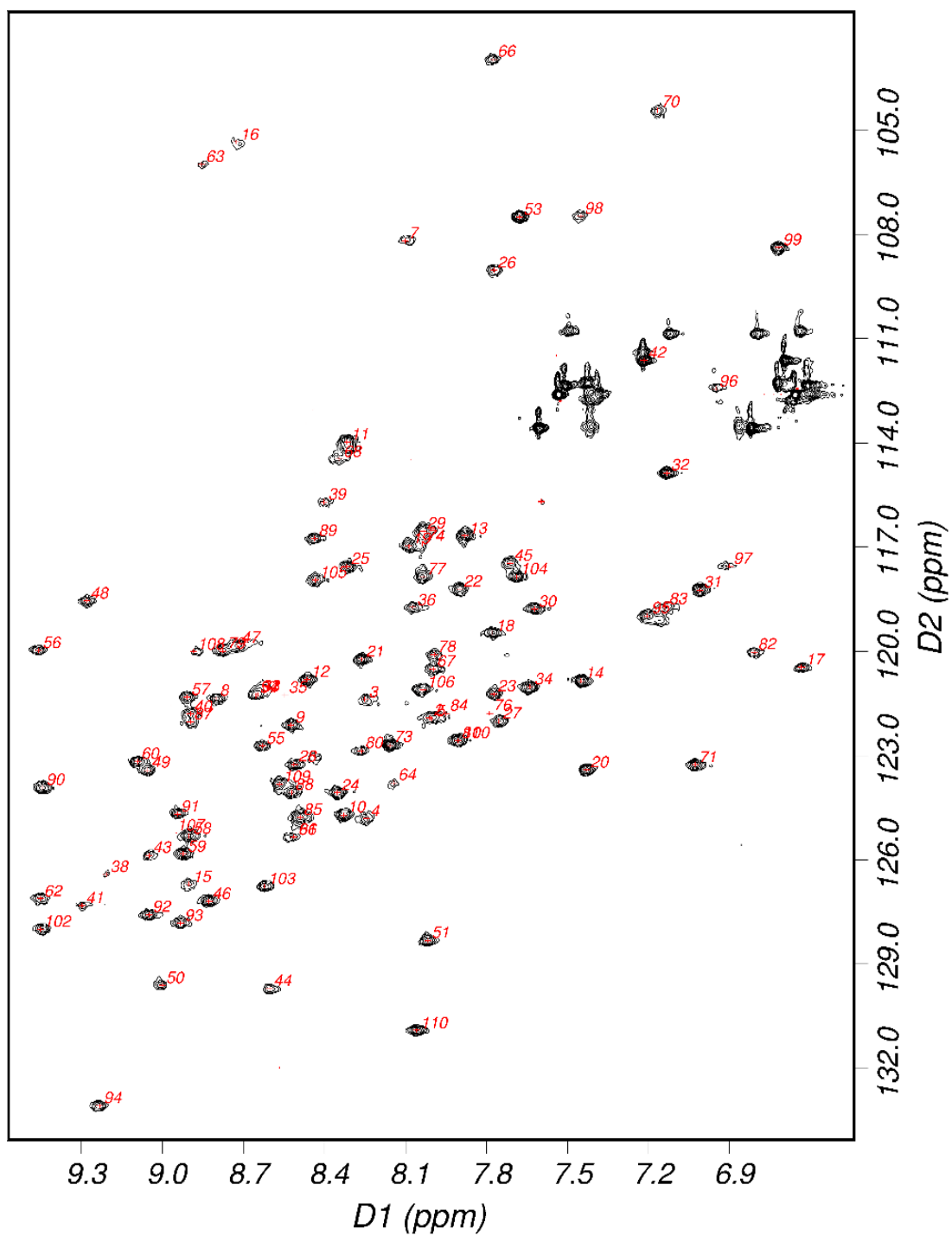
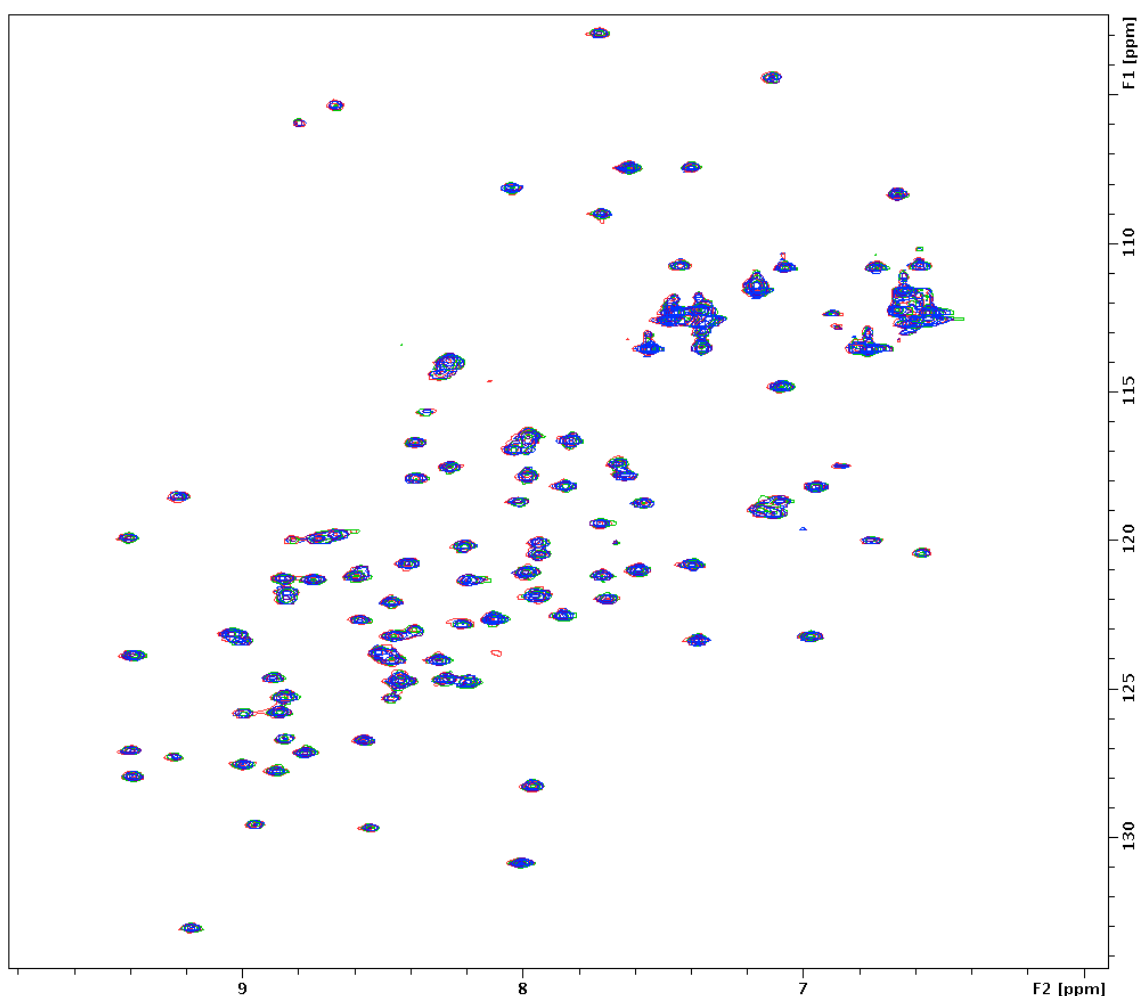


**Figure 5.18. HSQC Spectrum of hCC at 278 K**

An HSQC spectrum of 50  $\mu\text{M}$  hCC incubated in 15 mM Tris-TFA pH 7.5 at 278 K showing the amide assignment. D1 represents the  $^1\text{H}$  dimension and D2 represents the  $^{15}\text{N}$  dimension.

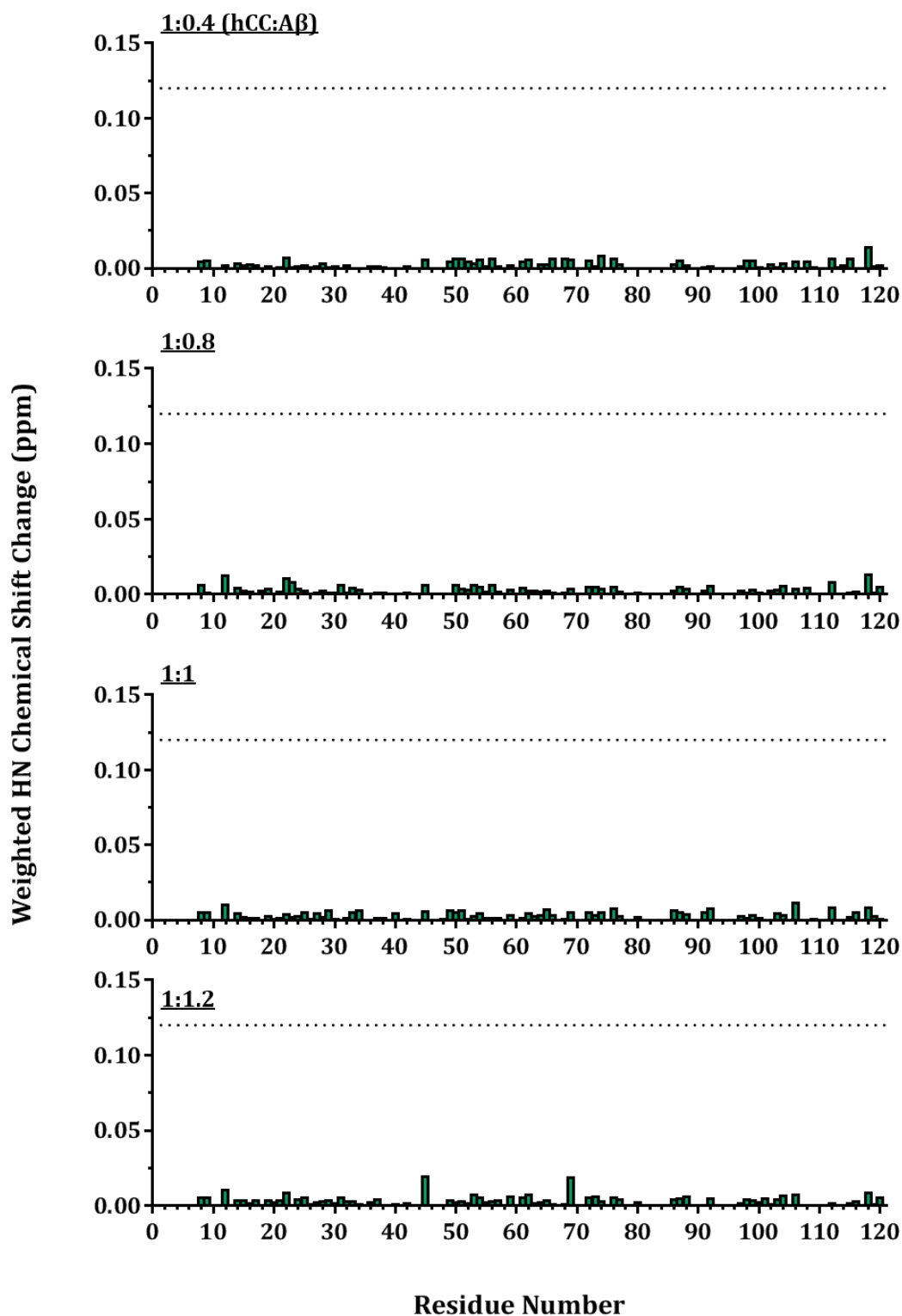
### *Titration with Monomeric A $\beta$ <sub>1-42</sub>*

Figure 5.19 shows an overlay of a reference HSQC spectrum overlaid with the four spectra that were obtained over the course of the titration of unlabelled monomeric <sup>15</sup>N-labelled hCC with unlabelled monomeric A $\beta$ <sub>1-42</sub>. As has been previously observed by Elshawaihde (2012) there are only very minor chemical shift changes. Figure 5.20 illustrates the calculated average chemical shift differences and indicates that no residues have a significant chemical shift change. The lack of chemical shift changes, even at equivalences beyond 1:1, indicates that there is no change in the local chemical environments of any of the residues.



**Figure 5.19. Titration of hCC with A $\beta$ <sub>1-42</sub>**

*A reference spectrum of <sup>15</sup>N labelled 50  $\mu$ M hCC in 15 mM Tris-TFA pH 7.5 at 278 K (blue) was overlaid with 4 spectra in which increasing amounts of A $\beta$ <sub>1-42</sub> have been added (shown in red, green, purple and blue). The four spectra correspond to additions of 200  $\mu$ l, 400  $\mu$ l, 500  $\mu$ l and 600  $\mu$ l of 50  $\mu$ M A $\beta$ <sub>1-42</sub> respectively. F2 represents the <sup>1</sup>H dimension and F1 represents the <sup>15</sup>N dimension.*



**Figure 5.20. Amide Chemical Shifts**

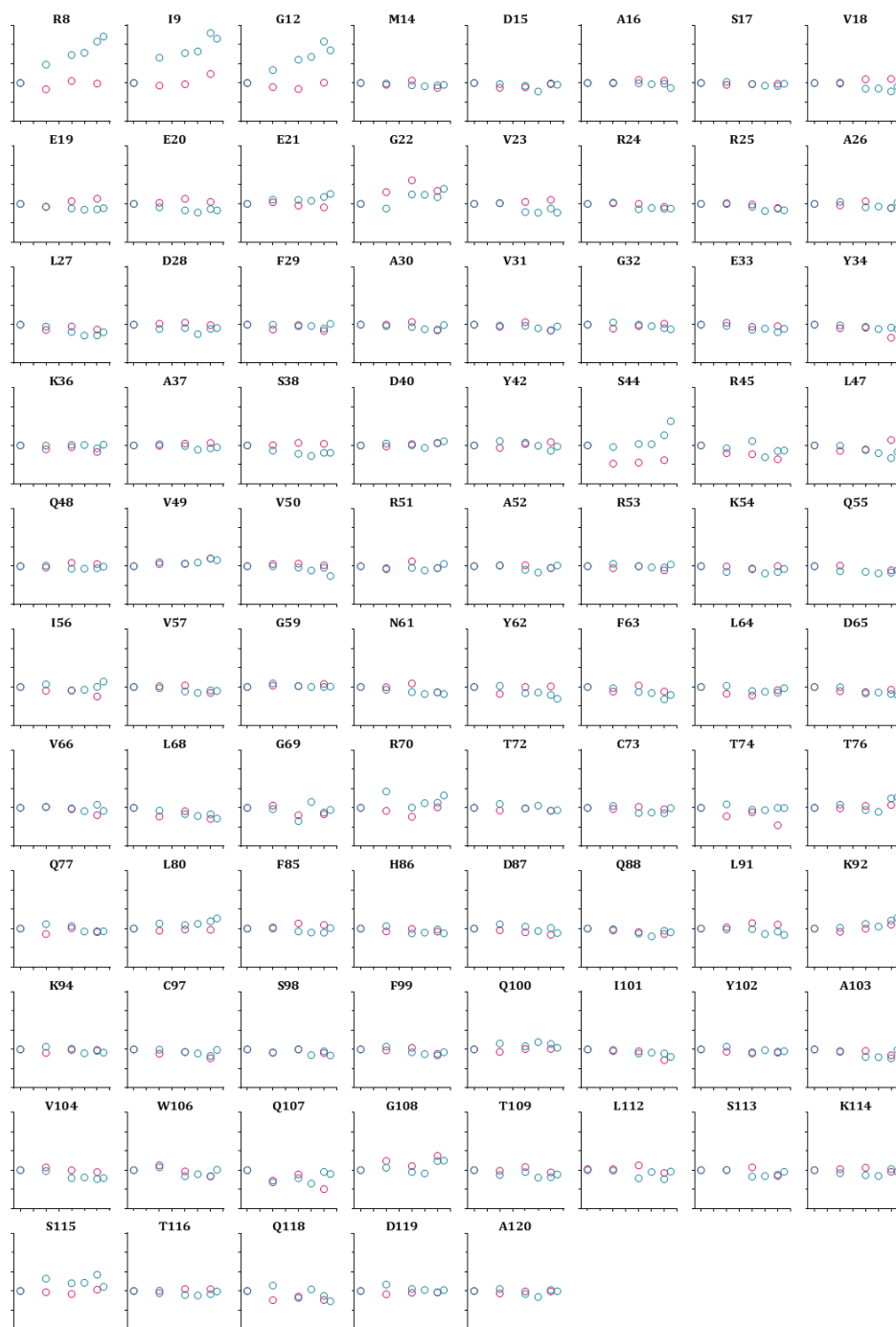
The changes in chemical shift observed in the HSQC spectrum of 50  $\mu\text{M}$  hCC in 15 mM Tris-TFA pH 7.5 at 278 K with the titration of monomeric  $A\beta_{1-42}$ , with each chart corresponding to a new addition. The stoichiometry is indicated at the top of each chart, and the chemical shift change required to be significant is shown as a dotted line.

Figure 5.21 shows the intensity change of each hCC amide observed in the A $\beta$  titration and in the control experiment. Significant increases in cross-peak intensity were observed at the N-terminal, particularly R8, I9 and G12. After 1 week there is also an increase in the intensity for S44. In the absence of A $\beta$ , a number of amide peaks belonging to the N-terminal region of the protein are often broadened or not present and has been attributed previously to the ability of this region to exchange at an intermediate rate between two or more conformations (Keeley, 2007). Following the addition of A $\beta$ <sub>1-42</sub>, these peaks gradually appear and sharpen, causing an increase in intensity to be observed, which indicates that the A $\beta$ <sub>1-42</sub> has influenced the ability of the hCC to change between these conformations.

The significance of this observation increases given very similar changes observed for these residues upon titration of hCC with the more soluble A $\beta$ <sub>1-40</sub> (Keeley, 2007). In this latter titration, an increase in amide peak intensity was also observed for residue A58 of loop 1 of the protease binding site, in addition to N-terminal residues. However the peak for A58 was not observed at all in the current experiment with A $\beta$ <sub>1-42</sub>.

The simplest scenario would be that in the absence of A $\beta$  two conformations are populated in intermediate exchange causing the amide peaks for these residues to broaden or disappear. The titration of A $\beta$ <sub>1-42</sub>, and presumably the subsequent interaction between the two molecules, favours one of these conformations, therefore removing the intermediate exchange effects observed through switching between the two and causing a sharpening of the relevant peaks, as was observed in the titration data. However, the chemical shift data shown in Figure 5.20 does not support such a simple model. A change in chemical shift should be observed as one of these conformations is favoured and becomes the predominant species, unless the chemical shift differences between the two conformations were unresolvable. This makes it necessary to adapt the simple model to introduce multiple conformations that can be populated, rather than the two originally suggested. The observed chemical shift represents an average of all of the chemical environments that an amide populates. If population of one of the conformations is prevented through interaction with A $\beta$ , it is possible that preventing the exposure to one chemical environment out of many will have a minimal effect on the observed chemical shift.

A comparison of the final time-point after 1 week incubation at 4°C with the final point of the reference spectrum showed minor reductions in intensity for several of the residues. The change in intensity was plotted for each of the residues as shown in Figure 5.22. However, it is difficult to distinguish whether these changes are significant or due to the noise of the experiment as the peaks for the reference spectrum appeared to undergo similar changes in intensity. This differs from the results observed previously, where a significant reduction in intensity was observed in 25 residues (Elshawaihde, 2012). The residues displaying a significant intensity reduction were plotted onto the structure of the molecule, which indicated that the region most affected by binding events between A $\beta$  and hCC was around the N-terminal  $\alpha$ -helix.



**Figure 5.21. Amide Peak Intensity**

The changes in intensity observed for hCC amides in the HSQC spectra of 50  $\mu\text{M}$  hCC in 15 mM Tris-TFA pH 7.5 at 278 K following the addition of buffer (pink) and  $\text{A}\beta_{1-42}$  (blue). The x-axis shows the ratio of buffer/ $\text{A}\beta$  to hCC extending from 0 to 1.2. The final point in the  $\text{A}\beta_{1-42}$  titration corresponds to the final titration point after incubation at 4°C for 1 week. The y-axis shows the relative intensity with a unit-less range from 0 to 2.5. All intensities have been scaled relative to the initial intensity of that residue (at 1). At each titration point spectra were scaled to account for the dilution factor in the titration and necessary changes in receiver gain throughout the experiment.

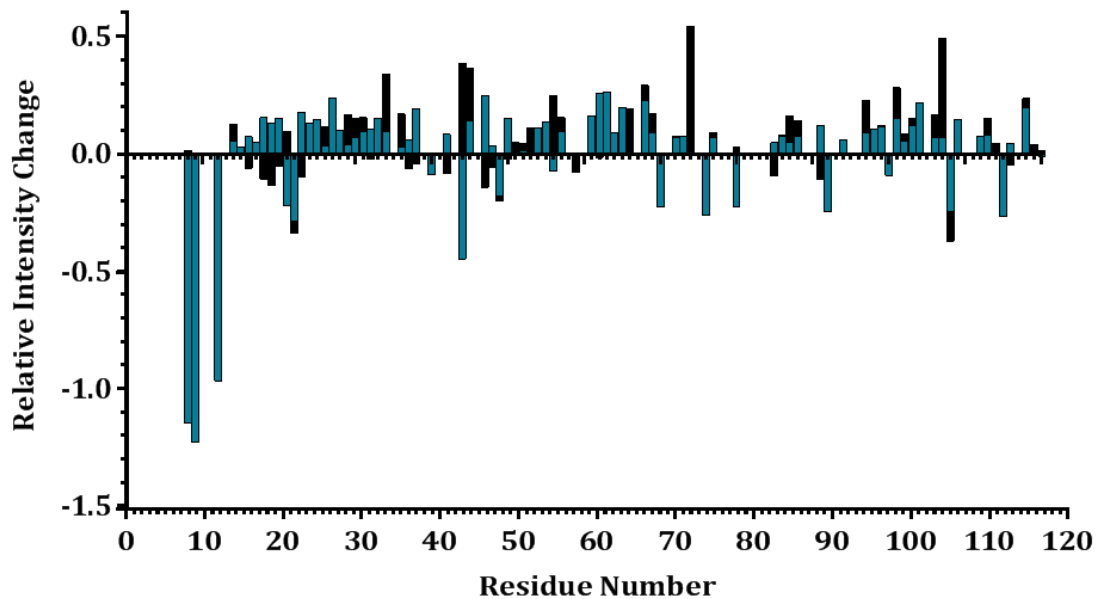


**Figure 5.22. Changes in Amide Peak Intensity**

The relative intensity change for each peak over the titration has been plotted against the residue number. Changes in the control experiment are shown in black, and changes in the titration with  $A\beta_{1-42}$  are shown in turquoise.

#### 5.3.7.2. Time-course of $^{15}N$ -labelled hCC with $A\beta_{1-42}$

The experiment described above suggests that there is no tight-binding interaction between monomeric hCC and monomeric  $A\beta_{1-42}$ . This is surprising as previous studies have indicated that a 1:1 complex forms between the two proteins (Sastre et al., 2004, Selenica et al., 2007). To establish whether hCC interacts with other species of  $A\beta$ , formed later in the aggregation process, a time-course was carried out of the two proteins incubated at 30°C. This procedure has been shown to be successful in monitoring the formation of a complex between  $A\beta_{1-40}$  and the cellular prion protein PrP<sup>C</sup> (Younan et al., 2013).

#### HSQC Spectrum of hCC at 303 K

The rate at which a protein tumbles in solution is proportional to the temperature of the sample. At low temperatures, the tumbling rate is slow due to the reduced energy available in the system, leading to a general broadening of the signal. Increasing the temperature to 30°C caused the majority of the peaks to sharpen. A wide dispersion of amide proton resonances (6-10 ppm) and upfield aliphatic proton peaks (below 0 ppm) in the initial  $^1H$  spectrum of 50  $\mu M$  hCC in 15 mM Tris-TFA pH 7.5 at 303 K signified

that hCC was folded. This was reflected in the HSQC spectrum where the amide chemical shifts are also well dispersed (Figure 5.23). At 30°C, the peaks for a further 4 residues have been lost from the 4°C spectrum, giving an assignment for 83 residues out of 120. Again, the excluded residues were either very weak, not present at all or overlapped. There was no evidence of the characteristic peak shifts that are associated with dimerisation in either the 1D or 2D spectra, indicating that the protein is in the required monomeric state.



### Time-course with $A\beta_{1-42}$

HSQC spectra, 12 in total, were obtained over 24 hours, with each experiment lasting 2 hours and 8 minutes. Figure 5.24 shows an overlay of the final spectrum with the reference spectrum which was obtained in the absence of  $A\beta_{1-42}$ . As was noted previously for the titration experiment, only very minor chemical shift changes were observed during the time-course of  $A\beta_{1-42}$  with hCC at 30°C (Figure 5.25).

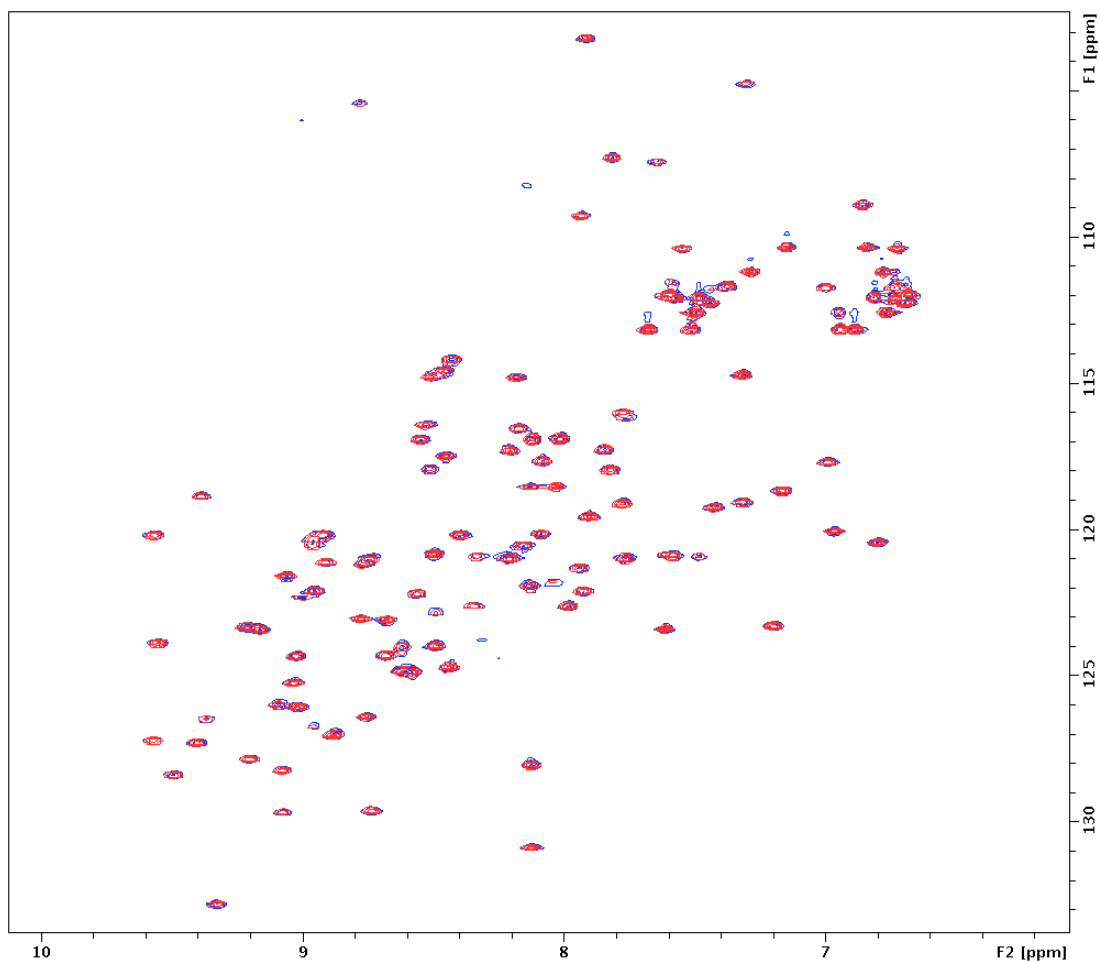


**Figure 5.24. Time-course of hCC in the Presence of  $A\beta_{1-42}$**

A reference spectrum of  $^{15}\text{-N}$  labelled 50  $\mu\text{M}$  hCC in 15 mM Tris-TFA pH 7.5 at 303 K (blue) was overlaid with the spectrum of an identical hCC sample which had been incubated in the presence of equimolar  $A\beta_{1-42}$  for 24 hours (red). F2 represents the  $^1\text{H}$  dimension and F1 represents the  $^{15}\text{N}$  dimension.

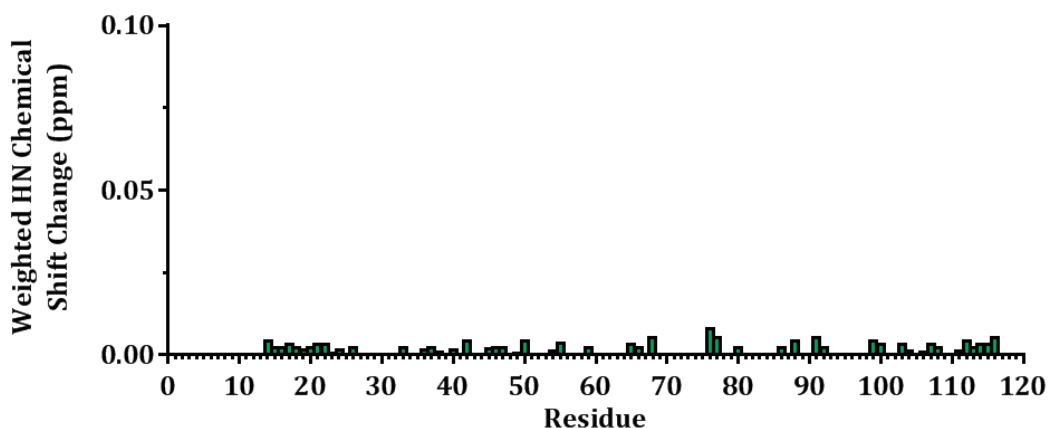


**Figure 5.25. Amide Chemical Shift Changes for hCC and A $\beta$ <sub>1-42</sub> Time-course**

*The changes in chemical shift observed in the HSQC spectrum of 50  $\mu$ M hCC in 15 mM Tris-TFA pH 7.5 at 303 K after incubation with 50  $\mu$ M A $\beta$ <sub>1-42</sub> for 24 hours.*

Amide peak intensity changes are shown in Figure 5.26 for both the A $\beta$  time-course and the control experiment. The hCC peak intensities in the presence of A $\beta$ <sub>1-42</sub> have been scaled to the reference spectrum (the first spectrum in the control experiment), which was given a value of 1. A small decrease in intensity was observed for many of the residues. However, the increase in intensity that was observed for R8 in the titration experiment was not seen in the time-course; the other two residues that demonstrated an increase in intensity, I9 and G12 were too weak to be detected in the latter experiment. The relative intensity change for each residue was plotted, as is illustrated in Figure 5.27. A minor decrease in intensity was observed for many of residues across the whole molecule in the presence of A $\beta$  compared to the control reaction. This indicates a change in chemical environment for these amides, presumably through interaction with A $\beta$ .



**Figure 5.26. Amide Peak Intensity**

The changes in intensity observed for hCC amides in the HSQC spectra of 50  $\mu\text{M}$  hCC in 15 mM Tris-TFA pH 7.5 at 303 K in the absence (pink) and presence (blue) of 50  $\mu\text{M}$   $A\beta_{1-42}$ . The x-axis shows the time-point of each experiment, with each experiment taking 2 hours and 8 minutes. The y-axis shows the relative intensity with a unit-less range from 0.5 to 1.5. All intensities have been scaled relative to the initial intensity of that residue in the reference spectrum of hCC in the absence of  $A\beta_{1-42}$ , which is given an intensity of 1.

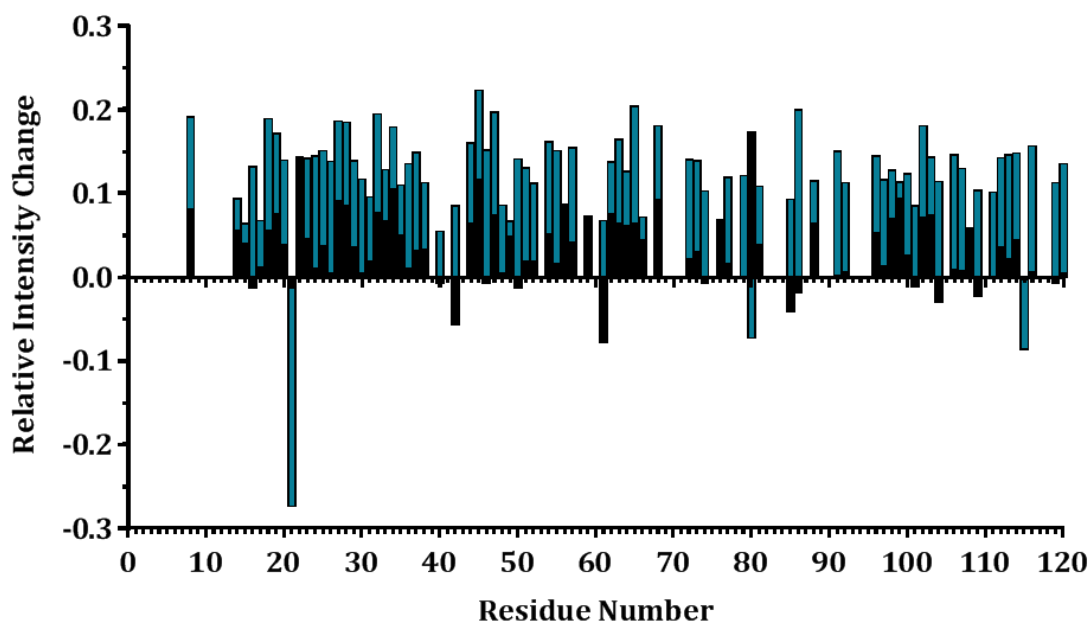


**Figure 5.27. Changes in Amide Peak Intensity**

*The relative intensity change for each peak over the titration has been plotted against the residue number. Changes in the control experiment are shown in black, and changes in the titration with Aβ<sub>1-42</sub> are shown in turquoise.*

The amide cross-peaks that experienced the greatest attenuation during the time-course were plotted onto the structure of the hCC molecule, as depicted in Figure 5.28. This highlights the regions of hCC that are most affected by the interaction with Aβ<sub>1-42</sub>. For comparative purposes, a structure of hCC showing the residues which have previously been observed to display significant changes in intensity in a titration of Aβ<sub>1-42</sub> at 4°C is also shown (Elshawaihde, 2012). These were thought to be mostly localised around the N-terminal α-helix, and that residues on the β-sheet in close proximity to this helix were also seeing an effect with the binding of Aβ<sub>1-42</sub>. A similar localisation of intensity change was not observed in the current experiment, with attenuation of a similar magnitude seen across the whole molecule, particularly in structured regions.

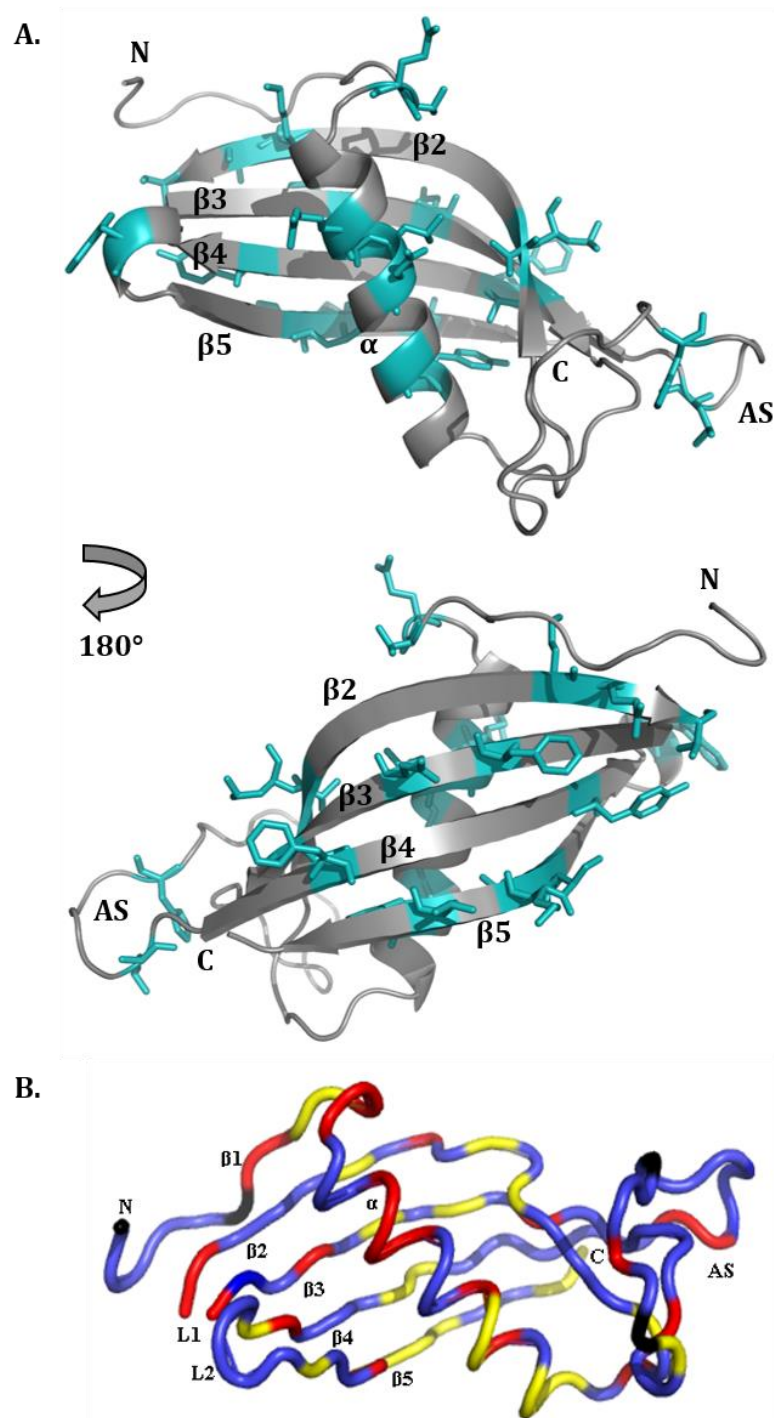


**Figure 5.28. Intensity Change Mapped onto hCC Structure**

A structural depiction of hCC based on the domain swapped dimer of hCC (PDB code: 1G96) adapted from Janowski et al. (2001) highlighting the residues which exhibited the most significant decrease in amide peak intensity (A). A58 which is found in loop 1 between strands 2 and 3 is not included in this depiction due to its involvement in the formation of the domain swapped dimer. A similar diagram taken from Elshawaihde (2012) shows the residues which displayed significant intensity decrease (red) and insignificant intensity decrease (yellow). Proline residues are represented in black and residues that showed no intensity change in blue.

Figure 5.29 shows an electron micrograph of the protein sample at the end-point of the time-course NMR experiment prepared immediately after the experiment and after 7 months in the fridge. An image of A $\beta_{1-42}$  fibrils formed through incubation in 15 mM Tris-TFA pH 7.5 at 30°C in the absence of hCC is also shown for comparative purposes. Amyloid fibrils are not observed in the NMR sample, suggesting that although the formation of a complex between A $\beta$  and hCC was not observed throughout the HSQC time-course, the hCC is having a dramatic effect on the assembly process of the A $\beta$ . Even after 7 months, amyloid fibrils were not observed in this sample.

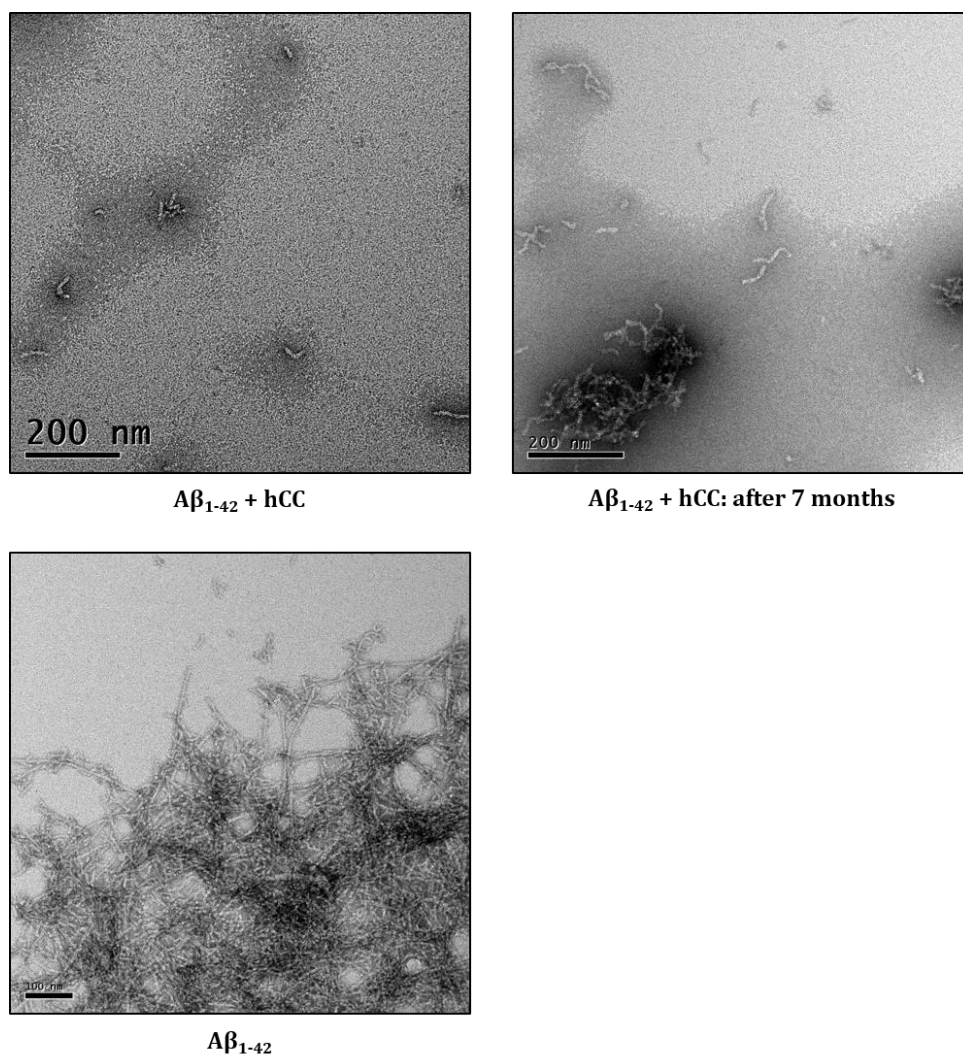


**Figure 5.29. TEM of NMR Time-course**

*Electron micrographs of the NMR time-course experiment of 50  $\mu$ M A $\beta_{1-42}$  incubated in the presence of 50  $\mu$ M A $\beta_{1-42}$  in 15 mM Tris-TFA pH 7.5 at 30°C after 24 hours and the same sample after 7 months. An image of a sample of A $\beta_{1-42}$  incubated in the absence of hCC in the same conditions is also shown. All images were taken at 21,000 x magnification.*

## 5.4. Discussion

Time-courses for the fibrillisation of A $\beta$  with and without hCC were carried out and presented for the first time in this thesis. It is demonstrated that hCC will inhibit the formation of amyloid fibrils by A $\beta$ <sub>1-42</sub> in a dose-dependent manner, requiring a 2:1 molar ratio of hCC to A $\beta$  to inhibit this reaction completely where no increase in ThT fluorescence intensity is observed. At equimolar concentrations, a considerable reduction in ThT fluorescence, but not a complete loss, demonstrates that a small amount of amyloid fibril is still present. This is not consistent with a model where hCC and A $\beta$  form a tightly bound monomer-monomer complex. The lack of quantitative measurements in the literature so far when examining the same phenomenon had not identified the need for an excess of hCC, at least at these concentrations of A $\beta$  peptide (e.g. Sastre et al. 2004). The effect of hCC is purely on the yield of amyloid fibrils and has no measurable effect on the fibrillisation kinetics of the A $\beta$  peptides that escape inhibition. This suggests the formation of a complex between hCC and A $\beta$  which is 2:1 but the persistence of free monomeric hCC in solution would suggest otherwise.

Observation of the sample by TEM indicated that instead of amyloid fibrils, protofibrillar species and granular aggregates had been produced. The species formed through the incubation of A $\beta$  with hCC have a protofibrillar appearance, however do not appear to aggregate further to produce mature fibrils when observed after several months. It is possible that hCC is stabilising these states and preventing their further aggregation to produce mature fibrils. A large amount of amorphous aggregate is also often observed. Measuring the protofibrillar species was a challenge due to their curled up nature, as well as image resolution, preventing a detailed summary of their width. However those that could be measured had a similar width to the mature fibrils. Comparison of these species to well characterised species of A $\beta$  such as protofibrils and ADDLs highlighted the protofibrillar appearance, although a greater degree of association was observed. Studies have reported a dramatic reduction in cytotoxicity when hCC is incubated with A $\beta$  (Kaeser et al., 2007, Mi et al., 2007, Tizon et al., 2010), demonstrating that the species forming do not display the toxic activity that is observed with A $\beta$  alone. Unfortunately attempts to perform cell assays and verify a reduction in cytotoxicity in the system described here were unsuccessful, however it could be assumed that the species being formed are similar to those found in the literature.

When incubated in the absence of hCC, A $\beta$  forms oligomers with a similar appearance to ADDLs very early on in the reaction and after 2 hours, only mature fibrils are observed in the TEM. In the presence of equimolar concentrations of hCC, species with different morphologies are observed. The hCC appears to be preventing the formation of fibrils but not of earlier intermediates, as aggregated species are still seen in the presence of hCC. If this were not the case and aggregation was being inhibited entirely, such as through stabilisation of the monomer, then no material would be observed in the TEM.

Size exclusion chromatography (SEC) demonstrated the formation of high molecular weight species by A $\beta$ <sub>1-42</sub> in the absence of hCC, however no distinct peaks were observed. SEC indicated that hCC binds very early on in the reaction, as a 25% reduction in the expected peak height of hCC was observed before the first point (15 min) of the time-course. This corresponds with the observations from the TEM time-course, in which aggregated species are observed at the first time-point. Surprisingly, as the reaction progressed no further decrease in peak height was seen, suggesting that further incorporation of the hCC is not occurring.

As previously observed there is an inconsistency between the results presented here, in which complex formation between monomeric hCC and monomeric A $\beta$ <sub>1-42</sub> is not observed by NMR, and published data which suggested the formation of a high-affinity complex between these molecules as established by ELISA (Sastre et al., 2004). It is thought that the variation in these results could be attributed to the fact the ELISA experiment is carried out on a surface, whereas the NMR experiment is in solution. A similar variation has been observed in experiments with transthyretin, suggesting solid-phase binding assays may not be entirely consistent with binding characteristics or inhibition of fibril formation observed in the liquid-phase (Li et al., 2013).

In order to identify the nature of the A $\beta$  species that interacts with hCC, the inhibitor was added after 20 minutes and 1 hour of initiating the A $\beta$  fibrillisation time-course. This also led to inhibition of the reaction and a reduction in ThT fluorescence intensity, although addition at these points was not as effective as when the hCC was added at the start of the reaction. Addition of hCC after 2 hours showed no change in ThT fluorescence intensity compared to the control experiment. This highlights that hCC needs to be present early on in the reaction, presumably whilst the species of A $\beta$  that it is interacting with are still present in sufficient number for the hCC to have an

inhibitory effect. This suggests the interacting A $\beta$  species are unlikely to be the mature fibrils, however it is plausible that protofibrillar species present early on in the reaction can bind hCC.

Different forms of hCC were also investigated in terms of their inhibitory activity. The addition of equimolar concentrations of hCC dimer at the beginning of the reaction also has an effect on the ThT fluorescence changes, but in a totally different way, showing an increase in lag phase, but not a decrease in fibril yield, compared to A $\beta$ <sub>1-42</sub> incubated in the absence of hCC. This indicates an alternative mechanism of inhibition by the dimer, where it is able to interfere with the progression of the reaction but not affect its outcome. A similar method of inhibition has been reported in the transthyretin system (Li et al., 2013) where TTR tetramer reduces A $\beta$  aggregation through binding to A $\beta$  monomer to inhibit A $\beta$  seed formation, whereas TTR monomers interact preferentially with A $\beta$  oligomers to slow large oligomer formation.

The study of the time-courses for A $\beta$  fibrillisation in the presence of inhibitors has highlighted at least two different mechanisms for the cystatins alone, perhaps 3 if the activity of cystatin B tetramers is also considered. The next step in this study was to identify the nature of the binding site and ideally purify a complex. The differential effects of the dimer and monomer, two proteins with remarkably similar properties, suggests binding must be localised to the protease binding site, which is unusually hydrophobic for the surface of a protein. The effect of A $\beta$  addition on the NMR <sup>15</sup>N-HSQC spectrum of hCC was investigated to look for clues as to possible binding sites.

Despite the inhibition of A $\beta$  fibril formation, no shifted amide cross-peaks were observed in HSQC spectra of hCC incubated with A $\beta$ , both in its monomeric form at 4°C and at a higher temperature (30°C) which should induce the formation of oligomers. The experiment carried out at 4°C showed that A $\beta$  disturbed the structural flexibility of the N-terminal of hCC, a region which is part of the protease binding site of the protein and changes upon dimerisation. The latter experiment showed minor decreases in amide peak intensity over time for many of the hCC residues. Mapping these residues onto the hCC structure demonstrated that the attenuated residues were spread across the whole molecule, with no localisation to any particular region. This confirmed the results of the chromatography, which was carried out at a higher ionic strength but where a percentage of the monomeric hCC was observed to disappear, presumably to go and form a large molecular weight complex with A $\beta$ . In previous

work, a titration of  $^{15}\text{N}$ -labelled hCC with  $\text{A}\beta_{1-42}$  at  $4^\circ\text{C}$  had suggested some possible localisation of these attenuated residues (Elshawaihde, 2012), however this effect was small and not observed consistently in any experiment carried out subsequently.

The data presented here indicate that folded monomeric hCC is not interacting with monomeric  $\text{A}\beta_{1-42}$ , yet it effectively inhibits  $\text{A}\beta$  fibril formation. This strongly suggests that hCC binds a species of  $\text{A}\beta_{1-42}$  other than monomer, most likely some form of oligomer. The gradual decrease in amide peak height over the course of the experiment could indicate that the species of  $\text{A}\beta$  that interacts forms only slowly, or potentially causes a slow perturbation of hCC, with an alternative conformer of hCC interacting with an oligomeric species of  $\text{A}\beta$ . A number of scenarios need to be examined:

Scenario number 1: hCC forms a very weak interaction with  $\text{A}\beta$  oligomers and so only 10% is bound under the conditions of the experiment. The ratio of  $k_{\text{on}}/k_{\text{off}}$  will give the binding affinity of the reaction, however as the on-rate ( $k_{\text{on}}$ ) will normally be diffusion-controlled, the off-rate ( $k_{\text{off}}$ ) will to some extent dictate the  $k_{\text{d}}$ . A weakly-bound complex will generally lead to fast dissociation of the protein, whereas the protein will dissociate slowly in a tightly-bound complex. Weak binding at the concentrations used ( $50\mu\text{M}$ ) would suggest fast or intermediate exchange. Since only 10% is bound at any one time and the size of the complex may be large, differences in chemical shift and the movement of the peak towards the bound form may be unresolvable and so all that is observed is a small decrease in amide peak height. This is consistent with what is observed here.

Scenario number 2: hCC forms a tight complex with  $\text{A}\beta$  oligomers but the species which is competent for binding is not the species that dominates in solution, but rather a sub-species of the folded ensemble, such as a specific proline(s) isomer. Again, only a small proportion of the hCC is bound ( $\sim 10\%$ ), but this time the binding of species is in slow exchange. The appearance of a new peak corresponding to the bound form may then be hard to identify above the noise of the experiment, and line broadening caused by intermediate exchange or a large relaxation time ( $t_2$ ) may be hard to detect. This is also consistent with what is observed here.

The presence of hCC in the  $\text{A}\beta$  fibrillisations does not appear to be having an effect on the lag time of the reaction, suggesting that the nucleation process is not being affected. The formation of a nucleus is highly concentration dependent, suggesting that hCC is not binding to monomeric  $\text{A}\beta$  and forming a stable complex, as this would mean that

the concentration of A $\beta$  monomers in the solution available to form a nucleus would be reduced and so the lag time of the reaction would increase. hCC is also not affecting the rate of fibril extension; those A $\beta$  molecules that are available to assemble and attach to the extension sites are doing so at the same rate as when hCC is not present. However, the amount of fibrils being produced is considerably less than in the absence of hCC, implying that the availability of assembly-competent A $\beta$  present in the solution is reduced.

A potential model for this system could be that the hCC is binding to an oligomeric species of A $\beta$  and reducing the amount of assembly-competent A $\beta$  that is present in solution to attach to the fibrils and elongate. By sequestering A $\beta$  oligomers, hCC is diverting the assembly pathway and causing the formation of stable non-toxic aggregates, thus preventing the formation of amyloid fibrils. This proposal is consistent with previous studies, in which hCC is shown to inhibit fibril formation and cause the production of amorphous aggregates (Sastre et al., 2004). An illustration of this model is shown in Figure 5.30. hCC is not inhibiting A $\beta$  fibril formation through prevention of the nucleation event, nor is it preventing the formation of oligomeric species and protofibrils. It is unknown whether the species that are forming are related to the species that form during the normal assembly of A $\beta$ , however the conversion of these species into amyloid fibrils appears to be prevented. NMR has confirmed that folded monomeric hCC is not interacting with monomeric A $\beta$ , as the formation of this complex was not observed. This suggests that hCC is interacting with an oligomeric form of A $\beta$ . It is suggested that inhibition of A $\beta$  fibrillisation by hCC is either through catalytic conversion, where the complex is weak and occurs only transiently (scenario 1) or through the binding of a minor species to A $\beta$  (scenario 2).

Figure 5.30 illustrates these two different mechanisms of action for hCC and compares the activity of the dimer which exerts its activity earlier by decreasing the effective concentration of A $\beta$  and thus slowing down the observed fibrillisation reaction. Further analysis will be required to understand the nature of the interaction sites but it is suggested here that the proteinase binding site may be involved.

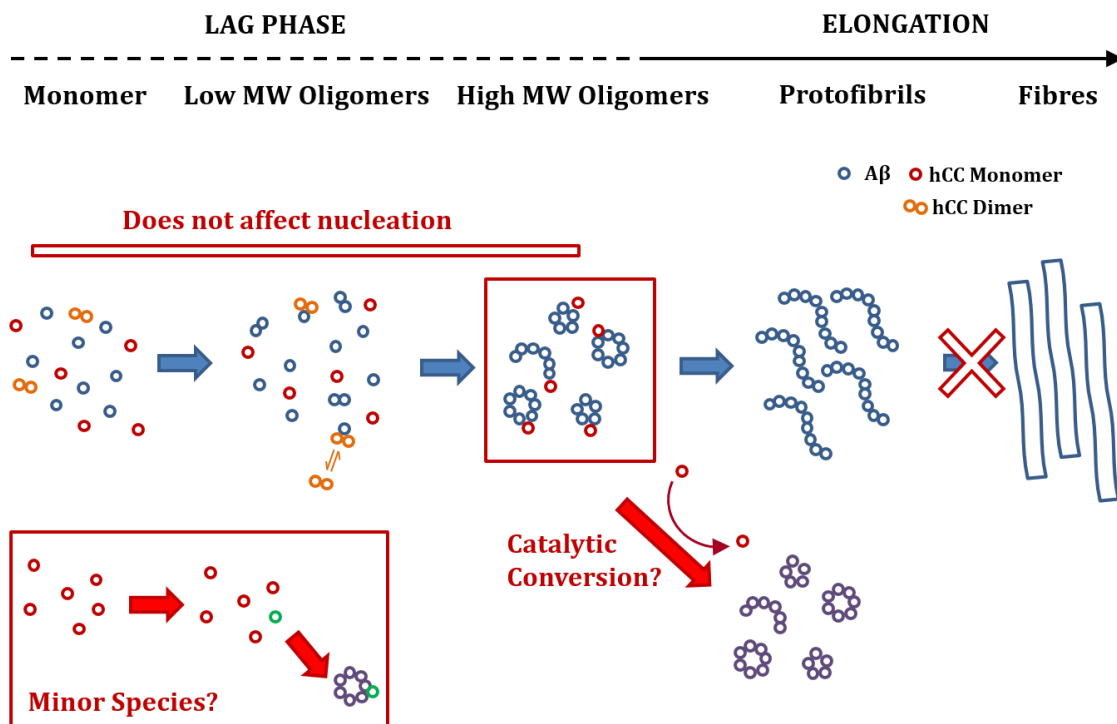


**Figure 5.30. Proposed Modulation of  $A\beta_{1-42}$  by hCC**

*Schematic illustrating the assembly pathway of  $A\beta_{1-42}$  into amyloid fibrils, from the formation of a nucleus through the production of oligomeric species before the assembly of protofibrils and finally mature fibrils. The potential mechanisms by which hCC is reducing  $A\beta_{1-42}$  toxicity at different points in the aggregation process are highlighted.*

## **Chapter Six: Final Conclusions and Future Work**

The current research project has focussed on exploring the nature of the interaction between hCC and A $\beta$  peptide, and investigating the aggregation of hCC into amyloid fibrils and oligomers. The main limitation to the work described in this thesis has been the ability to produce sufficient quantities both of recombinant hCC and A $\beta$ .

Establishing a system to allow the production of recombinant A $\beta$  was highly desirable, and initially it was hoped that the peptide produced would be used for the interaction study with hCC, in addition to further NMR experiments using isotopically labelled A $\beta$ . The expression and purification protocol described in Chapter 3 was adapted from a protocol described by Utsumi et al. (2009), utilising a ubiquitin tag to increase the expression and solubility of the peptide. The ubiquitin is removed through hydrolysis by a specific yeast hydrolase GST-YUH1, and purification of the hydrolysis products had previously been described using reverse-phase chromatography. This proved unsuccessful, so further methods of purification were explored. These included size-exclusion chromatography, Ni<sup>2+</sup>-NTA affinity chromatography and aggregation methods. Optimisation of the protocol led to the production of pure A $\beta$ <sub>1-40</sub> peptide using Ni<sup>2+</sup>-NTA chromatography, however low yields were still obtained and the amount of peptide produced was not comparable to the expected yield. Establishing a method of purifying the peptide by reverse-phase HPLC would reduce the number of purification steps required, thereby potentially increasing the yield. This process would also buffer exchange the peptide into acetonitrile, which can be readily removed through lyophilisation, in addition to removing any contaminating buffer salts.

The difficulties in producing large quantities of hCC has hindered previous attempts to study the fibrillation pathway of this protein (Keeley, 2007, Elshawaihde, 2012). Further complications have arisen with the observation that oligomeric species are formed in conjunction with the fibrils. The equilibrium between these assemblies and the high association which leads to the coating of the fibrils by the oligomers has meant that purification of either species has been a challenge.

It has been demonstrated here that WT hCC will form amyloid fibrils under two different conditions, at pH 4.0 and at pH 2.0. Both of these are far from physiological, especially when combined with the high temperature and agitation required for fibril assembly. However, structural insights obtained in this system could be used as a model

for the pathogenic variant L68Q, a protein that readily aggregates under physiological conditions. Production of this mutant is extremely challenging due to its tendency to aggregate during expression, even at the low levels used here. It is also shown that hCC fibrils can be formed at lower protein concentrations than has previously been reported, with a ten-fold dilution from 225  $\mu\text{M}$  to 22.5  $\mu\text{M}$  still leading to the formation of significant amounts of amyloid at pH 4.0.

hCC will form oligomeric species in both of the conditions described above. Although the production of hCC oligomers at pH 4.0 have been described previously (Wahlbom et al., 2007), hCC oligomers have not been reported to form at pH 2.0. Both of these oligomer populations are circular, or spherical, with a uniform morphology throughout the samples but a large variation in size. These could conceivably be the same species forming at both conditions but observed from different angles. Although hCC readily makes oligomers through *in vitro* incubation of the pure protein, other members of the cystatin family do not, although small amounts have been isolated from preparations of cystatin B directly after over-expression in *E. coli* (Davis, 2013).

The current favoured hypothesis for amyloid neurotoxicity is that oligomeric intermediates are the toxic species in many neurodegenerative diseases. The species formed by hCC, particularly at pH 4 where the annular morphology is observed, have the properties of species associated with toxicity in a number of different systems. Indeed, Wahlbom et al. (2007) report that hCC oligomers produced at pH 4.0 bind to the oligomer-specific antibody A11 in a dot blot. Unfortunately, attempts to characterise further the toxicity of the hCC oligomer samples were unsuccessful due to inherent difficulties with the cell assays.

The hCC species appear highly stable, and remain in solution after extended incubation periods. Interestingly in these samples, oligomers which have adhered to the fibril surface are observed. These oligomers coat the fibril and do not appear to dissociate in any of the conditions tested here except possibly for high concentrations of the denaturant guanidine hydrochloride. It has recently been proposed that amyloid fibrils can act as a surface to catalyse the formation of nuclei in a secondary nucleation mechanism, thereby increasing the rate of fibrillogenesis (Buell et al., 2014). In the hCC system it is possible that amyloid fibrils are exerting a surface effect to catalyse the formation of stable oligomeric species, and that once these species form they remain associated with the fibril structure. This may explain the stability of the complex if these

oligomers are essentially an integral part of the fibril. In this scenario, the kinetics of the process would be such that following the reaction over time would show the production of fibrils before oligomers, or at least an increase of oligomers as the fibrils are produced. This was not observed. Alternatively, instead of catalysing oligomer formation, the fibril surface could be acting either to stabilise the oligomers once they have formed, or to segregate them away from solution. In both these cases oligomers will be prevented from aggregating further. This would require the formation of fibrils and oligomers simultaneously and would suggest the processes are occurring in parallel, indicating that the oligomers are unlikely to be on-pathway to amyloid formation.

Purification methods developed below were used to further verify that disturbing the ratio of fibrils to oligomers in solution did not lead to “re-equilibration” by inter-conversion of one species into the other, but rather, to the persistence of these individual species in solution. This contrasts strongly with data reported by Wahlbom et al. (2007) where they observed the formation of fibrils from a solution of oligomers at a rate far exceeding fibrillisation of hCC monomers.

Ultrafiltration proved to be successful in purifying the oligomers away from contaminating fibrils. This method is also thought to remove any contaminating monomer from the sample, however due to difficulties in analysing these samples by SEC and SDS-PAGE it is difficult to verify whether this is indeed the case. Producing a pure sample of hCC fibrils proved challenging, attempts were hindered by the variations in the products produced upon incubation of the protein in the different conditions combined with the problems of producing large amounts of protein. Optimising the conditions so that fibrils are produced in conditions at which very few oligomers form (such as 22.5  $\mu\text{M}$  hCC at pH 4.0) should then enable a more efficient isolation of the fibrils through centrifugation. An alternative method for the production of pure fibrils could be through repeated rounds of seeding, but the requirement for large amounts of protein makes this route costly.

A preliminary investigation into the hCC fibril structure was performed using elastase to probe unprotected regions. Although the limited proteolysis results presented here do not define a protected fibril core in the same way as has been described for cystatin B, novel insights into the structure of hCC fibrils have been established.

The proteolysis reactions were carried out at pH 8.0 on fibrillar hCC then the resulting fibrillar pellets were washed then analysed after dissolution in guanidine hydrochloride.

Rapid hydrolysis was observed throughout many regions of the protein showing a lack of sensitive areas, or the ability of “nicked” hCC to remain incorporated within the fibril pellet. For example, where cleavage occurs in the central part of the molecule (between V60 and N61) a partner fragment can often also be identified, suggesting that the fibrillar hCC can indeed be nicked. This site is located between strands 2 and 3 of the original monomer structure. Peptides from both sides of this cut site were observed (i.e. both halves of the molecule) suggesting that this region of the molecule, unlike in its cystatin B counterpart fibrils, is vulnerable to hydrolysis. This also indicates that hCC does not retain a monomer-like fold within the fibril, as the loop where these residues are positioned is the region which is responsible for the inhibitory activity of hCC.

Consistent with results obtained for its counterpart cystatin B, regions of hCC which are susceptible to proteolysis are the N-terminal of the molecule, in particular the region up to the end of the  $\alpha$ -helix, and the area between strands 4 and 5. This suggests that, as for cystatin B, the N-terminal region is disordered and is not part of the fibril core whereas the susceptibility of the region between strands 4 and 5 could indicate that this region is protruding out of the structure.

This study has highlighted additional complications in the identification of the peptide fragments produced by proteolysis due to the presence of the two disulphide bonds in the hCC molecule. A comparison of the digestion samples in both native and reducing conditions would confirm the identification of the linked peptides. N-terminal sequencing could be used in conjunction with MS to identify, or confirm the presence of, additional fragments particularly those with an ambiguous cut site. Limited proteolysis using alternative enzymes such as proteinase K or pepsin would verify the sensitivity of the regions described above. The determination of structural features from oligomeric species is highly desirable, and the stability of the species formed by hCC could make these an ideal model. Current limitations into structural studies with these oligomers is the low yields and difficulties with manipulation.

The interaction between hCC and A $\beta$ <sub>1-42</sub> was explored by ThT fluorescence assays, TEM and NMR, which led to the proposal that monomeric hCC is inhibiting the formation of amyloid fibrils by A $\beta$  through binding to an oligomeric form of the peptide. A comparison of the inhibition mechanism of hCC in A $\beta$  fibril formation with methods of inhibition by transthyretin and neuroserpin highlights the differences between these mechanisms, indicating the alternative processes that have evolved to try

and prevent the aggregation of A $\beta$  through targeting the reaction at different points. It is thought that TTR tetramer binds to A $\beta$  monomer and reduces the formation of nucleating species (Li et al., 2013). Neuroserpin forms a specific binary complex with A $\beta_{1-42}$  with a 1:1 stoichiometry (Kinghorn et al., 2006). Although the addition of neuroserpin accelerates the aggregation of A $\beta$ , the species formed are small amorphous aggregates with a distinctly different appearance to mature fibrils. It is proposed that these are off pathway non-toxic oligomers. hCC is not binding to monomeric A $\beta$  but instead appears to be binding to an oligomeric species causing the formation of non-toxic assemblies. In a similar fashion PrP<sup>C</sup> selectively binds to oligomers (Lauren et al., 2009), however in this system the resulting species are more toxic than those produced in the absence of PrP<sup>C</sup>.

The nature of these interactions, and why they have such diverse effects, must be to do with differences in the binding and subsequent dissociation of the interacting proteins, and therefore must be related to their structure. It is therefore important to understand these interfaces, particularly considering one promotes the toxicity of A $\beta$  whilst others show an inhibitory effect. The inhibitory and amyloid-promoting associations of different forms of  $\beta_2m$  have been studied in Karamanos et al. (2014), which demonstrated that a similar head-to-head interaction was observed in both complexes. The interface for the inhibitory complex is stabilised by hydrophobic interactions, whereas the amyloid-promoting interface involves electrostatic interactions.

Although the formation of the complex between A $\beta$  and hCC was not observable using HSQC, it is possible that alternative NMR methods, for example relaxation experiments, could be performed to monitor this interaction. Mutagenesis of particular residues, such as in the hydrophobic protease binding region, could be used to monitor the effect of this region on A $\beta$  fibril inhibition through ThT fluorescence assays. A study using short peptides of hCC could be exploited to examine which region of hCC is involved in binding A $\beta$ , as has been successful in the transthyretin system (Du et al., 2012). In addition to this, it may be interesting to examine the effect of mixtures of modulating proteins on A $\beta$  fibril assembly. A further characterisation of the species produced through the incubation of hCC and A $\beta$  would be required for a more detailed insight into the mechanism of inhibition. Events at a surface may be quite different to what is occurring in solution, or they might provide the ideal experimental system for observing a complex between hCC and A $\beta$ .

## References

- ABRAHAMSON, M., ALVAREZ-FERNANDEZ, M. & NATHANSON, C. M. 2003. Cystatins. In: SAKLATVALA, J., NAGASE, H. & SALVESEN, G. (eds.) *Proteases and the Regulation of Biological Processes*. London: Portland Press Ltd.
- ABRAHAMSON, M., BARRETT, A. J., SALVESEN, G. & GRUBB, A. 1986. Isolation of 6 cysteine proteinase inhibitors from human urine - Their physicochemical and enzyme kinetic properties and concentrations in biological fluids. *Journal of Biological Chemistry*, 261, 1282-1289.
- ABRAHAMSON, M. & GRUBB, A. 1994. Increased body temperature accelerates aggregation of the Leu 68 → Gln mutant cystatin C, the amyloid forming protein in hereditary cystatin C amyloid angiopathy. *Proceedings of the National Academy of Sciences of the United States of America*, 91, 1416-1420.
- ABRAHAMSON, M., MASON, R. W., HANSSON, H., BUTTLE, D. J., GRUBB, A. & OHLSSON, K. 1991. Human cystatin C - Role of the N-terminal segment in the inhibition of human cysteine proteinases and in its inactivation by leukocyte elastase. *Biochemical Journal*, 273, 621-626.
- ABRAHAMSON, M., RITONJA, A., BROWN, M. A., GRUBB, A., MACHLEIDT, W. & BARRETT, A. J. 1987. Identification of the probable inhibitory reactive sites of the cysteine proteinase inhibitors human cystatin C and chicken cystatin. *Journal of Biological Chemistry*, 262, 9688-9694.
- ALEXANDRESCU, A. T. 2001. An NMR-based quenched hydrogen exchange investigation of model amyloid fibrils formed by cold shock protein A. *Pacific Symposium Biocomputing* 6, 67-78.
- ALEXANDRESCU, A. T. 2005. Amyloid accomplices and enforcers. *Protein Science*, 14, 1-12.
- ALVAREZ-FERNANDEZ, M., BARRETT, A. J., GERHARTZ, B., DANDO, P. M., NI, J. A. & ABRAHAMSON, M. 1999. Inhibition of mammalian legumain by some cystatins is due to a novel second reactive site. *Journal of Biological Chemistry*, 274, 19195-19203.
- ALZHEIMER'S SOCIETY UK. 2014. About dementia statistics. Available at [http://www.alzheimers.org.uk/site/scripts/documents\\_info.php?documentID=341](http://www.alzheimers.org.uk/site/scripts/documents_info.php?documentID=341) [Accessed 28<sup>th</sup> September 2014]
- ANCOLIO, K., DUMANCHIN, C., BARELLI, H., WARTER, J. M., BRICE, A., CAMPION, D., FREBOURG, T. & CHECLER, F. 1999. Unusual phenotypic alteration of  $\beta$ -amyloid precursor protein ( $\beta$ -APP) maturation by a new Val 715 → Met  $\beta$ -APP 770 mutation responsible for probable early-onset Alzheimer's disease. *Proceedings of the National Academy of Sciences of the United States of America*, 96, 4119-4124.
- ANNAERT, W. & DE STROOPER, B. 2002. A cell biological perspective on Alzheimer's disease. *Annual Review of Cell and Developmental Biology*, 18, 25-51.
- ARTIMO, P., JONNALAGEDDA, M., ARNOLD, K., BARATIN, D., CSARDI, G., DE CASTRO, E., DUVAUD, S., FLEGEL, V., FORTIER, A., GASTEIGER, E., GROSDIDIER, A., HERNANDEZ, C., IOANNIDIS, V., KUZNETSOV, D., LIECHTI, R., MORETTI, S., MOSTAGUIR, K., REDASCHI, N., ROSSIER, G., XENARIOS, I. & STOCKINGER, H. 2012. ExPASy: SIB bioinformatics resource portal. *Nucleic Acids Research*, 40, W597-W603.
- ATLAS, D., LEVIT, S., SCHECHTE, I. & BERGER, A. 1970. Active site of elastase - Partial mapping by means of specific peptide substrates. *FEBS Letters*, 11, 281-283.
- BABBES, A. R. H., POWERS, E. T. & KELLY, J. W. 2008. Quantification of the thermodynamically linked quaternary and tertiary structural stabilities of transthyretin and its disease-associated variants: The relationship between stability and amyloidosis. *Biochemistry*, 47, 6969-6984.
- BALGUERIE, A., DOS REIS, S., RITTER, C., CHAIGNEPAIN, S., COULARY-SALIN, B., FORGE, V., BATHANY, K., LASCU, I., SCHMITTER, J. M., RIEK, R. & SAUPE, S. J. 2003. Domain

- organization and structure-function relationship of the HET-s prion protein of *Podospora anserina*. *Embo Journal*, 22, 2071-2081.
- BARNHART, M. M. & CHAPMAN, M. R. 2006. Curli biogenesis and function. *Annual Review of Microbiology*, 60, 131-147.
- BARRETT, A. J. 1987. The cystatins - A new class of peptidase inhibitors. *Trends in Biochemical Sciences*, 12, 193-196.
- BARRETT, A. J., DAVIES, M. E. & GRUBB, A. 1984. The place of human  $\gamma$ -trace (cystatin C) amongst the cysteine proteinase inhibitors. *Biochemical and Biophysical Research Communications*, 120, 631-636.
- BARROW, C. J. & ZAGORSKI, M. G. 1991. Solution structures of  $\beta$ -peptide and its constituent fragments - Relation to amyloid deposition. *Science*, 253, 179-182.
- BAUMANN, F., TOLNAY, M., BRABECK, C., PAHNKE, J., KLOZ, U., NIEMANN, H. H., HEIKENWALDER, M., RULICKE, T., BURKLE, A. & AGUZZI, A. 2007. Lethal recessive myelin toxicity of prion protein lacking its central domain. *Embo Journal*, 26, 538-547.
- BENILOVA, I., KARRAN, E., DE STROOPER, B. 2012. The toxic A $\beta$  oligomer and Alzheimer's disease: an emperor in need of clothes. *Nature Neuroscience*, 15, 349-357.
- BENILOVA, I. & DE STROOPER, B. 2013. Promiscuous Alzheimer's amyloid: Yet another partner. *Science*, 341, 1354-1355.
- BERNACKI, J.P. & MURPHY, R.M. 2009. Model discrimination and mechanistic interpretation of kinetic data in protein aggregation studies. *Biophysical Journal*, 96, 2871-2887.
- BERTINI, I., GONNELLI, L., LUCHINAT, C., MAO, J. F. & NESI, A. 2011. A new structural model of A $\beta_{40}$  fibrils. *Journal of the American Chemical Society*, 133, 16013-16022.
- BEYER, K., LAO, J. I., GOMEZ, M., RIUTORT, N., LATORRE, P., MATE, J. L. & ARIZA, A. 2001. Alzheimer's disease and the cystatin C gene polymorphism: An association study. *Neuroscience Letters*, 315, 17-20.
- BIERE, A. L., OSTASZEWSKI, B., STIMSON, E. R., HYMAN, B. T., MAGGIO, J. E. & SELKOE, D. J. 1996. Amyloid  $\beta$  peptide is transported on lipoproteins and albumin in human plasma. *Journal of Biological Chemistry*, 271, 32916-32922.
- BIESCHKE, J., COHEN, E., MURRAY, A., DILLIN, A. & KELLY, J. W. 2009. A kinetic assessment of the *C. elegans* amyloid disaggregation activity enables uncoupling of disassembly and proteolysis. *Protein Science*, 18, 2231-2241.
- BITAN, G., KIRKITADZE, M. D., LOMAKIN, A., VOLLERS, S. S., BENEDEK, G. B. & TEPLow, D. B. 2003. Amyloid  $\beta$  protein (A $\beta$ ) assembly: A $\beta_{40}$  and A $\beta_{42}$  oligomerize through distinct pathways. *Proceedings of the National Academy of Sciences of the United States of America*, 100, 330-335.
- BLAKE, C. & SERPELL, L. 1996. Synchrotron X-ray studies suggest that the core of the transthyretin amyloid fibril is a continuous  $\beta$ -sheet helix. *Structure*, 4, 989-998.
- BOADA, M., ORTIZ, P., ANAYA, F., HERNANDEZ, I., MUNOZ, J., NUNEZ, L., OLAZARAN, J., ROCA, I., CUBERAS, G., TARRAGA, L., BUENDIA, M., PLA, R. P., FERRER, I. & PAEZ, A. 2009. Amyloid targeted therapeutics in Alzheimer's disease: Use of human albumin in plasma exchange as a novel approach for A $\beta$  mobilization. *Drug News & Perspectives*, 22, 325-339.
- BOADA, M., RAMOS-FERNÁNDEZ, E., GUIVERNAU, B., MUÑOZ, F.J., COSTA, M., ORTIZ, A.M., JORQUERA, J.I., NÚÑEZ, L., TORRES, M. & PÁEZ, A. 2014. Treatment of Alzheimer's disease using combination therapy with plasma exchange and haemapheresis with albumin and intravenous immunoglobulin: Rationale and treatment approach of the AMBAR (Alzheimer Management By Albumin Replacement) study. *Neurologia*, in press.

- BOBEK, L. A. & LEVINE, M. J. 1992. Cystatins - Inhibitors of cysteine proteinases. *Critical Reviews in Oral Biology & Medicine*, 3, 307-332.
- BODE, W., ENGH, R., MUSIL, D., THIELE, U., HUBER, R., KARSHIKOV, A., BRZIN, J., KOS, J. & TURK, V. 1988. The 2.0 Å X-ray crystal structure of chicken egg-white cystatin and its possible mode of interaction with cysteine proteinases. *Embo Journal*, 7, 2593-2599.
- BODE, W., MEYER, E. & POWERS, J. C. 1989. Human-leukocyte and porcine pancreatic elastase - X-ray crystal-structures, mechanism, substrate-specificity, and mechanism-based inhibitors. *Biochemistry*, 28, 1951-1963.
- BUCCIANTINI, M., GIANNONI, E., CHITI, F., BARONI, F., FORMIGLI, L., ZURDO, J. S., TADDEI, N., RAMPONI, G., DOBSON, C. M. & STEFANI, M. 2002. Inherent toxicity of aggregates implies a common mechanism for protein misfolding diseases. *Nature*, 416, 507-511.
- BUELL, A.K., DOBSON, C.M. & KNOWLES, T.P. J. 2014. The physical chemistry of the amyloid phenomenon: Thermodynamics and kinetics of filamentous protein aggregation. *Essays in biochemistry*, 56, 11-39.
- BURNS, A. & ILIFFE, S. 2009. Alzheimer's disease. *British Medical Journal*, 338, 13.
- BUTKO, P., BUFORD, J. P., GOODWIN, J. S., STROUD, P. A., MCCORMICK, C. L. & CANNON, G. C. 2001. Spectroscopic evidence for amyloid-like interfacial self-assembly of hydrophobin Sc3. *Biochemical and Biophysical Research Communications*, 280, 212-215.
- BUTTERFIELD, S. M. & LASHUEL, H. A. 2010. Amyloidogenic protein membrane interactions: Mechanistic insight from model systems. *Angewandte Chemie-International Edition*, 49, 5628-5654.
- BUXBAUM, J. N., YE, Z., REIXACH, N., FRISKE, L., LEVY, C., DAS, P., GOLDE, T., MASLIAH, E., ROBERTS, A. R. & BARTFAI, T. 2008. Transthyretin protects Alzheimer's mice from the behavioral and biochemical effects of A $\beta$  toxicity. *Proceedings of the National Academy of Sciences of the United States of America*, 105, 2681-2686.
- CAMPIONI, S., MANNINI, B., ZAMPAGNI, M., PENSALFINI, A., PARRINI, C., EVANGELISTI, E., RELINI, A., STEFANI, M., DOBSON, C. M., CECCHI, C. & CHITI, F. 2010. A causative link between the structure of aberrant protein oligomers and their toxicity. *Nature Chemical Biology*, 6, 140-147.
- CARULLA, N., CADDY, G. L., HALL, D. R., ZURDO, J., GAIRI, M., FELIZ, M., GIRALT, E., ROBINSON, C. V. & DOBSON, C. M. 2005. Molecular recycling within amyloid fibrils. *Nature*, 436, 554-558.
- CAUGHEY, B. & LANSBURY, P. T. 2003. Protofibrils, pores, fibrils, and neurodegeneration: Separating the responsible protein aggregates from the innocent bystanders. *Annual Review of Neuroscience*, 26, 267-298.
- CHAPMAN, M. R., ROBINSON, L. S., PINKNER, J. S., ROTH, R., HEUSER, J., HAMMAR, M., NORMARK, S. & HULTGREN, S. J. 2002. Role of *Escherichia coli* curli operons in directing amyloid fiber formation. *Science*, 295, 851-855.
- CHEN, S. G., YADAV, S. P. & SUREWICZ, W. K. 2010. Interaction between human prion protein and amyloid- $\beta$  (A $\beta$ ) oligomers. Role of N-terminal residues. *Journal of Biological Chemistry*, 285, 26377-26383.
- CHIMON, S., SHAIBAT, M. A., JONES, C. R., CALERO, D. C., AIZEZI, B. & ISHII, Y. 2007. Evidence of fibril-like  $\beta$ -sheet structures in a neurotoxic amyloid intermediate of Alzheimer's  $\beta$ -amyloid. *Nature Structural & Molecular Biology*, 14, 1157-1164.
- CHIOU, A., HÄGGLÖF, P., ORTE, A., CHEN, A. Y., DUNNE, P. D., BELORGEY, D., KARLSSON-LI, S., LOMAS, D. A. & KLENERMAN, D. 2009. Probing neuroserpin polymerization and

- interaction with amyloid- $\beta$  peptides using single molecule fluorescence. *Biophysical Journal*, 97, 2306–2315.
- CHITI, F. & DOBSON, C. M. 2006. Protein misfolding, functional amyloid, and human disease. *Annual Review of Biochemistry*, 75, 333-366.
- CHITI, F. & DOBSON, C. M. 2009. Amyloid formation by globular proteins under native conditions. *Nature Chemical Biology*, 5, 15-22.
- CHOI, S. H., LEIGHT, S. N., LEE, V. M. Y., LI, T., WONG, P. C., JOHNSON, J. A., SARAIVA, M. J. & SISODIA, S. S. 2007. Accelerated A $\beta$  deposition in APP<sup>swe</sup>/PS1 Delta E9 mice with hemizygous deletions of TTR (transthyretin). *Journal of Neuroscience*, 27, 7006-7010.
- CHOTHIA, C & JANIN, J. 1975. Principles of protein-protein recognition. *Nature*, 256, 705-708.
- CITRON, M. 2010. Strategies for disease modification in Alzheimer's disease. *Nature Reviews Drug Discovery*, 9, 387-398.
- CLELAND, J. L., POWELL, M. F. & SHIRE, S. J. 1993. The development of stable protein formulations - A close look at protein aggregation, deamidation, and oxidation. *Critical Reviews in Therapeutic Drug Carrier Systems*, 10, 307-377.
- COELHO, T., MAIA, L.F., DA SILVA, A.M., CRUZ, M.W., PLANTE-BORDENEUVE, V., SUHR, O.B., CONCEICAO, I., SCHMIDT, H.H.J., TRIGO, P., KELLY, J.W., LABAUDINIÈRE, R., CHAN, J.S., PACKMAN, J. & GROGAN, D.R. 2013. Long-term effects of tafamidis for the treatment of transthyretin familial amyloid polyneuropathy. *Journal of Neurology*, 260, 2802-2814.
- COHEN, D. H., FEINER, H., JENSSON, O. & FRANGIONE, B. 1983. Amyloid fibril in Hereditary Cerebral Hemorrhage with Amyloidosis (HCHWA) is related to the gastroentero-pancreatic neuroendocrine protein,  $\gamma$ -trace. *Journal of Experimental Medicine*, 158, 623-628.
- COHEN, F. E. & KELLY, J. W. 2003. Therapeutic approaches to protein-misfolding diseases. *Nature*, 426, 905-909.
- COHEN, E., BIESCHKE, J., PERCIAVALLE, R. M., KELLY, J. W. & DILLIN, A. 2006. Opposing activities protect against age-onset proteotoxicity. *Science*, 313, 1604-1610.
- COHEN, S. I. A., LINSE, S., LUHESHI, L. M., HELLSTRAND, E., WHITE, D. A., RAJAH, L., OTZEN, D. E., VENDRUSCOLO, M., DOBSON, C. M. & KNOWLES, T. P. J. 2013. Proliferation of amyloid- $\beta$  42 aggregates occurs through a secondary nucleation mechanism. *Proceedings of the National Academy of Sciences of the United States of America*, 110, 9758-9763.
- COLES, M., BICKNELL, W., WATSON, A., FAIRLIE, D. & CRAIK, D. 1998. Solution structure amyloid  $\beta$ -peptide (1-40) in a water-micelle environment. Is the membrane-spanning domain where we think it is? *Biochemistry*, 37, 11064-11077.
- COLLINGE, J. 2001. Prion diseases of humans and animals: Their causes and molecular basis. *Annual Review of Neuroscience*, 24, 519-550.
- COLLETIER, J.-P., LAGANOWSKY, A., LANDAU, M., ZHAO, M., SORIAGA, A. B., GOLDSCHMIDT, L., FLOT, D., CASCIO, D., SAWAYA, M. R. & EISENBERG, D. 2011. Molecular basis for amyloid- $\beta$  polymorphism. *Proceedings of the National Academy of Sciences of the United States of America*, 108, 16938-16943.
- COSTA, R., GONCALVES, A., SARALVA, M. J. & CARDOSO, I. 2008. Transthyretin binding to A $\beta$  peptide - Impact on A $\beta$  fibrillogenesis and toxicity. *Febs Letters*, 582, 936-942.
- CRAWFORD, F. C., FREEMAN, M. J., SCHINKA, J. A., ABDULLAH, L. I., GOLD, M., HARTMAN, R., KRIVIAN, K., MORRIS, M.D., RICHARDS, D., DUARA, R., ANAND, R. & MULLAN, M. J. 2000. A polymorphism in the cystatin C gene is a novel risk factor for late-onset Alzheimer's disease. *Neurology*, 55, 763–768.

- D'ADAMIO, L. 2010. Role of cystatin C in neuroprotection and its therapeutic implications. *American Journal of Pathology*, 177, 2163-2165.
- DANDO, P. M., FORTUNATO, M., SMITH, L., KNIGHT, C. G., MCKENDRICK, J. E. & BARRETT, A. J. 1999. Pig kidney legumain: an asparaginyl endopeptidase with restricted specificity. *Biochemical Journal*, 339, 743-749.
- DAVIS, R. L., SHRIMPTON, A. E., HOLOHAN, P. D., BRADSHAW, C., FEIGLIN, D., COLLINS, G. H., SONDEREGGER, P., KINTER, J., BECKER, L. M., LACBAWAN, F., KRASNEWICH, D., MUENKE, M., LAWRENCE, D. A., YERBY, M. S., SHAW, C. M., GOOPTU, B., ELLIOTT, P. R., FINCH, J. T., CARRELL, R. W. & LOMAS, D. A. 1999. Familial dementia caused by polymerisation of mutant neuroserpin. *Nature*, 401, 376-379.
- DAVIS, P. J. 2013. *Structural Studies of Cystatin B Amyloid Fibre and Oligomer*. PhD thesis, University of Sheffield.
- DE STROOPER, B. & ANNAERT, W. 2000. Proteolytic processing and cell biological functions of the amyloid precursor protein. *Journal of Cell Science*, 113, 1857-1870.
- DENG, A., IRIZARRY, M. C., NITSCH, R. M., GROWDON, J. H. & REBECK, G. W. 2001. Elevation of cystatin C in susceptible neurons in Alzheimer's disease. *American Journal of Pathology*, 159, 1061-1068.
- DILL, K. A. & CHAN, H. S. 1997. From Levinthal to pathways to funnels. *Nature Structural Biology*, 4, 10-19.
- DOBSON, C. M. 2003. Protein folding and misfolding. *Nature*, 426, 884-890.
- DOBSON, C. M. 2004. Principles of protein folding, misfolding and aggregation. *Seminars in Cell & Developmental Biology*, 15, 3-16.
- DU, J. & MURPHY, R. M. 2010. Characterization of the interaction of  $\beta$ -amyloid with transthyretin monomers and tetramers. *Biochemistry*, 49, 8276-8289.
- DU, J. L., CHO, P. Y., YANG, D. T. & MURPHY, R. M. 2012. Identification of  $\beta$ -amyloid binding sites on transthyretin. *Protein Engineering Design & Selection*, 25, 337-345.
- EKIEL, I. & ABRAHAMSON, M. 1996. Folding-related dimerization of human cystatin C. *Journal of Biological Chemistry*, 271, 1314-1321.
- EKIEL, I., ABRAHAMSON, M., FULTON, D. B., LINDAHL, P., STORER, A. C., LEVADOUX, W., LAFRANCE, M., LABELLE, S., POMERLEAU, Y., GROLEAU, D., LESAUTEUR, L. & GEHRING, K. 1997. NMR structural studies of human cystatin C dimers and monomers. *Journal of Molecular Biology*, 271, 266-277.
- ELSHAWAIHDE, A. 2012. *Role of Human Cystatin C in Alzheimer's Disease*. PhD thesis, University of Sheffield.
- ENGH, R.A., DIECKMANN, T., BODE, W., AUERSWALD, E.A., TURK, V., HUBER, R. & OSCHKINAT, H. (1993) Conformational variability of chicken cystatin – Comparison of structures determined by X-ray diffraction and NMR spectroscopy. *Journal of Molecular Biology*, 234, 1060-1069.
- FANDRICH, M. 2012. Oligomeric intermediates in amyloid formation: Structure determination and mechanisms of toxicity. *Journal of Molecular Biology*, 421, 427-440.
- FANDRICH, M. & DOBSON, C. M. 2002. The behaviour of polyamino acids reveals an inverse side chain effect in amyloid structure formation. *Embo Journal*, 21, 5682-5690.
- FANDRICH, M., FLETCHER, M. A. & DOBSON, C. M. 2001. Amyloid fibrils from muscle myoglobin - Even an ordinary globular protein can assume a rogue guise if conditions are right. *Nature*, 410, 165-166.

- FERRER, I., BLANCO, R., CARMONA, M., PUIG, B., RIBERA, R., REY, M. J. & RIBALTA, T. 2001. Prion protein expression in senile plaques in Alzheimer's disease. *Acta Neuropathologica*, 101, 49-56.
- FINCKH, U., VON DER KAMMER, H., VELDEN, J., MICHEL, T., ANDRESEN, B., DENG, A., ZHANG, J., MULLER-THOMSEN, T., ZUCHOWSKI, K., MENZER, G., MANN, U., PAPASSOTIROPOULOS, A., HEUN, R., ZURDEL, J., HOLST, F., BENUSSI, L., STOPPE, G., REISS, J., MISEREZ, A. R., STAEHELIN, H. B., REBECK, G. W., HYMAN, B. T., BINETTI, G., HOCK, C., GROWDON, J. H. & NITSCH, R. M. 2000. Genetic association of a cystatin C gene polymorphism with late-onset Alzheimer disease. *Archives of Neurology*, 57, 1579-1583.
- FINDER, V. H., VODOPIVEC, I., NITSCH, R. M. & GLOCKSHUBER, R. 2010. The recombinant amyloid- $\beta$  peptide: A $\beta_{1-42}$  aggregates faster and is more neurotoxic than synthetic A $\beta_{1-42}$ . *Journal of Molecular Biology*, 396, 9-18.
- FOWLER, D. M., KOULOV, A. V., ALORY-JOST, C., MARKS, M. S., BALCH, W. E. & KELLY, J. W. 2006. Functional amyloid formation within mammalian tissue. *Plos Biology*, 4, 100-107.
- FOWLER, D. M., KOULOV, A. V., BALCH, W. E. & KELLY, J. W. 2007. Functional amyloid - from bacteria to humans. *Trends in Biochemical Sciences*, 32, 217-224.
- FRARE, E., MOSSUTO, M. F., DE LAURETO, P. P., DUMOULIN, M., DOBSON, C. M. & FONTANA, A. 2006. Identification of the core structure of lysozyme amyloid fibrils by proteolysis. *Journal of Molecular Biology*, 361, 551-561.
- GARAI, K., CRICK, S. L., MUSTAFI, S. M. & FRIEDEN, C. 2009. Expression and purification of amyloid- $\beta$  peptides from *Escherichia coli*. *Protein Expression and Purification*, 66, 107-112.
- GASTEIGER, E., HOOGLAND, C., GATTIKER, A., DUVAUD, S., WILKINS, M. R., APPEL, R. D. & BAIROCH, A. 2005. Protein identification and analysis tools on the ExPASy server. In: WALKER, J., (ed). *The Proteomics Protocols Handbook*. Humana Press.
- GHISO, J., PONSESTEL, B. & FRANGIONE, B. 1986. Hereditary Cerebral Amyloid Angiopathy - the amyloid fibrils contain a protein which is a variant of cystatin C, an inhibitor of lysosomal cysteine proteases. *Biochemical and Biophysical Research Communications*, 136, 548-554.
- GIMBEL, D. A., NYGAARD, H. B., COFFEY, E. E., GUNTHER, E. C., LAUREN, J., GIMBEL, Z. A. & STRITTMATTER, S. M. 2010. Memory Impairment in transgenic Alzheimer mice requires cellular prion protein. *Journal of Neuroscience*, 30, 6367-6374.
- GIUNTA, S., VALLI, M. B., GALEAZZI, R., FATTORETTI, P., CORDER, E. H. & GALEAZZI, L. 2005. Transthyretin inhibition of amyloid- $\beta$  aggregation and toxicity. *Clinical Biochemistry*, 38, 1112-1119.
- GIURLEO, J. T., HE, X. & TALAGA, D. S. 2008.  $\beta$ -Lactoglobulin assembles into amyloid through sequential aggregated intermediates. *Journal of Molecular Biology*, 381, 1332-1348.
- GLABE, C. G. 2006. Common mechanisms of amyloid oligomer pathogenesis in degenerative disease. *Neurobiology of Aging*, 27, 570-575.
- GLABE, C. G. 2008. Structural classification of toxic amyloid oligomers. *Journal of Biological Chemistry*, 283, 29639-29643.
- GLENNER, G. G., EANES, E. D. & PAGE, D. L. 1972. Relation of properties of Congo Red-stained amyloid fibrils to  $\beta$ -conformation. *Journal of Histochemistry & Cytochemistry*, 20, 821-826.
- GOLD, R. & SHALITIN, Y. 1975. Specificity of porcine elastase. *Biochimica et Biophysica Acta*, 410, 421-425.
- GOLDSBURY, C., FREY, P., OLIVIERI, V., AEBI, U. & MULLER, S. A. 2005. Multiple assembly pathways underlie amyloid- $\beta$  fibril polymorphisms. *Journal of Molecular Biology*, 352, 282-298.

- GOLDSBURY, C. S., WIRTZ, S., MULLER, S. A., SUNDERJI, S., WICKI, P., AEBI, U. & FREY, P. 2000. Studies on the in vitro assembly of A $\beta$  1-40: Implications for the search for A $\beta$  fibril formation inhibitors. *Journal of Structural Biology*, 130, 217-231.
- GOLDSCHMIDT, L., TENG, P. K., RIEK, R. & EISENBERG, D. 2010. Identifying the amyloids, proteins capable of forming amyloid-like fibrils. *Proceedings of the National Academy of Sciences of the United States of America*, 107, 3487-3492.
- GOODMAN, Y. & MATTSON, M. P. 1994. Secreted forms of  $\beta$ -amyloid precursor protein protect hippocampal-neurons against amyloid- $\beta$ -peptide-induced oxidative injury. *Experimental Neurology*, 128, 1-12.
- GRIFFITH, J. S. 1967. Self-replication and scrapie. *Nature*, 215, 1043-1044.
- GRUBB, A. & LOFBERG, H. 1982. Human  $\gamma$ -trace, a basic microprotein: amino acid sequence and presence in the adenohypophysis. *Proceedings of the National Academy of Sciences of the United States of America*, 79, 3024-3027.
- GRUBB, A. & LOFBERG, H. 1985. Human  $\gamma$ -trace - structure, function and clinical use of concentration measurements. *Scandinavian Journal of Clinical & Laboratory Investigation*, 45, 7-13.
- GRZONKA, Z., JANKOWSKA, E., KASPRZYKOWSKI, F., KASPRZYKOWSKA, R., LAMKIEWICZ, L., WICZK, W., WIECZERZAK, E., CIARKOWSKI, J., DRABIK, P., JANOWSKI, R., KOZAK, M., JASKOLSKI, M. & GRUBB, A. 2001. Structural studies of cysteine proteases and their inhibitors. *Acta Biochimica Polonica*, 48, 1-20.
- GUIJARRO, J. I., SUNDE, M., JONES, J. A., CAMPBELL, I. D. & DOBSON, C. M. 1998. Amyloid fibril formation by an SH3 domain. *Proceedings of the National Academy of Sciences of the United States of America*, 95, 4224-4228.
- HAAN, J. & ROOS, R. A. C. 1992. Comparison between the Icelandic and Dutch forms of Hereditary Cerebral Amyloid Angiopathy. *Clinical Neurology and Neurosurgery*, 94, S82-S83.
- HAASS, C., SCHLOSSMACHER, M. G., HUNG, A. Y., VIGOPELFREY, C., MELLON, A., OSTASZEWSKI, B. L., LIEBERBURG, I., KOO, E. H., SCHENK, D., TEPLow, D. B. & SELKOE, D. J. 1992. Amyloid  $\beta$ -peptide is produced by cultured cells during normal metabolism. *Nature*, 359, 322-325.
- HAASS, C. & SELKOE, D. J. 2007 Soluble protein oligomers in neurodegeneration: Lessons from the Alzheimer's amyloid  $\beta$ -peptide. *Nature Reviews Molecular Cell Biology*, 8, 101-112.
- HABICHT, G., HAUPT, C., FRIEDRICH, R. P., HORTSCHANSKY, P., SACHSE, C., MEINHARDT, J., WIELIGMANN, K., GELLERMANN, G. P., BRODHUN, M., GOTZ, J., HALBHUBER, K. J., ROCKEN, C., HORN, U. & FANDRICH, M. 2007. Directed selection of a conformational antibody domain that prevents mature amyloid fibril formation by stabilizing A $\beta$  protofibrils. *Proceedings of the National Academy of Sciences of the United States of America*, 104, 19232-19237.
- HAMILTON, J. A. & BENSON, M. D. 2001. Transthyretin: a review from a structural perspective. *Cellular and Molecular Life Sciences*, 58, 1491-1521.
- HAMMARSTROM, P., SCHNEIDER, F. & KELLY, J. W. 2001. Trans-suppression of misfolding in an amyloid disease. *Science*, 293, 2459-2462.
- HARD, T. & LENDEL, C. 2012. Inhibition of Amyloid Formation. *Journal of Molecular Biology*, 421, 441-465.
- HARDY, J. 1997. Amyloid, the presenilins and Alzheimer's disease. *Trends in Neuroscience*, 20, 154-159.
- HARDY, J. & SELKOE, D. J. 2002. Medicine - The amyloid hypothesis of Alzheimer's disease: Progress and problems on the road to therapeutics. *Science*, 297, 353-356.

- HARTL, F. U., BRACHER, A. & HAYER-HARTL, M. 2011. Molecular chaperones in protein folding and proteostasis. *Nature*, 475, 324-332.
- HASAGAWA, K., YAMAGUCHI, I., OMATA, S., GEJYO, F. AND NAIKI, H. 1999. Interaction between A $\beta$ <sub>1-42</sub> and A $\beta$ <sub>1-40</sub> in Alzheimer's  $\beta$ -amyloid fibril formation *in vivo*. *Biochemistry*, 38, 15514-15521.
- HELLSTRAND, E., BOLAND, B., WALSH, D. M. & LINSE, R. 2010. Amyloid  $\beta$ -protein aggregation produces highly reproducible kinetic data and occurs by a two-phase process. *ACS Chemical Neuroscience*, 1, 13-18.
- HIRSCHFIELD, G. M. & HAWKINS, P. N. 2003. Amyloidosis: new strategies for treatment. *International Journal of Biochemistry & Cell Biology*, 35, 1608-1613.
- HOLLINGWORTH, P., HAROLD, D., SIMS, R., GERRISH, A., LAMBERT, J.-C., CARRASQUILLO, M. M., ABRAHAM, R., HAMSHERE, M. L., PAHWA, J. S., MOSKVINA, V., DOWZELL, K., JONES, N., STRETTON, A., THOMAS, C., RICHARDS, A., IVANOV, D., WIDDOWSON, C., CHAPMAN, J., LOVESTONE, S., POWELL, J., PROITSI, P., LUPTON, M. K., BRAYNE, C., RUBINSZTEIN, D. C., GILL, M., LAWLOR, B., LYNCH, A., BROWN, K. S., PASSMORE, P. A., CRAIG, D., MCGUINNESS, B., TODD, S., HOLMES, C., MANN, D., SMITH, A. D., BEAUMONT, H., WARDEN, D., WILCOCK, G., LOVE, S., KEHOE, P. G., HOOPER, N. M., VARDY, E. R. L. C., HARDY, J., MEAD, S., FOX, N. C., ROSSOR, M., COLLINGE, J., MAIER, W., JESSEN, F., RUTHER, E., SCHURMANN, B., HEUN, R., KOLSCH, H., VAN DEN BUSSCHE, H., HEUSER, I., KORNHUBER, J., WILTFANG, J., DICHGANS, M., FROLICH, L., HAMPEL, H., GALLACHER, J., HULL, M., RUJESCU, D., GIEGLING, I., GOATE, A. M., KAUWE, J. S. K., CRUCHAGA, C., NOWOTNY, P., MORRIS, J. C., MAYO, K., SLEEGERS, K., BETTENS, K., ENGELBORGH, S., DE DEYN, P. P., VAN BROECKHOVEN, C., LIVINGSTON, G., BASS, N. J., GURLING, H., MCQUILLIN, A., GWILLIAM, R., DELOUKAS, P., AL-CHALABI, A., SHAW, C. E., TSOLAKI, M., SINGLETON, A. B., GUERREIRO, R., MUHLEISEN, T. W., NOTHEN, M. M., MOEBUS, S., JOCKEL, K.-H., KLOPP, N., WICHMANN, H. E., PANKRATZ, V. S., SANDO, S. B., AASLY, J. O., BARCIKOWSKA, M., WSZOLEK, Z. K., DICKSON, D. W., GRAFF-RADFORD, N. R., PETERSEN, R. C., et al. 2011. Common variants at ABCA7, MS4A6A/MS4A4E, EPHA1, CD33 and CD2AP are associated with Alzheimer's disease. *Nat Genet.*, 43 (5), 429-435
- HORNBERG, A., ENEQVIST, T., OLOFSSON, A., LUNDGREN, E. & SAUER-ERIKSSON, A. E. 2000. A comparative analysis of 23 structures of the amyloidogenic protein transthyretin. *Journal of Molecular Biology*, 302, 649-669.
- HORTSCHANSKY, P., SCHROECKH, V., CHRISTOPEIT, T., ZANDOMENEGHI, G. & FANDRICH, M. 2005. The aggregation kinetics of Alzheimer's  $\beta$ -amyloid peptide is controlled by stochastic nucleation. *Protein Science*, 14, 1753-1759.
- HOSHINO, M., KATOU, H., HAGIHARA, Y., HASEGAWA, K., NAIKI, H. & GOTO, Y. 2002. Mapping the core of the  $\beta$ <sub>2</sub>-microglobulin amyloid fibril by H/D exchange. *Nature Structural Biology*, 9, 332-336.
- HUBBARD, S. J. 1998. The structural aspects of limited proteolysis of native proteins. *Biochimica et Biophysica Acta - Protein Structure and Molecular Enzymology*, 1382 (2), 161-206
- ICONOMIDOU, V. A., VRIEND, G. & HAMODRAKAS, S. J. 2000. Amyloids protect the silkworm oocyte and embryo. *Febs Letters*, 479, 141-145.
- IRVINE, G. B., EL-AGNAF, O. M., SHANKAR, G. M. & WALSH, D. M. 2008. Protein aggregation in the brain: The molecular basis for Alzheimer's and Parkinson's diseases. *Molecular Medicine*, 14, 451-464.
- JACKSON, G. S., MURRAY, I., HOSSZU, L. L. P., GIBBS, N., WALTHO, J. P., CLARKE, A. R. & COLLINGE, J. 2001. Location and properties of metal-binding sites on the human prion protein. *Proceedings of the National Academy of Sciences of the United States of America*, 98, 8531-8535.

- JAHN, T.R., MAKIN, O.S., MORRIS, K.L., MARSHALL, K.E., TIAN, P., SIKORSKI, P. & SERPELL, L.C. 2010. The common architecture of cross- $\beta$  amyloid. *Journal of Molecular Biology*, 395, 717-727.
- JANOWSKI, R., KOZAK, M., JANKOWSKA, E., GRZONKA, Z., GRUBB, A., ABRAHAMSON, M. & JASKOLSKI, M. 2001. Human cystatin C, an amyloidogenic protein, dimerizes through three-dimensional domain swapping. *Nature Structural Biology*, 8, 316-320.
- JARRETT, J. T., BERGER, E. P. & LANSBURY, P. T. 1993. The carboxy terminus of the  $\beta$ -amyloid protein is critical for the seeding of amyloid formation - implications for the pathogenesis of Alzheimer's disease. *Biochemistry*, 32, 4693-4697.
- JARRETT, J. T. & LANSBURY, P. T. 1993. Seeding one-dimensional crystallization of amyloid - a pathogenic mechanism in Alzheimer's disease and scrapie. *Cell*, 73, 1055-1058.
- JIMENEZ, J. L., GUIJARRO, J. L., ORLOVA, E., ZURDO, J., DOBSON, C. M., SUNDE, M. & SAIBIL, H. R. 1999. Cryo-electron microscopy structure of an SH3 amyloid fibril and model of the molecular packing. *Embo Journal*, 18, 815-821.
- JIMENEZ, J. L., NETTLETON, E. J., BOUCHARD, M., ROBINSON, C. V., DOBSON, C. M. & SAIBIL, H. R. 2002. The protofilament structure of insulin amyloid fibrils. *Proceedings of the National Academy of Sciences of the United States of America*, 99, 9196-9201.
- KAESER, S. A., HERZIG, M. C., COOMARASWAMY, J., KILGER, E., SELENICA, M. L., WINKLER, D. T., STAUFENBIEL, M., LEVY, E., GRUBB, A. & JUCKER, M. 2007. Cystatin C modulates cerebral  $\beta$ -amyloidosis. *Nature Genetics*, 39, 1437-1439.
- KANG, J., LEMAIRE, H. G., UNTERBECK, A., SALBAUM, J. M., MASTERS, C. L., GRZESCHIK, K. H., MÜLTHAUP, G., BEYREUTHER, K. & MÜLLERHILL, B. 1987. The precursor of Alzheimer's disease amyloid A $\beta$  protein resembles a cell surface receptor. *Nature*, 325, 733-736.
- KARAMANOS, T. K., KALVERDA, A. P., THOMPSON, G. S. & RADFORD, S. E. 2014. Visualization of transient protein-protein interactions that promote or inhibit amyloid assembly. *Molecular Cell*, 55, 214-226.
- KAUR, G., MOHAN, P., PAWLIK, M., DEROSA, S., FAJICULAY, J., CHE, S. L., GRUBB, A., GINSBERG, S. D., NIXON, R. A. & LEVY, E. 2010. Cystatin C rescues degenerating neurons in a cystatin B knockout mouse model of progressive myoclonus epilepsy. *American Journal of Pathology*, 177, 2256-2267.
- KAYED, R., HEAD, E., THOMPSON, J. L., MCINTIRE, T. M., MILTON, S. C., COTMAN, C. W. & GLABE, C. G. 2003. Common structure of soluble amyloid oligomers implies common mechanism of pathogenesis. *Science*, 300, 486-489.
- KAYED, R., HEAD, E., SARSOZA, F., SAING, T., COTMAN, C. W., NECULA, M., MARGOL, L., WU, J., BREYDO, L., THOMPSON, J.L., RASOOL, S., GURLO, T., BUTLER, P. & GLABE, C. 2007. Fibril-specific, conformation-dependent antibodies recognize a generic epitope common to amyloid fibrils and fibrillar oligomers that is absent in prefibrillar oligomers. *Molecular Neurodegeneration*, 2, 18
- KAYED, R., PENSALFINI, A., MARGOL, L., SOKOLOV, Y., SARSOZA, F., HEAD, E., HALL, J. & GLABE, C. 2009. Annular protofibrils are a structurally and functionally distinct type of amyloid oligomer. *Journal of Biological Chemistry*, 284, 4230-4237.
- KEELEY, E. 2007. *Folding, Dimerisation and the Interaction with A $\beta_{1-40}$  of Human Cystatin C*. PhD thesis, University of Sheffield.
- KELLY, J. W. 2000. Mechanisms of amyloidogenesis. *Nature Structural Biology*, 7, 824-826.
- KHETERPAL, I., WILLIAMS, A., MURPHY, C., BLEDSOE, B. & WETZEL, R. 2001. Structural features of the A $\beta$  amyloid fibril elucidated by limited proteolysis. *Biochemistry*, 40, 11757-11767.

- KINGHORN, K. J., CROWTHER, D. C., SHARP, L. K., NERELIUS, C., DAVIS, R. L., CHANG, H. T., GREEN, C., GUBB, D. C., JOHANSSON, J. & LOMAS, D. A. 2006. Neuroserpin binds A $\beta$  and is a neuroprotective component of amyloid plaques in Alzheimer disease. *Journal of Biological Chemistry*, 281, 29268-29277.
- KINGHAM, P. J. & POCOCK, J. M. 2001. Microglial secreted cathepsin B induces neuronal apoptosis. *Journal of Neurochemistry*, 2001, 76, 1475-1484.
- KODALI, R. & WETZEL, R. 2007. Polymorphism in the intermediates and products of amyloid assembly. *Current Opinion in Structural Biology*, 17, 48-57.
- KOŁODZIEJCZYK, R., MICHALSKA, K., HERNANDEZ-SANTOYO, A., WAHLBOM, M., GRUBB, A. & JASKOLSKI, M. 2010. Crystal structure of human cystatin C stabilized against amyloid formation. *Febs Journal*, 277, 1726-1737.
- KOO, E.H. & SQUAZZO, S.L. 1994. Evidence that production and release of amyloid- $\beta$  protein involves the endocytic pathway. *The Journal of Biological Chemistry*, 269, 17386-17389,
- KRANENBURG, O., BOUMA, B., KROON-BATENBURG, L. M. J., REIJERKERK, A., WU, Y. P., VOEST, E. E. & GEBBINK, M. 2002. Tissue type plasminogen activator is a multiligand cross- $\beta$  structure receptor. *Current Biology*, 12, 1833-1839.
- KUMAR-SINGH, S., DE JONGHE, C., CRUTS, M., KLEINERT, R., WANG, R., MERCKEN, M., DE STROOPER, B., VANDERSTICHELE, H., LOFGREN, A., VANDERHOEVEN, I., BACKHOVENS, H., VANMECHELEN, E., KROISEL, P. M. & VAN BROECKHOVEN, C. 2000. Nonfibrillar diffuse amyloid deposition due to a  $\gamma(42)$ -secretase site mutation points to an essential role for N-truncated A $\beta_{42}$  in Alzheimer's disease. *Human Molecular Genetics*, 9, 2589-2598.
- KUO, Y. M., KOKJOHN, T. A., KALBACK, W., LUEHRS, D., GALASKO, D. R., CHEVALLIER, N., KOO, E. H., EMMERLING, M. R. & ROHER, A. E. 2000. Amyloid- $\beta$  peptides interact with plasma proteins and erythrocytes: Implications for their quantitation in plasma. *Biochemical and Biophysical Research Communications*, 268, 750-756.
- LAMB, B. T., SISODIA, S. S., LAWLER, A. M., SLUNT, H. H., KITT, C. A., KEARNS, W. G., PEARSON, P. L., PRICE, D. L. & GEARHART, J. D. 1993. Introduction and expression of the 400 kilobase precursor amyloid protein gene in transgenic mice. *Nat Genet*, 5, 22-30.
- LANG, A. E. & LOZANO, A. M. 1998. Parkinson's disease - First of two parts. *New England Journal of Medicine*, 339, 1044-1053.
- LANSBURY, P. T. 1999. Evolution of amyloid: What normal protein folding may tell us about fibrillogenesis and disease. *Proceedings of the National Academy of Sciences of the United States of America*, 96, 3342-3344.
- LASHUEL, H. A., HARTLEY, D., PETRE, B. M., WALZ, T. & LANSBURY, P. T. 2002. Neurodegenerative disease - Amyloid pores from pathogenic mutations. *Nature*, 418, 291-291.
- LASHUEL, H. A. & LANSBURY, P. T. 2006. Are amyloid diseases caused by protein aggregates that mimic bacterial pore-forming toxins? *Quarterly Reviews of Biophysics*, 39 (2), 167-201.
- LAUREN, J., GIMBEL, D. A., NYGAARD, H. B., GILBERT, J. W. & STRITTMATTER, S. M. 2009. Cellular prion protein mediates impairment of synaptic plasticity by amyloid- $\beta$  oligomers. *Nature*, 457, 1128-U84.
- LEE, E. K., HWANG, J. H., SHIN, D. Y., KIM, D. I. & YOO, Y. J. 2005. Production of recombinant amyloid-beta peptide 42 as an ubiquitin extension. *Protein Expression and Purification*, 40, 183-189.
- LESNE, S., KOH, M. T., KOTILINEK, L., KAYED, R., GLABE, C. G., YANG, A., GALLAGHER, M. & ASHE, K. H. 2006. A specific amyloid- $\beta$  protein assembly in the brain impairs memory. *Nature*, 440, 352-357.

- LEUNG-TACK, J., TAVERA, C., GENSAC, M. C., MARTINEZ, J. & COLLE, A. 1990a. Modulation of phagocytosis-associated respiratory burst by human cystatin C - Role of the N-terminal tetrapeptide Lys-Pro-Pro-Arg. *Experimental Cell Research*, 188, 16-22.
- LEUNG-TACK, L., TAVERA, C., MARTINEZ, J. & COLLE, A. 1990b. Neutrophil chemotactic activity is modulated by human cystatin C an inhibitor of cysteine proteases. *Inflammation*, 14, 247-258.
- LEVY, E., LOPEZOTIN, C., GHISO, J., GELTNER, D. & FRANGIONE, B. 1989. Stroke in Icelandic patients with Hereditary Amyloid Angiopathy is related to a mutation in the cystatin C gene, an inhibitor of cysteine proteases. *Journal of Experimental Medicine*, 169, 1771-1778.
- LEVY, E., SASTRE, M., KUMAR, A., GALLO, G., PICCARDO, P., GHETTI, B. & TAGLIAVINI, F. 2001. Codeposition of cystatin C with amyloid- $\beta$  protein in the brain of Alzheimer disease patients. *Journal of Neuropathology and Experimental Neurology*, 60, 94-104.
- LI, X. & BUXBAUM, J. N. 2011. Transthyretin and the brain re-visited: Is neuronal synthesis of transthyretin protective in Alzheimer's disease? *Molecular Neurodegeneration*, 6, 79-96.
- LI, X. Y., MASLIAH, E., REIXACH, N. & BUXBAUM, J. N. 2011. Neuronal production of transthyretin in human and murine Alzheimer's disease: Is it protective? *Journal of Neuroscience*, 31, 12483-12490.
- LI, X. Y., ZHANG, X., LADIWALA, A. R. A., DU, D. G., YADAV, J. K., TESSIER, P. M., WRIGHT, P. E., KELLY, J. W. & BUXBAUM, J. N. 2013. Mechanisms of transthyretin inhibition of  $\beta$ -amyloid aggregation *in vitro*. *Journal of Neuroscience*, 33, 19423-19433.
- LINDAHL, P., NYCANDER, M., YLINENJARVI, K., POL, E. & BJORK, I. 1992. Characterization by rapid kinetic and equilibrium methods of the interaction between N-terminally truncated forms of chicken cystatin and the cysteine proteinases papain and actinidin. *Biochemical Journal*, 286, 165-171.
- LINK, C. D. 1995. Expression of human  $\beta$ -amyloid peptide in transgenic *Caenorhabditis elegans*. *Proceedings of the National Academy of Sciences of the United States of America*, 92, 9368-9372.
- LIU, L. & MURPHY, R. M. 2006. Kinetics of inhibition of  $\beta$ -amyloid aggregation by transthyretin. *Biochemistry*, 45, 15702-15709.
- LORENZO, A. & YANKNER, B. A. 1994.  $\beta$ -amyloid neurotoxicity requires fibril formation and is inhibited by Congo Red. *Proceedings of the National Academy of Sciences of the United States of America*, 91, 12243-12247.
- LU, J. X., QIANG, W., YAU, W. M., SCHWIETERS, C. D., MEREDITH, S. C. & TYCKO, R. 2013. Molecular structure of  $\beta$ -amyloid fibrils in Alzheimer's disease brain tissue. *Cell*, 154, 1257-1268.
- LUE, L.F., KUO, Y.M., ROHER, A.E., BRACHOVA, L., SHEN, Y., SUE, L., BEACH, T., KURTH, J.H., RYDEL, R.E. & ROGERS, J. 2000. Soluble amyloid- $\beta$  peptide concentration as a predictor of synaptic change in Alzheimer's disease. *American journal of pathology*, 155, 853-862.
- MA, B. & NUSSINOV, R. 2006. Simulations as analytical tools to understand protein aggregation and predict amyloid conformation. *Current Opinion in Chemical Biology*, 10, 445-452.
- MACAO, B., HOYER, W., SANDBERG, A., BRORSSON, A. C., DOBSON, C. M. & HARD, T. 2008. Recombinant amyloid- $\beta$  peptide production by coexpression with an affibody ligand. *BMC Biotechnology*, 8, 11.
- MACKIC, J. B., WEISS, M. H., MIAO, W., KIRKMAN, E., GHISO, J., CALERO, M., BADING, J., FRANGIONE, B. & ZLOKOVIC, B. V. 1998. Cerebrovascular accumulation and increased blood-brain barrier permeability to circulating Alzheimer's amyloid- $\beta$  peptide in aged squirrel monkey with cerebral amyloid angiopathy. *Journal of Neurochemistry*, 70, 210-215.

- MAKIN, O. S., ATKINS, E., SIKORSKI, P., JOHANSSON, J. & SERPELL, L. C. 2005. Molecular basis for amyloid fibril formation and stability. *Proceedings of the National Academy of Sciences of the United States of America*, 102, 315-320.
- MAKIN, O. S. & SERPELL, L. C. 2005. Structures for amyloid fibrils. *Febs Journal*, 272, 5950-5961.
- MARUYAMA, K., IKEDA, S. I., ISHIHARA, T., ALLSOP, D. & YANAGISAWA, N. 1990. Immunohistochemical characterization of cerebrovascular amyloid in 46 autopsied cases using antibodies to  $\beta$ -protein and cystatin C. *Stroke*, 21, 397-403.
- MATSUZAKI, K. 2007. Physicochemical interactions of amyloid peptide with lipid bilayers. *Biochimica Et Biophysica Acta-Biomembranes*, 1768, 1935-1942.
- MAZURKOLECKA, B., FRACKOWIAK, J. & WISNIEWSKI, H. M. 1995. Apolipoproteins  $\epsilon 3$  and  $\epsilon 4$  induce, and transthyretin prevents accumulation of the Alzheimer's  $\beta$ -amyloid peptide in cultured vascular smooth muscle cells. *Brain Research*, 698, 217-222.
- MCLAURIN, J., YANG, D. S., YIP, C. M. & FRASER, P. E. 2000. Review: Modulating factors in amyloid- $\beta$  fibril formation. *Journal of Structural Biology*, 130, 259-270.
- MCCLEAN, C.A., CHERNY, R.A., FRASER, F.W., FULLER, S.J., SMITH, M.J., BEYREUTHER, K., BUSH, A.I. & MASTERS, C.L. 1999. Soluble pool of A $\beta$  amyloid as a determinant of severity of neurodegeneration in Alzheimer's disease. *Annals of Neurology*, 46, 860-866.
- MEINHARDT, J., SACHSE, C., HORTSCHANSKY, P., GRIGORIEFF, N. & FANDRICH, M. 2009. A $\beta_{1-40}$  fibril polymorphism implies diverse interaction patterns in amyloid fibrils. *Journal of Molecular Biology*, 386, 869-877.
- MEYER-LUEHMANN, M., COOMARASWAMY, J., BOLMONT, T., KAESER, S., SCHAEFER, C., KILGER, E., NEUENSCHWANDER, A., ABRAMOWSKI, D., FREY, P., JATON, A.L., VIGOURET, J.-M., PAGANETTI, P., WALSH, D.M., MATHEWS, P.M., GHISO, J., STAUFENBIEL, M., WALKER, L.C. & JUCKER, M. 2006. Exogenous induction of cerebral  $\beta$ -amyloidogenesis is governed by agent and host. *Science*, 313, 1781-1784.
- MI, W., PAWLIK, M., SASTRE, M., JUNG S. S., RADVINSKY, D. S., KLEIN, A. M., SOMMER, J., SCHMIDT, S.D., NIXON, R.A., MATHEWS, P. M. & LEVY, E. 2007. Cystatin C inhibits amyloid- $\beta$  deposition in Alzheimer's disease mouse models. *Nature Genetics*, 39, 1440-1442.
- MORGAN, G. J., GIANNINI, S., HOUNSLOW, A. M., CRAVEN, C. J., ZEROVNIK, E., TURK, V., WALTHO, J. P. & STANFORTH, R. A. 2008. Exclusion of the native alpha-helix from the amyloid fibrils of a mixed alpha/beta protein. *Journal of Molecular Biology*, 375, 487-498.
- MUELLER-STEINER, S., ZHOU, Y., ARAI, H., ROBERSON, E.D., SUN, B., CHEN, J., WANG, X., YU, G., ESPOSITO, L., MUCKE, L., GAN, L. 2006. Anti-amyloidogenic and neuroprotective functions of cathepsin B: Implications for Alzheimer's disease. *Neuron*, 51, 703-714.
- MURRAY, A. N., SOLOMON, J. P., WANG, Y.-J., BALCH, W. E. & KELLY, J. W. 2010. Discovery and characterization of a mammalian amyloid disaggregation activity. *Protein Science*, 19, 836-846.
- MUSSAP, M. & PLEBANI, M. 2004. Biochemistry and clinical role of human cystatin C. *Critical Reviews in Clinical Laboratory Sciences*, 41, 467-550.
- MYERS, S. L., THOMSON, N. H., RADFORD, S. E. & ASHCROFT, A. E. 2006. Investigating the structural properties of amyloid-like fibrils formed in vitro from  $\beta_2$ -microglobulin using limited proteolysis and electrospray ionisation mass spectrometry. *Rapid Communications in Mass Spectrometry*, 20, 1628-1636.
- NAGATA-UCHIYAMA, M., YAGUCHI, M., HIRANO, Y. & UEDA, T. 2007. Expression and purification of uniformly N-15-labelled amyloid- $\beta$  peptide 1-40 in *Escherichia coli*. *Protein and Peptide Letters*, 14, 788-792.

- NÄSLUND, J., HAROUTUNIAN, V., MOHS, R., DAVIS, K. L., DAVIES, P., GREENGARD, P. & BUXBAUM, J. D. 2000. Correlation between elevated levels of amyloid- $\beta$  peptide in the brain and cognitive decline. *Journal American Medical Association*, 283, 1571-1577.
- NICOLL, A. J., PANICO, S., FREIR, D. B., WRIGHT, D., TERRY, C., RISSE, E., HERRON, C. E., O'MALLEY, T., WADSWORTH, J. D. F., FARROW, M. A., WALSH, D. M., SAIBIL, H. R. & COLLINGE, J. 2013. Amyloid- $\beta$  nanotubes are associated with prion protein-dependent synaptotoxicity. *Nature Communications*, 4, 2416.
- NIELSEN, L., KHURANA, R., COATS, A., FROKJAER, S., BRANGE, J., VYAS, S., UVERSKY, V.N. & FINK, A.L. 2001. Effect of environmental factors on the kinetics of insulin fibril formation: Elucidation of the molecular mechanism. *Biochemistry*, 40 (20), 6036-6046
- NILSSON, M., WANG, X., RODZIEWICZ-MOTOWIDLO, S., JANOWSKI, R., LINDSTROM, V., ONNERFJORD, P., WESTERMARK, G., GRZONKA, Z., JASKOLSKI, M. & GRUBB, A. 2004. Prevention of domain swapping inhibits dimerization and amyloid fibril formation of cystatin C - Use of engineered disulfide bridges, antibodies, and carboxymethylpapain to stabilize the monomeric form of cystatin C. *Journal of Biological Chemistry*, 279, 24236-24245.
- NORTH, M. J., MOTTRAM, J. C. & COOMBS, G. H. 1990. Cysteine proteinases of parasitic protozoa. *Parasitology Today*, 6, 270-275.
- OHNISHI, S. & TAKANO, K. 2004. Amyloid fibrils from the viewpoint of protein folding. *Cellular and Molecular Life Sciences*, 61, 511-524.
- OLAFSSON, I., GUDMUNDSSON, G., ABRAHAMSON, M., JENSSON, O. & GRUBB, A. 1990. The amino terminal portion of cerebrospinal fluid cystatin C in Hereditary Cystatin C Amyloid Angiopathy is not truncated - Direct sequence analysis from agarose gel electropherograms. *Scandinavian Journal of Clinical & Laboratory Investigation*, 50, 85-93.
- ORLIKOWSKA, M., JANKOWSKA, E., KOLODZIEJCZYK, R., JASKOLSKI, M. & SZYMANSKA, A. 2011. Hinge-loop mutation can be used to control 3D domain swapping and amyloidogenesis of human cystatin C. *Journal of Structural Biology*, 173, 406-413.
- PALSDOTTIR, A., SNORRADOTTIR, A. O. & THORSTEINSSON, L. 2006. Hereditary Cystatin C Amyloid Angiopathy: Genetic, clinical, and pathological aspects. *Brain pathology (Zurich, Switzerland)*, 16, 55-9.
- PARAVASTU, A. K., LEAPMAN, R. D., YAU, W.-M. & TYCKO, R. 2008. Molecular structural basis for polymorphism in Alzheimer's  $\beta$ -amyloid fibrils. *Proceedings of the National Academy of Sciences of the United States of America*, 105, 18349-18354.
- PARAVASTU, A. K., QAHWASH, I., LEAPMAN, R. D., MEREDITH, S. C. & TYCKO, R. 2009. Seeded growth of  $\beta$ -amyloid fibrils from Alzheimer's brain-derived fibrils produces a distinct fibril structure. *Proceedings of the National Academy of Sciences of the United States of America*, 106, 7443-7448.
- PEPYS, M. B. 1996. *Oxford Textbook of Medicine*, Oxford, Oxford : Oxford University Press, 1996.
- PERUTZ, M. F. 1999. Glutamine repeats and neurodegenerative diseases: Molecular aspects. *Trends in Biochemical Sciences*, 24, 58-63.
- PETKOVA, A. T., LEAPMAN, R. D., GUO, Z. H., YAU, W. M., MATTSON, M. P. & TYCKO, R. 2005. Self-propagating, molecular level polymorphism in Alzheimer's  $\beta$ -amyloid fibrils. *Science*, 307, 262-265.
- PETKOVA, A. T., YAU, W. M. & TYCKO, R. 2006. Experimental constraints on quaternary structure in Alzheimer's  $\beta$ -amyloid fibrils. *Biochemistry*, 45, 498-512.
- PRUSINER, S. B. 1982. Novel proteinaceous infectious particles cause scrapie. *Science*, 216, 136-144.
- PRUSINER, S. B. 1998. Prions. *Proceedings of the National Academy of Sciences of the United States of America*, 95, 13363-13383.

- RAWLINGS, N. D. & BARRETT, A. J. 1990. Evolution of proteins of the cystatin superfamily. *Journal of Molecular Evolution*, 30, 60-71.
- REIXACH, N., DEECHONGKIT, S., JIANG, X., KELLY, J. W. & BUXBAUM, J. N. 2004. Tissue damage in the amyloidoses: Transthyretin monomers and nonnative oligomers are the major cytotoxic species in tissue culture. *Proceedings of the National Academy of Sciences of the United States of America*, 101, 2817-2822.
- REVESZ, T., GHISO, J., LASHLEY, T., PLANT, G., ROSTAGNO, A., FRANGIONE, B. & HOLTON, J. L. 2003. Cerebral amyloid angiopathies: A pathologic, biochemical, and genetic view. *Journal of Neuropathology and Experimental Neurology*, 62, 885-898.
- RICHARDSON, J. S. & RICHARDSON, D. C. 2002. Natural  $\beta$ -sheet proteins use negative design to avoid edge-to-edge aggregation. *Proceedings of the National Academy of Sciences of the United States of America*, 99, 2754-2759.
- RIETSCHEL, B., ARREY, T. N., MEYER, B., BORNEMANN, S., SCHUERKEN, M., KARAS, M. & POETSCH, A. 2009. Elastase Digests new ammunition for shotgun membrane proteomics. *Molecular & Cellular Proteomics*, 8, 1029-1043.
- ROCHET, J. C. & LANSBURY, P. T. 2000. Amyloid fibrillogenesis: themes and variations. *Current Opinion in Structural Biology*, 10, 60-68.
- RUSHWORTH, J. V. & HOOPER, N. M. 2010. Lipid rafts: Linking Alzheimer's amyloid- $\beta$  production, aggregation, and toxicity at neuronal membranes. *International journal of Alzheimer's disease*, 2011, 603052.
- SAMBROOK, J., FRITSCH, E. F. & MANIATIS, T. 1989. *Molecular Cloning: A Laboratory Manual. Second Edition vols. 1 2 and 3.*
- SANCHEZ, L., MADURGA, S., PUKALA, T., VILASECA, M., LOPEZ-IGLESIAS, C., ROBINSON, C. V., GIRALT, E. & CARULLA, N. 2011. A $\beta$ <sub>40</sub> and A $\beta$ <sub>42</sub> amyloid fibrils exhibit distinct molecular recycling properties. *Journal of the American Chemical Society*, 133, 6505-6508.
- SANDBERG, A., LUHESHI, L. M., SOLLVANDER, S., DE BARROS, T. P., MACAO, B., KNOWLES, T. P. J., BIVERSTAL, H., LENDEL, C., EKHOLM-PETTERSON, F., DUBNOVITSKY, A., LANNFELT, L., DOBSON, C. M. & HARD, T. 2010. Stabilization of neurotoxic Alzheimer amyloid- $\beta$  oligomers by protein engineering. *Proceedings of the National Academy of Sciences of the United States of America*, 107, 15595-15600.
- SANDERS, A., CRAVEN, C. J., HIGGINS, L. D., GIANNINI, S., CONROY, M. J., HOUNSLOW, A. M., WALTHO J. P., AND STANIFORTH R. A. (2004). Cystatin forms a tetramer through structural rearrangement of domain swapped dimers prior to amyloidogenesis. *Journal of Molecular Biology*, 336, 165-178.
- SASTRE, M., CALERO, M., PAWLIK, M., MATHEWS, P. M., KUMAR, A., DANILOV, V., SCHMIDT, S. D., NIXON, R. A., FRANGIONE, B. & LEVY, E. 2004. Binding of cystatin C to Alzheimer's amyloid- $\beta$  inhibits in vitro amyloid fibril formation. *Neurobiology of Aging*, 25, 1033-1043.
- SCHEIDT, H. A., MORGADO, I., ROTHEMUND, S., HUSTER, D. & FANDRICH, M. 2011. Solid-state NMR spectroscopic investigation of A $\beta$  protofibrils: Implication of A $\beta$ -sheet remodeling upon maturation into terminal amyloid fibrils. *Angewandte Chemie-International Edition*, 50, 2837-2840.
- SCHEUNER, D., ECKMAN, C., JENSEN, M., SONG, X., CITRON, M., SUZUKI, N., BIRD, T. D., HARDY, J., HUTTON, M., KUKULL, W., LARSON, E., LEVYLAHAD, E., VIITANEN, M., PESKIND, E., POORKAJ, P., SCHELLENBERG, G., TANZI, R., WASCO, W., LANNFELT, L., SELKOE, D. & YOUNKIN, S. 1996. Secreted amyloid- $\beta$  protein similar to that in the senile plaques of Alzheimer's disease is increased in vivo by the presenilin 1 and 2 and APP mutations linked to familial Alzheimer's disease. *Nature Medicine*, 2, 864-870.

- SCHWARZMAN, A. L., GREGORI, L., VITEK, M. P., LYUBSKI, S., STRITTMATTER, W. J., ENGHILDE, J. J., BHASIN, R., SILVERMAN, J., WEISGRABER, K. H., COYLE, P. K., ZAGORSKI, M. G., TALAFIOUS, J., EISENBERG, M., SAUNDERS, A. M., ROSES, A. D. & GOLDGABER, D. 1994. Transthyretin sequesters amyloid- $\beta$  protein and prevents amyloid formation. *Proceedings of the National Academy of Sciences of the United States of America*, 91, 8368-8372.
- SELENICA, M. L., WANG, X., OSTERGAARD-PEDERSEN, L., WESTLIND-DANIELSSON, A. & GRUBB, A. 2007. Cystatin C reduces the *in vitro* formation of soluble A $\beta_{1-42}$  oligomers and protofibrils. *Scandinavian Journal of Clinical & Laboratory Investigation*, 67, 179-190.
- SELKOE, D. J. & SCHENK, D. 2003. Alzheimer's disease: Molecular understanding predicts amyloid-based therapeutics. *Annual Review of Pharmacology and Toxicology*, 43, 545-584.
- SEMISOTNOV, G. V., KIHARA, H., KOTOVA, N. V., KIMURA, K., AMEMIYA, Y., WAKABAYASHI, K., SERDYUK, I. N., TIMCHENKO, A. A., CHIBA, K., NIKAIIDO, K., IKURA, T. & KUWAJIMA, K. 1996. Protein globularization during folding. A study by synchrotron small-angle X-ray scattering. *Journal of Molecular Biology*, 262, 559-574.
- SERIO, T. R., CASHIKAR, A. G., KOWAL, A. S., SAWICKI, G. J., MOSLEHI, J. J., SERPELL, L., ARNSDORF, M. F. & LINDQUIST, S. L. 2000. Nucleated conformational conversion and the replication of conformational information by a prion determinant. *Science*, 289, 1317-1321.
- SERPELL, L. C. 2000. Alzheimer's amyloid fibrils: Structure and assembly. *Biochimica Et Biophysica Acta-Molecular Basis of Disease*, 1502, 16-30.
- SERPELL, L. C. & SMITH, J. M. 2000. Direct visualisation of the  $\beta$ -sheet structure of synthetic Alzheimer's amyloid. *Journal of Molecular Biology*, 299, 225-231.
- SHANKAR, G. M., BLOODGOOD, B. L., TOWNSEND, M., WALSH, D. M., SELKOE, D. J. & SABATINI, B. L. 2007. Natural oligomers of the Alzheimer amyloid- $\beta$  protein induce reversible synapse loss by modulating an NMDA-type glutamate receptor dependent signaling pathway. *Journal of Neuroscience*, 27, 2866-2875.
- SHAHNAWAZ, M., THAPA, A. & PARK, I. S. 2007. Stable activity of a deubiquitylating enzyme (Usp2-cc) in the presence of high concentrations of urea and its application to purify aggregation-prone peptides. *Biochemical and Biophysical Research Communications*, 359, 801-805.
- SHAO, H., JAO, S., MA, J. & ZAGORSKI, M. 1999. Solution structures of micelle-bound amyloid- $\beta_{1-40}$  and - $\beta_{1-42}$  peptides of Alzheimer's disease. *Journal of Molecular Biology*, 285, 755-773.
- SHIRAHAM, T. & COHEN, A. S. 1967. High-resolution electron microscopic analysis of amyloid fibril. *Journal of Cell Biology*, 33, 679-708.
- SIPE, J. D., BENSON, M. D., BUXBAUM, J. N., IKEDA, S.-I., MERLINI, G., SARAIVA, M. J. M. & WESTERMARK, P. 2010. Amyloid fibril protein nomenclature: 2010 recommendations from the nomenclature committee of the International Society of Amyloidosis. *Amyloid*, 17, 101-104.
- SIPE, J. D., BENSON, M. D., BUXBAUM, J. N., IKEDA, S.-I., MERLINI, G., SARAIVA, M. J. M. & WESTERMARK, P. 2012. Amyloid fibril protein nomenclature: 2012 recommendations from the nomenclature committee of the International Society of Amyloidosis. *Amyloid*, 19, 167-170.
- SIPE, J. D. & COHEN, A. S. 2000. Review: History of the amyloid fibril. *Journal of Structural Biology*, 130, 88-98.
- SISODIA, S.S., ANNAERT, W., KIM, S.-H. & DE STROOPER, B. 2001.  $\gamma$ -Secretase: Never more enigmatic. *Trends in neuroscience*, 24, S1-S6.
- SKERGET, K., VILFAN, A., POMPE-NOVAK, M., TURK, V., WALTHO, J. P., TURK, D. & ZEROVNIK, E. 2009. The mechanism of amyloid-fibril formation by stefin B: Temperature and

protein concentration dependence of the rates. *Proteins - Structure, Function and Bioinformatics*, 74, 425-436.

- SKERGET, K., TALER-VERCIC, A., BAVDEK, A., HODNIK, V., CERU, S., TUSEK-ZNIDARIC, M., KUMM, T., PITSI, D., POMPE-NOVAK, M., PALUMAA, P., SORIANO, S., KOPITAR-JERALA, N., TURK, V., ANDERLUH, G. & ZEROVNIK, E. 2010. Interaction between oligomers of Stefin B and Amyloid- $\beta$  *in vitro* and in cells. *Journal of Biological Chemistry*, 285 (5), 3201-3210.
- SLEEGERS, K., LAMBERT, J.-C., BERTRAM, L., CRUTS, M., AMOUYEL, P. & VAN BROECKHOVEN, C. 2010. The pursuit of susceptibility genes for Alzheimer's disease: Progress and prospects. *Trends in Genetics*, 26, 84-93.
- SMALL, D. H., MOK, S. S. & BORNSTEIN, J. C. 2001. Alzheimer's disease and AP toxicity: From top to bottom. *Nature Reviews Neuroscience*, 2, 595-598.
- SOUZA, J. M., GIASSON, B. I., CHEN, Q., LEE, V. M. & ISCHIROPOULOS, H. 2000. Dityrosine cross-linking promotes formation of stable  $\alpha$ -synuclein polymers. Implication of nitrative and oxidative stress in the pathogenesis of neurodegenerative synucleinopathies. *Journal of Biological Chemistry*, 275, 18344-18349.
- SOUSA, M. M., CARDOSO, I., FERNANDES, R., GUIMARAES, A. & SARAIVA, M. J. 2001. Deposition of transthyretin in early stages of familial amyloidotic polyneuropathy - Evidence for toxicity of nonfibrillar aggregates. *American Journal of Pathology*, 159, 1993-2000.
- STANIFORTH, R. A., GIANNINI, S., HIGGINS, L. D., CONROY, M. J., HOUNSLOW, A. M., JERALA, R., CRAVEN, C. J. & WALTHO, J. P. 2001. Three-dimensional domain swapping in the folded and molten-globule states of cystatins, an amyloid-forming structural superfamily. *Embo Journal*, 20, 4774-4781.
- STANYON, H. F. & VILES, J. H. 2012. Human serum albumin can regulate amyloid- $\beta$  peptide fiber growth in the brain interstitium. Implications for Alzheimer's disease. *Journal of Biological Chemistry*, 287, 28163-28168.
- STEIN, T. D., ANDERS, N. J., DECARLI, C., CHAN, S. L., MATTSON, M. P. & JOHNSON, J. A. 2004. Neutralization of transthyretin reverses the neuroprotective effects of secreted amyloid precursor protein (APP) in APP(Sw) mice resulting in tau phosphorylation and loss of hippocampal neurons: Support for the amyloid hypothesis. *Journal of Neuroscience*, 24, 7707-7717.
- STEIN, T. D. & JOHNSON, J. A. 2002. Lack of neurodegeneration in transgenic mice overexpressing mutant amyloid precursor protein is associated with increased levels of transthyretin and the activation of cell survival pathways. *Journal of Neuroscience*, 22, 7380-7388.
- STEINHOFF, T., MORITZ, E., WOLLMER, M. A., MOHAJERI, M. H., KINS, S. & NITSCH, R. M. 2001. Increased cystatin C in astrocytes of transgenic mice expressing the K670N-M671L mutation of the amyloid precursor protein and deposition in brain amyloid plaques. *Neurobiology of Disease*, 8, 647-654.
- STEVENS, L. A., CORESH, J., GREENE, T. & LEVEY, A. S. 2006. Medical progress - Assessing kidney function - Measured and estimated glomerular filtration rate. *New England Journal of Medicine*, 354, 2473-2483.
- STICHT, H., BAYER, P., WILLBOLD, D., DAMES, S., HILBICH, C., BEYREUTHER, K., FRANK, R. & ROSCH, P. 1995. Structure of amyloid A $\beta_{1-40}$  peptide of Alzheimer's disease, *European Journal of Biochemistry*, 233, 293-298.
- STINE, W. B., DAHLGREN, K. N., KRAFFT, G. A. & LADU, M. J. 2003. In vitro characterization of conditions for amyloid- $\beta$  peptide oligomerization and fibrillogenesis. *Journal of Biological Chemistry*, 278, 11612-11622.

- STOEHR, J., CONDELLO, C., WATTS, J.C., BLOCH, L., OEHLER, A., NICK, M., DEARMOND, S.J., GILES, K., DEGRADO, W.F. & PRUSINER, S.B. 2014. Distinct synthetic A $\beta$  prion strains producing different amyloid deposits in bigenic mice. *Proceedings of the National Academy of Sciences of the United States of America*, 111, 10329-10334.
- STOREY, E. & CAPPAL, R. 1999. The amyloid precursor protein of Alzheimer's disease and the A $\beta$  peptide. *Neuropathology and Applied Neurobiology*, 25, 81-97.
- SUN, B. G., ZHOU, Y. G., HALABISKY, B., LO, I., CHO, S. H., MUELLER-STEINER, S., DEVIDZE, N., WANG, X., GRUBB, A. & GAN, L. 2008. Cystatin C-cathepsin B axis regulates amyloid- $\beta$  levels and associated neuronal deficits in an animal model of Alzheimer's disease. *Neuron*, 60, 247-257.
- SUNDE, M., SERPELL, L. C., BARTLAM, M., FRASER, P. E., PEPYS, M. B. & BLAKE, C. C. F. 1997. Common core structure of amyloid fibrils by synchrotron X-ray diffraction. *Journal of Molecular Biology*, 273, 729-739.
- TAUPIN, P., RAY, J., FISCHER, W. H., SUHR, S. T., HAKANSSON, K., GRUBB, A. & GAGE, F. H. 2000. FGF-2-responsive neural stem cell proliferation requires CCG, a novel autocrine/paracrine cofactor. *Neuron*, 28, 385-397.
- THAPA, A., SHAHNAWAZ, M., KARKI, P., DAHAL, G. R., SHAROAR, M. G., SHIN, S. Y., LEE, J. S., CHO, B. & PARK, I. S. 2008. Purification of inclusion body-forming peptides and proteins in soluble form by fusion to *Escherichia coli* thermostable proteins. *Biotechniques*, 44, 787-796.
- THINAKARAN, G. & KOO, E. H. 2008. Amyloid precursor protein trafficking, processing, and function. *Journal of Biological Chemistry*, 283, 29615-29619.
- THOMAS, T., THOMAS, G., MCLENDON, C., SUTTON, T. & MULLAN, M. 1996.  $\beta$ -Amyloid mediated vasoactivity and vascular endothelial damage. *Nature*, 380, 168-171.
- THOMPSON, R. C. & BLOUT, E. R. 1973. Restrictions on binding of proline-containing peptides to elastase. *Biochemistry*, 12, 51-57.
- THORNTON, E., VINK, R., BLUMBERGS, P. C. & VAN DEN HEUVEL, C. 2006. Soluble amyloid precursor protein a reduces neuronal injury and improves functional outcome following diffuse traumatic brain injury in rats. *Brain Research*, 1094, 38-46.
- TIZON, B., RIBE, E. M., MI, W., TROY, C. M. & LEVY, E. 2010. Cystatin C protects neuronal cells from amyloid- $\beta$ -induced toxicity. *Journal of Alzheimers Disease*, 19, 885-894.
- TJERNBERG, L., HOSIA, W., BARK, N., THYBERG, J., & JOHANSSON, J. 2002. Charge attraction and beta propensity are necessary for amyloid fibril formation of tetrapeptides. *Journal of Biological Chemistry*, 277, 43243-43246.
- TURK, V. & BODE, W. 1991. The cystatins - Protein inhibitors of cysteine proteinases. *Febs Letters*, 285, 213-219.
- TYCKO, R., SCIARETTA, K.L., ORGEL, J. & MEREDITH, S.C. 2009. Evidence for novel  $\beta$ -sheet structures in Iowa mutant  $\beta$ -amyloid fibrils. *Biochemistry*, 48, 6072-6084.
- TYCKO, R. 2011. Solid-state NMR studies of amyloid fibril structure. *Annual Review of Physical Chemistry*, 62, 279-299.
- UPTAIN, S. M. & LINDQUIST, S. 2002. Prions as protein-based genetic elements. *Annual Review of Microbiology*, 56, 703-741.
- UTSUMI, M., YAMAGUCHI, Y., SASAKAWA, H., YAMAMOTO, N., YANAGISAWA, K. & KATO, K. 2009. Up-and-down topological mode of amyloid- $\beta$  peptide lying on hydrophilic/hydrophobic interface of ganglioside clusters. *Glycoconjugate Journal*, 26, 999-1006.

- VETRIVEL, K. S. & THINAKARAN, G. 2010. Membrane rafts in Alzheimer's disease  $\beta$ -amyloid production. *Biochimica Et Biophysica Acta-Molecular and Cell Biology of Lipids*, 1801, 860-867.
- VIGOPELFREY, C., LEE, D., KEIM, P., LIEBERBURG, I. & SCHENK, D. B. 1993. Characterization of  $\beta$ -amyloid peptide from human cerebrospinal fluid. *Journal of Neurochemistry*, 61, 1965-1968.
- VILES, J. H., COHEN, F. E., PRUSINER, S. B., GOODIN, D. B., WRIGHT, P. E. & DYSON, H. J. 1999. Copper binding to the prion protein: Structural implications of four identical cooperative binding sites. *Proceedings of the National Academy of Sciences of the United States of America*, 96, 2042-2047.
- VINTERS, H. V., NISHIMURA, G. S., SECOR, D. L. & PARDRIDGE, W. M. 1990. Immunoreactive A4 and  $\gamma$ -trace peptide colocalization in amyloidotic arteriolar lesions in brains of patients with Alzheimer's disease. *Am J Pathol*, 137, 233-40.
- WAHLBOM, M., WANG, X., LINDSTROM, V., CARLEMALM, E., JASKOLSKI, M. & GRUBB, A. 2007. Fibrillogenic oligomers of human cystatin C are formed by propagated domain swapping. *Journal of Biological Chemistry*, 282, 18318-18326.
- WALSH, D. M., LOMAKIN, A., BENEDEK, G. B., CONDRON, M. M. & TEPLow, D. B. 1997. Amyloid- $\beta$  protein fibrillogenesis - Detection of a protofibrillar intermediate. *Journal of Biological Chemistry*, 272, 22364-22372.
- WALSH, D. M., HARTLEY, D. M., KUSUMOTO, Y., FEZoui, Y., CONDRON, M. M., LOMAKIN, A., BENEDEK, G. B., SELKOE, D. J. & TEPLow, D. B. 1999. Amyloid  $\beta$ -protein fibrillogenesis - Structure and biological activity of protofibrillar intermediates. *Journal of Biological Chemistry*, 274, 25945-25952.
- WALSH, D. M., KLYUBIN, I., FADEEVA, J. V., CULLEN, W. K., ANWYL, R., WOLFE, M. S., ROWAN, M. J. & SELKOE, D. J. 2002. Naturally secreted oligomers of amyloid- $\beta$  protein potently inhibit hippocampal long-term potentiation *in vivo*. *Nature*, 416, 535-539.
- WALSH, D. M., THULIN, E., MINOGUE, A. M., GUSTAVSSON, N., PANG, E., TEPLow, D. B. & LINSE, S. 2009. A facile method for expression and purification of the Alzheimer's disease-associated amyloid- $\beta$  peptide. *FEBS Journal*, 276, 1266-1281.
- WANG, J., DICKSON, D.W., TROJANOWSKI, J.Q. & LEE, V.M.-Y. 1999. The levels of soluble versus insoluble brain A $\beta$  distinguish Alzheimer's disease from normal and pathologic aging. *Experimental Neurology* 158, 328-337.
- WARFEL, A. H., ZUCKERFRANKLIN, D., FRANGIONE, B. & GHISO, J. 1987. Constitutive secretion of cystatin C ( $\gamma$ -trace) by monocytes and macrophages and its down-regulation after stimulation. *Journal of Experimental Medicine*, 166, 1912-1917.
- WATTS, J.C., CONDELLO, C., STOEHR, J., OEHLER, A., LEE, J., DEARMOND, S.J., LANNFELT, L., INGELSSON, M., GILES, K. & PRUSINER, S.B. 2014. Serial propagation of distinct strains of A $\beta$  prions from Alzheimer's disease patients. *Proceedings of the National Academy of Sciences of the United States of America*, 111, 10323-10328.
- WELLER, J.A.R. & NICOLL, R.O. 2003. Cerebral amyloid angiopathy: Pathogenesis and effects on the ageing and Alzheimer brain. *Neurological Research*, 25, 611-616.
- WHITE, H. E., HODGKINSON, J. L., JAHN, T. R., COHEN-KRAUSZ, S., GOSAL, W. S., MULLER, S., ORLOVA, E. V., RADFORD, S. E. & SAIBIL, H. R. 2009. Globular tetramers of  $\beta_2$ -microglobulin assemble into elaborate amyloid fibrils. *Journal of Molecular Biology*, 389, 48-57.
- WILHELMUS, M. M. M., DE WAAL, R. M. W. & VERBEEK, M. M. 2007. Heat shock proteins and amateur chaperones in amyloid- $\beta$  accumulation and clearance in Alzheimer's disease. *Molecular Neurobiology*, 35, 203-216.

- WOLFE, L. S., CALABRESE, M. F., NATH, A., BLAHO, D. V., MIRANKER, A. D. & XIONG, Y. 2010. Protein-induced photophysical changes to the amyloid indicator dye thioflavin T. *Proceedings of the National Academy of Sciences of the United States of America*, 107, 16863-16868.
- XUE, W.-F., HOMANS, S. W., & RADFORD, S. E. 2009a. Amyloid fibril length distribution quantified by atomic force microscopy single particle image analysis. *Protein Engineering Design & Selection*, 22, 489-496.
- XUE, W.-F., HELLEWELL, A. L., GOSAL, W. S., HOMANS, S. W., HEWITT, E. W. & RADFORD, S. E. 2009b. Fibril fragmentation enhances amyloid cytotoxicity. *Journal of Biological Chemistry*, 284, 34272-34282.
- XUE, W.-F. & RADFORD, S.E. 2013. An imaging and systems modeling approach to fibril breakage enables prediction of amyloid behavior. *Biophysical Journal*, 105, 2811-2819.
- YAMADA, M. 2000. Cerebral amyloid angiopathy: An overview. *Neuropathology*, 20, 8-22.
- YAMADA, M., SODEYAMA, N., ITOH, Y., SUEMATSU, N., OTOMO, E., MATSUSHITA, M. & MIZUSAWA, H. 1997. Association of presenilin 1 polymorphism with cerebral amyloid angiopathy in the elderly. *Stroke*, 28, 2219-2221.
- YAMAMOTO, N., HASEGAWA, K., MATSUZAKI, K., NAIKI, H. & YANAGISAWA, K. 2004. Environment and mutation dependent aggregation behavior of Alzheimer's amyloid- $\beta$  protein. *Journal of Neurochemistry*, 90, 62-69.
- YANG, D. T., JOSHI, G., CHO, P. Y., JOHNSON, J. A. & MURPHY, R. M. 2013. Transthyretin as both a sensor and a scavenger of  $\beta$ -amyloid oligomers. *Biochemistry*, 52, 2849-2861.
- YOBURN, J. C., TIAN, W., BROWER, J. O., NOWICK, J. S., GLABE, C. G. & VAN VRANKEN, D. L. 2003. Dityrosine cross-linked A $\beta$  peptides: fibrillar beta-structure in A $\beta$ <sub>1-40</sub> is conducive to formation of dityrosine cross-links but a dityrosine cross-link in A $\beta$ <sub>8-14</sub> does not induce  $\beta$ -structure. *Chemical Research Toxicology*, 16, 531-535.
- YOSHIKE, Y., AKAGI, T. & TAKASHIMA, A. 2007. Surface structure of amyloid- $\beta$  fibrils contributes to cytotoxicity. *Biochemistry*, 46, 9805-9812.
- YOUNAN, N. D., SARELL, C. J., DAVIES, P., BROWN, D. R. & VILES, J. H. 2013. The cellular prion protein traps Alzheimer's A $\beta$  in an oligomeric form and disassembles amyloid fibers. *FASEB Journal*, 27, 1847-1858.
- ZAGORSKI, M. G. & BARROW, C. J. 1992. NMR studies of amyloid  $\beta$ -peptides - proton assignments, secondary structure, and mechanism of an  $\alpha$ -helix -  $\beta$ -sheet conversion for a homologous, 28 residue, N-terminal fragment. *Biochemistry*, 31, 5621-5631.
- ZAGORSKI, M. G., YANG, J., SHAO, H. Y., MA, K., ZENG, H. & HONG, A. 1999. Methodological and chemical factors affecting amyloid beta peptide amyloidogenicity. *Methods in Enzymology - Amyloid, Prions, and Other Protein Aggregates*, 309, 189-204.
- ZANUY, D., HASPEL, N., TSAI, H. H., MA, B. Y., GUNASEKARAN, K., WOLFSON, H. J. & NUSSINOV, R. 2004. Side chain interactions determine the amyloid organization: a single layer  $\beta$ -sheet molecular structure of the calcitonin peptide segment 15-19. *Physical Biology*, 1, 89-99.
- ZHANG, R., HU, X. Y., KHANT, H., LUDTKE, S. J., CHIU, W., SCHMID, M. F., FRIEDEN, C. & LEE, J. M. 2009. Interprotofilament interactions between Alzheimer's A $\beta$ <sub>1-42</sub> peptides in amyloid fibrils revealed by cryoEM. *Proceedings of the National Academy of Sciences of the United States of America*, 106, 4653-4658.
- ZEROVNIK, E., POMPE-NOVAK, M., SKARABOT, M., RAVNIKAR, M., MUSEVIC, I. & TURK, V. 2002. Human stefin B readily forms amyloid fibrils *in vitro*. *Biochimica Et Biophysica Acta-Protein Structure and Molecular Enzymology*, 1594, 1-5.

- ZHI, P., CHIA, C. & GLEESON, P.A. 2011. Intracellular trafficking of the  $\beta$ -secretase and processing of amyloid precursor protein. *IUBMB Life*, 63, 721–729.
- ZOU, W. Q., XIAO, X. Z., YUAN, J., PUOTI, G., FUJIOKA, H. S., WANG, X. L., RICHARDSON, S., ZHOU, X. C., ZOU, R., LI, S. H., ZHU, X. W., MCGEER, P. L., MCGEEHAN, J., KNEALE, G., RINCON-LIMAS, D. E., FERNANDEZ-FUNEZ, P., LEE, H. G., SMITH, M. A., PETERSEN, R. B. & GUO, J. P. 2011. Amyloid- $\beta_{42}$  interacts mainly with insoluble prion protein in the Alzheimer brain. *Journal of Biological Chemistry*, 286, 15095-15105.